SPATIO-TEMPORAL VARIATION OF ESTUARINE MIXING, SUSPENDED SEDIMENT AND PHYTOPLANKTON IN A HIGHLY TURBID ESTUARY

GUBASH AZHIKODAN

September, 2014

TOKYO METROPOLITAN UNIVERSITY

SPATIO-TEMPORAL VARIATION OF ESTUARINE MIXING, SUSPENDED SEDIMENT AND PHYTOPLANKTON IN A HIGHLY TURBID ESTUARY

By

GUBASH AZHIKODAN

A dissertation submitted in partial fulfilment of the requirements for the Degree of Doctor of Engineering in Civil and Environmental Engineering

Department of Civil and Environmental Engineering

Graduate School of Urban Environmental Sciences

Tokyo Metropolitan University

Tokyo, Japan

September, 2014

Dedicated to

My

Loving Parents

Doctoral Examination Committee

Dr. Katsuhide Yokoyama (Supervisor)

Associate Professor, Department of Civil and Environmental Engineering,
Graduate School of Urban Environmental Sciences,
Tokyo Metropolitan University (TMU),
Email: k-yoko@tmu.ac.jp

Dr. Akira Kawamura

Professor, Department of Civil and Environmental Engineering,
Graduate School of Urban Environmental Sciences,
Tokyo Metropolitan University (TMU),
Email: kawamura@tmu.ac.jp

Dr. Yasuhiro Arai

Associate Professor, Department of Civil and Environmental Engineering,
Graduate School of Urban Environmental Sciences,
Tokyo Metropolitan University (TMU),
Email: y-arai@tmu.ac.jp

Preface

I came to Japan from India as a doctoral student on 27th September, 2011 when I was granted "Asian Human Resource Fund" financially supported by the Tokyo Metropolitan Government, Japan as a part of the research project entitled, "Solutions for the water related problems in Asian metropolitan areas" for doing PhD at Tokyo Metropolitan University (TMU) under the guidance of Associate Professor Katsuhide Yokoyama.

I have completed my schooling in 2003 with Science background. Later I qualified Engineering Entrance Examination (2003) conducted by the Government of Kerala State, India. Then I chose Agricultural Engineering as my field of study and joined Kelappaji College of Agricultural Engineering and Technology, Tavanur under Kerala Agricultural University, Govt. of Kerala for B. Tech studies in 2003. During B. Tech from 2003 to 2007 I have undergone various training programs which helped me to develop in an overall way. I have also participated in inter-university athletic meet and that helped me to improve my team spirit and communication skills.

After graduation I cleared Graduate Aptitude Test in Engineering (GATE) and joined Indian Institute of Technology (IIT) Kharagpur as a post graduate student with the specialization of Water Management at School of Water resources. In IIT I underwent rigorous training in various interdisciplinary subjects related to the field of water management. These helped me to broaden my views about various issues related to water management. Also I attended DAAD supported Summer School on "Teaching and research for Sustainability", 21st June to 4th July, 2009 at the Leibniz University of Hannover, Germany. I also have spent five months (January to May, 2010) in Leibniz University of Hannover, Germany as part of my masters research. These opportunities helped me to improve my international exposure.

I feel that life at TMU helped me to gain a lot of knowledge and experience as a researcher. The Chikugo River estuary, which was located Kyushu district of Southwestern Japan become the study area of my research.

This PhD thesis is one of the requirements of my PhD program from October 2011 to September 2014 at the Department of Civil and Environmental Engineering,

Graduate School of Urban Environmental Sciences, Tokyo Metropolitan University under Associate Professor Katsuhide Yokoyama. The PhD thesis was constructed based on three peer-reviewed scientific papers that were accepted to publish in globally referred journals and two peer-reviewed scientific papers published in international conferences.

The thesis describe the interaction of physical, chemical and phytoplankton processes in a highly turbid estuary which may provide useful information for hydraulic and water resource engineers for the better management of the aquatic ecosystems.

Obviously, successful completion of this PhD research is not my merit alone. This study would not have been possible without the valuable support and guidance from my teachers, colleagues, and friends during my doctoral study in TMU. Therefore, I would take this opportunity to express my heartfelt gratitude to them for their support and encouragement.

First and foremost, I wish to express my sincere gratitude, deep sense of indebtedness and heartfelt thanks to my supervisor Associate Professor Katsuhide Yokoyama, for his helpful and inspiring guidance, valuable suggestions, persistent encouragement and advice throughout the period of my PhD study. It has been an honor to be his PhD student. I could never have accomplished without his timely support, countless help and valuable advice at every stage of my research period.

I express my sincere gratitude to Professor Akira Kawamura and Associate Professor Yasuhiro Arai for accepting to be the members of my Doctoral Examination Committee and spending valuable time to review my thesis and providing me constructive suggestions and comments which greatly helped to enhance the quality of the thesis.

I also wish to thank my M. Tech supervisor, Professor S. N. Panda, Department of Agricultural and Food Engineering, Indian Institute of Technology Kharagpur for his constant support and encouragement to get PhD admission at Tokyo Metropolitan University.

I wish to express my special thanks to my lab mates Mr. Onozaki Toru, Ms. Atsuka Iwatsuki, Mr. Yu Morimura, Mr. Kazutoshi Kiyama, Mr. Ryohei Tomita, Ms. Masuzaki Yumiko, Mr. Kamei Keisuke, Mr. Ryosuke Hara, Mr. Yasushi Iketani, Mr. Ken Morishita, Mr. Tatunori Hashimoto, Mr. Hiroshige Ueda and others for their support and timely help in lab as well as in field.

I wish to express special thanks to my friends Dr. Bijal K Bahuleyan, Mr. Fazalurahman Kuttassery, Mr. Jishad Abubacker, Mrs. Naseera Jishad and Mr. Vivek R Nair, for their timely help and close association during my stay in TMU. I also wish to express special gratitude to my dear friends Mr. Vishnu C Satheesan and Ms. Rekha Sukumary for their encouragement and prayers.

I wish to express my heartfelt gratitude to Tokyo Metropolitan Government for providing financial support during my doctoral study through Asian Human Resource Fund Scholarship. I also want to express heartiest thanks to Ms. Yuki Yamada, Ms. Rie Sasaki, Ms. Naoko Sekiguchi and many others in the International Center of TMU for their co-operation during my doctoral studies.

Words cannot be expressed my indebtedness to my parents whose blessings, love and emotional support helped me in completing this work and accomplish studies successfully. I would like to thank my brothers Mr. Fazilu Rahman A and Mr. Feroz A as well as my sisters Mrs. Fijula Ameer and Mrs. Finsiya Ramsy for their care and love. Special thanks to my beloved one for her care and love to me. I cannot forget her energetic support and timely encouragement during my stressful and difficult moments in my doctoral study.

I heartily thank to all those who have contributed in one or another way for successful completion of my doctoral study.

Above all I bow my head before the Almighty whose blessings empowered and guided me to reach the destination.

Gubash Azhikodan

Tokyo Metropolitan University

Tokyo, September 2014.

Publications

Scientific Papers

2014

1. Azhikodan, G., Yokoyama, K., 2014. Temporal and Spatial Variation of Mixing and Movement of Suspended Sediment in the Macrotidal Chikugo River Estuary. *Journal of Coastal Research*, Accepted.
2. Azhikodan, G., Yokoyama, K., 2014. Estuarine Mixing and Spatial Distribution of Phytoplankton in the Chikugo River Estuary. *Journal of JSCE, Ser. B2 (Coastal Engineering)*, Accepted.
3. Azhikodan, G, Yokoyama, K., Morimura, Y., 2014. Effect of Mixing on Turbidity Maximum Movement during Semilunar Tidal Cycle in the Chikugo River Estuary. *Journal of JSCE, Ser. B1 (Hydraulic Engineering)*, Vol. 70, No. 4, pp. I_37-I_42.

2013

4. Azhikodan, G., Yokoyama, K., 2013. Turbidity Maximum Movement during Semilunar Tidal Cycle in the Chikugo River Estuary. *Proceedings of Hydro International, IIT Madras, India*, ISBN: 978-93-80689-18-0, pp.521-529.
5. Azhikodan, G., Yokoyama, K., Morimura, Y., 2013. Temporal and Spatial Distribution of Salinity and Suspended Sediment in a Macrotidal Estuary. *Proceedings of International Symposium on Answers to Asian Aquatic Problems, Japan*, pp. 47-56.

2012

6. Azhikodan, G., Yokoyama, K., 2012. Influence of Tidal Mixing on Suspended Sediment Transport and Phytoplankton Dynamics in the Chikugo River Estuary, Japan. *Proceedings of the 10th Intl. Conference on Hydroscience & Engg., U.S.A*, No. 40137245, pp. 1-6.

Conference Oral Presentations

2014

1. Azhikodan, G., Yokoyama, K., Morimura, Y., 2014. Effect of Mixing on Turbidity Maximum Movement during Semilunar Tidal Cycle in the Chikugo River Estuary. 58th Conference on Hydraulic Engineering, JSCE, March 4-6, Kobe, Japan.

2013

2. Azhikodan, G., Yokoyama, K., 2013. Turbidity Maximum Movement during Semilunar Tidal Cycle in the Chikugo River Estuary. XVIII Conference on Hydraulics, Water Resources, Coastal and Environmental Engg., Hydro International, December 4-6, IIT Madras, India.
3. Azhikodan, G., Yokoyama, K., 2013. Temporal and Spatial Distribution of Salinity and Suspended Sediment in a Macrotidal Estuary. International Symposium on Answers to Asian Aquatic Problems (AAA+ 2013), November 16, Tokyo, Japan.

2012

4. Azhikodan, G., Yokoyama, K., 2012. Influence of Tidal Mixing on Suspended Sediment Transport and Phytoplankton Dynamics in the Chikugo River Estuary, Japan. 10th Intl. Conference on Hydroscience & Engg., (ICHE 2012), November 4-7, Orlando, Florida, U.S.A.
5. Azhikodan, G., Yokoyama, K., Iwatsuki, A., 2012. Temporal Variation of Mixing Condition in Chikugo River Estuary during a Semilunar Tidal Cycle and its Influence on Phytoplankton Growth. The 11th Seoul-Tokyo International Symposium of Water and Environmental Engineering, August 29, Tokyo, Japan.

Summary

Estuaries are subjected to the influence of both marine and freshwater environments, and receive high levels of fine sediments and nutrients. The abundant production of fish and shellfish in the estuary are supported by the primary production. Therefore, the magnitude and location of the estuarine turbidity maximum (ETM) zone and its effect on phytoplankton life cycle should be clarified in order to manage the productive natural environment of an estuary.

Many studies have focused on seasonal changes of estuarine mixing, suspended sediment dynamics and phytoplankton distribution. However the combined discussion about the spatial variations of mixing, salinity intrusion, suspended sediment transport, formation of ETM and their influence on phytoplankton growth during semilunar tidal cycle were rarely seen. Additionally light availability for the photosynthesis is scarcely studied in highly turbid estuaries. It is crucial to fully understand the effects of mixing and suspended sediment concentration (SSC) on phytoplankton growth. There are four significant issues to consider when analyzing the physical process of salinity intrusion and ETM movement: semidiurnal and semi-lunar tidal variations, spatial distribution, and synchronism of data acquisition. This paper describes the effect of salinity intrusion and mixing on the SSC dynamics and how it regulates the light availability on the activity of phytoplankton in the Chikugo River estuary on a fortnightly time scale for the entire estuary.

The objectives of the studies are (i) to study the spatial and temporal (semidiurnal and fortnightly) variability of salinity intrusion, estuarine mixing and its effects on the location and movement of ETM in the Chikugo River Estuary during a semilunar tidal cycle; (ii) to study the spatial and temporal variability of phytoplankton process based on the estuarine mixing and suspended sediment concentration variability in the Chikugo River Estuary during a semilunar tidal cycle.

This dissertation is composed of five chapters.

Chapter 1 is the introduction that provides the research background and objectives of this study. Previous studies about estuarine mixing and ETM dynamics were also reviewed.

Chapter 2 is the materials and methods that provides the information about the study area, field measurement, analysis of water quality and data analysis. A field

survey was carried out in the Chikugo River estuary during two weeks. Spatial distributions of salinity and turbidity were measured continuously using CTD probe with turbidity sensor, and the obtained turbidity data was converted to the SSC. Water samples were collected from the surface layer (0 to 10 cm) and chlorophyll-a (Chl-a) and pheophytin-a (Pheo-a) was analyzed in the laboratory.

In this study, five indices were defined to discuss the estuarine mixing and movement of ETM: flow ratio, salinity interface gradient (SIG), mixing strength (MS), salinity intrusion length (SIL) and length of ETM (ETML). Furthermore, six indices were used to discuss the growth and migration of phytoplankton: light attenuation coefficient (K), ratio of photic depth to mixing depth (Zp/Zm), surface salinity reach (SSR), surface SSC maximum (SSM), Pheo-a length and Chl-a length.

Chapter 3 focuses on the influence of estuarine mixing on the ETM movement. The estuary gradually changed from a vertically well-mixed condition during spring tide to a stratified condition during the neap tide via a partially mixed condition during intermediate half tides. The relationship between flow ratio and average SSC produced a uniformly linear relation during the fortnightly tidal cycle. SSC was high when the salinity was 0.5 psu in the upper estuary and 10 psu in the lower estuary. For the same mixing strength (MS), SSC in the lower estuary was higher than that in the upper estuary. Based on the flow ratio, salinity and MS, the occurrence of the ETM and its development at a macrotidal estuary was a consequence of three processes: bed sediment erosion by sea water in the lower estuary, sediment transport in the estuarine channel by the tidal current and freshwater flow, and sediment accumulation at the salinity front in the upper estuary.

In Chapter 4, influence of estuarine mixing and ETM on the phytoplankton process was studied. The photic depth became less than 0.2 m during spring tide and it gradually increased during the half tides and reached 4 m during neap tide. Strong relation between K and SSC indicate that the SSC was the key driver of light availability in the Chikugo river estuary. Although light scarcely penetrated into the water column during spring tide, a definite quantity of living phytoplankton (Chl-a) existed throughout the semilunar tidal cycle. Mean concentration of Chl-a in the daytime and in the upper estuary against Zp/Zm showed the hysteresis loop and it was found that phytoplankton growth has a time lag of three days. Good relationship between SSR and Chl-a length showed that the phytoplankton mainly inhabit in brackish water below 1psu.

Pheo-a (dead phytoplankton cells) had high correlation for SSC, K and Zp/Zm. This shows that phytoplankton deactivation and Pheo-a production were caused by the light limitation due to suspended sediment. Good relationship between location of SSM and Pheo-a length indicated that the detritus migrated by adhering to inorganic sediment. It was concluded that estuarine mixing, development of the ETM and phytoplankton process interact.

Chapter 5 gives the summary of main conclusions of each chapter and the future issues.

Contents

Preface…….. i
Publications……..iv
Summary…….. vi
Contents…… ix
List of Figures…….. xii
List of Tables…… xvi

Chapter 1
Introduction 1

1.1 Background 1
1.2 Physical Processes in Estuaries 3
1.3 Aquatic Ecosystems in an Estuary 6
1.4 Scope of the Study 7
1.5 Objectives and Thesis Structure 8

Chapter 2
Materials and Methods 11

2.1 Study Site 11
2.2 In-situ Observation 13
2.3 Laboratory Analysis of SSC and Phytoplankton 21
2.4 Data Analysis 21
2.4.1 Data Analysis of Mixing and ETM 21
a. SIG 21
b. Flow Ratio 22
c. MS 24
d. SIL and ETML 25
2.4.2 Data Analysis of Phytoplankton 25
a. Light Attenuation (K) 25
b. Ratio of Photic Depth to Mixing Depth 26

c. SSR and SSM 27
d. Chl-a length and Pheo-a length 27
e. Chl-a rate 27

Chapter 3

Salinity Intrusion, Mixing and Suspended Sediment Dynamics 28

Abstract 28
3.1 Results 29
3.1.1 River Discharge and Rainfall 29
3.1.2 Semidiurnal Estuarine Variability 30
a. Spring Tide 30
b. Half Tide 31
c. Neap Tide 31
d. Neap Tide to Spring Tide 32
3.1.3 Semilunar Estuarine Variability 66
3.2 Discussion 68
3.2.1 Magnitude of the ETM 68
3.2.2 Flow Ratio 69
3.2.3 Salinity Intrusion and Movement of ETM 73
3.2.4 MS and SSC 77
3.2.5 The ETM Process 81
3.3 Conclusions 82

Chapter 4

Effect of Estuarine Mixing and ETM on the Phytoplankton Process 84

Abstract 84
4.1 Results 85
4.1.1 Weather 85
4.1.3 Relationship between in-situ Chl-a and analysed phytoplankton 86
4.1.3 Spring - Neap - Spring Transition 90
a. Spring Tide to Neap Tide Transition 90
b. Neap Tide to Spring Tide Transition 91
4.2 Discussion 126
4.2.1 Light Attenuation in the Water Column 126

4.2.2 Phytoplankton 130
a. Semidiurnal Variation of Phytoplankton 130
b. Semilunar Variation of Phytoplankton 132
c. Spatial Variation of Phytoplankton 134
4.2.3 Zp:Zm Ratio and Activity of Phytoplankton 137
4.2.4 Time lag of Phytoplankton Growth 140
4.2.5 Migration of Phytolankton 142
4.3 Conclusions 143

Chapter 5
Conclusions 144

5.1 Salinity Intrusion, Mixing and Suspended Sediment Dynamics 144
5.2 Estuarine Mixing and ETM on Phytoplankton Process 145
5.3 Future Works 146

References 148

List of Figures

Fig.1.1	Schematic representation of an estuary	1
Fig. 1.2	Schematic diagram of (a) a highly stratified estuary, (b) a partially mixed estuary, and (c) a vertically well-mixed estuary	4
Fig. 2.1	Study area	12
Fig. 2.2	A Photograph of AAQ sensors	14
Fig. 2.3	A photograph of light sensor connected with AAQ	15
Fig. 2.4	A photograph of data collection using AAQ-1183	15
Fig. 2.5	A photograph of turbidity sensor	17
Fig. 2.6	A photograph of salinity sensor	18
Fig. 2.7	A photograph of acoustic Doppler current profiler (ADCP) instrument	19
Fig. 2.8	A photograph of water level logger	20
Fig. 2.9	A Schematic diagram of 10 psu isohaline in an estuary	22
Fig. 2.10	An example of a semidiurnal tide in an estuary	23
Fig. 2.11	A schematic diagram of Tidal Prism of an estuary during a specific tidal cycle	23
Fig. 2.12	The area of the estuary during a water level of 3.248 m	23
Fig. 2.13	Schematic diagram of salinity distribution in an estuary	25
Fig. 2.14	Schematic diagram of light attenuation through the water column	26
Fig. 2.15	Photic depth and mixing depth during (a) spring tide, and (b) neap tide	27
Fig. 3.1	Time series of (a) river discharge for the year 2010, (b) river discharge and rainfall for September 11 to 25, 2010, and (c) water level for September 11 to 25, 2010	30
Fig. 3.2 – Fig. 3.8	(a) temporal variation of tide and longitudinal and vertical distributions of (b) salinity in psu, (c) SSC in mg/l and (d) Chl-a in µg/l during September 11 (Round 1 to 7)	33-39
Fig. 3.9 – Fig. 3.11	(a) temporal variation of tide and longitudinal and vertical distributions of (b) salinity in psu, (c) SSC in mg/l and (d) Chl-a in µg/l during September 13 (Round 1 to 3)	40-42
Fig. 3.12 – Fig. 3.14	(a) temporal variation of tide and longitudinal and vertical distributions of (b) salinity in psu, (c) SSC in mg/l and (d) Chl-a in µg/l during September 15 (Round 1 to 3)	43-45
Fig. 3.15 – Fig. 3.21	(a) temporal variation of tide and longitudinal and vertical distributions of (b) salinity in psu, (c) SSC in mg/l and (d) Chl-a in µg/l during September 17 (Round 1 to 7)	46-52

Fig. 3.22 – Fig. 3.24	(a) temporal variation of tide and longitudinal and vertical distributions of (b) salinity in psu, (c) SSC in mg/l and (d) Chl-a in µg/l during September 18 (Round 1 to 3)	53-55
Fig. 3.25	(a) temporal variation of tide and longitudinal and vertical distributions of (b) salinity in psu, (c) SSC in mg/l and (d) Chl-a in µg/l during September 19 (Round 1)	56
Fig. 3.26 – Fig. 3.28	(a) temporal variation of tide and longitudinal and vertical distributions of (b) salinity in psu, (c) SSC in mg/l and (d) Chl-a in µg/l during September 20 (Round 1 to 3)	57-59
Fig. 3.29 – Fig. 3.31	(a) temporal variation of tide and longitudinal and vertical distributions of (b) salinity in psu, (c) SSC in mg/l and (d) Chl-a in µg/l during September 22 (Round 1 to 3)	60-62
Fig. 3.32 – Fig. 3.34	(a) temporal variation of tide and longitudinal and vertical distributions of (b) salinity in psu, (c) SSC in mg/l and (d) Chl-a in µg/l during September 25 (Round 1 to 3)	63-65
Fig. 3.35	Longitudinal and vertical distributions of (a) salinity, and (b) SSC during the semilunar tidal cycle. Data measured during flood tide were used	67
Fig. 3.36	Temporal variation of (a) water level, (b) SIG, (c) tidal discharge, (d) flow ratio, (e) bottom velocity at 14.6 km upstream, (f) bottom SSC of estuary at 14.6 km upstream and river at 25 km upstream gauge station, and (g) salinity in the surface and bottom at 14.6 km upstream (h) location of saltwater intrusion and the ETM	71
Fig. 3.37	A plot of the flow ratio against SSC. The average bottom SSC at 14.6 km upstream was calculated for the duration of each flood and ebb tide. The relationship was plotted during spring tide (black), half tides (red and green), and neap tide (blue)	72
Fig. 3.38	Time-distance isopleth of (a) salinity and (b) SSC at flood phase on the surface	74
Fig. 3.39	Relationship between salinity and SSC for (a) the lower estuary, (b) the middle estuary, and (c) the upper estuary	76
Fig. 3.40	(a) Temporal variation of the water level and (b) spatio-temporal distribution of MS	78
Fig. 3.41	Relationship between MS and depth averaged SSC for (a) the lower estuary, (b) the middle estuary, and (c) the upper estuary	80
Fig. 4.1	Weather conditions of the study area during September 11 to 25, 2010	86
Fig. 4.2	In-situ Chl-a (surface) vs laboratory analysed Chl-a (surface) for (a) September 11, (b) September 13, (c) September 15, (d) September 17, (e) September 18, (f) September 20, (g) September 22, and (h) September 25	88

Fig. 4.3	In-situ Chl-a (surface) vs laboratory analysed Pheo-a (surface) for (a) September 11, (b) September 13, (c) September 15, (d) September 17, (e) September 18, (f) September 20, (g) September 22, and (h) September 25	89
Fig. 4.4 – Fig. 4.10	(a) temporal variation of tide; longitudinal and vertical distributions of (b) salinity in psu, (c) SSC in mg/l, and (d) light intensity in µmol/m^2s; and (e) longitudinal distributions of Chl-a (surface) and Pheo-a (surface) during September 11 (Round 1 to 7)	93-99
Fig. 4.11 – Fig. 4.13	(a) temporal variation of tide; longitudinal and vertical distributions of (b) salinity in psu, (c) SSC in mg/l, and (d) light intensity in µmol/m^2s; and (e) longitudinal distributions of Chl-a (surface) and Pheo-a (surface) during September 13 (Round 1 to 3)	100-102
Fig. 4.14 – Fig. 4.16	(a) temporal variation of tide; longitudinal and vertical distributions of (b) salinity in psu, (c) SSC in mg/l, and (d) light intensity in µmol/m^2s; and (e) longitudinal distributions of Chl-a (surface) and Pheo-a (surface) during September 15 (Round 1 to 3)	103-105
Fig. 4.17 – Fig. 4.23	(a) temporal variation of tide; longitudinal and vertical distributions of (b) salinity in psu, (c) SSC in mg/l, and (d) light intensity in µmol/m^2s; and (e) longitudinal distributions of Chl-a (surface) and Pheo-a (surface) during September 17 (Round 1 to 7)	106-112
Fig. 4.24 – Fig. 4.26	(a) temporal variation of tide; longitudinal and vertical distributions of (b) salinity in psu, (c) SSC in mg/l, and (d) light intensity in µmol/m^2s; and (e) longitudinal distributions of Chl-a (surface) and Pheo-a (surface) during September 18 (Round 1 to 3)	113-115
Fig. 4.27	(a) temporal variation of tide; longitudinal and vertical distributions of (b) salinity in psu, (c) SSC in mg/l, and (d) light intensity in µmol/m^2s; and (e) longitudinal distributions of Chl-a (surface) and Pheo-a (surface) during September 19 (Round 1)	116
Fig. 4.28 – Fig. 4.30	(a) temporal variation of tide; longitudinal and vertical distributions of (b) salinity in psu, (c) SSC in mg/l, and (d) light intensity in µmol/m^2s; and (e) longitudinal distributions of Chl-a (surface) and Pheo-a (surface) during September 20 (Round 1 to 3)	117-119
Fig. 4.31 – Fig. 4.33	(a) temporal variation of tide; longitudinal and vertical distributions of (b) salinity in psu, (c) SSC in mg/l, and (d) light intensity in µmol/m^2s; and (e) longitudinal distributions of Chl-a (surface) and Pheo-a (surface) during September 22 (Round 1 to 3)	120-122

Fig. 4.34 – Fig. 4.36	(a) temporal variation of tide; longitudinal and vertical distributions of (b) salinity in psu, (c) SSC in mg/l, and (d) light intensity in μmol/m^2s; and (e) longitudinal distributions of Chl-a (surface) and Pheo-a (surface) during September 25 (Round 1 to 3)	123-125
Fig. 4.37	Spatio-temporal distribution of (a) Light attenuation coefficient (K) in m^{-1}, (b) Photic Depth (Zp) in m, and (c) Zp:Zm ratio (Zp/Zm)	127
Fig. 4.38	Relationship between (a) light attenuation coefficient and depth averaged SSC in the photic zone and (b) light attenuation coefficient and Zp:Zm ratio	129
Fig. 4.39	(1) Surface Salinity, (2) Surface SSC, (3) Chl-a, and (4) Pheo-a during (a) spring and (b) neap tide	131
Fig. 4.40	Temporal variations of (a) tide, (b) SIG, (c) chl-a, (d) pheo-a, and (e) chl-a rate	133
Fig. 4.41	Spatial variation of Chl-a and Pheo-a with Zp:Zm ratio, salinity and SSC during September 11 at high tide	135
Fig. 4.42	Spatial variation of Chl-a and Pheo-a with Zp:Zm ratio, salinity and SSC during September 13 at high tide	135
Fig. 4.43	Spatial variation of Chl-a and Pheo-a with Zp:Zm ratio, salinity and SSC during September 15 at high tide	135
Fig. 4.44	Spatial variation of Chl-a and Pheo-a with Zp:Zm ratio, salinity and SSC during September 17 at high tide	136
Fig. 4.45	Spatial variation of Chl-a and Pheo-a with Zp:Zm ratio, salinity and SSC during September 18 at low tide	136
Fig. 4.46	Spatial variation of Chl-a and Pheo-a with Zp:Zm ratio, salinity and SSC during September 20 at low tide	136
Fig. 4.47	Spatial variation of Chl-a and Pheo-a with Zp:Zm ratio, salinity and SSC during September 22 at low tide	137
Fig. 4.48	Spatial variation of Chl-a and Pheo-a with Zp:Zm ratio, salinity and SSC during September 25 at high tide	137
Fig. 4.49	Zp:Zm ratio against Chl-a, Pheo-a and Chl-a rate	139
Fig. 4.50	Zp:Zm ratio vs chl-a for brackish water	140
Fig. 4.51	Time series of the (a) water level and (b) slope of the relationship between in-situ Chl-a and analysed Chl-a	141
Fig. 4.52	(a) Chl-a length against Surface SIL, and (b) Pheo-a length against Surface SSC length	143

List of Tables

Table 1.1	Tidal range classification of estuaries (Davies, 1964)	5
Table 2.1	Specifications of AAQ sensors	14
Table 2.2	Specifications of turbidity sensor	17
Table 2.3	Specifications of salinity sensor	18
Table 2.4	Specifications of acoustic Doppler current profiler (ADCP) instrument	19
Table 2.5	Specification of water level logger	20

Chapter 1

Introduction

This chapter provides the research background and objectives of this study. Previous studies about estuarine mixing and ETM dynamics were also reviewed.

1.1 Background

An estuary can be defined as a semi-enclosed coastal body of water which has free connection to the open sea and within which seawater is measurably diluted with freshwater derived from land drainage (Cameron and Pritchard, 1963; Pritchard, 1967) (Fig. 1.1).

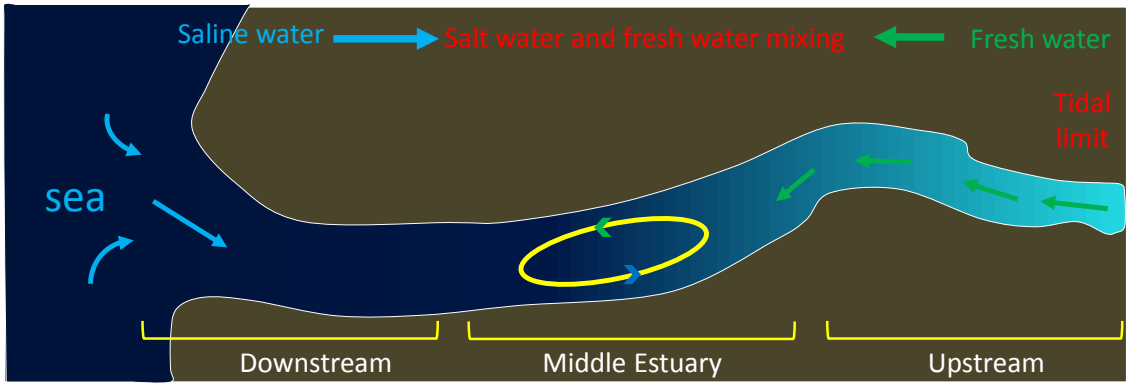

Fig. 1.1 Schematic representation of an estuary.

Estuaries are dynamic environments that display a transitional behavior between rivers and oceans. Estuaries are subjected to the influence of both marine and freshwater environments, and receive high levels of fine sediments and nutrients, which make them very productive aquatic ecosystems. There are highly productive aquatic ecosystems in an estuary with varieties of fish communities which can see only in the estuary. The abundant production of fish and shellfish are supported by the primary production. The characteristics of an estuary depend up local conditions such as weather, tidal cycle, river discharge, currents, and tidal mixing. In addition, estuaries are dynamic at both

spatial and temporal scales.

Major cities of the world have been built on the flood plains around the estuaries. For example, Shanghai on the Yangtze river estuary in China, Bangkok on the Chao Phraya River estuary in Thailand, London on the Thames estuary in the United Kingdom, Hamburg on the Elbe River estuary in Germany, and New Orleans on the Mississippi River estuary in the United States.

Estuaries are the source of food and have a significant commercial value as it provide economic, cultural and ecological benefit to the society. Because of this, estuarine ecosystems are over exploited by the people, which resulted in the severe contamination of estuary and loss of estuarine habitats.

Estuarine ecosystems are threatened by manmade activities and natural phenomenon. The estuarine water is contaminated by pollutants and other toxic chemicals from sewage, industrial wastes and agricultural run-off. This may affect the life of estuarine habitats like fishes. The pollutants that have the greatest impact on the health of estuaries include toxic substances like chemicals and heavy metals, nutrient pollution (or eutrophication), and pathogens such as bacteria or viruses. For e.g., contamination of Amur river by the Chinese and Russian industrial pollution destroyed fish stocks and damaged its estuary soil. Over exploitation of the harvestable communities results the reduction in fishes and other estuarine habitats. It may affect other serious issues to the estuarine system. For e.g., the flourishing oyster population in the Chesapeake Bay was declined dramatically because of the overfishing. Historically, oyster filtered entire water column of the estuary every 3 days. After the collapse of the oyster population the filtering process takes long time and this resulted decline in water quality, eutrophication and other problems. Generally oysters filter particulate carbon, nutrients and other inorganic particles from the water column (Rothschild *et al.*, 1994; Newell, 1988).

Estuaries experience various environmental gradients (such as semidiurnal and semilunar variation of tidal ranges, temporal and spatial changes in salinity, a well-developed estuarine turbidity maximum), many valuable and unique species live in habitats with specific parameters suitable to that particular species. The combination of environmental elements in estuaries is very complicated, and the habitat requirements may be highly specific. Therefore, human impact may have significant effects on ecosystems in estuaries.

River estuaries are important regions for both human beings and wildlife.

Furthermore, there are large environmental fluctuations in river estuaries. Therefore, it is necessary to understand and predict temporally and spatially complex phenomena, such as mixing of freshwater and saltwater, water quality, sediment transport, and morphodynamics, and their relationship to ecosystems, in order to manage the water environment appropriately and to minimize the impact of river engineering on biodiversity and wildlife.

1.2 Physical Processes in Estuaries

Freshwater collides with saltwater in a river mouth estuary. Two fluids of different densities thus mix and form a gradation of salinity. Estuaries are classified as vertically stratified, partially mixed, or well mixed. Although there are no clear criteria for this classification, an approximate explanation of each type is given below.

Mixing in an estuary is affected by the interaction of tidal flow and freshwater flow. Tidal flow is determined by tidal amplitude and tidal prism, that is, the capacity for saltwater intrusion. A combination of weak tidal flow and large freshwater flow produces vertical stratification, termed as salt wedge. Salt wedges are often found in microtidal estuaries with a tidal range of less than 2 m. Sea water runs up along the river bottom landward and river water flows in the surface zone sea ward, with a steep pycnocline between two layers (Fig. 1.2a). Since the vertical density gradient in the transition zone is very large, suspended or dissolved materials in the bottom layer cannot migrate to the surface layer, and vice versa. The speed of flow of the salt wedge is slow (dozens of centimeters per second), due to high stability; however, sea water may gradually travel landward for hundreds of kilometers in land, due to residual currents. Examples are Mississippi estuary, United States (Dyer, 1997), Vellar estuary, India (Dyer and Ramamoorthy, 1969), and Yura estuary, Japan (Kasai *et al.*, 2010 and Watanabe *et al.*, 2014).

Conversely, a combination of large tidal flow and weak freshwater flow produces well-mixed conditions (Fig. 1.2c). Well-mixed salinity patterns are often found in macrotidal estuaries with a tidal range larger than 4 m. because of large tidal variations, salt water is intensely mixed with freshwater, and a vertically homogeneous water column is formed at the interface between saltwater and freshwater. Saltwater rapidly intrudes into an estuary and freshwater is pushed back landward during flood tides, while both saltwater and freshwater in an estuary are discharged to the sea during

ebb tides. Although the current speed in well-mixed estuary exceeds 1.0 m/s (far greater than the migration speed of a salt wedge), the landward mileage of a salinity front in a well-mixed estuary is shorter than that of a salt wedge. Active turbulence occurs in a well-mixed estuary, and water and suspended matter circulate vertically; as a result, bottom material reaches the surface easily. Examples are Delaware estuary, United States (Sommerfield and Wong, 2011), Scheldt estuary, Netherlands (Baeyens, 1998),

Partially mixed estuaries are often located in mesotidal coastal areas with a tidal range of 2-4 m. Salinity patterns under partially mixed conditions are transitional between those of a salt wedge and those characteristic of a well-mixed distribution (Fig. 1.2b). Examples are James river estuary, Virginia, United States (Feuillet and Fleischer, 1980) and Tamar estuary, England (Uncles, 2002).

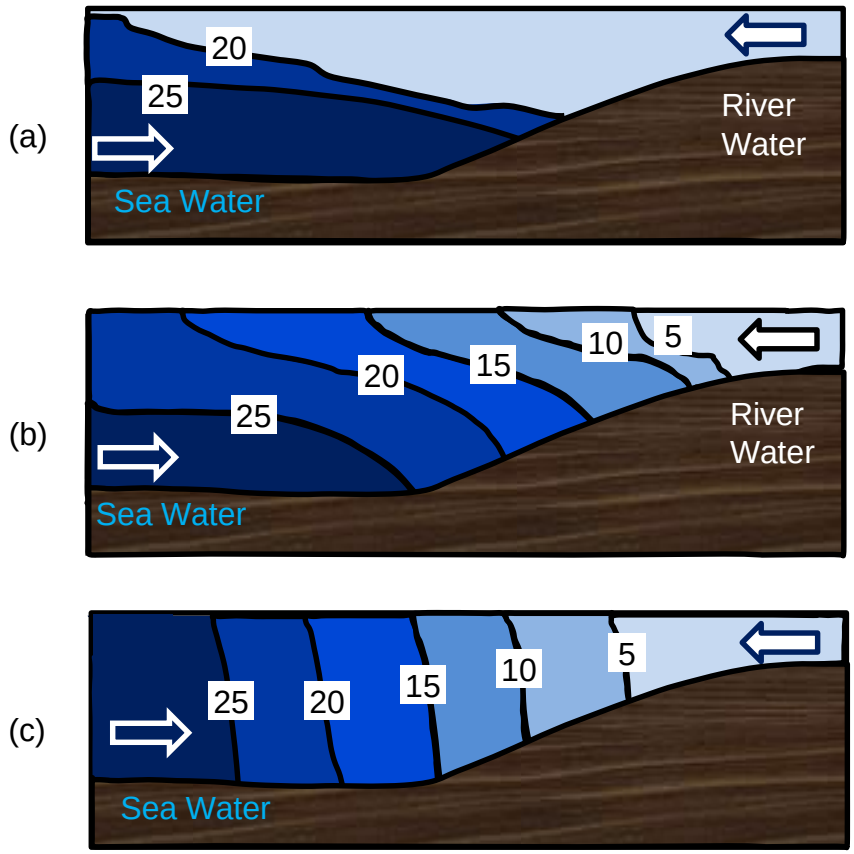

Fig. 1.2 Schematic diagram of (a) a highly stratified estuary, (b) a partially mixed estuary, and (c) a vertically well-mixed estuary.

Mixing in an estuary has an important role in the distribution of sediments, nutrients, and pollutants in a coastal area. Mixing can be highly variable, depending on tidal variations and river discharge (Dyer, 1997). Therefore tidal discharge and river

discharge have the significant role in different processes in an estuary.

Based on tidal ranges, Davies (1964) classified estuaries in to four types (Table 1.1).

Table 1.1 Tidal range classification of estuaries (Davies, 1964).

Type	Tidal Range	Examples
Microtidal	<2 m range	St. Lucie (Florida)
Mesotidal	< 4 m, >2 m	Guadiana (southwestern Iberia)
Macrotidal	< 6 m, > 4 m	Tamar, Thames (UK), Scheldt (Belgium), Delaware (USA), Tay (Scotland), Konkoure (Republic of Guinea)
Hypertidal	> 6 m	Seine (France)

The presence of a locally elevated suspended sediment concentration (SSC) is termed the estuarine turbidity maximum (ETM) and is found in coastal plain estuaries throughout the world (Schubel, 1968). Estuarine productivity is strongly affected by the SSC when it increases from 10 to 100 mg/l (Peterson and Festa, 1984). The ETM can significantly influence estuarine ecosystems by regulating the availability of light (Cloern, 1987) and nutrients. For *e.g.*, Guadiana estuary in Iberia (Domingues *et al.*, 2012), San Francisco Bay in United States (Cloern, 1987), Seine estuary in France (Romana, 1979), Amazon river mouth in Brazil (Edmond *et al*., 1981), Delaware estuary in United States (Pennock, 1985), Gironde in France (Allen *et al.*, 1990).

Different mechanisms may be responsible for the magnitude and location of the ETM zone depending up the mixing conditions, the strength of the estuarine circulation, and the concentration of suspended sediment due to tidal flat and river discharge (Dyer, 1986; Festa and Hansen, 1978; Patchineelam and Kjerfve, 2004). Many studies have been undertaken to investigate estuarine mixing and suspended sediment dynamics in various estuaries worldwide.

Wolanski *et al.* (1995) investigated the ETM dynamics in the Fly River estuary, Papua New Guinea, and reported that a turbidity maximum existed only at spring tides. They also suggested that the turbidity maximum was due to the simultaneous influence of the baroclinic circulation and tidal pumping. Grabemann *et al.*, (1997) conducted a comparative investigation of the Tamar (England) and Weser (Germany) estuaries, which have similar mean tidal ranges and mean tidal current speeds, and reported that both estuaries have a strong ETM zone in their lower salinity reaches, despite their

differences in morphology and freshwater inflows. They also reported that the Tamar estuary had a much higher SSC than the Weser estuary did because tidal asymmetry was stronger in the Tamar than it was in the Weser. The SSC in the macrotidal Daly estuary, Australia, did not vary in direct relation to the current speed, especially at ebb tide when a number of high turbidity events occurred (Wolanski *et al.*, 2004). Chen *et al.* (2005) identified the existence of three ETM zones in the macrotidal Scheldt estuary, Belgium, which were related to the energy distribution patterns in the estuary. Jago *et al.* (2006) found that the ETM occurred at high water in the macrotidal Taf estuary, southwest Wales, United Kingdom, and they described a new mechanism for ETM formation from resuspension and advection by flood tidal currents, which differ from the classical mechanisms of gravitational circulation and tidal pumping. They also predicted that the highest SSC occurred when a spring tide coincided with low river discharge. That indicates the influence of river discharge on ETM formation. Cook *et al.* (2007) measured the ETM in the Delaware estuary, U.S. Atlantic coast, during spring 2003 and reported that the SSC and tidal sediment flux varied spatially in the estuary with the magnitude of the local current and the proximity of patches of easily resuspendable sediment. The seaward residual current that compensates for Stokes drift in a flood tide appears to be a significant mechanism for sediment transport to the estuarine turbidity maximum zone.

1.3 Aquatic Ecosystems in an Estuary

In general, phytoplankton growth is influenced by light attenuation in water column of slack water area such as lake, reservoir and ocean. Smith and Baker (1978) found strong correlation between light attenuation and chlorophyll-like pigment concentration of ocean waters. Many studies show that change in SSC play the dominant role on the light attenuation and strongly influenced the photic depth in shallow lakes of Lake Balaton (Somlyody and Koncsos, 1991), Lake Veluwe (Van Dijk and Achterberg, 1992), Lake Malaren (Pierson *et al.*, 2003), Lake Taihu (Shi *et al.*, 2014).

Estuarine phytoplankton growth was regulated by both nutrients and light availability (Bruno *et al.*, 1980; Pennock, 1987; Domingues *et al.*, 2005; Gameiro *et al.*, 2007). Phytoplankton production in a turbid Westerschelde estuary, Netherlands was mainly driven by light compared with nutrients (Van Spaendonk *et al.*, 1993). However,

previous studies on phytoplankton dynamics in estuaries were mainly focused on the effects of nutrient availability on the growth of phytoplankton, dominant species, and seasonal variations of chlorophyll-a (Chl-a). Temporal and spatial variability of phytoplankton production in the Delaware estuary was studied by Pennock and Sharp (1986) over several seasonal cycles of 5 year period in a monthly basis. Spatial and temporal dynamics of phytoplankton communities in Schelde estuary was studied by the Muylaert *et al.* (2000) to find the origin and composition of phytoplankton communities in a freshwater tidal estuary with the monthly sampling of 1996. Kasai *et al*. (2010) explains the seasonal changes of salinity intrusion and its implication on phytoplankton dynamics of Yura estuary, effects of tidal currents were negligible due to the low tidal influence.

Light availability for the photosynthesis is limited by SSC especially in highly turbid estuaries (May *et al.*, 2003). It is crucial to fully understand the effects of mixing and suspended sediment concentration (SSC) on phytoplankton growth. There are few studies that investigated the effect of physical dynamics such as mixing, movement of salinity and ETM on the state of phytoplankton in macro-tidal estuaries. A few studies have been undertaken to assess the ETM and ecosystems of the highly turbid macro-tidal Chikugo River estuary and Ariake Sea (Suzuki *et al.*, 2008; 2009; 2012; 2013). Because these studies have focused on the ecology of the area or specifically fish or zooplankton, SSC and salinity distributions were measured during high water at spring tide and it took 4–5 hours to make observations from the uppermost to the lower most station. Although an outline of the ETM distribution and the distribution of organisms was recorded, the synchronicity of the data acquisition was too weak to analyze the detailed relationship between salinity intrusion and movement of the ETM.

The seasonal study may not give a clear explanation on the growth of plankton in an estuarine system and how environmental conditions influence them. Since the growth of phytoplankton takes place within few days, in order to understand the effect of physical process on phytoplankton growth, semidiurnal and semilunar studies are to be carried out.

1.4 Scope of the Study

There are four significant issues to consider when analyzing the physical process of salinity intrusion and ETM movement: semidiurnal and semi-lunar tidal variations,

spatial distribution, and synchronism of data acquisition. The movement of salinity, suspended sediment, and the formation of the ETM may be affected by the tidal range and tidal cycle. It is well known that the maximum concentration of suspended sediment is observed during a flood or ebb tide in the semidiurnal tidal cycle. Furthermore, the spring-neap-spring tidal cycle also affects the salinity mixing and movement of the ETM. Although many studies have focused on estuarine mixing and suspended sediment dynamics, only a few have addressed both spatial and fortnightly tidal variations for the estuaries (Allen *et al.*, 1980; Gelfebaum, 1983). Semidiurnal and seasonal variations have received significant attention compared to fortnightly variations (Patchineelam and Kjerfve, 2004).

Sufficiently documented studies in river estuary that satisfy all these factors are rare in the world.

1.5 Objectives and Thesis Structure

1. To study the spatial and temporal (semidiurnal and fortnightly) variability of salinity intrusion, estuarine mixing and its effects on the location and movement of ETM in the Chikugo River Estuary during a semilunar tidal cycle.
2. To study the spatial and temporal variability of phytoplankton process based on the estuarine mixing and suspended sediment concentration variability in the Chikugo River Estuary during a semilunar tidal cycle.

This dissertation is composed of five chapters.

Chapter 1 is the introduction that provides the research background and objectives of this study. Previous studies about estuarine mixing and ETM dynamics were also reviewed.

Chapter 2 is the materials and methods that provides the information about the study area, field measurement, analysis of water quality and data analysis. A field survey was carried out in the Chikugo River estuary during two weeks. Spatial distributions of salinity and turbidity were measured continuously using CTD probe with turbidity sensor, and the obtained turbidity data was converted to the SSC. Water samples were collected from the surface layer (0 to 10 cm) and chlorophyll-a (Chl-a)

and pheophytin-a (Pheo-a) was analyzed in the laboratory.

In this study, five indices were defined to discuss the estuarine mixing and movement of ETM: flow ratio, salinity interface gradient (SIG), mixing strength (MS), salinity intrusion length (SIL) and length of ETM (ETML). Furthermore, six indices were used to discuss the growth and migration of phytoplankton: light attenuation coefficient (K), ratio of photic depth to mixing depth (Zp:Zm ratio), surface salinity reach (SSR), surface SSC maximum (SSM), Pheo-a length and Chl-a length.

Chapter 3 focuses on the influence of estuarine mixing on the ETM movement. The estuary gradually changed from a vertically well-mixed condition during spring tide to a stratified condition during the neap tide via a partially mixed condition during intermediate half tides. The relationship between flow ratio and average SSC produced a uniformly linear relation during the fortnightly tidal cycle. SSC was high when the salinity was 0.5 psu in the upper estuary and 10 psu in the lower estuary. For the same mixing strength (MS), SSC in the lower estuary was higher than that in the upper estuary. Based on the flow ratio, salinity and MS, the occurrence of the ETM and its development at a macrotidal estuary was a consequence of three processes: bed sediment erosion by sea water in the lower estuary, sediment transport in the estuarine channel by the tidal current and freshwater flow, and sediment accumulation at the salinity front in the upper estuary.

In Chapter 4, influence of estuarine mixing and ETM on the phytoplankton process was studied. The photic depth became less than 0.2 m during spring tide and it gradually increased during the half tides and reached 4 m during neap tide. Strong relation between K and SSC indicate that the SSC was the key driver of light availability in the Chikugo river estuary. Although light scarcely penetrated into the water column during spring tide, a definite quantity of living phytoplankton (Chl-a) existed throughout the semilunar tidal cycle. Mean concentration of Chl-a in the daytime and in the upper estuary against Zp:Zm ratio showed the hysteresis loop and it was found that phytoplankton growth has a time lag of three days. Good relationship between SSR and Chl-a length showed that the phytoplankton mainly inhabit in brackish water below 1psu.

Pheo-a (dead phytoplankton cells) had high correlation for SSC, K and Zp:Zm ratio. This shows that phytoplankton deactivation and Pheo-a production were caused by the light limitation due to suspended sediment. Good relationship between location of SSM and Pheo-a length indicated that the detritus migrated by adhering to inorganic

sediment. It was concluded that estuarine mixing, development of the ETM and phytoplankton process interact.

Chapter 5 gives the summary of main conclusions of each chapter and the future issues.

Chapter 2

Materials and Methods

This chapter provides the information about the study area, field measurement, analysis of water quality and data analysis. A field survey was carried out in the Chikugo River estuary during two weeks. Spatial distributions of salinity and turbidity were measured continuously using CTD probe with turbidity sensor, and the obtained turbidity data was converted to the SSC. Water samples were collected from the surface layer (0 to 10 cm) and chlorophyll-a (Chl-a) and pheophytin-a (Pheo-a) was analyzed in the laboratory.

2.1 Study Site

The Ariake Sea is a large semi-enclosed shallow sea in Japan. Many harvestable communities can only be found in the area. The Chikugo River estuary and offshore tidal flats are strongly affected by the intrusion of freshwater from the Chikugo River and the high tidal range (5 m) of the bay.

The Chikugo River is the largest river draining into the western part of the Ariake Sea and is situated in the Kyushu district of Southwestern Japan (Fig. 2.1). The total length of the river is nearly 143 km. It ranks as the 22nd largest river in Japan with a drainage basin of 2,860 km^2, a mean discharge of 54 m^3/s (during the dry season), and a mean annual storm discharge of 2,800 m^3/s.

The Chikugo River estuary has a width varying from 1,000 m at the river mouth to 250 m at a distance 23 km upstream. There is a branch off the main estuarine channel 10 km from the river mouth, which rejoins the main channel 6.5 km from the Ariake Sea. Another branch forms at 6.5 km and subsequently discharges into the Ariake Sea. The bottom sediments in the tidal flat consist mainly of silt and clay (below 0.075 mm), whereas the section between the river mouth and 10 km upstream consists mainly of fine sand (0.075–2 mm). The section between 10 km and 20 km upstream consists mainly of silt and clay. The region upstream of 20 km consists mainly of sand. The estuary experiences semidiurnal conditions with a tidal amplitude of 5 m at spring tide

and 1.5 m at neap tide. The estuary is classified as a mesotidal/macrotidal estuary (Davies, 1964). The tidal currents in the estuary increase by over 1 m/s during spring tide. A considerable tidal influence extends to a barrage, which is situated 23 km upstream from the river mouth.

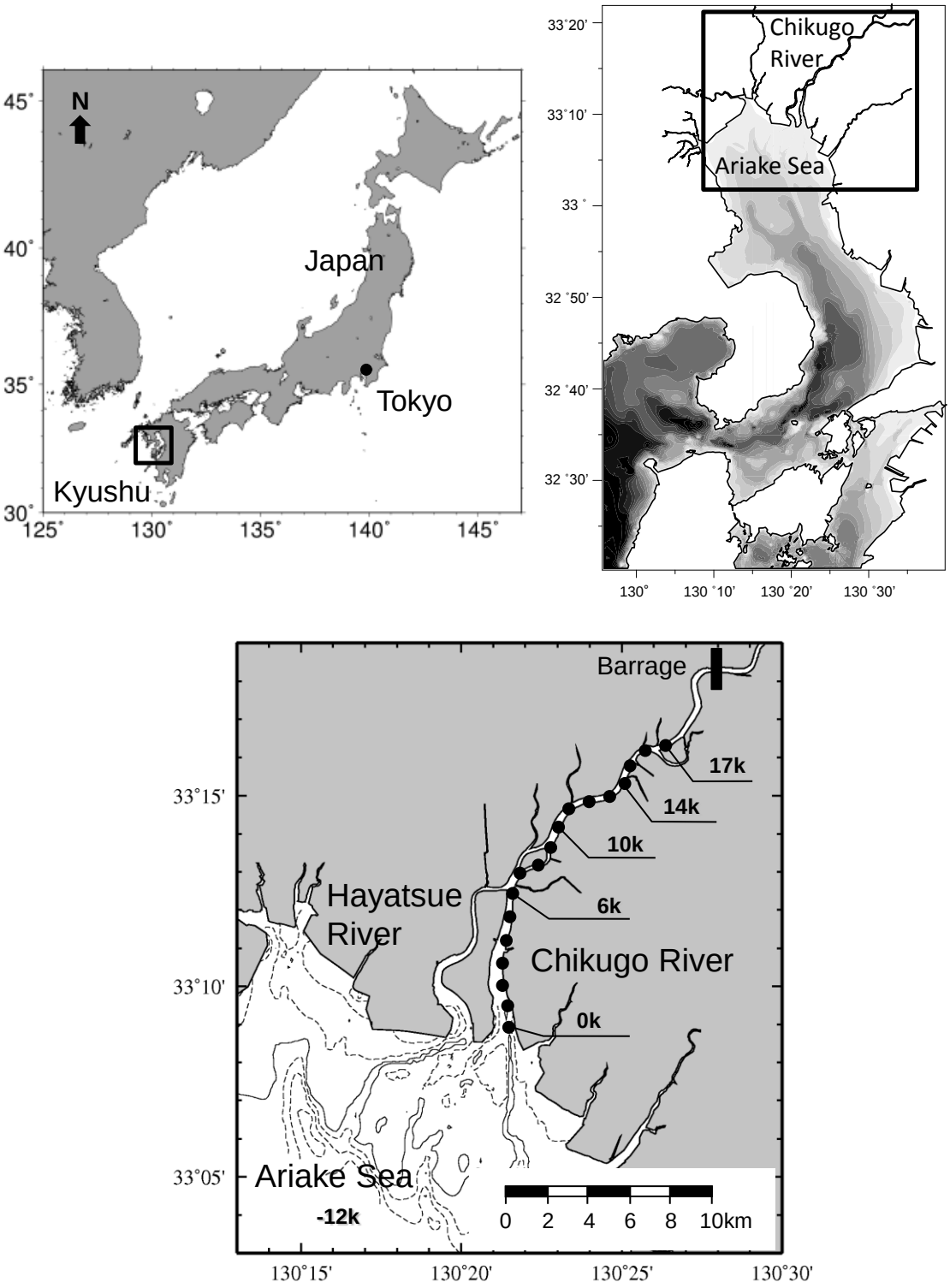

Fig. 2.1 Map and location of the study area, Chikugo River estuary.

2.2 In-situ Observation

A detailed field survey was conducted in the Chikugo River estuary during a semi-lunar tidal cycle from September 11 to 25, 2010. These observations were undertaken in the mid channel at 1 km intervals starting from the river mouth (0 km) to 17 km upstream with a total of 18 measurement stations. Vertical profiles of water quality parameters, including salinity, turbidity, chlorophyll fluorescence and temperature, were measured using a CTD probe with an optical backscatter sensor (AAQ-1183, JFE Advantech, Japan) (Fig. 2.2). Photon flux density was measured using another data collector synchronizing with the acquisition of water quality data (Fig. 2.3).The details of sensors were given in Table 2.1. The value of these parameters was recorded at depth intervals of 0.1 m throughout the vertical profile at the speed of 5 Hz.

A high-speed boat equipped with a differential global positioning system (D-GPS) was used to undertake the field survey (Fig. 2.4). Data was collected at each station over a 2 min period, and the travel time between stations was a further 2 min at a boat speed of approximately 25 km/h. This allowed data collection with one boat within 75 min for all 18 stations. Accounting for the 45 min period necessary to return to the starting point from the last station, each sampling period completed in 2 h, and it was possible to complete seven sampling periods within the semidiurnal tidal cycle for spring and neap tides. Water samples for the determination of suspended sediments were collected from the surface layer (0 to 10 cm) at all 18 measurement stations. For intermediate half tides, measurements were taken three times in 2 h intervals during low tide, flood tide, and high tide during the semidiurnal cycle.

Fig. 2.2 A Photograph of AAQ sensors.

Table 2.1 Specifications of AAQ sensors.

Product name	AAQ-1183 (JFE Advantech, Nishinomiya, Hyogo, Japan)				
Parameter	Depth	Temperature	Salinity	Chlorophyll	Turbidity
Type	Semiconductor Pressure Transducer	Thermistor	Practical Salinity Equation	Fluorescent Scattering Light	Back-scattering Light
Measurement range	0 ～ 100 m	-5 ～ 40℃	0 ～ 40	0 ～ 400μg/l	0～1000FTU (Formazine)
Resolution	0.002 m	0.001℃	0.001	0.01μg/l	0.03FTU
Accuracy	0.30%	±0.02℃	±0.03	±1%	±2%

Fig. 2.3 A photograph of light sensor connected with AAQ-1183.

Fig. 2.4 A photograph of data collection using AAQ-1183.

A self-recording turbidity sensor (Infinity-Turb, JFE Advantech, Japan) and salinity sensor (infinity-CTW ACTW-USB with wiper, JFE Advantech, Japan) were attached to a bridge pier (14.6 km) at a position near the river bed (Fig. 2.5 and Fig. 2.6). The parameters and specifications of the sensor were given in Table 2.2 and Table 2.3. A self-recording acoustic Doppler current profiler (Aquadopp 1MHz, Nortek AS) was mounted on the channel bed (Fig. 2.7). The specifications of the velocity profile were given in Table 2.4. Turbidity, salinity and velocity data were collected at a location 14.6 km upstream in 10 min intervals. Water level data was collected in every 10 min at 14.6 km using a HOBO U20 water level logger (Fig. 2.8) with a resolution of 0.21 cm (Onset, USA). The specifications of the water logger were given in Table 2.5.

A gauge station was located in the freshwater region (25 km from river mouth) which is at the upstream of Chikugo river barrage. River discharge monitored at the gauge station and rainfall data of the area were collected from Japanese Ministry of Land, Infrastructure, Transport and Tourism. In this study, a turbidity sensor with a resolution of 1 mg/l was attached at the gauge station and data were collected in 60 min intervals.

Fig. 2.5 A photograph of turbidity sensor.

Table 2.2 Specifications of turbidity sensor.

Sensor type	**Infinity-Turb, JFE Advantech ACLW-CMP**	
Parameter	Chlorophyll	Turbidity
Measurement range	0.1 ～ 400 ppb	① 0～1000FTU (Formazin) ② 0～5000ppm (Kaolin)
Accuracy	±1%	±2%
Resolution	0.01 ppb	① 0.03FTU (Formazin) ② 0.01ppm (Kaolin)
Excitation waves	470nm	880nm
Emission waves	680～1000 nm	880nm

Fig. 2.6 A photograph of salinity sensor.

Table 2.3 Specifications of salinity sensor.

Sensor type	**INFINITY-CTW ACTW-USB with wiper, JFE Advantech**
Parameter	Electric conductivity
Principle	7-electrode type
Measurement range	2 to 70mS/cm
Resolution	0.001mS/cm
Accuracy	±0.01mS/cm (2 to 65mS/cm)
Measuring mode	Continuous mode, Burst mode
Measuring interval	0.1 to 600 seconds
Dimensions	ø70mm×342mm(including sensor card)
Weight	Approx. 1.5kg in air, 0.6kg in water

Fig. 2.7 A photograph of acoustic Doppler current profiler (ADCP) instrument.

Table 2.4 Specifications of acoustic Doppler current profiler (ADCP) instrument.

Product name	Aquadopp (Nortek AS, Rud, Norway)
Acoustic Frequency	1 MHz
Maximum profiling range	12–20m
Velocity Range:	±10m/s
Accuracy:	1% of measured value ±0.5cm/s
No. of sensors	4
Wave transmission angle	20° from the center line
Dimensions	Length 405.5mm and diameter 228mm
Weight	2.4kg (in air), 0kg (in water)

Fig. 2.8 A photograph of water level logger.

Table 2.5 Specification of water level logger.

Sensor type	**HOBO water level logger U20**
Measurement range	9 m
Accuracy	±0.5 cm
Sampling intervals	1s～18hours possible
Size	25×150 mm
Weight	210 g
Resolution	0.21 cm water

2.3 Laboratory Analysis of SSC and Phytoplankton

Both sediment and phytoplankton samples were filtered through a 0.7 μm glass fiber filter. The filtered samples were transported to a Tokyo laboratory for analysis. Dry weight of sediment samples was recorded and SSC was determined. SSC was plotted against the in-situ turbidity value (TB) measured at the same stations and a formula for the conversion of TB to SSC was derived. The vertical profile of SSC at each station was calculated from the measured *TB* using eq. (1).

$$SSC = 1.05TB + 4 \cdot 10^{-4} TB^2 + 6 \cdot 10^{-14} TB^5 \quad (1)$$

The average bottom SSC at 14.6 km upstream was calculated for the duration of each flood and ebb tide.

Historically, phytoplankton standing stocks were explained by using Chlorophyll pigments in estuaries, lakes and coastal waters (Boyer *et al.*, 2009; Cloern *et al*., 1989; Cloern and Jassby, 2010; Zhai *et al*., 2011). The filtered sample of phytoplankton was placed in 12 ml Dimethylformamide (DMF). The Chl-a concentration in the extracts were determined by the fluorometry using a Turner Designs 10-AU fluorometer. Pheophytin-a (Pheo-a) concentrations are then calculated using fluorescence values based on Holm-Hansen method.

2.4 Data Analysis

2.4.1 Data Analysis of Mixing and ETM

In this study, five indices were defined to discuss the estuarine mixing and movement of ETM: flow ratio, salinity interface gradient (SIG), mixing strength (MS), salinity intrusion length (SIL) and length of ETM (ETML).

(a) SIG

To classify the salinity mixing, the salinity interface gradient (SIG) was defined, which is defined as the slope of the 10 psu isohaline (Fig. 2.9):

$$SIG = H \Big/ \left(X_b - X_s \right) \quad (2)$$

where X_b is the distance from 0 km to the position where 10 psu appears on the bottom, X_s is the distance from 0 km to the position where 10 psu appears at the surface, and H is the water depth around the 10 psu area. The estuary is classified using the salinity

interface gradient. When the water depth is 5 m, and the position where 10 psu appears on the bottom advances 1 km or less than the position at the surface (SIG ≥ 0.005), the condition is defined as well mixed. When the difference in distance between X_b and X_s ranges from 1 to 5 km at the same depth (0.005 > SIG ≥ 0.001), the condition is defined as partially mixed. A SIG < 0.001 is defined as highly stratified.

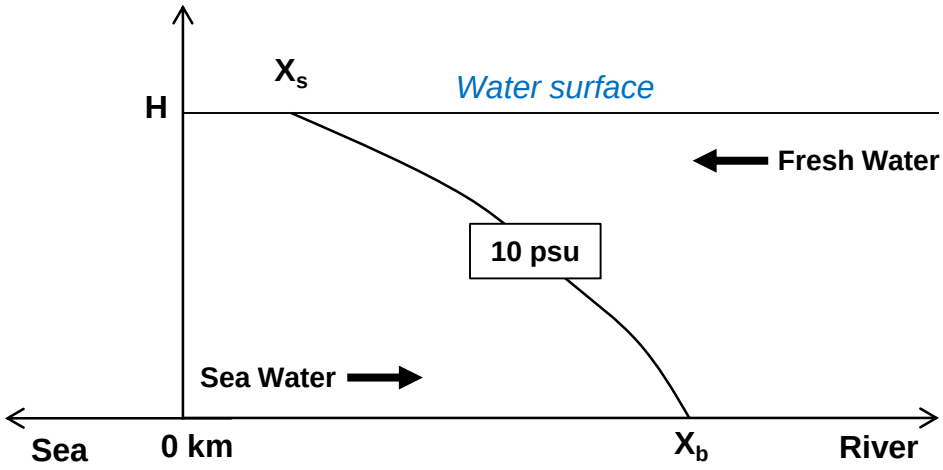

Fig. 2.9 A Schematic diagram of 10 psu isohaline in an estuary.

(b) Flow Ratio

The flow ratio was used to investigate the dominant factors affecting the mixing and SSC. The actual daily value was calculated using the tidal range of every half day to determine an accurate tidal discharge. Freshwater discharge and tidal discharge are key factors that affect mixing in an estuary. The balance of these two driving forces can be expressed as a flow ratio (*FR*):

$$FR = \sum_{t=i}^{t=j} Q_f(t) \Big/ (V_H - V_L) \qquad (3)$$

where $Q_f(t)$ is the freshwater discharge at the gauge station (25 km), i is the time of low or high tide, j is the time of high or low tide (Fig. 2.10), V_H is the estuary volume at high tide, and V_L is the estuary volume at low tide, and therefore (V_H–V_L) is the tidal prism, which is the volume of salt-water intrusion during an ebb and flood tide (Fig. 2.11). Estuary volume was calculated using the topography data of the estuarine cross section at every 200 m longitudinally and the tidal amplitude during every low tide and high tide at 14.6 km (Fig. 2.12).

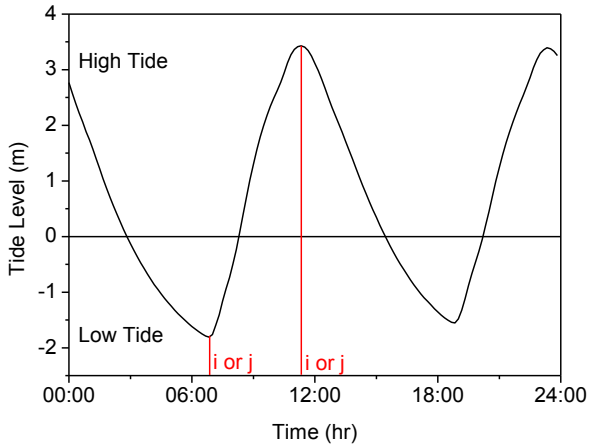

Fig. 2.10 An example of a semidiurnal tide in an estuary.

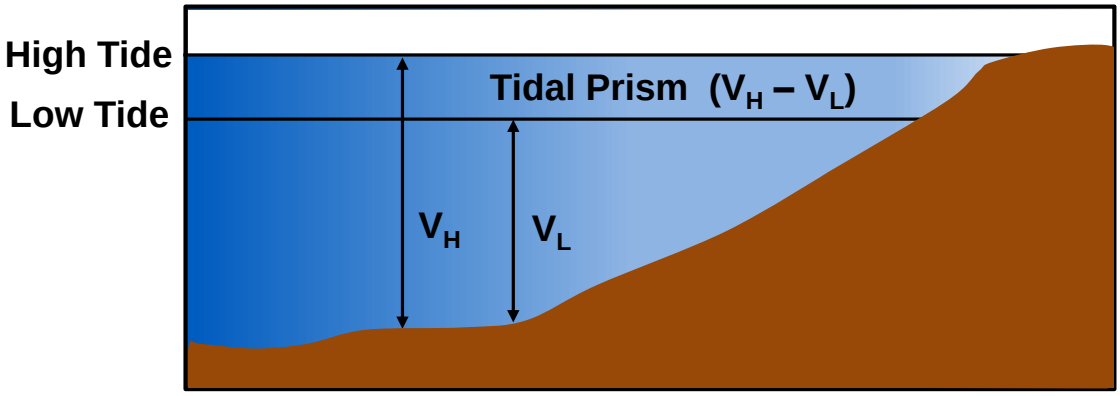

Fig. 2.11 A schematic diagram of Tidal Prism of an estuary during a specific tidal cycle.

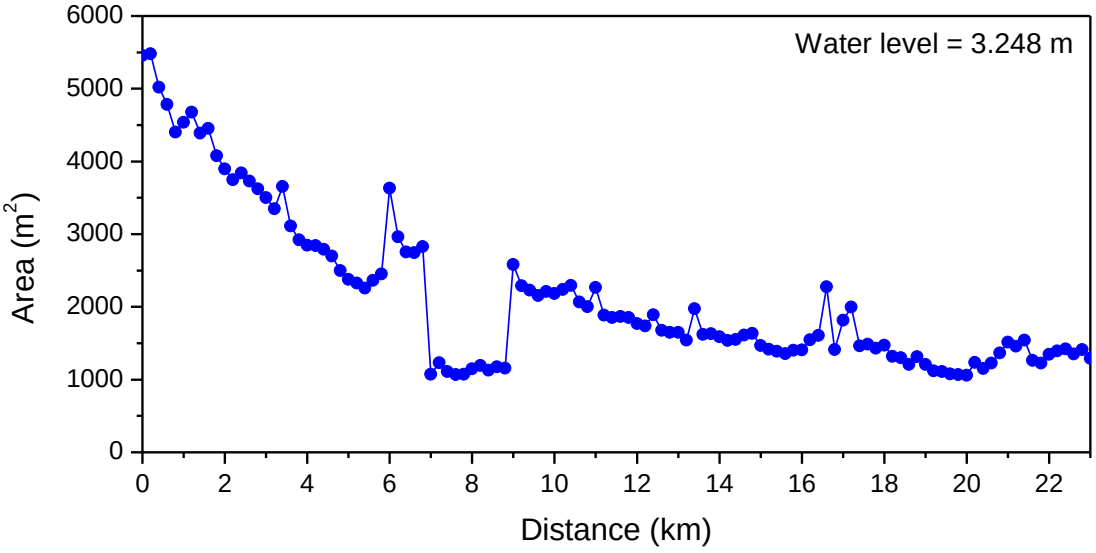

Fig. 2.12 The area of the estuary during a water level of 3.248 m.

(c) MS

In general, the mixing condition of the estuary is discussed using the salinity stratification number. The salinity stratification number (S_n) is defined as,

$$S_n = \frac{S_b - S_s}{\bar{S}} \quad (4)$$

where S_b and S_s are the salinity at the bottom and surface respectively and $\bar{S}$ is the depth averaged salinity (Dyer, 1997). This index can be used to explain the mixing condition of the estuary. If $S_n < 0.15$, the estuary is well mixed and if $S_n > 0.32$ it is stratified.

However, it is difficult to use this index to analyze the mixing condition spatially. For example, when S_b is 10.0 and S_s is 9.0, S_n becomes 0.105 and the estuary is classified as well-mixed. However, when S_b is 2.0 and S_s is 1.0 at the front of the well-mixed salinity intrusion, S_n becomes 0.667, and the estuary is classified as stratified. Furthermore, when S_b is 20.0 and S_s is 10.0, S_n becomes 0.667, which also results in a stratified classification. This shows the difficulty in explaining the vertical mixing of the salinity intrusion by using S_n.

Therefore we use the index of mixing strength (MS), which is the vertical gradient of salinity, is defined as:

$$MS = \frac{S_b - S_s}{H} \quad (5)$$

where S_b and S_s are the salinity at bottom and surface respectively. H is the depth (m) of the water column (Fig. 2.13). Because MS is similar to the vertical density gradient and stability of stratification, the index value becomes the inverse of the actual mixing force. The MS is small when the salinity distribution is vertically uniform, and is high in stratified conditions. When the estuary is vertically well mixed, MS is less than 0.1; MS will be 0.1 to 1 when the estuary is partially mixed; and MS becomes greater than 1 when the estuary is stratified.

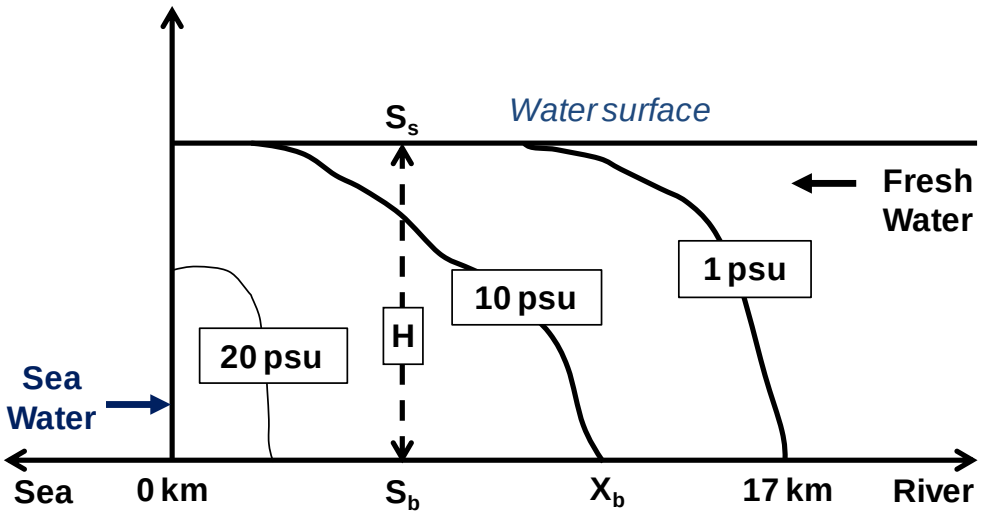

Fig. 2.13 Schematic diagram of salinity distribution in an estuary.

(d) SIL and ETML

In this study, salinity intrusion length (SIL) was defined as the distance from the estuary mouth (0 km) to the tip of the salt wedge, which has a salinity of 1 psu on the bottom. The location of the ETM was calculated with distance from the estuary mouth to the position where the maximum depth-averaged SSC occurred during each cruise.

2.4.2 Data Analysis of Phytoplankton

Furthermore, six indices were used to discuss the growth and migration of phytoplankton: light attenuation coefficient (K), ratio of photic depth to mixing depth (Zp/Zm), surface salinity reach (SSR), surface SSC maximum (SSM), Pheo-a length and Chl-a length.

(a) Light Attenuation (K)

The light attenuation in the water column was calculated using Lambert Beer equation assuming that light was attenuated exponentially with depth (Fig. 2.14).

$$I_z = I_0 \times e^{-kz} \qquad (2)$$

where I_z is the light intensity at depth z (m), I_0 is the light intensity at surface and k is the attenuation coefficient.

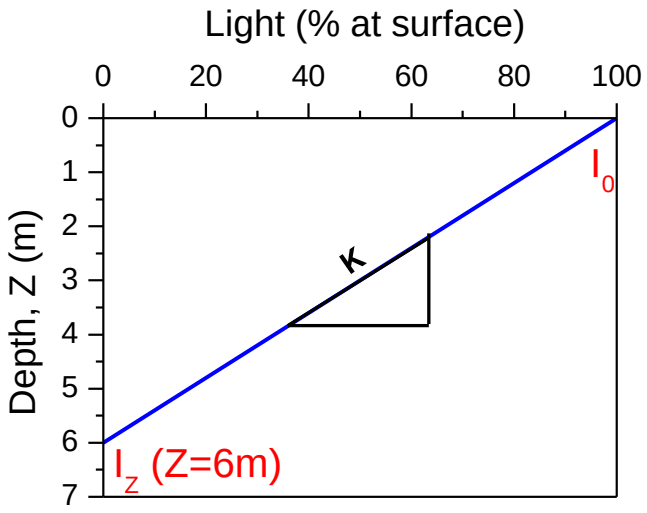

Fig. 2.14 Schematic diagram of light attenuation through the water column.

(b) Ratio of Photic Depth to Mixing Depth

The ratio of mixing depth (Zm) and photic depth (Zp) was proposed by Cloern (1987) and used by many researchers (Barbosa *et al*., 2010; Domingues *et al*., 2011) for understanding the degree of light limitation in estuaries. The maximum depth of the light zone suitable for phytoplankton photosynthesis is termed as the photic depth (Zp), and is calculated using Zp = 4.61/k assuming that irradiance at Zp is 1% of the irradiance at surface (Fig. 2.15). Mixing depth, Zm (m) represents the depth of the mixed layer. The mixing depth during September 11 and 25 represents the whole water column since the whole estuary was in well mixed condition. The mixing depth during other days was determined as the depth where salinity variations were 1 psu from the surface layer (Fig. 2.15).

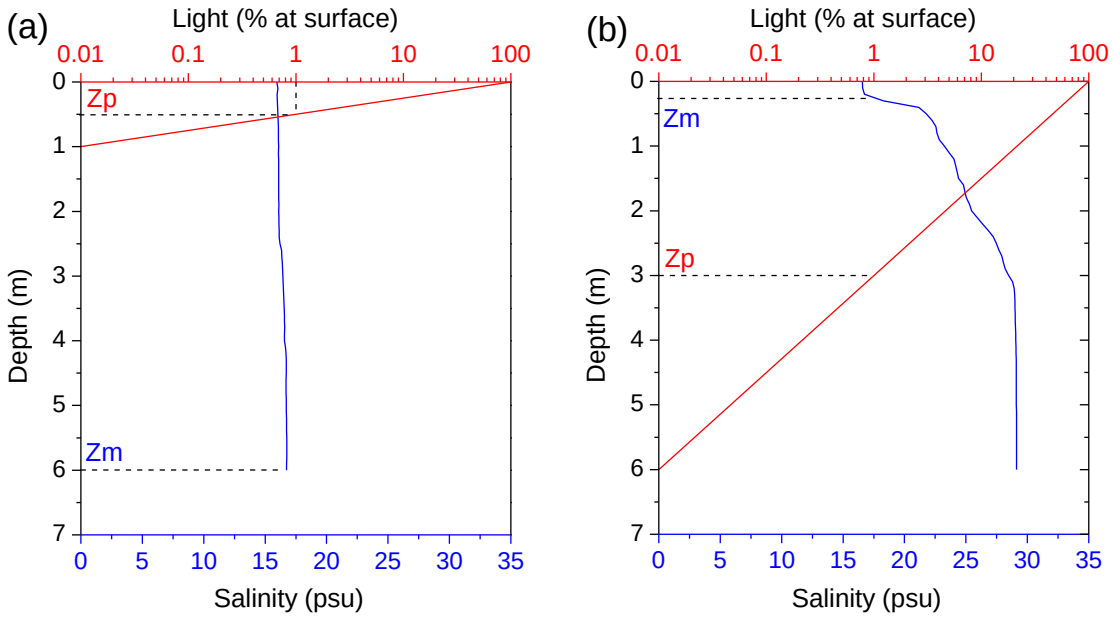

Fig. 2.15 Photic depth and mixing depth during (a) spring tide, and (b) neap tide.

(c) SSR and SSM

Surface salinity reach (SSR) was defined as the distance from 0 km to the position where salinity indicates 1 psu at the surface. Surface SSC maximum (SSM) was calculated as the distance from 0 km to the position where surface SSC reached maximum.

(d) Chl-a length and Pheo-a length

Chl-a length and Pheo-a length were defined as the location of their peak concentration and calculated as the distance from 0 km to the position where the highest concentration occurs at the surface.

(e) Chl-a Rate

Chl-a rate is defined as the rate of living phytoplankton (Chl-a) in total phytoplankton (Chl-a and Pheo-a).

Chapter 3

Salinity Intrusion, Mixing and Suspended Sediment Dynamics

This chapter focuses on the influence of estuarine mixing on the ETM movement.

Abstract

The effect of mixing on the movement of the estuarine turbidity maximum (ETM) was examined in the highly turbid Chikugo River estuary, Japan in consideration of four significant issues: semidiurnal and semi-lunar tidal variations, spatial distribution, and synchronism of data acquisition. Vertical profiles of salinity and turbidity were measured for two weeks at 1 km intervals from the river mouth (0 km) to 17 km upstream with a short duration for every cruise. Spring-neap transition and the spatial variation of mixing and SSC was found during the semilunar tidal cycle. The estuary gradually changed from a vertically well-mixed condition during spring tide to a stratified condition during the neap tide via a partially mixed condition during the intermediate half tides. The relationship between the flow ratio and the SSC showed that ETM growth was dominated by both tidal forcing and freshwater flow. SSC was high when the salinity was 0.5 psu in the upper estuary and 10 psu in the lower estuary. For the same mixing strength (MS), SSC in the lower estuary was greater than that in the upper estuary. Based on flow ratio, salinity and MS, the occurrence of the ETM and its development at the macrotidal estuary was a consequence of three processes: bed sediment erosion by seawater in the lower estuary, sediment transport in the estuarine channel by the tidal current and freshwater flow, and sediment accumulation at the salinity front in the upper estuary.

Content of this chapter was constructed from following papers:

Azhikodan, G. and Yokoyama, K. 2014. Temporal and Spatial Variation of Mixing and Movement of Suspended Sediment in the Macrotidal Chikugo River Estuary, *Journal of Coastal Research*, Accepted.

Azhikodan, G., Yokoyama, K. and Morimura, Y. 2014. Effect of Mixing on Turbidity Maximum Movement during Semilunar Tidal Cycle in the Chikugo River Estuary, *Journal of JSCE, Ser. B1 (Hydraulic Engineering)*, Vol. 70, No. 4, pp. I_37-I_42, 2014.

Azhikodan, G. and Yokoyama, K. 2013. Turbidity Maximum Movement during Semilunar Tidal Cycle in the Chikugo River Estuary, *Proceedings of Hydro International, India*, ISBN: 978-93-80689-18-0, pp.521-529.

Azhikodan, G. and Yokoyama, K. 2012. Influence of Tidal Mixing on Suspended Sediment Transport and Phytoplankton Dynamics in the Chikugo River Estuary, Japan, *Proceedings of the 10th Intl. Conference on Hydroscience & Engg., U.S.A*, No. 40137245, pp. 1-6.

3.1 Results

3.1.1 River Discharge and Rainfall

The time series of the hourly river discharge for the year 2010 is shown in Fig. 3.1a. Additionally, the time series of hourly freshwater discharge, the hourly rainfall, and the water level (at the station 14.6 km upstream) during field measurements is shown in Fig. 3.1b and Fig. 3.1c. The freshwater discharge in the dry season was 40 m^3/s, and the mean annual peak discharge was 2,800 m^3/s. The period when the freshwater discharge exceeded 500 m^3/s was 11 days, and the period when the freshwater discharge exceeded 200 m^3/s was 39 days on average (Fig. 3.1a).

Rainfall events of up to 20 mm occurred on September 13, 22, and 23 (Fig. 3.1b). A sudden peak discharge on September 13 and 23 was observed because of those rainfall events. The freshwater discharge patterns revealed significant temporal variation with the influence of rainfall. Freshwater discharges in the Chikugo River estuary during the period from September 11 to 25 ranged from 50 m^3/s (during the normal period) to more than 300 m^3/s during rainy days.

The shaded area in the water level indicates the actual measurement time during the period of the field survey (Fig. 3.1c). On September 11 and 25, a spring tide occurred with a tidal range of 5.1 m and 4.7 m, respectively. A neap tide occurred on September 17 with a tidal range of 2 m.

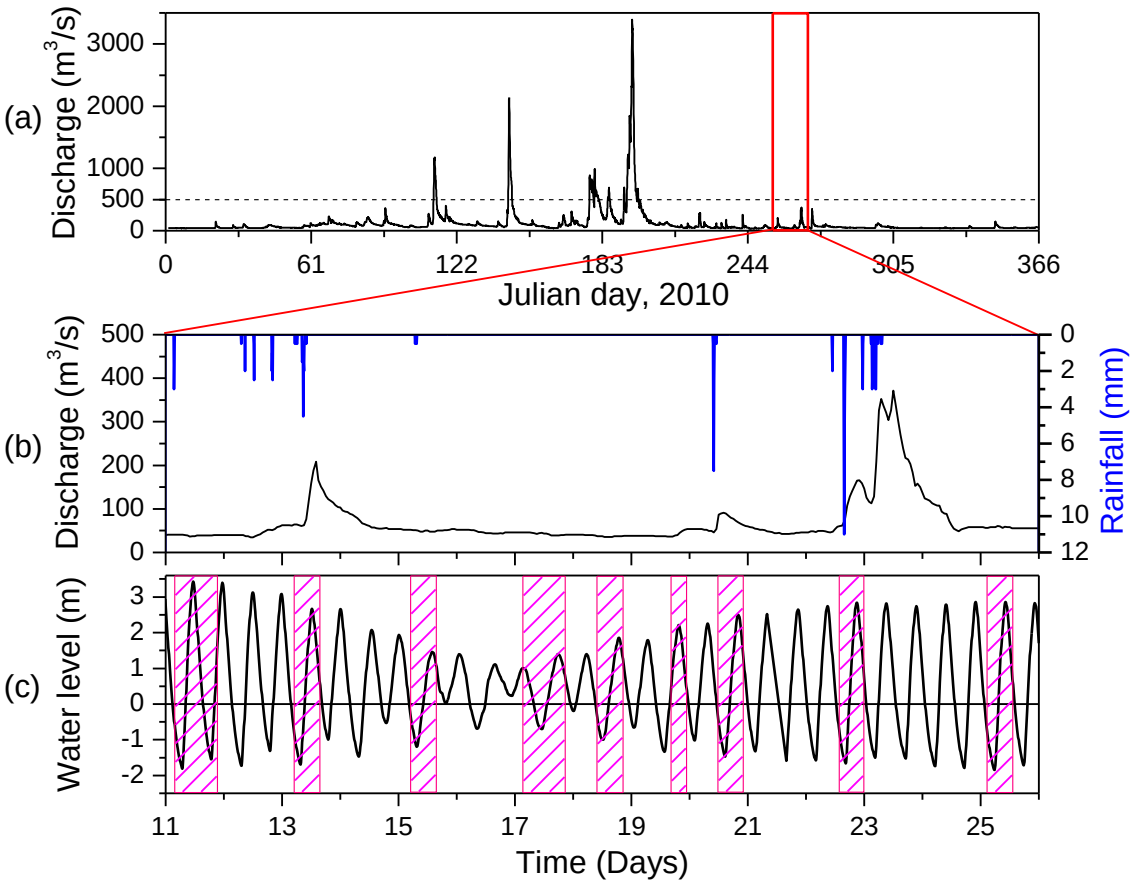

Fig. 3.1 Time series of (a) river discharge for the year 2010, (b) river discharge and rainfall for September 11 to 25, 2010, and (c) water level for September 11 to 25, 2010.

3.1.2 Semidiurnal Estuarine Variability

The temporal variation of the tide, vertical and longitudinal distributions of the salinity, SSC and in-situ Chl-a by fluorescent sensor during each tidal cruise of the fortnightly tidal cycles (September 11 to 25) were shown in Fig. 3.2 to Fig. 3.34. The blue shade on the tide shows the time of measurement for respective cruise.

(a) Spring Tide

Salinity distribution during spring tide (September 11) with a tidal amplitude of 5.2 m had a vertically uniform distribution throughout the semidiurnal tidal cycle (Fig. 3.2 to Fig. 3.8). The water was extremely turbid with an SSC of 1000 – 2000 mg/l especially during flood water. During low water (Fig. 3.2 and Fig. 3.3) there was no salinity intrusion and ETM zone was found near 7 to 9 km. During flood water (Fig. 3.4) saline water intruded up to 10 km. ETM zone moves 5 km landward and reached

near 12 to 14 km stations. During high water (Fig. 3.5), salt water intruded a maximum distance of approximately 14 km. ETM zone moved further 3 km upstream from the ETM at flood water and reached 15-17 km. The SSC in the ETM zone decreased compared with the SSC in the flood water. This is because particles settled down at 15 to 17 km stations during the slack tide. During ebb water (Fig. 3.6), saline water retreated back 4 km seaward and reached 10 km. ETM zone was found 4 km downstream from the ETM at high water , near 11 to 14 km stations and SSC increased as the particles start to resuspend by strong current. The saline water went back to sea during the next low water (Fig. 3.8) with ETM zone at 7 to 9 km which is similar to the previous low water (Fig. 3.2 and Fig. 3.3).

Distribution of Chl-a was found very similar to the SSC distribution throughout the spring tidal cycle. Since the water was extremely turbid, phytoplankton could not grow up due to light limitations. However, chl-a values was also showing very high. In-situ chl-a sensor may be affected by the suspended sediment.

(b) Half Tide

The salinity intrusion and movement of ETM during the half tides of September 13 (Fig. 3.9 to Fig. 3.11) and 15 (Fig. 3.12 to Fig. 3.14) were found similar to the spring tide. During 13, the tidal amplitude decreased to 4.1 m and the vertical salinity distributions was little bit inclined compared with spring tide. The SSC in the ETM zone was nearly 1000 mg/l. Then during the following half tide (September 15), the tidal amplitude decreased to 2.4 m and the isohalines were inclined more than that of September 13. The SSC in the maximum zone decreased to 500 mg/l. Distributions of Chl-a were found very similar to the SSC distribution during the half tides.

(c) Neap Tide

The tidal amplitude decreased to 1.7 m during the neap tide (September 17), and there was little effect on mixing, which resulted in strong salinity stratification throughout the semidiurnal tidal cycle (Fig. 3.15 to Fig. 3.21). It was formed two layer of salinity stratification with bottom salt water and surface fresh water. The distance traveled by the saltwater intrusion exceeded 17 km, which was longer than the distance recorded during the spring tide and half tide. Estuarine water was found very clear throughout the neap tide with an SSC of 20–50 mg/l, and an ETM zone was not found.

The Chl-a distribution during the neap tide was clearly seen because of the low SSC in the water column. Chl-a distribution was very low during the morning (Fig. 3.15d). Then gradually Chl-a concentration increases towards evening. During neap tide and next half tide, sky was clear with sunny weather and the phytoplankton grew with these good conditions.

(d) Neap Tide to Spring Tide

Two layer of salinity stratification was present till low water phase of September 18 (Fig. 3.22b) and the inclination of isohalines started to change gradually during flood (Fig. 3.23b) and high water (Fig. 3.24b). Seawater intrusion was also exceeded 17 km and the water was still clear with low SSC (Fig. 3.22 to Fig. 3.24) as it was during neap tide. Distribution of Chl-a were also similar to neap tide (Fig. 3.15 to Fig. 3.21).

The salinity, SSC and Chl-a distribution during September 20 (Fig. 3.26 to Fig. 3.28) were found similar to their distributions during September 15 (Fig. 3.12 to Fig. 3.14) despite little greater salinity intrusion during September 20. The salinity, SSC and Chl-a distribution during September 22 (Fig. 3.29 to Fig. 3.31) were found similar to their distributions during September 13 (Fig. 3.9 to Fig. 3.11). Despite lesser intrusion during September 25 as it was during September 11, the salinity, SSC and Chl-a distribution during September 25 (Fig. 3.32 to Fig. 3.34) were found similar to their distributions during September 11 (Fig. 3.2 to Fig. 3.8).

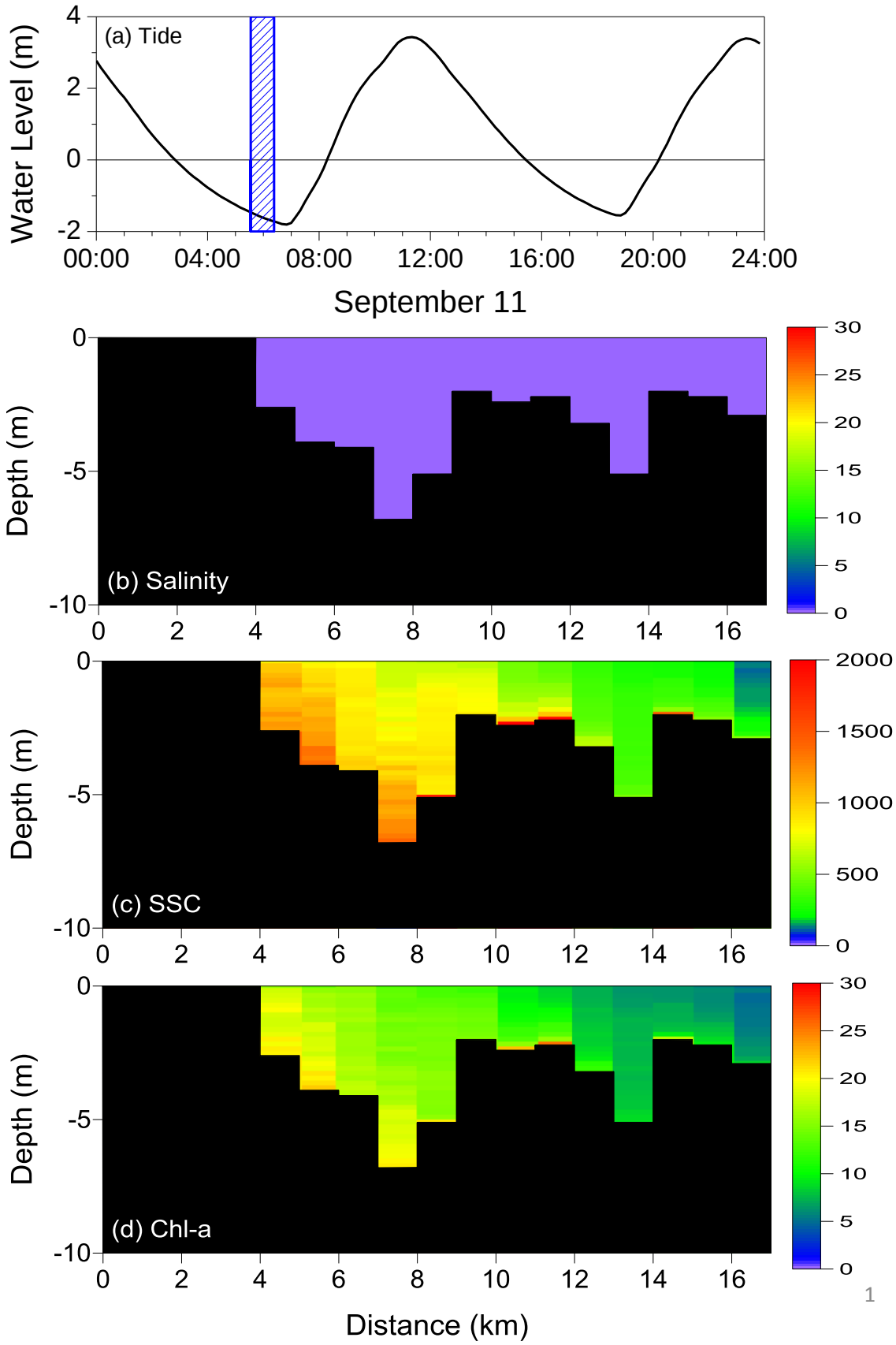

Fig. 3.2 (a) temporal variation of tide and longitudinal and vertical distributions of (b) salinity in psu, (c) SSC in mg/l and (d) Chl-a in µg/l during September 11 (Round 1).

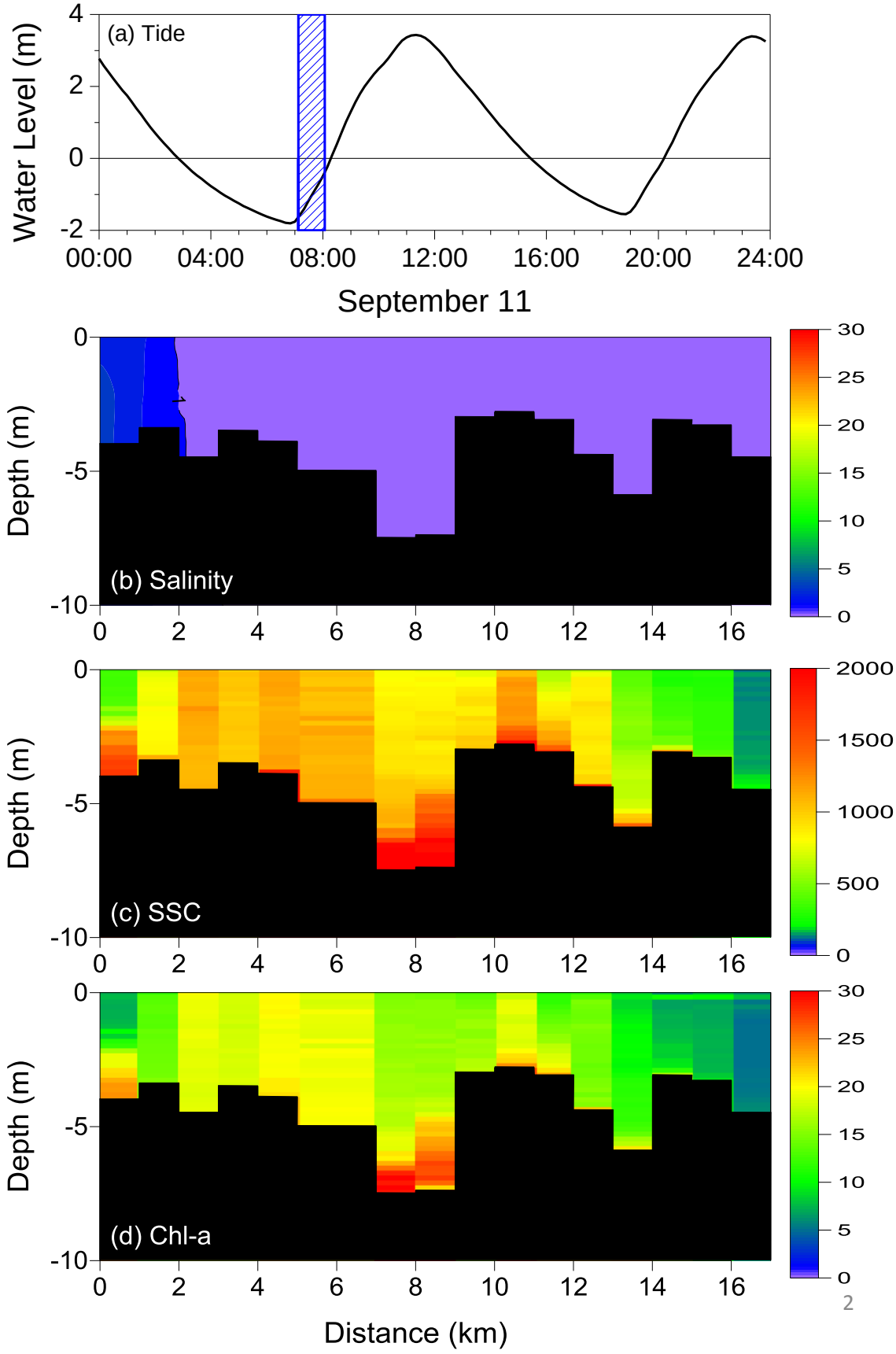

Fig. 3.3 (a) temporal variation of tide and longitudinal and vertical distributions of (b) salinity in psu, (c) SSC in mg/l and (d) Chl-a in µg/l during September 11 (Round 2).

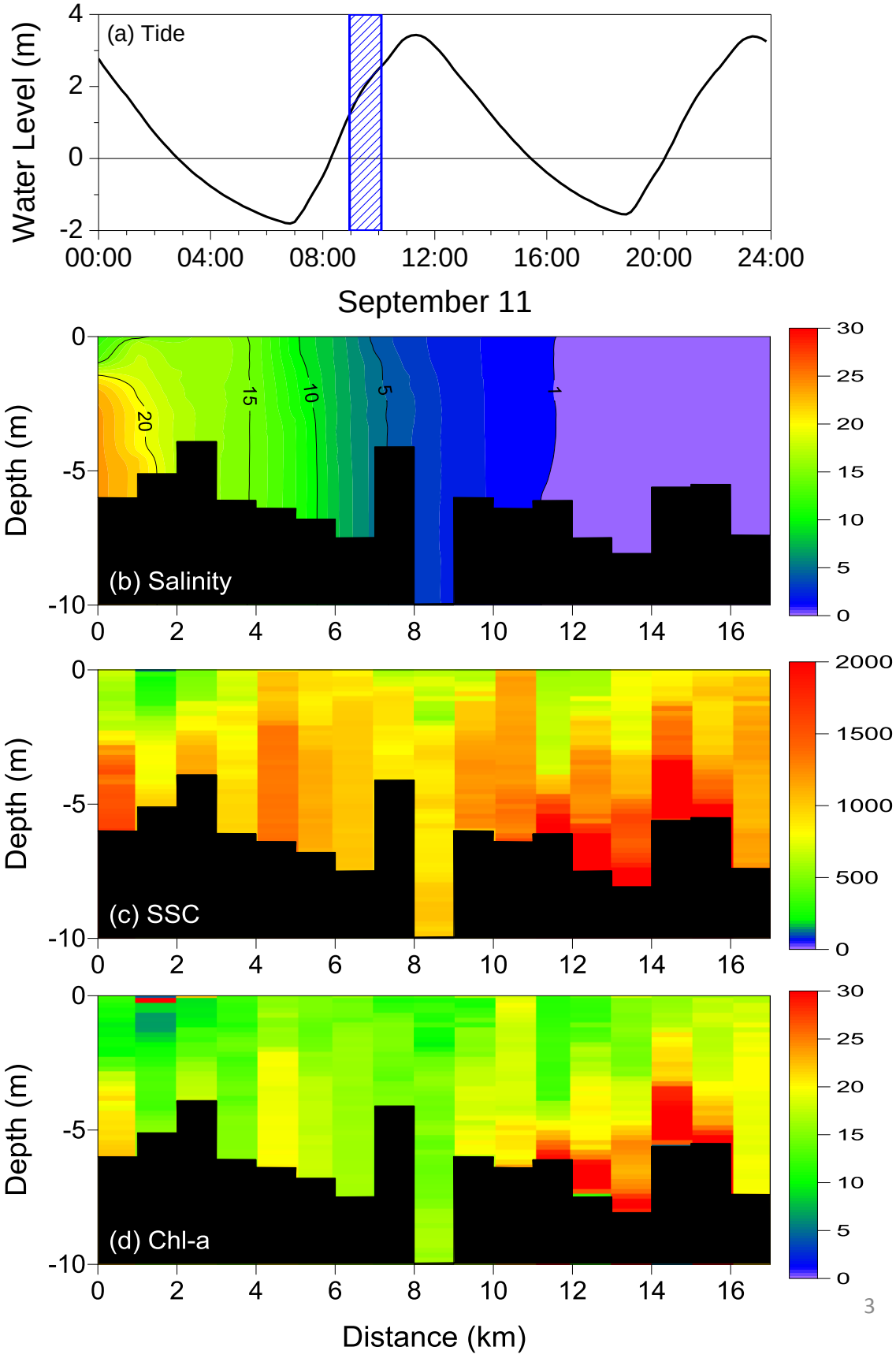

Fig. 3.4 (a) temporal variation of tide and longitudinal and vertical distributions of (b) salinity in psu, (c) SSC in mg/l and (d) Chl-a in µg/l during September 11 (Round 3).

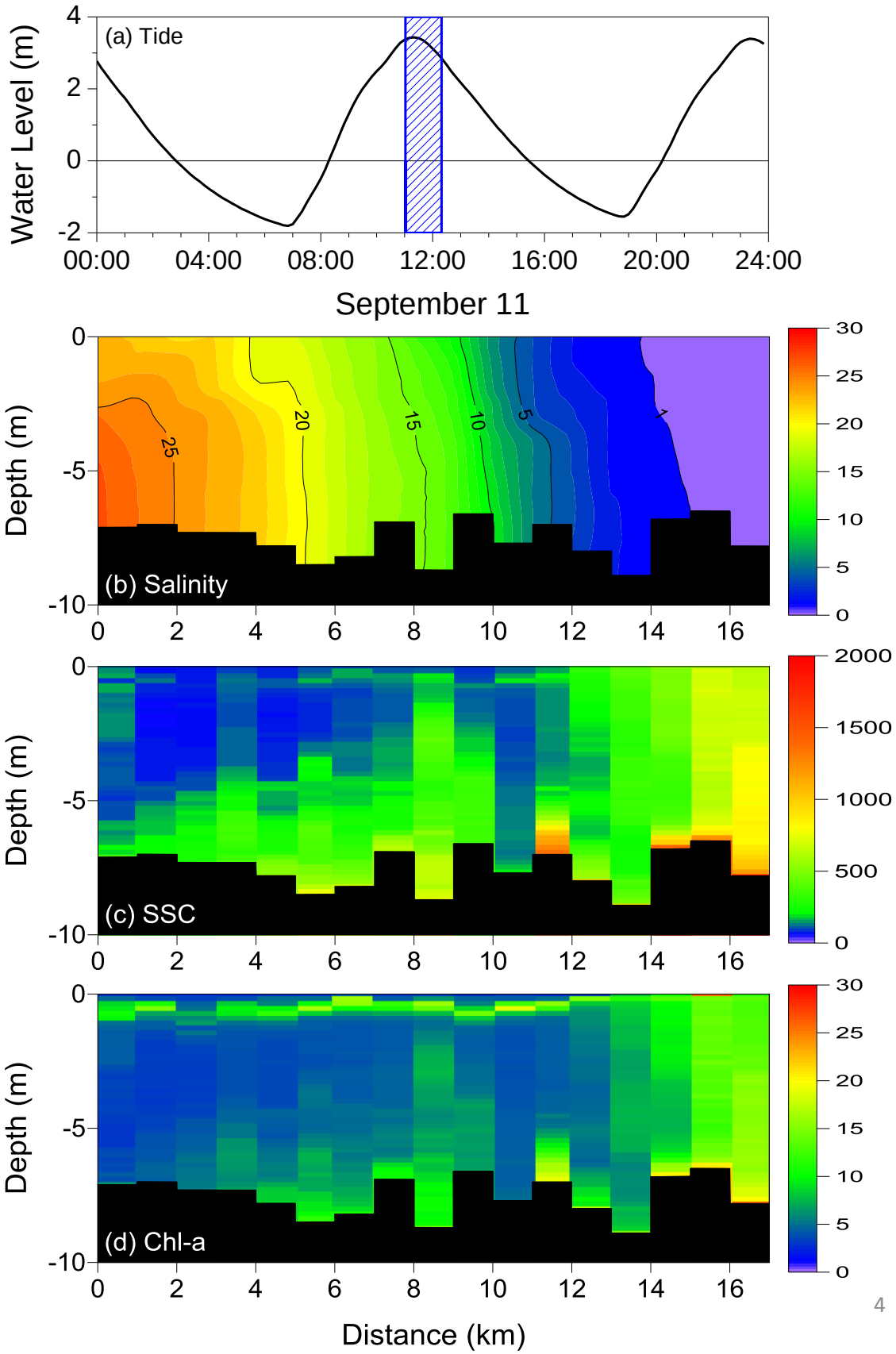

Fig. 3.5 (a) temporal variation of tide and longitudinal and vertical distributions of (b) salinity in psu, (c) SSC in mg/l and (d) Chl-a in µg/l during September 11 (Round 4).

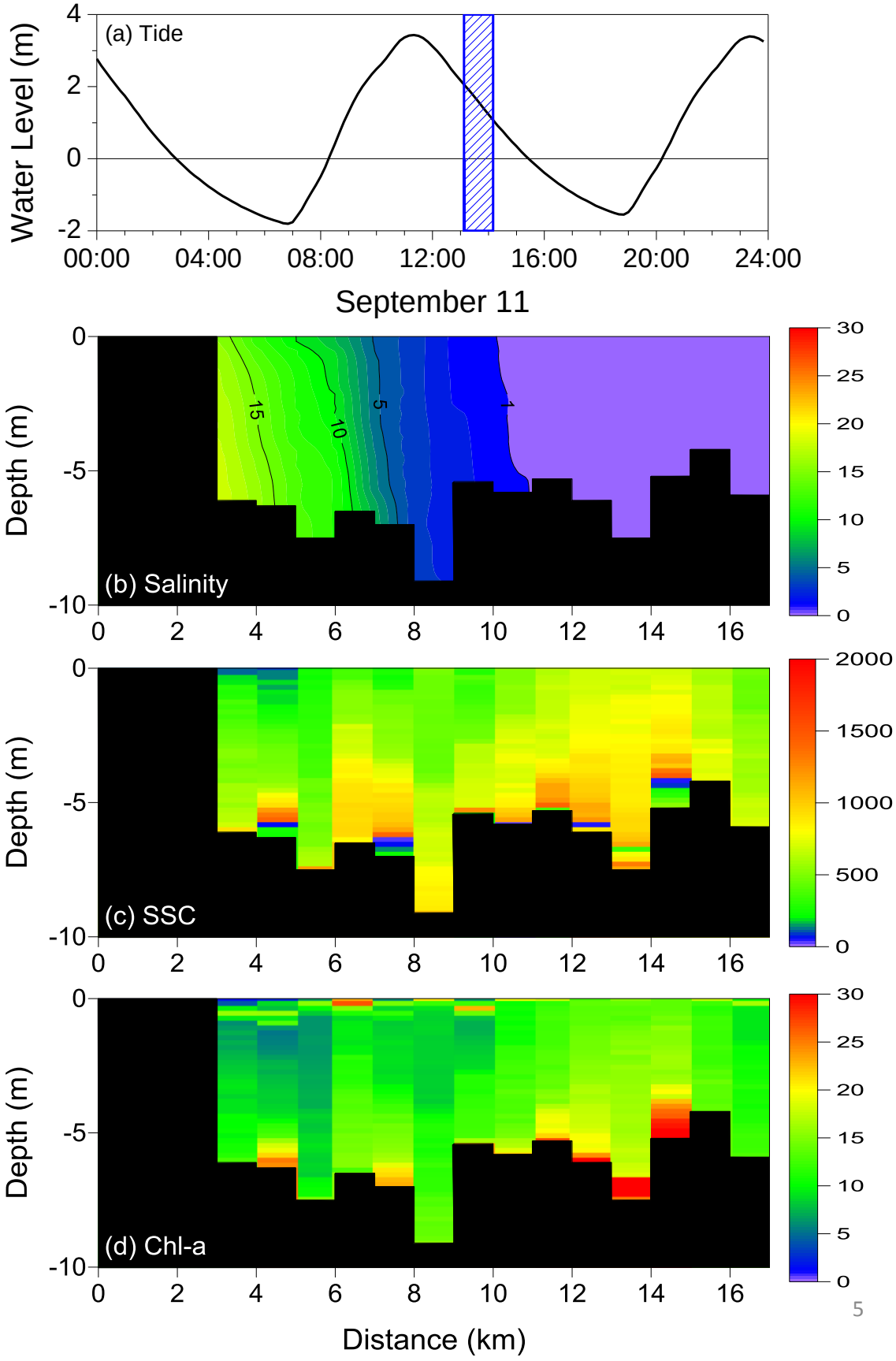

Fig. 3.6 (a) temporal variation of tide and longitudinal and vertical distributions of (b) salinity in psu, (c) SSC in mg/l and (d) Chl-a in µg/l during September 11 (Round 5).

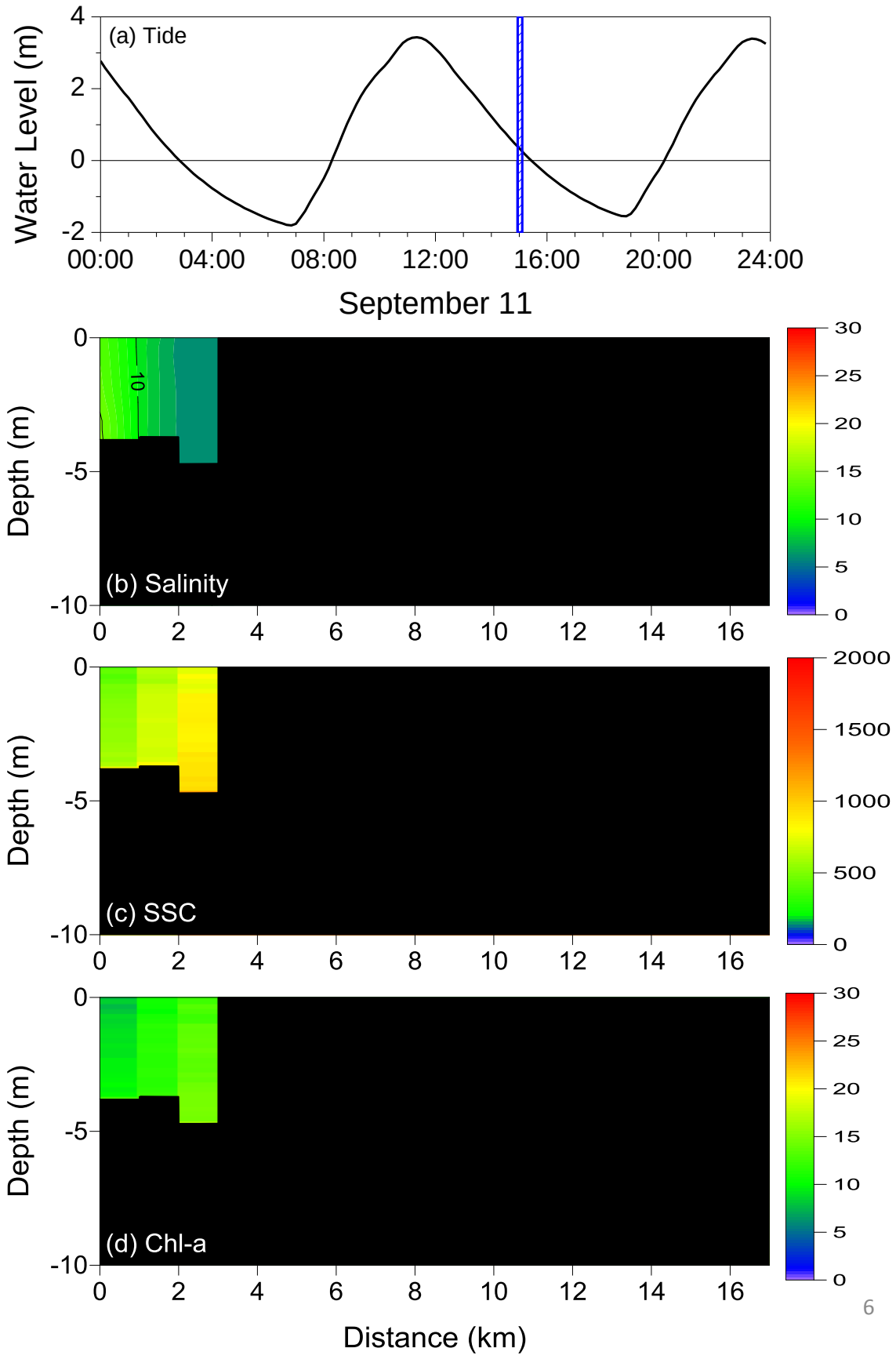

Fig. 3.7 (a) temporal variation of tide and longitudinal and vertical distributions of (b) salinity in psu, (c) SSC in mg/l and (d) Chl-a in µg/l during September 11 (Round 6).

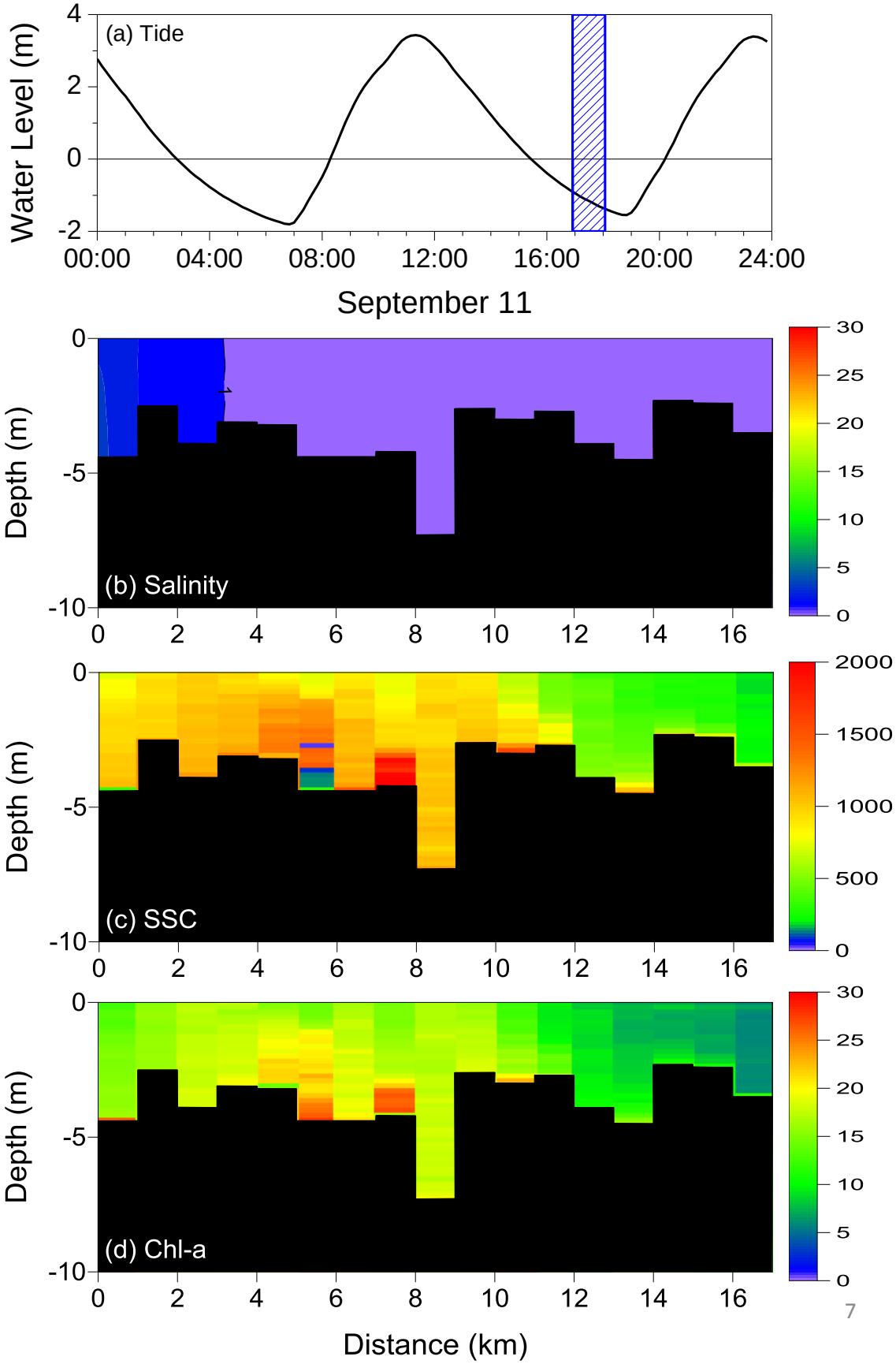

Fig. 3.8 (a) temporal variation of tide and longitudinal and vertical distributions of (b) salinity in psu, (c) SSC in mg/l and (d) Chl-a in µg/l during September 11 (Round 7).

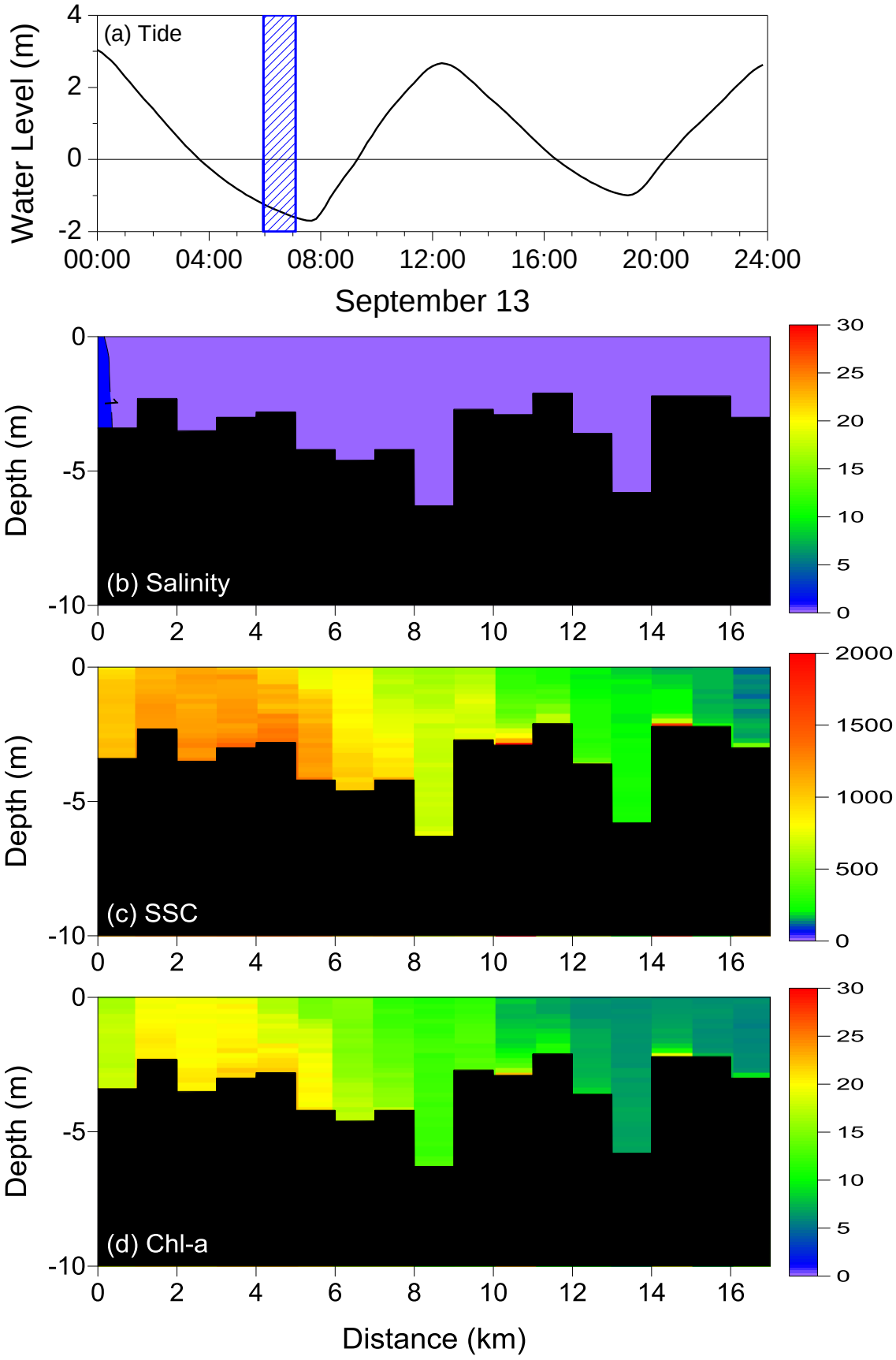

Fig. 3.9 (a) temporal variation of tide and longitudinal and vertical distributions of (b) salinity in psu, (c) SSC in mg/l and (d) Chl-a in µg/l during September 13 (Round 1).

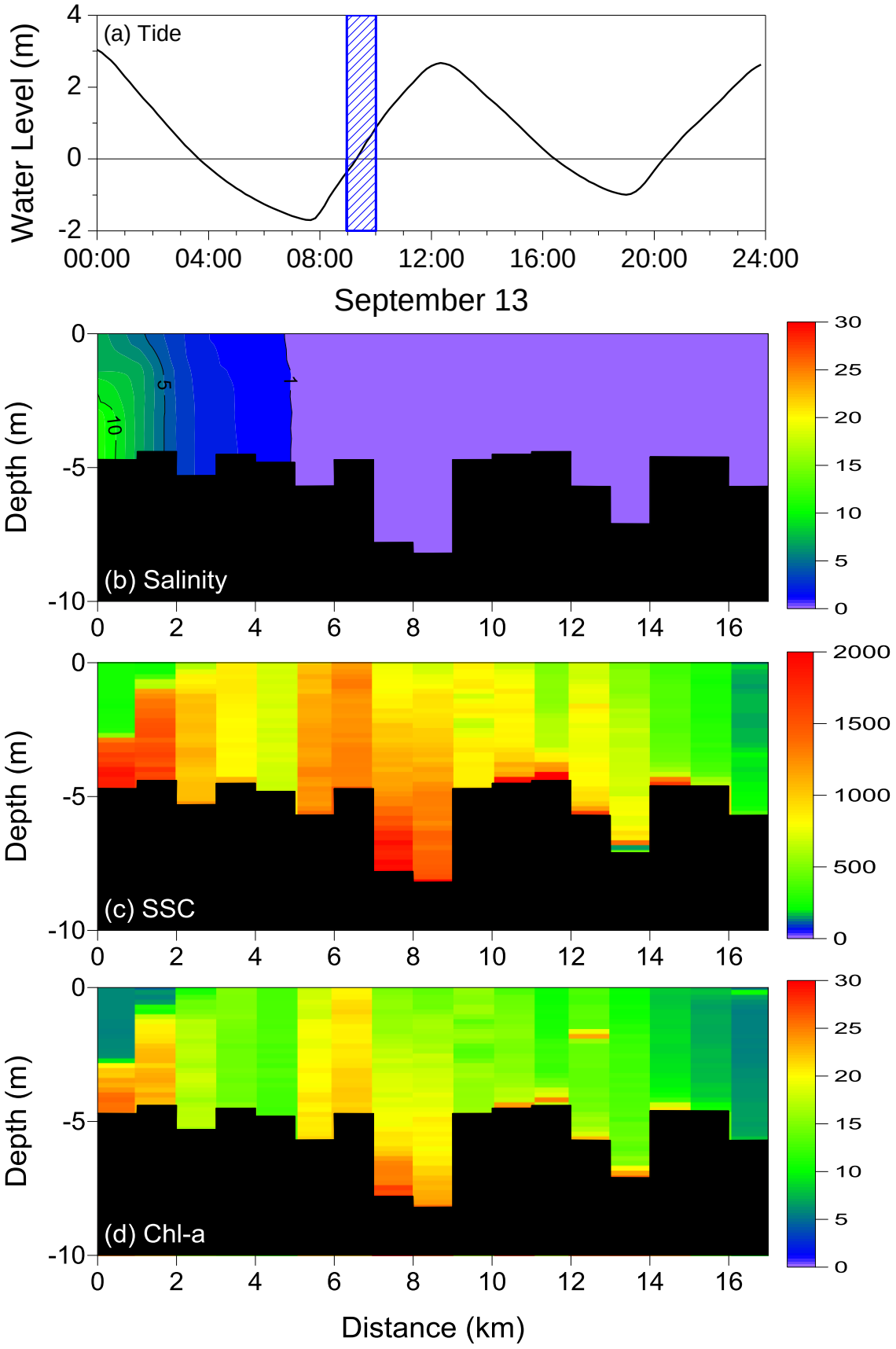

Fig. 3.10 (a) temporal variation of tide and longitudinal and vertical distributions of (b) salinity in psu, (c) SSC in mg/l and (d) Chl-a in µg/l during September 13 (Round 2).

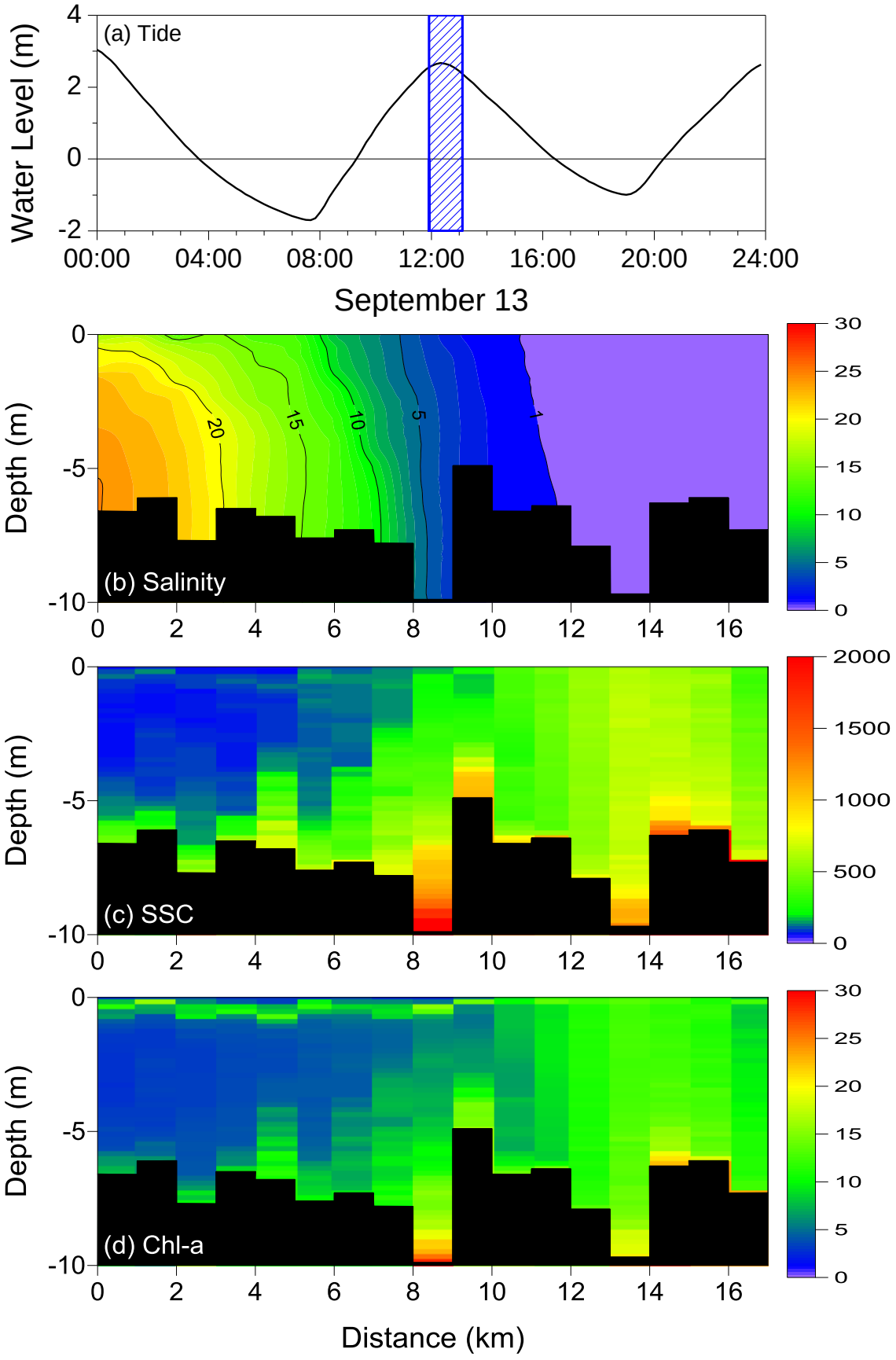

Fig. 3.11 (a) temporal variation of tide and longitudinal and vertical distributions of (b) salinity in psu, (c) SSC in mg/l and (d) Chl-a in µg/l during September 13 (Round 3).

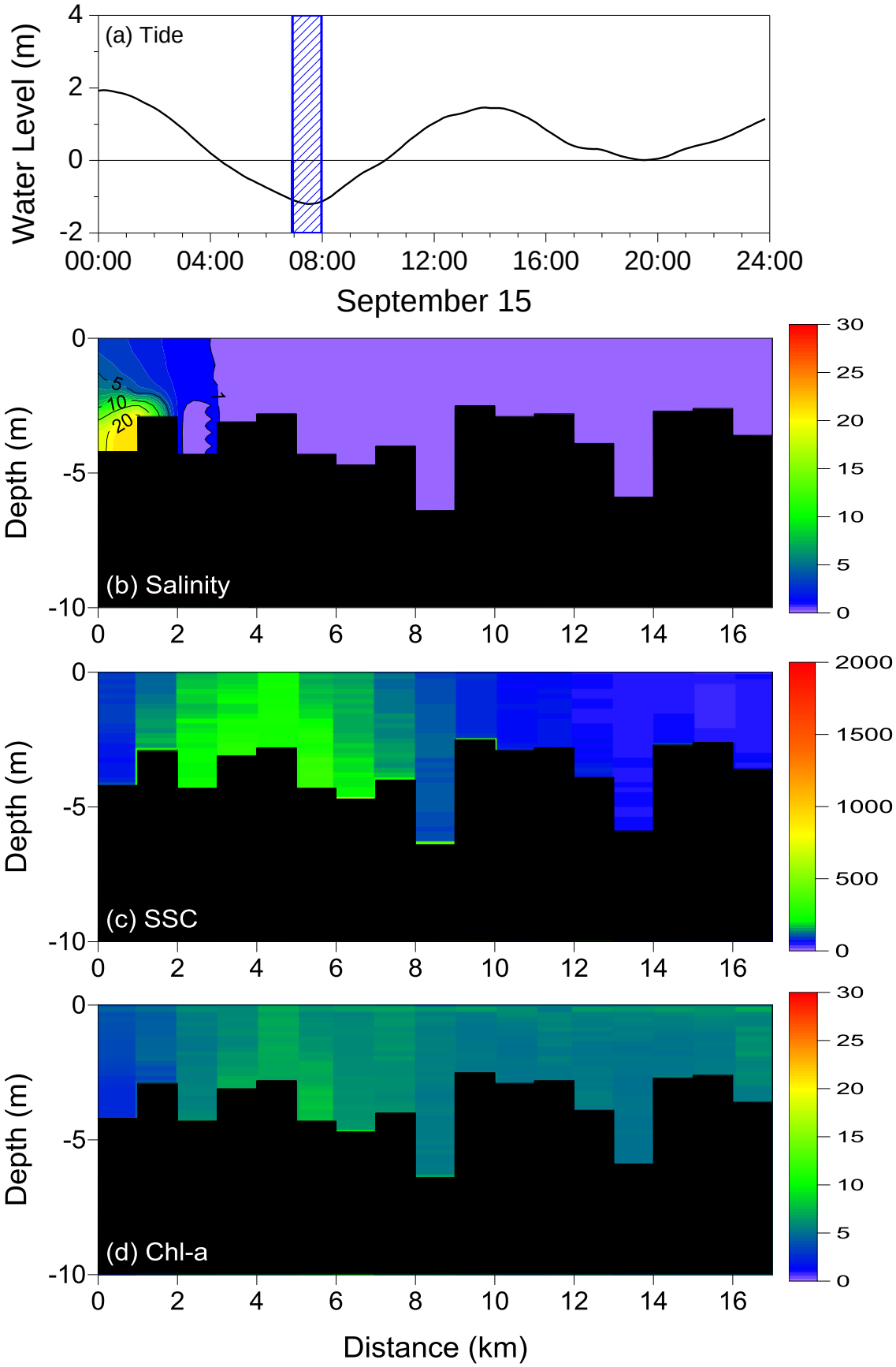

Fig. 3.12 (a) temporal variation of tide and longitudinal and vertical distributions of (b) salinity in psu, (c) SSC in mg/l and (d) Chl-a in µg/l during September 15 (Round 1).

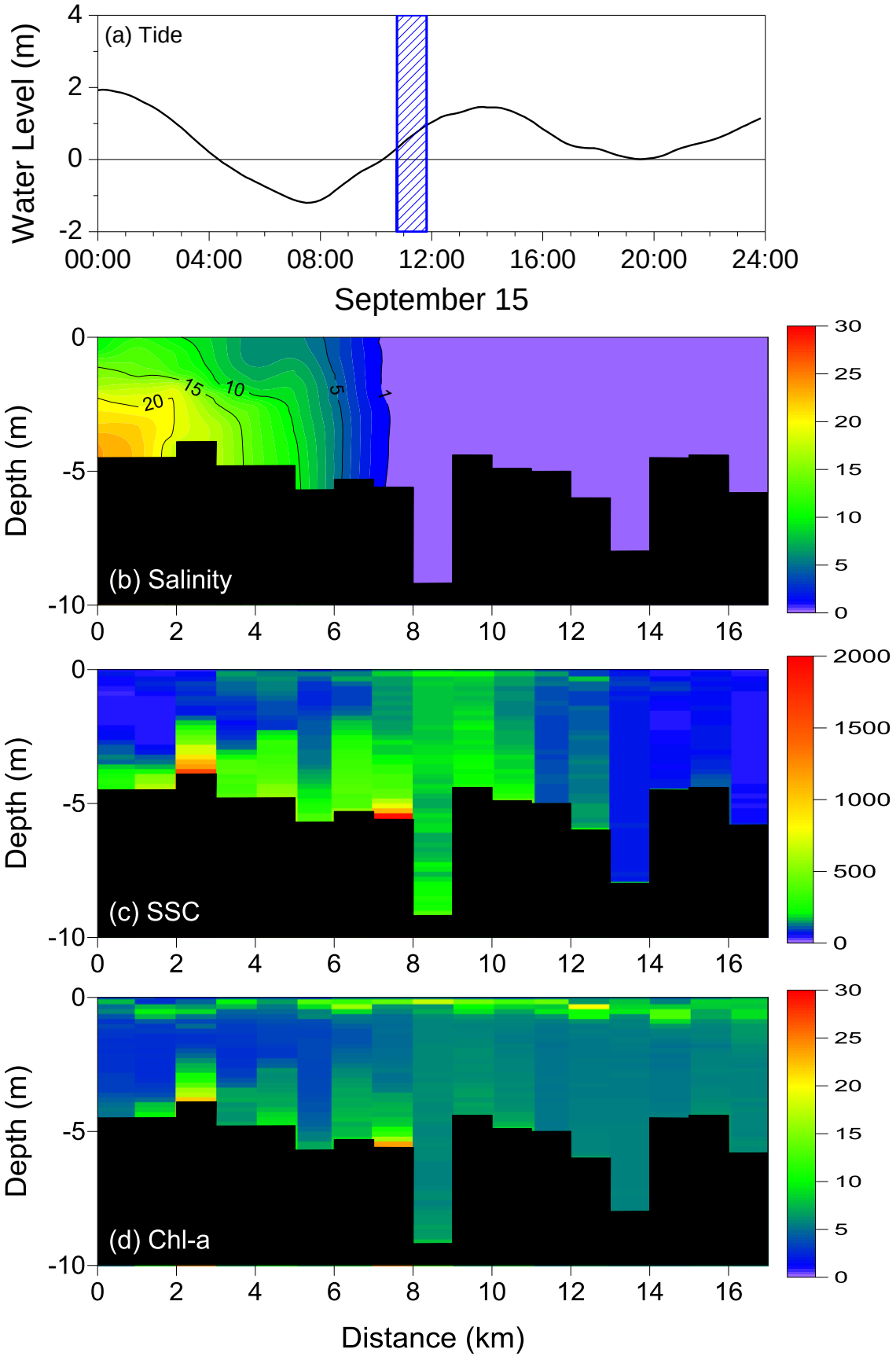

Fig. 3.13 (a) temporal variation of tide and longitudinal and vertical distributions of (b) salinity in psu, (c) SSC in mg/l and (d) Chl-a in µg/l during September 15 (Round 2).

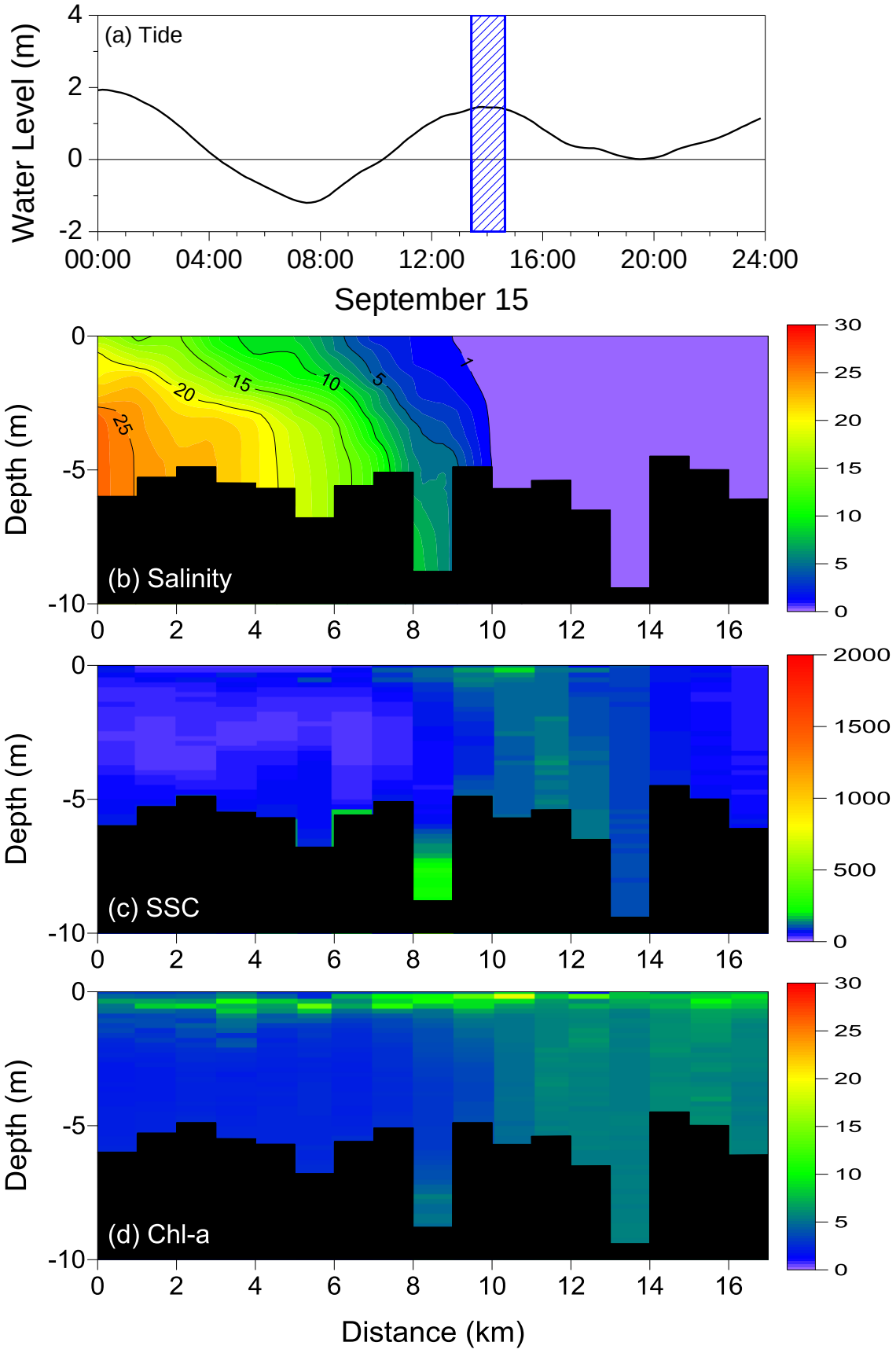

Fig. 3.14 (a) temporal variation of tide and longitudinal and vertical distributions of (b) salinity in psu, (c) SSC in mg/l and (d) Chl-a in µg/l during September 15 (Round 3).

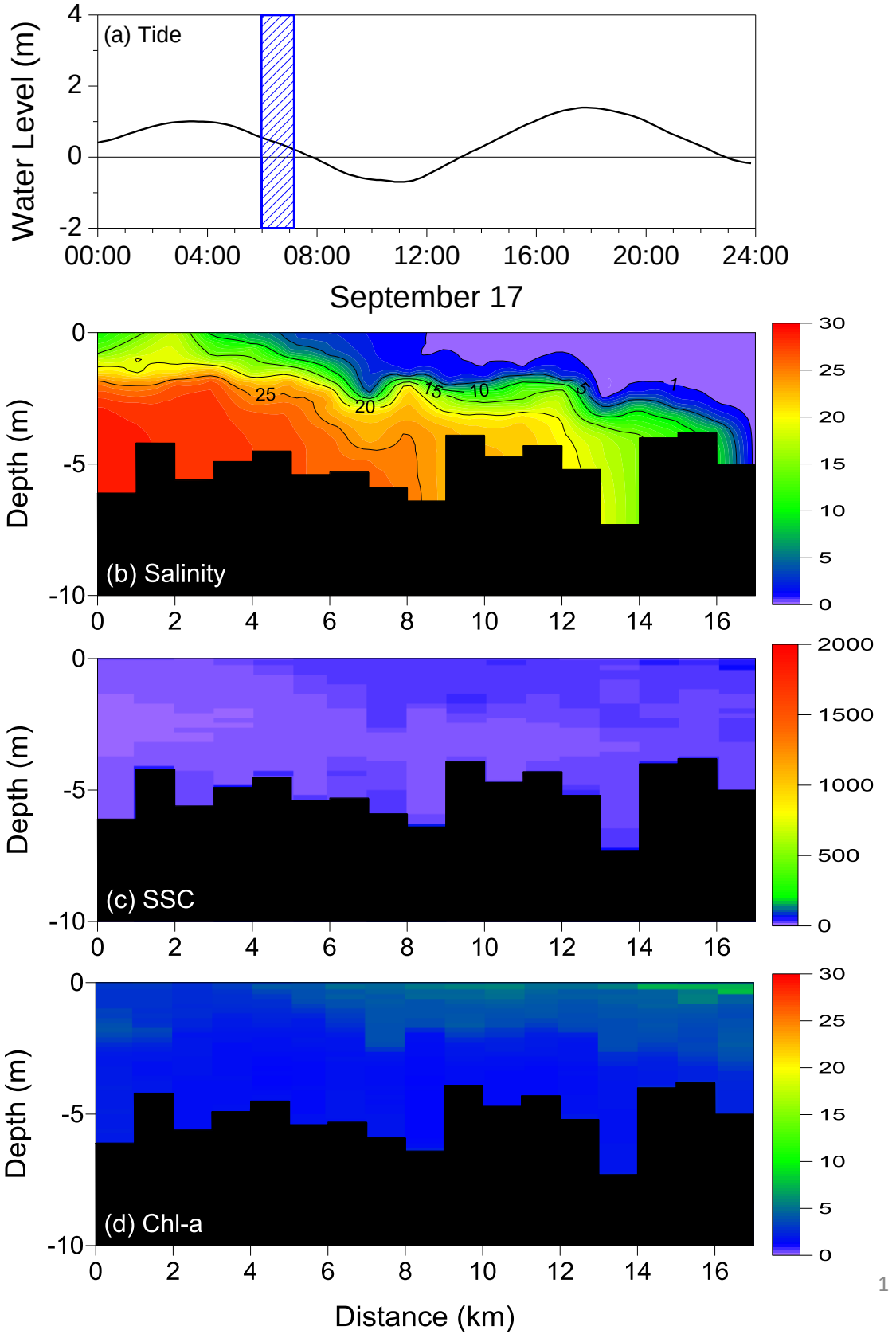

Fig. 3.15 (a) temporal variation of tide and longitudinal and vertical distributions of (b) salinity in psu, (c) SSC in mg/l and (d) Chl-a in µg/l during September 17 (Round 1).

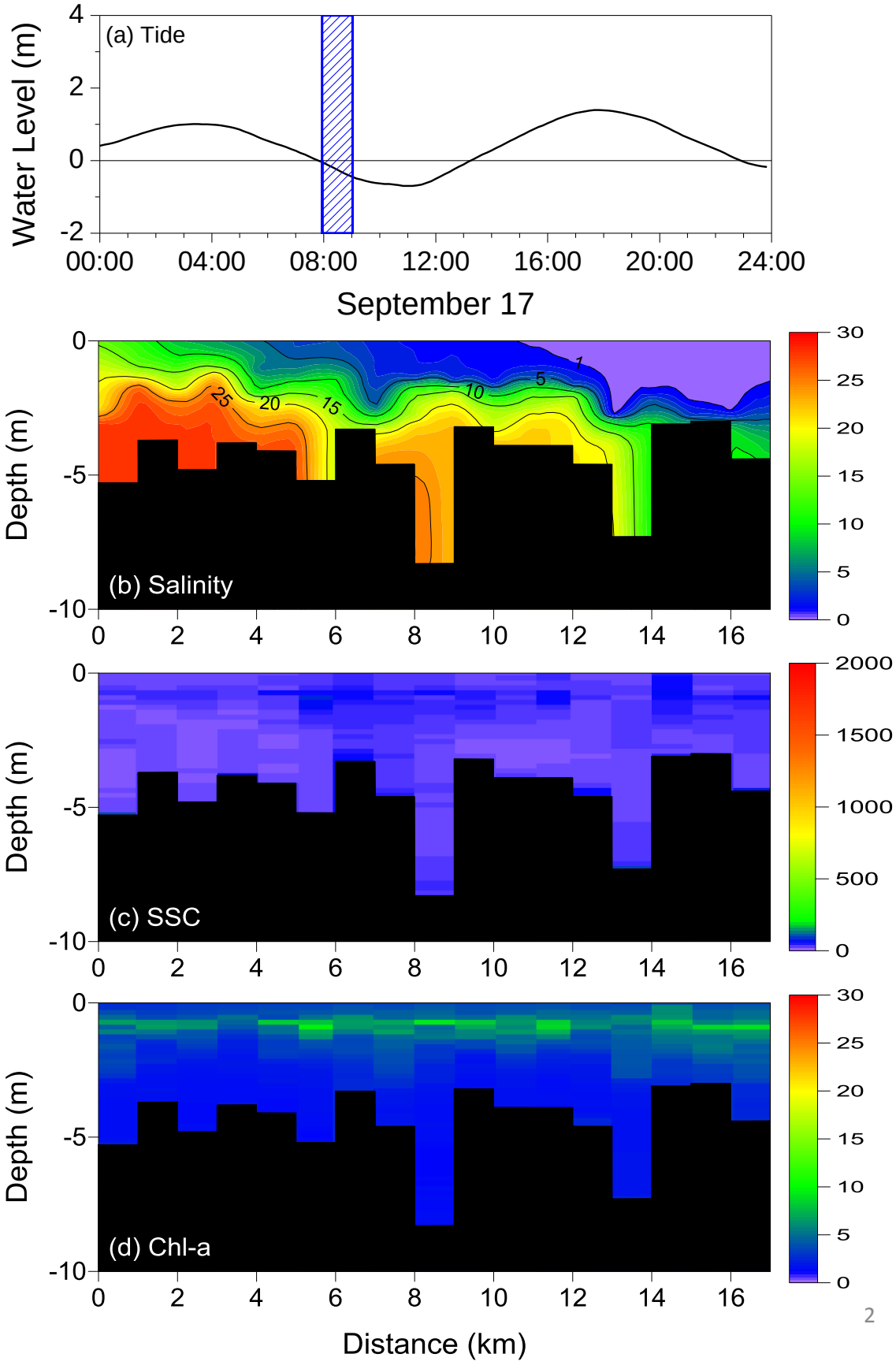

Fig. 3.16 (a) temporal variation of tide and longitudinal and vertical distributions of (b) salinity in psu, (c) SSC in mg/l and (d) Chl-a in µg/l during September 17 (Round 2).

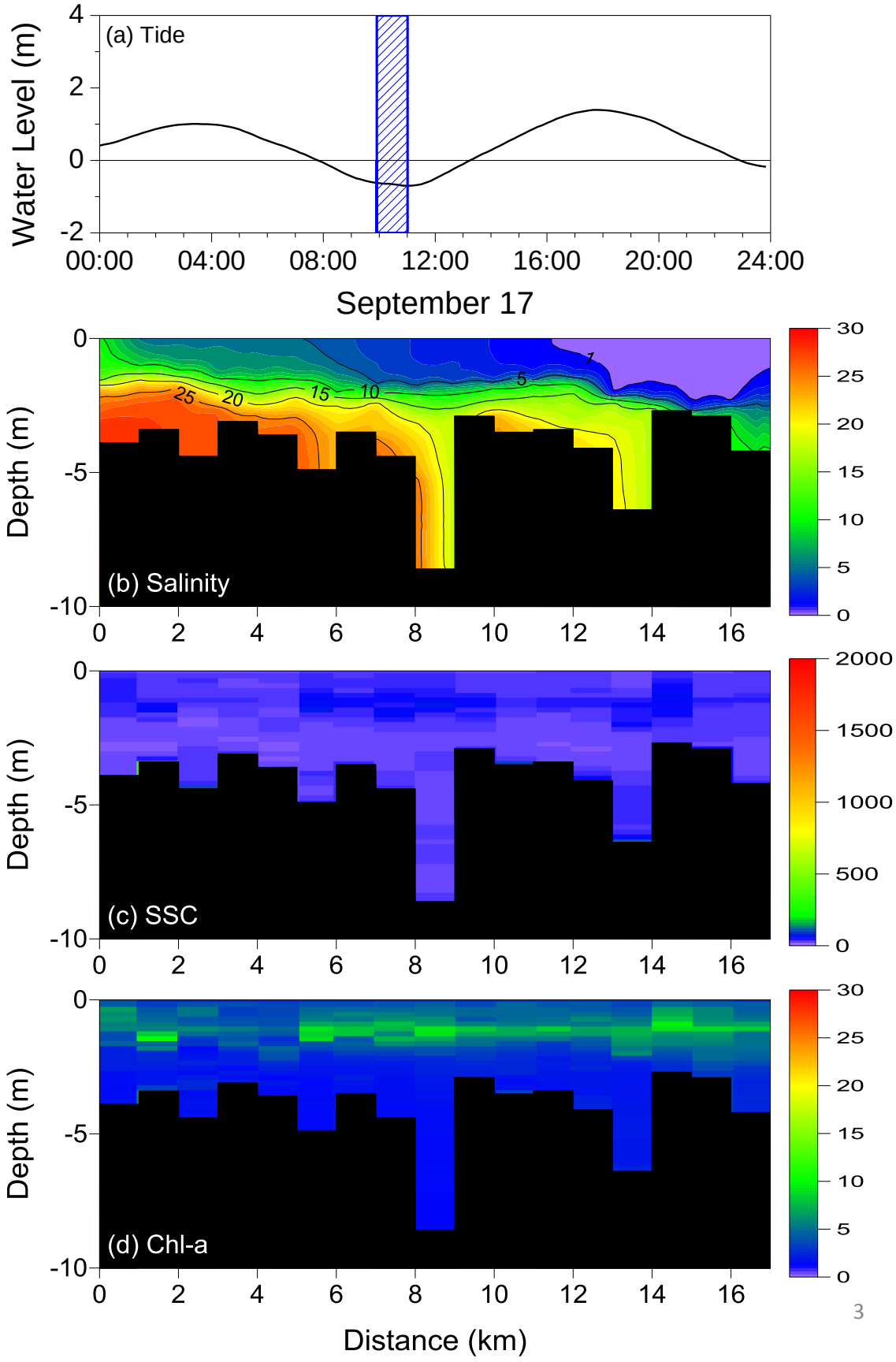

Fig. 3.17 (a) temporal variation of tide and longitudinal and vertical distributions of (b) salinity in psu, (c) SSC in mg/l and (d) Chl-a in µg/l during September 17 (Round 3).

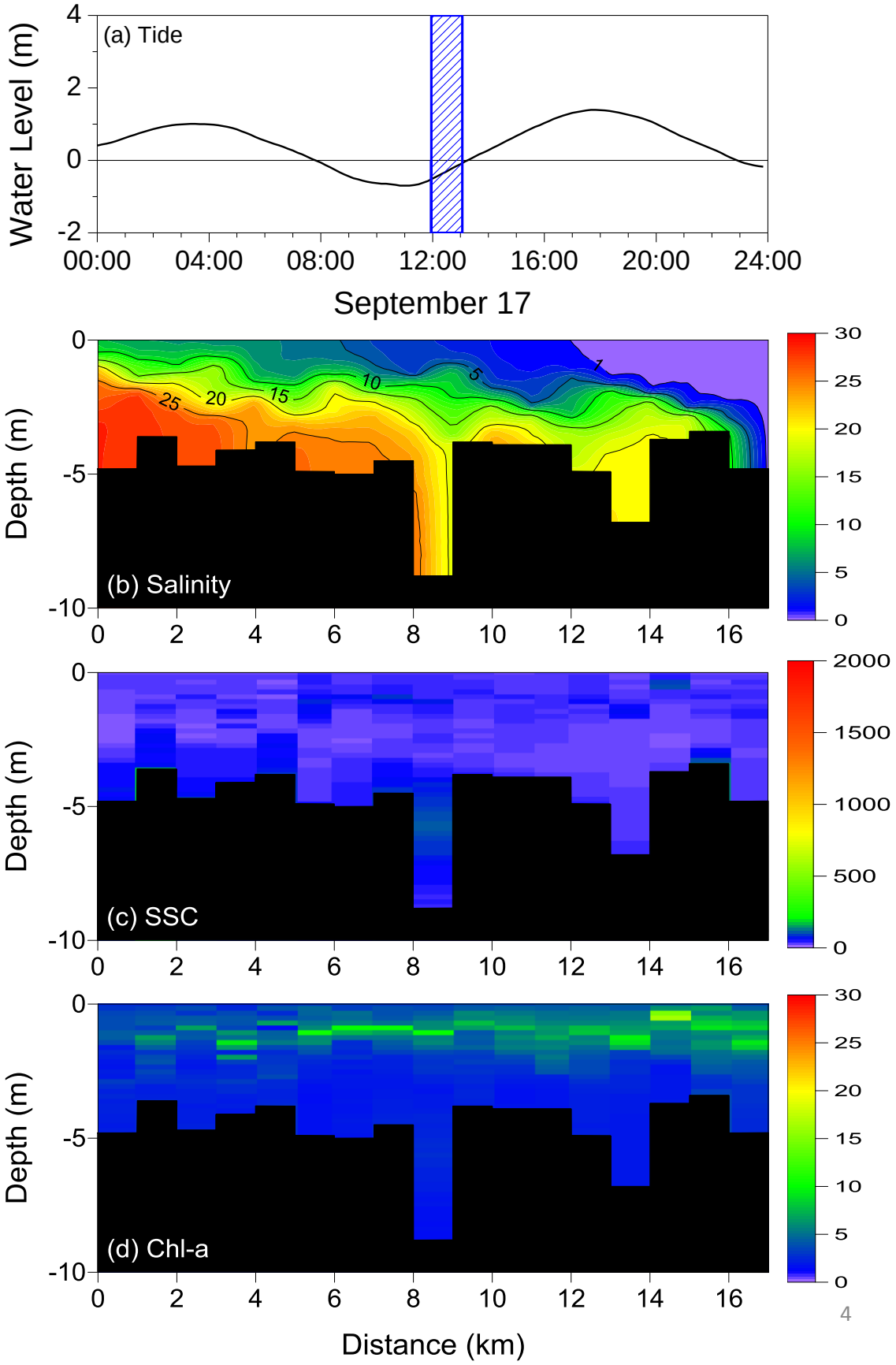

Fig. 3.18 (a) temporal variation of tide and longitudinal and vertical distributions of (b) salinity in psu, (c) SSC in mg/l and (d) Chl-a in µg/l during September 17 (Round 4).

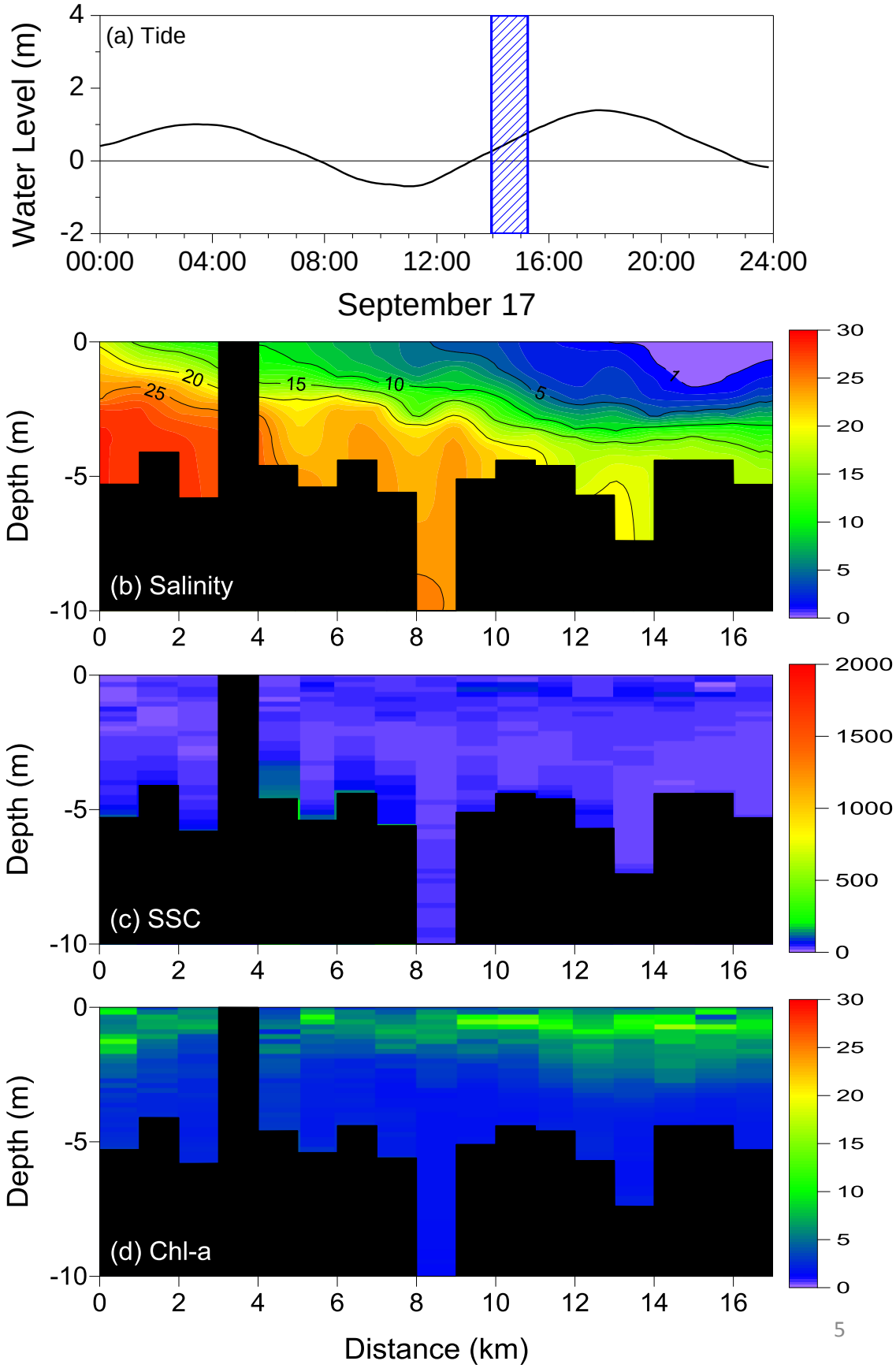

Fig. 3.19 (a) temporal variation of tide and longitudinal and vertical distributions of (b) salinity in psu, (c) SSC in mg/l and (d) Chl-a in µg/l during September 17 (Round 5).

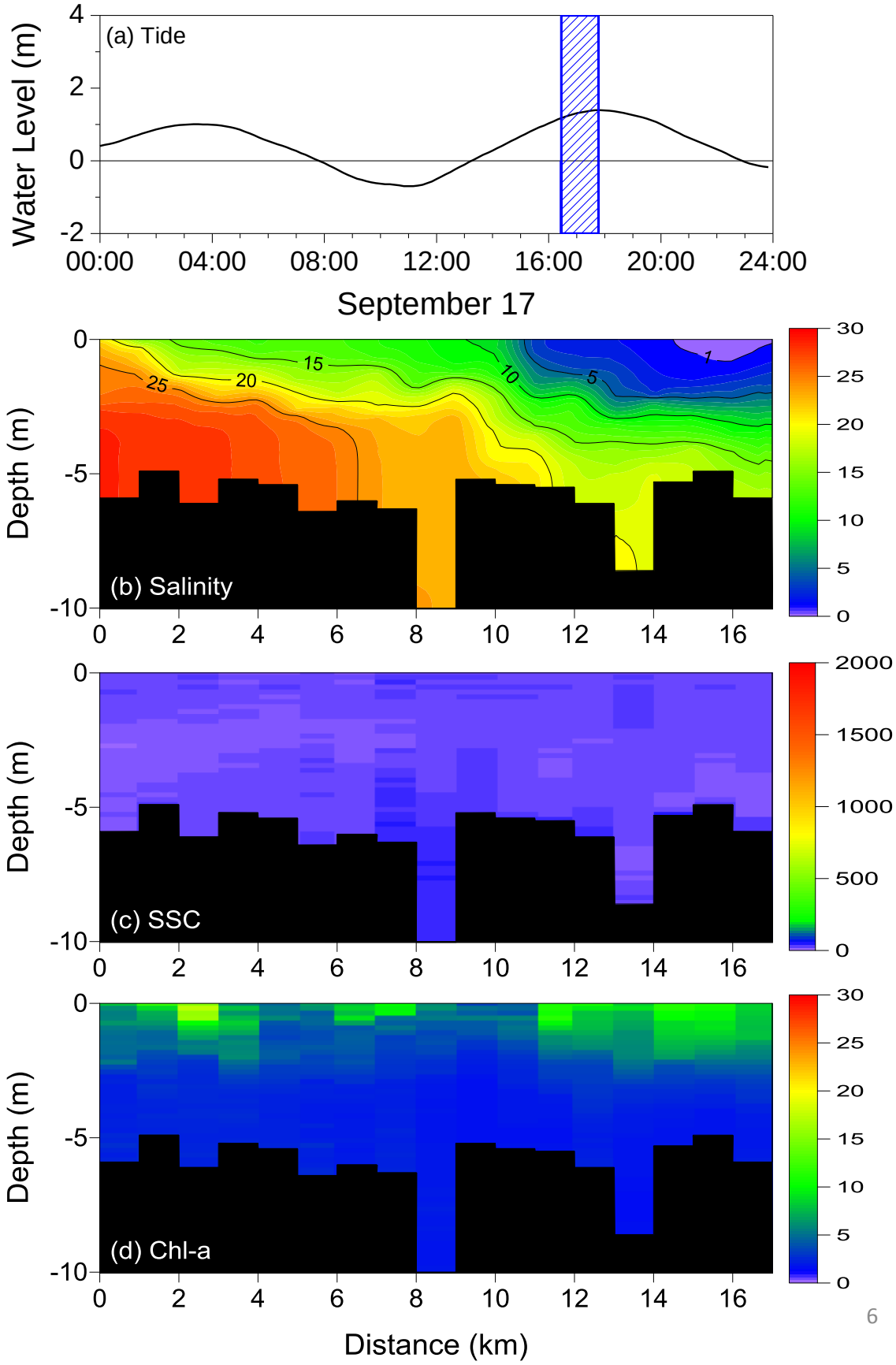

Fig. 3.20 (a) temporal variation of tide and longitudinal and vertical distributions of (b) salinity in psu, (c) SSC in mg/l and (d) Chl-a in µg/l during September 17 (Round 6).

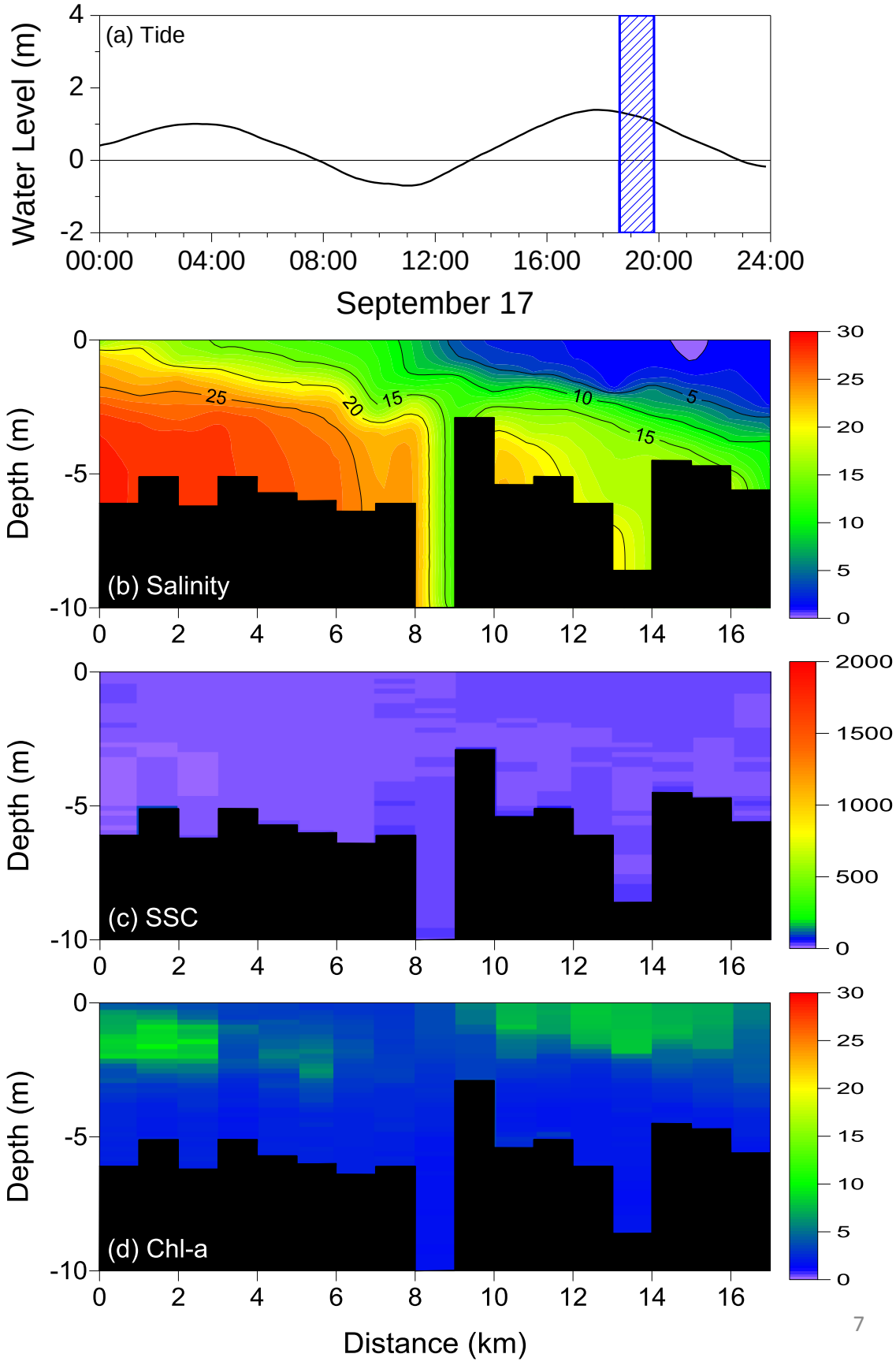

Fig. 3.21 (a) temporal variation of tide and longitudinal and vertical distributions of (b) salinity in psu, (c) SSC in mg/l and (d) Chl-a in µg/l during September 17 (Round 7).

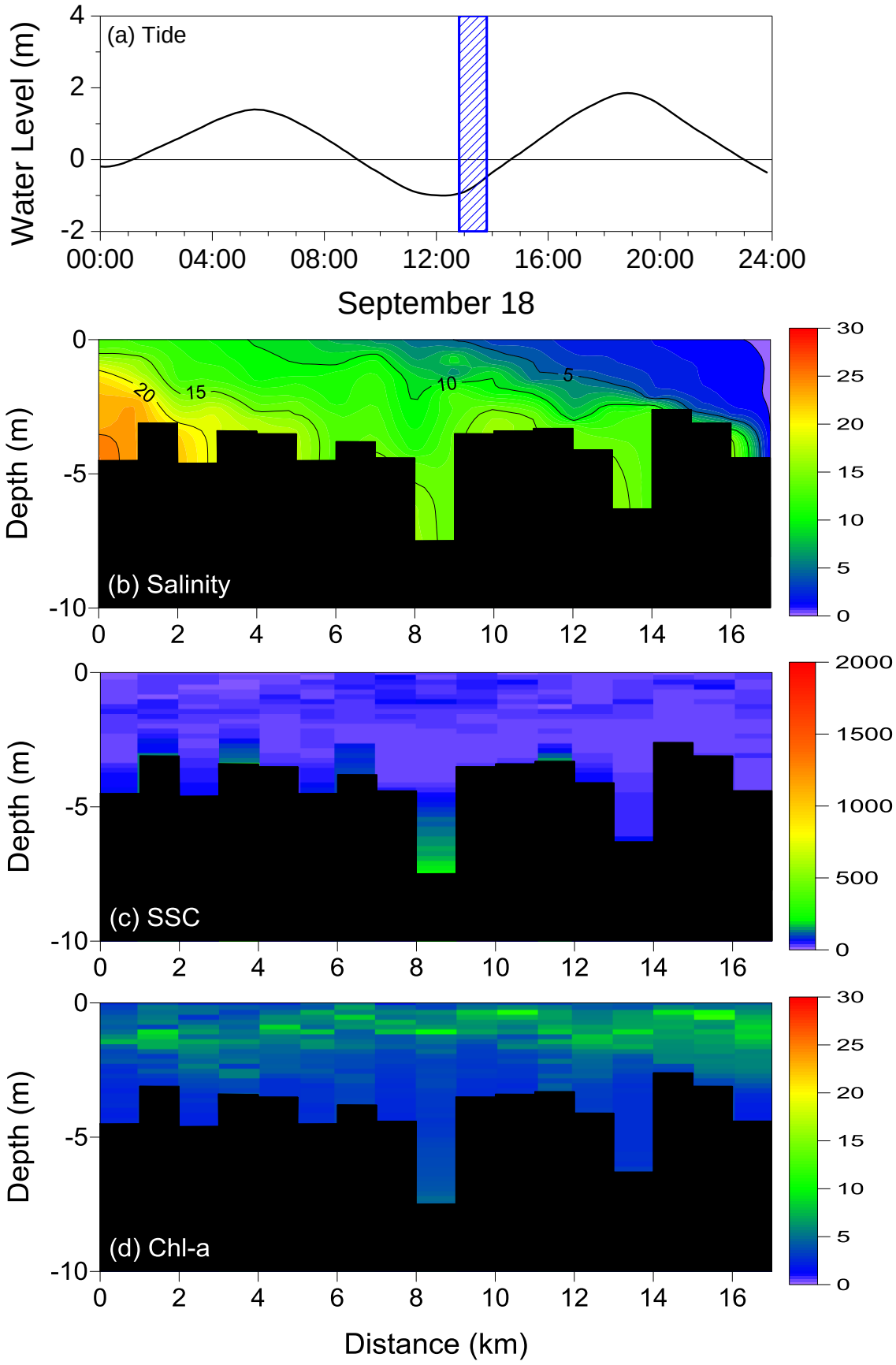

Fig. 3.22 (a) temporal variation of tide and longitudinal and vertical distributions of (b) salinity in psu, (c) SSC in mg/l and (d) Chl-a in µg/l during September 18 (Round 1).

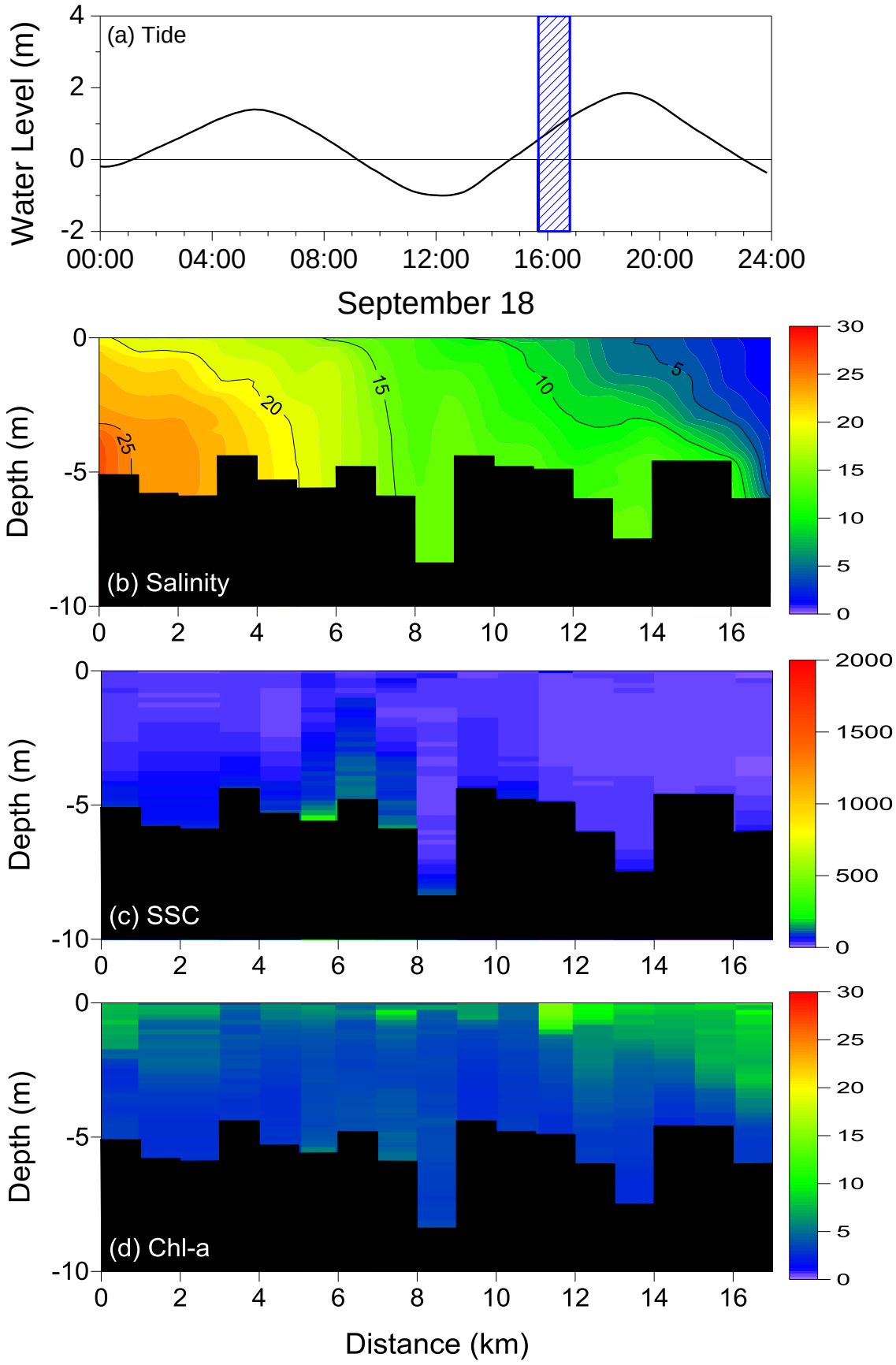

Fig. 3.23 (a) temporal variation of tide and longitudinal and vertical distributions of (b) salinity in psu, (c) SSC in mg/l and (d) Chl-a in µg/l during September 18 (Round 2).

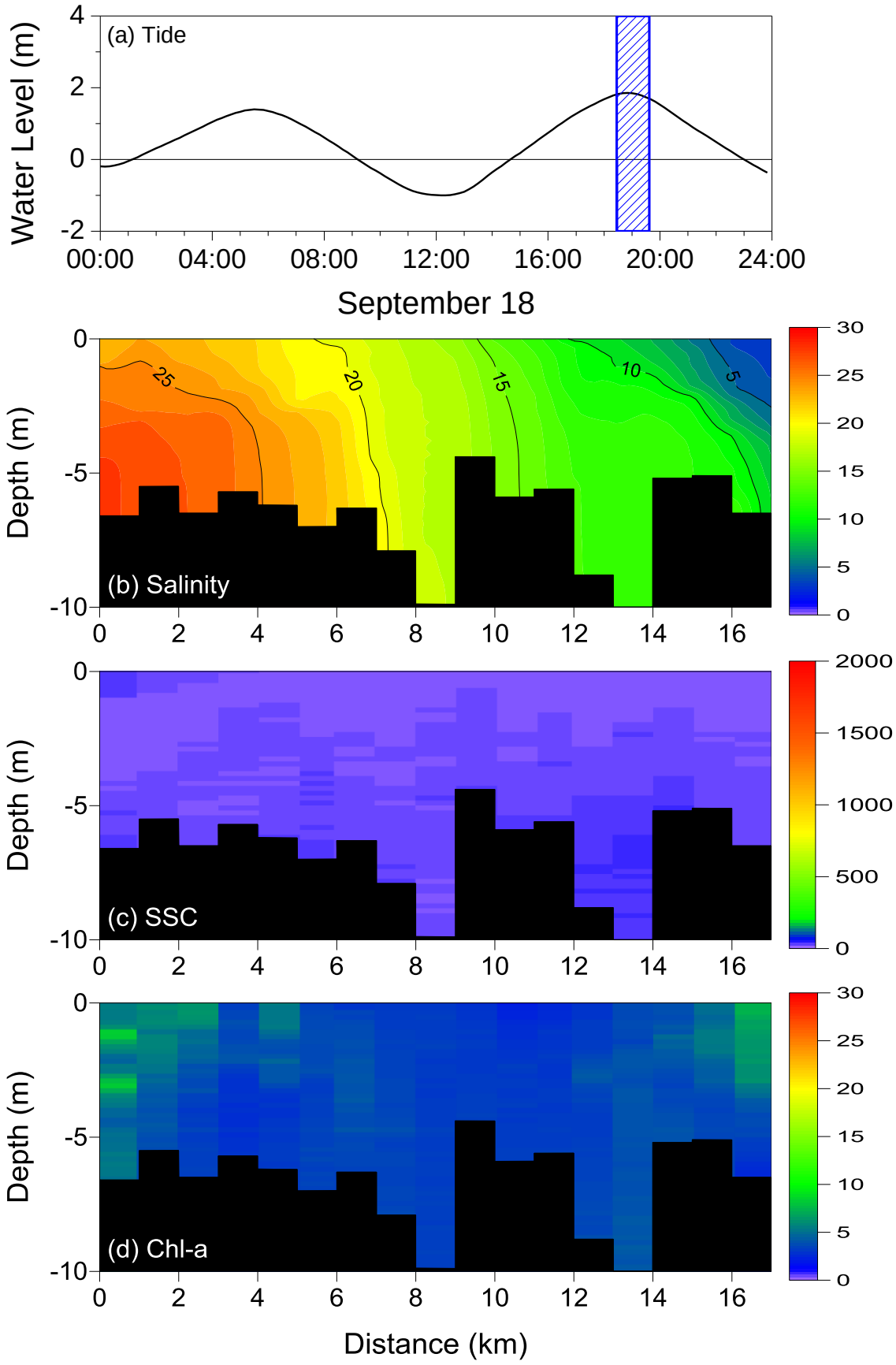

Fig. 3.24 (a) temporal variation of tide and longitudinal and vertical distributions of (b) salinity in psu, (c) SSC in mg/l and (d) Chl-a in µg/l during September 18 (Round 3).

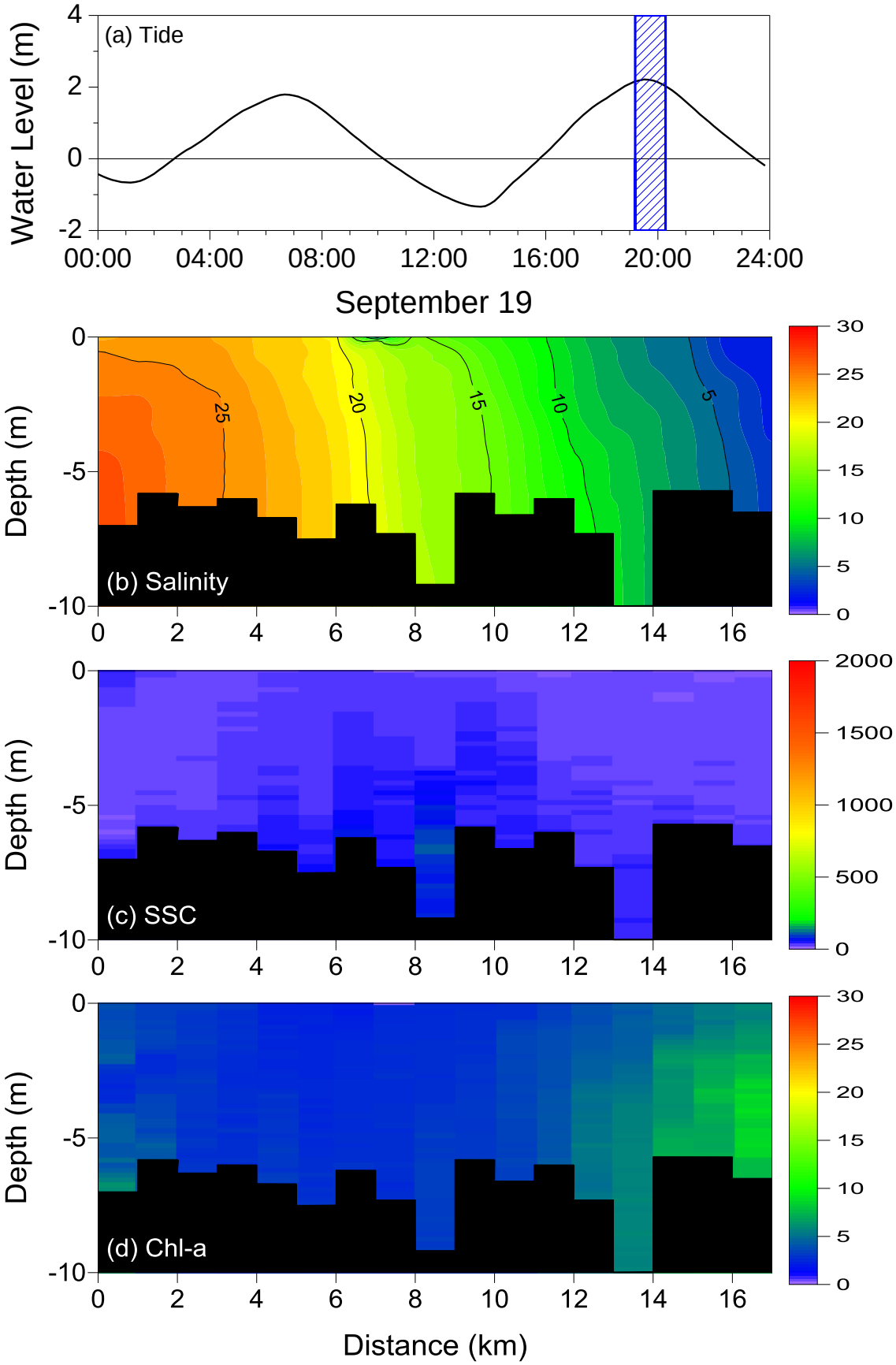

Fig. 3.25 (a) temporal variation of tide and longitudinal and vertical distributions of (b) salinity in psu, (c) SSC in mg/l and (d) Chl-a in µg/l during September 19 (Round 1).

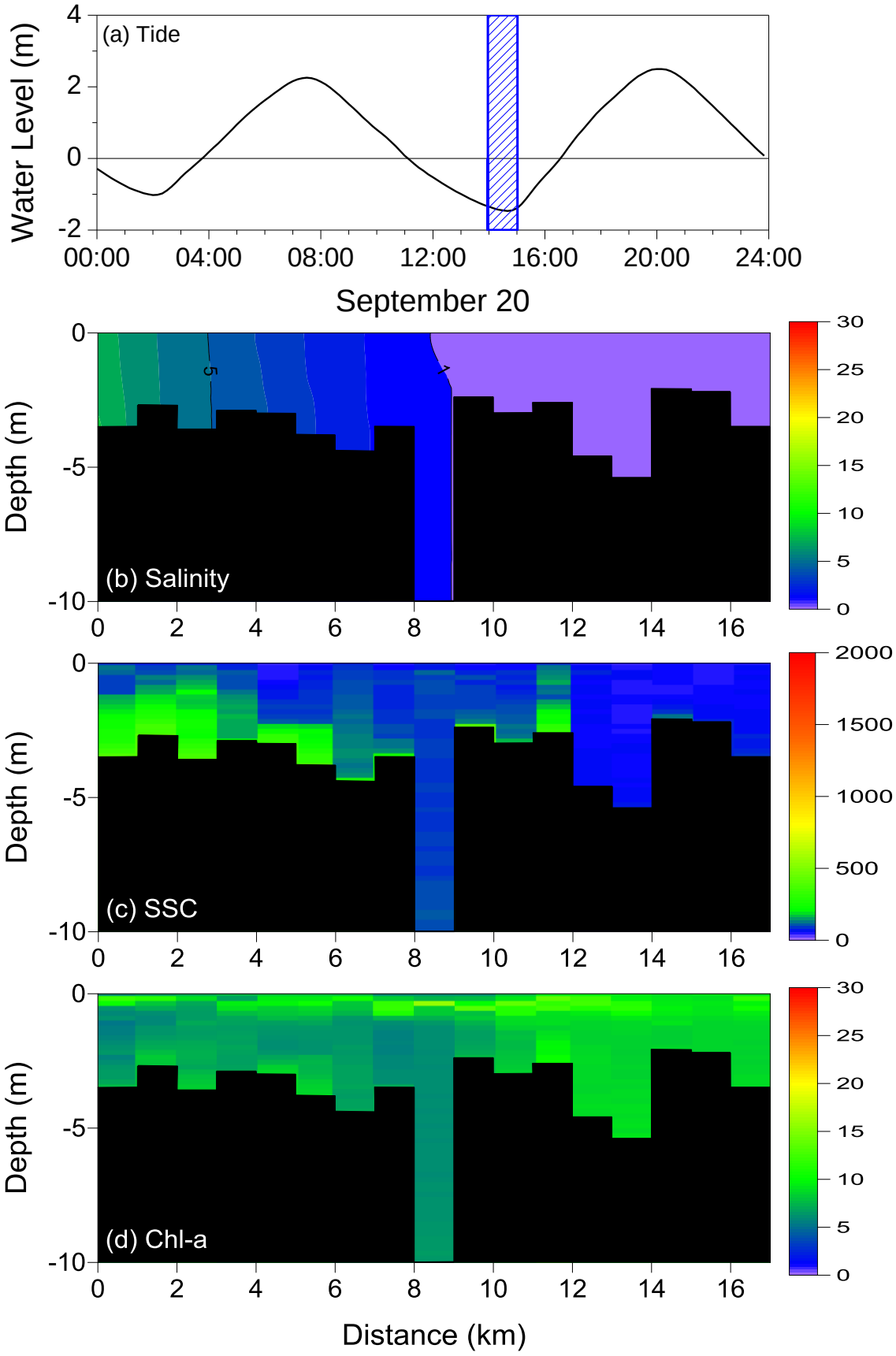

Fig. 3.26 (a) temporal variation of tide and longitudinal and vertical distributions of (b) salinity in psu, (c) SSC in mg/l and (d) Chl-a in µg/l during September 20 (Round 1).

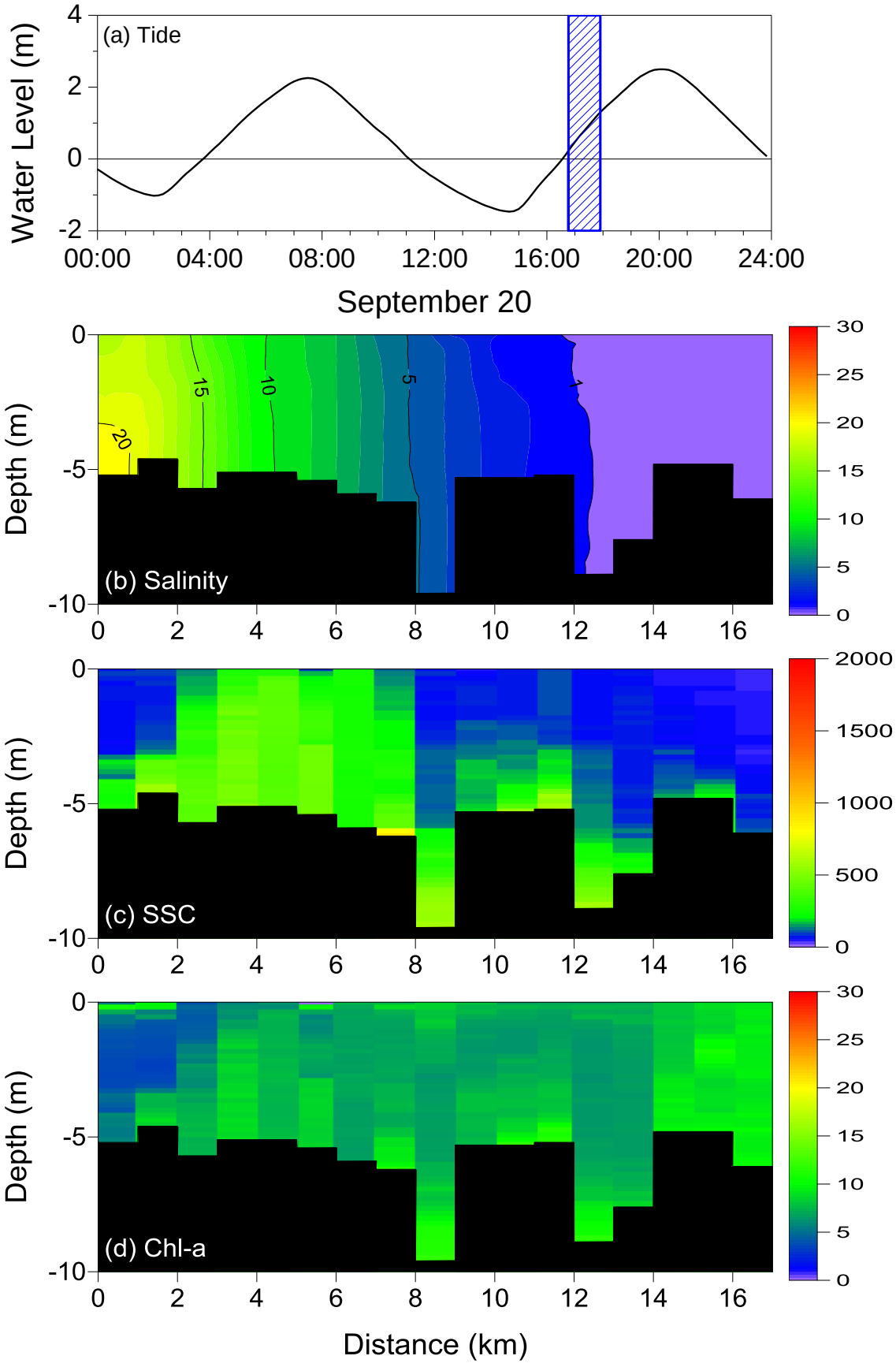

Fig. 3.27 (a) temporal variation of tide and longitudinal and vertical distributions of (b) salinity in psu, (c) SSC in mg/l and (d) Chl-a in µg/l during September 20 (Round 2).

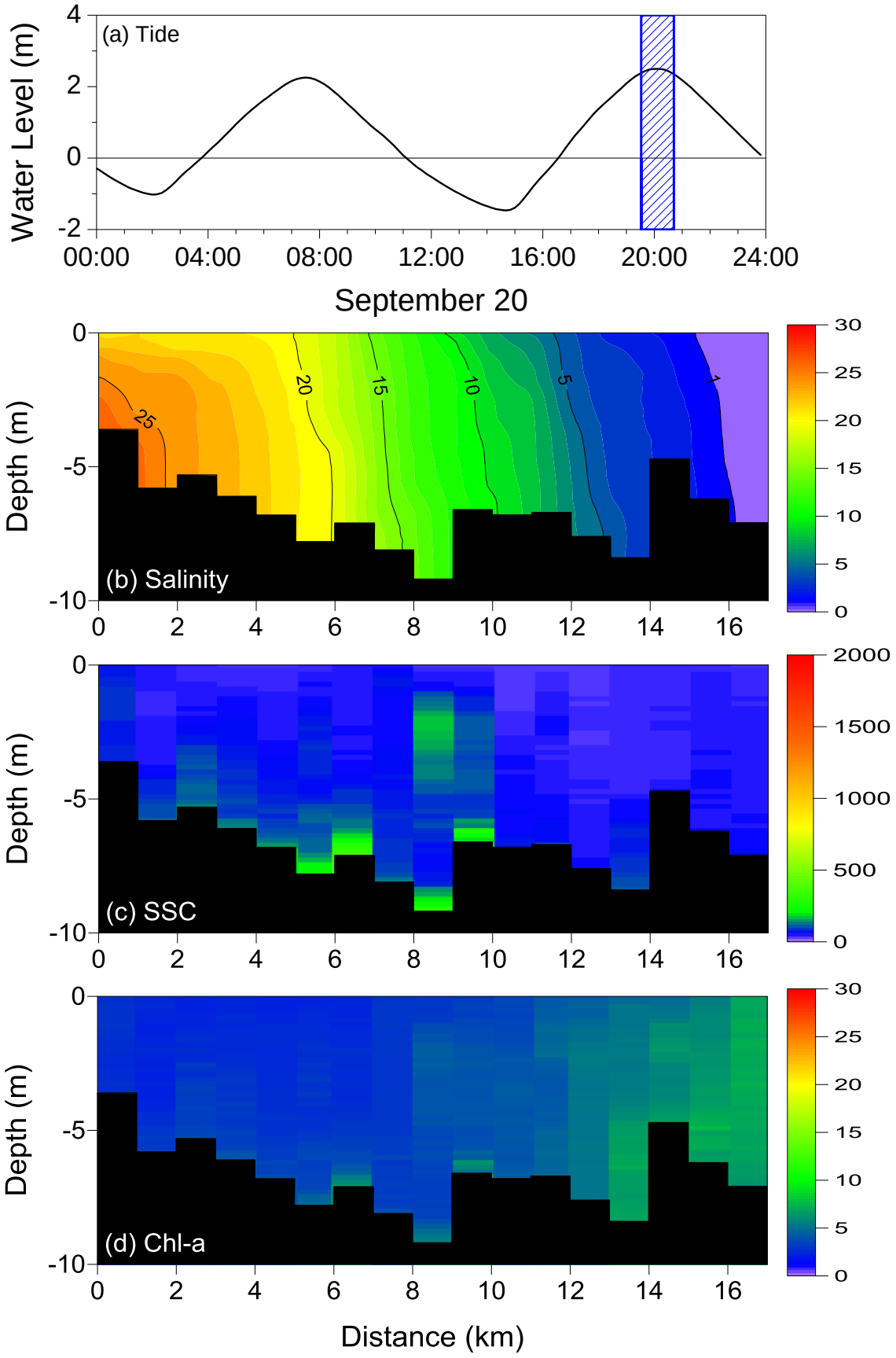

Fig. 3.28 (a) temporal variation of tide and longitudinal and vertical distributions of (b) salinity in psu, (c) SSC in mg/l and (d) Chl-a in µg/l during September 20 (Round 3).

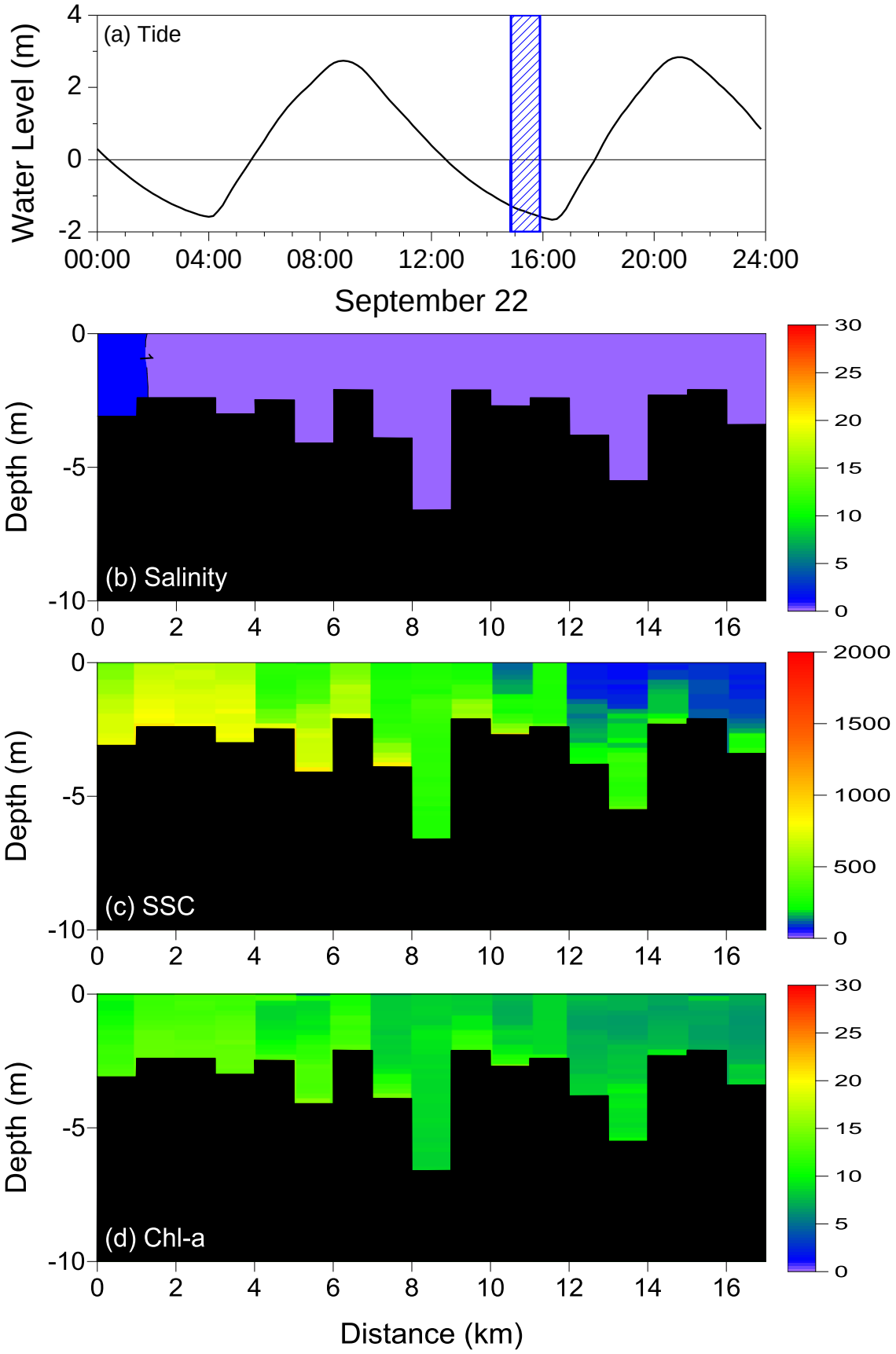

Fig. 3.29 (a) temporal variation of tide and longitudinal and vertical distributions of (b) salinity in psu, (c) SSC in mg/l and (d) Chl-a in µg/l during September 22 (Round 1).

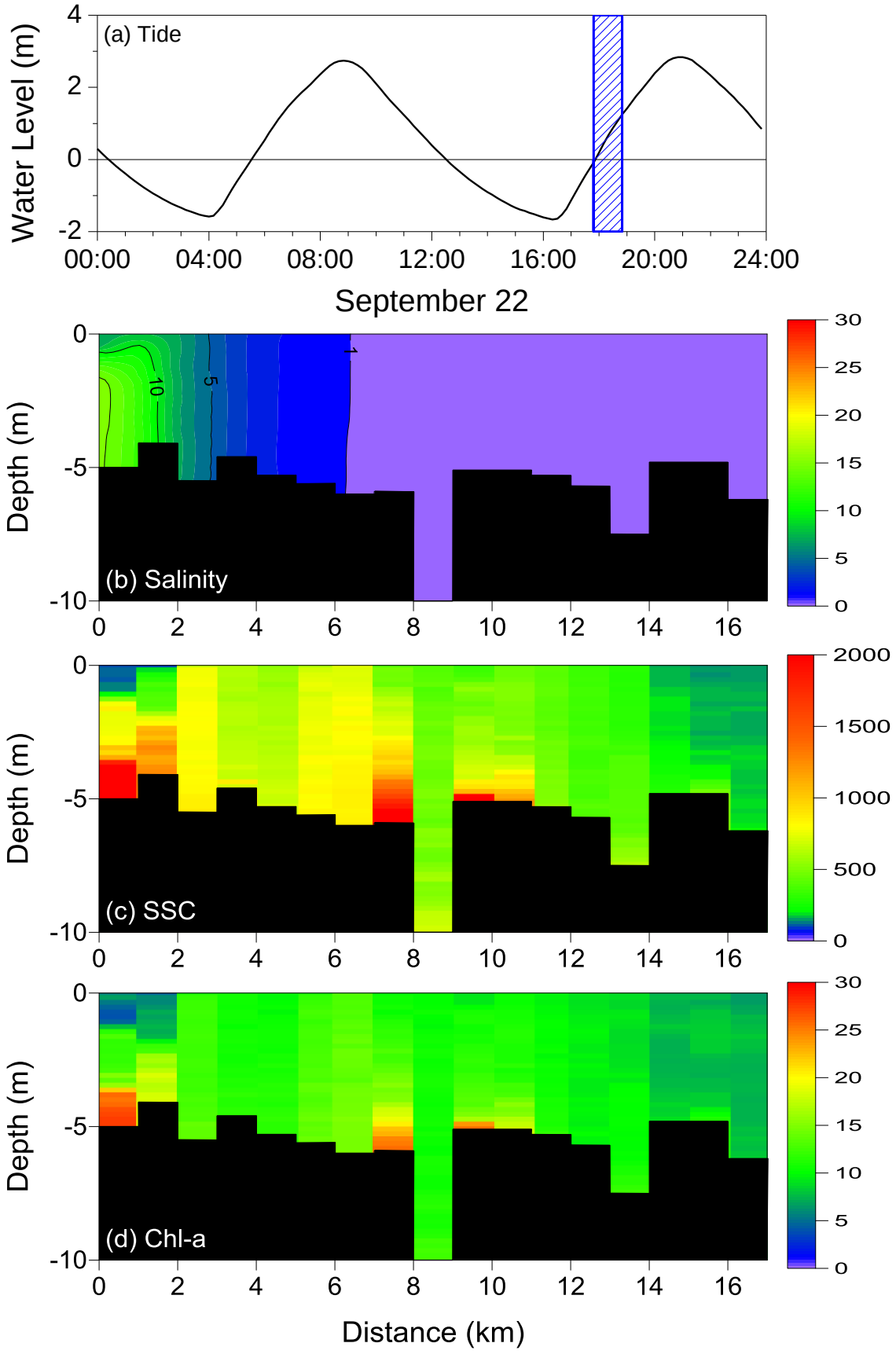

Fig. 3.30 (a) temporal variation of tide and longitudinal and vertical distributions of (b) salinity in psu, (c) SSC in mg/l and (d) Chl-a in µg/l during September 22 (Round 2).

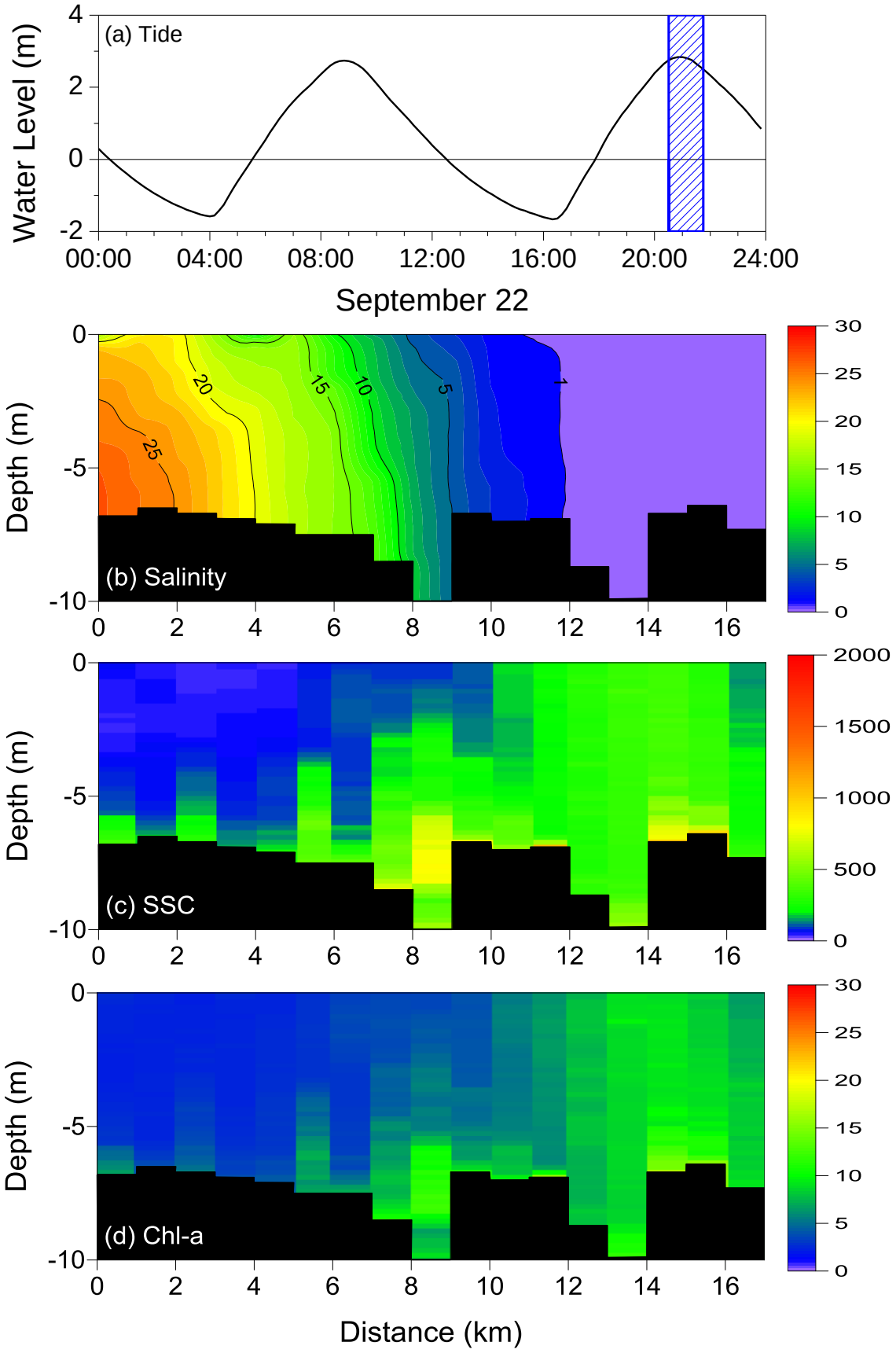

Fig. 3.31 (a) temporal variation of tide and longitudinal and vertical distributions of (b) salinity in psu, (c) SSC in mg/l and (d) Chl-a in µg/l during September 22 (Round 3).

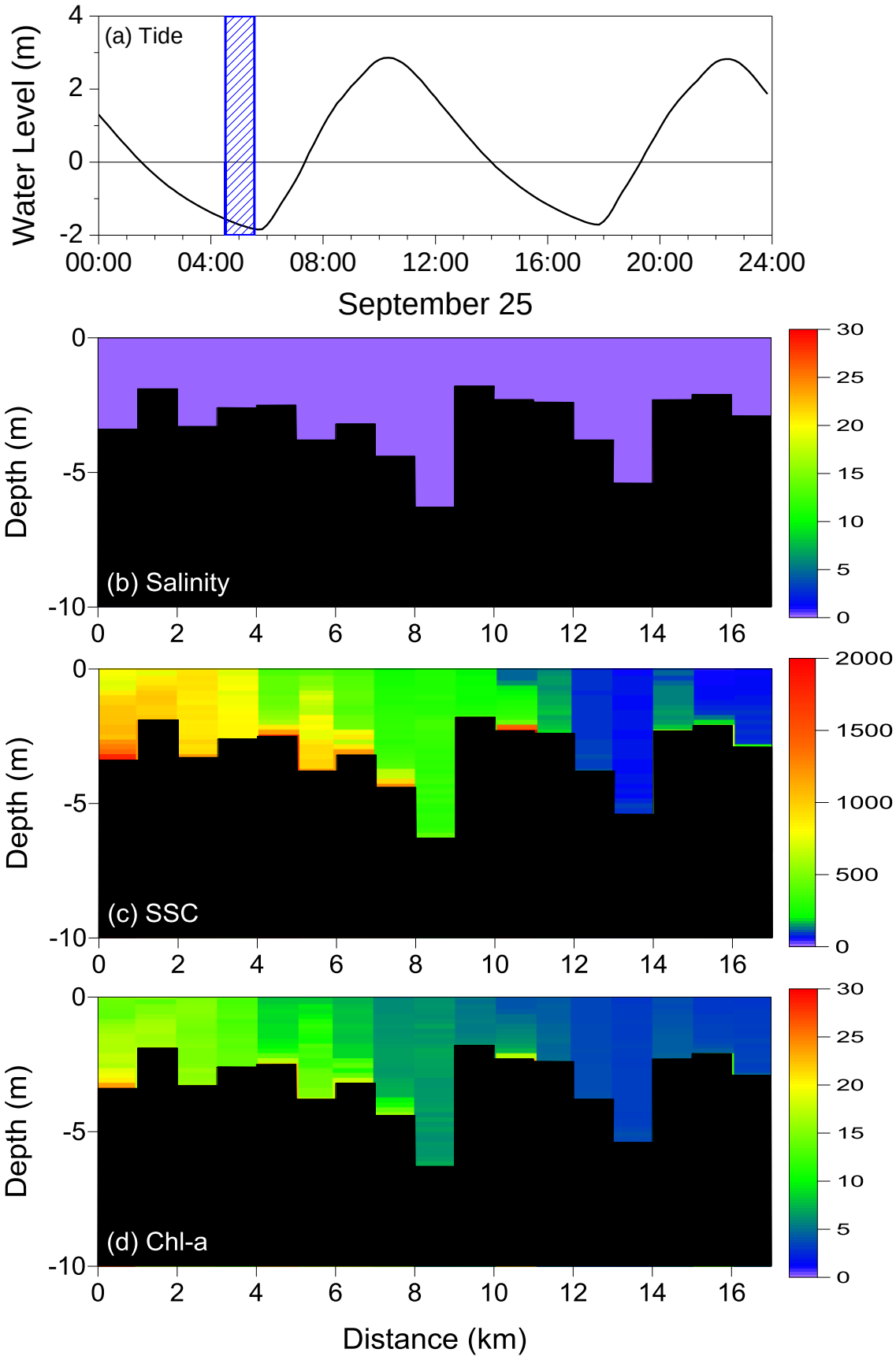

Fig. 3.32 (a) temporal variation of tide and longitudinal and vertical distributions of (b) salinity in psu, (c) SSC in mg/l and (d) Chl-a in µg/l during September 25 (Round 1).

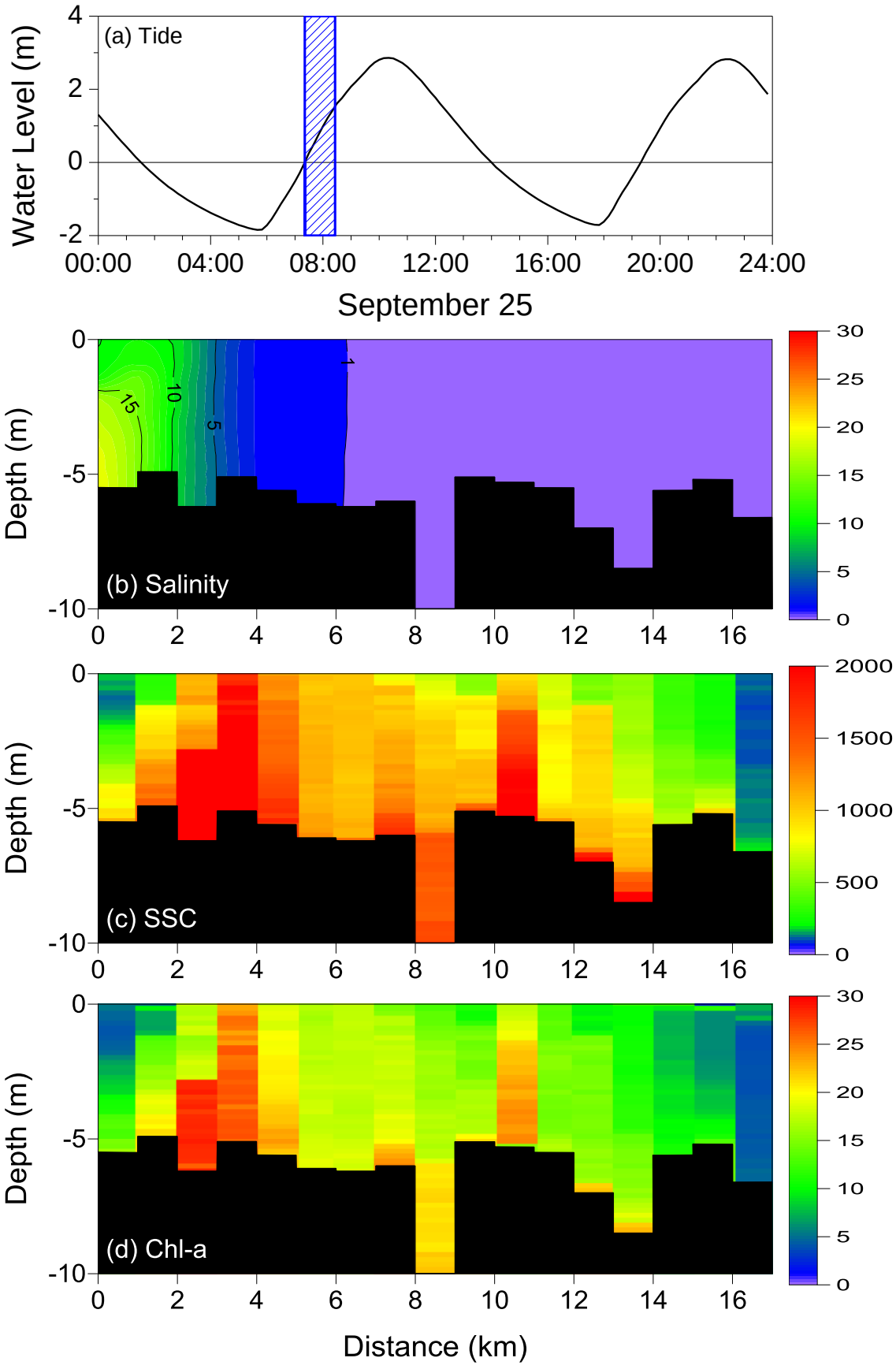

Fig. 3.33 (a) temporal variation of tide and longitudinal and vertical distributions of (b) salinity in psu, (c) SSC in mg/l and (d) Chl-a in µg/l during September 25 (Round 2).

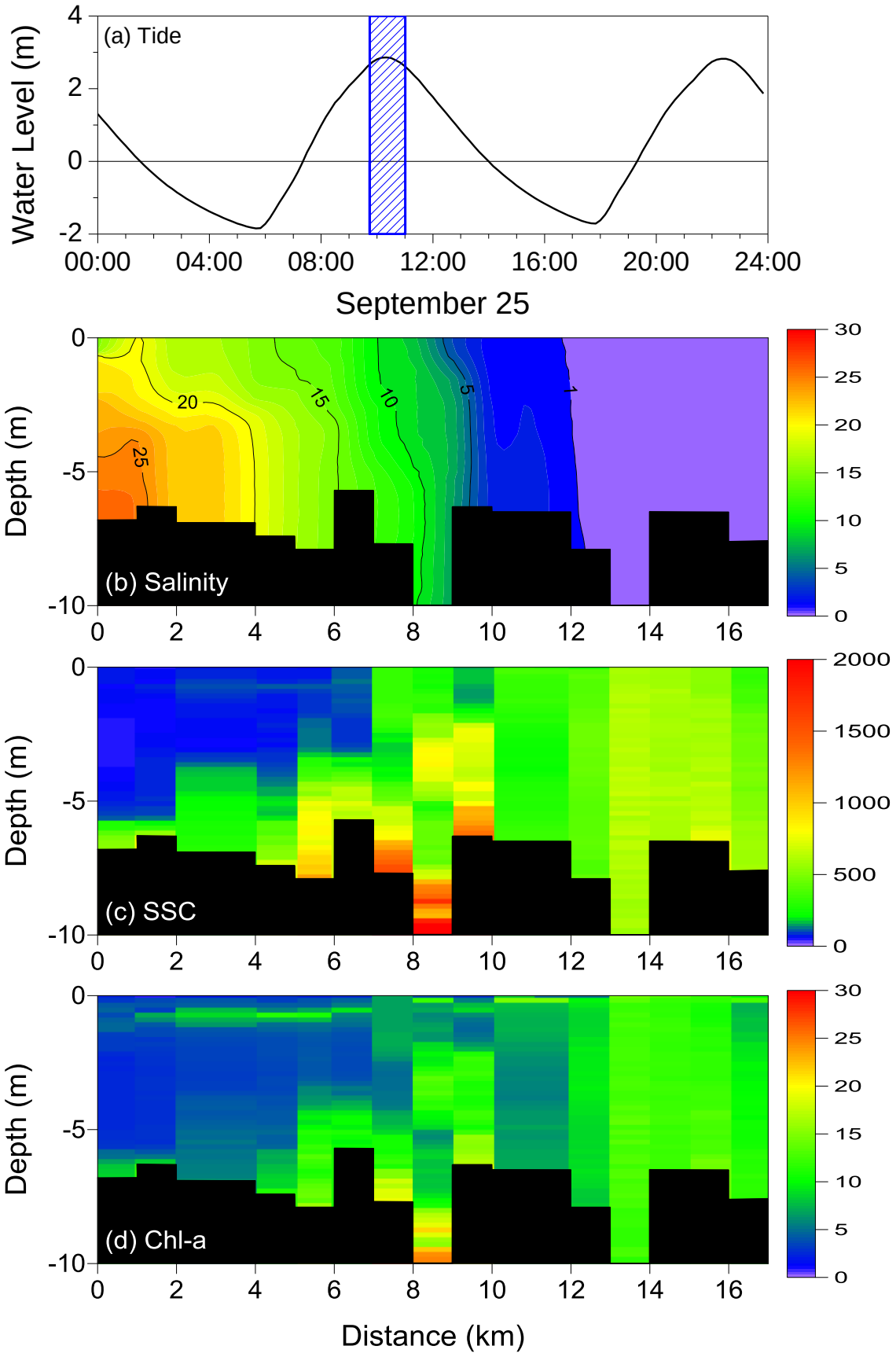

Fig. 3.34 (a) temporal variation of tide and longitudinal and vertical distributions of (b) salinity in psu, (c) SSC in mg/l and (d) Chl-a in µg/l during September 25 (Round 3).

3.1.3 Semilunar Estuarine Variability

The vertical and horizontal spatial distributions of the salinity and SSC in the flood water phase during the fortnightly tidal cycles were collected and shown in Fig. 3.35. Salinity during the spring tide [Fig. 3.35(a1)] with a tidal amplitude of 5.2 m had a vertically uniform distribution, and the estuary was therefore classified as well-mixed. During the following half tide [Fig. 3.35(a3)], the tidal amplitude decreased to 2.4 m. The 10-psu contour line was inclined, and the 10-psu salinity level appeared at the surface at 3.5 km and on the bottom at 7.5 km. Therefore, the estuary was classified as partially mixed at this time. Subsequently, the tidal amplitude decreased to 1.7 m during the neap tide [Fig. 3.35(a4)] and there was little effect on mixing, which resulted in strong salinity stratification. The distance traveled by the saltwater intrusion exceeded 17 km, which was longer than the distance recorded during the spring tide and half tide. The mixing condition again changed from stratified during the neap tide [Fig. 3.35(a4)] to well-mixed during spring tide [Fig. 3.35(a8)] *via* a partially mixed condition during the intermediate half tides. The saline water intrusion was limited to within the lower estuary on September 22 [Fig. 3.35(a7)] and 25 [Fig. 3.35(a8)].

There were large variations in SSC during the fortnightly tidal cycle. The estuarine water was extremely turbid during the spring tide [Fig. 3.35(b1)]. The ETM zone was observed to extend from 14 to 16 km upstream with an SSC greater than 1,000 mg/l, and its location corresponded to the saltwater front. The SSC decreased to 500 mg/l in the maximum zone, and decreased to 50–80 mg/l around the river mouth and upper estuary during the half tide [Fig. 3.35(b3)]. Although the concentration decreased during the half tides, the peak concentration occurred at the location that corresponded to the salinity front. The estuary became almost clear during the neap tide [Fig. 3.35(b4)], with an SSC of 20–50 mg/l, and an ETM zone was not found. The SSC again started to increase gradually during the succeeding half tides and the water became extremely turbid during the next spring tide with an SSC of 1000–-2000 mg/l [Fig. 3.35(b8)]. The SSC was high in the middle estuary on September 22 [Fig. 3.35(b7)] and 25 [Fig. 3.35(b8)]. Although it was spring tide on both the first and last day of field observations, the locations of the ETM zone were different and the ETM on the last day was located near the river mouth.

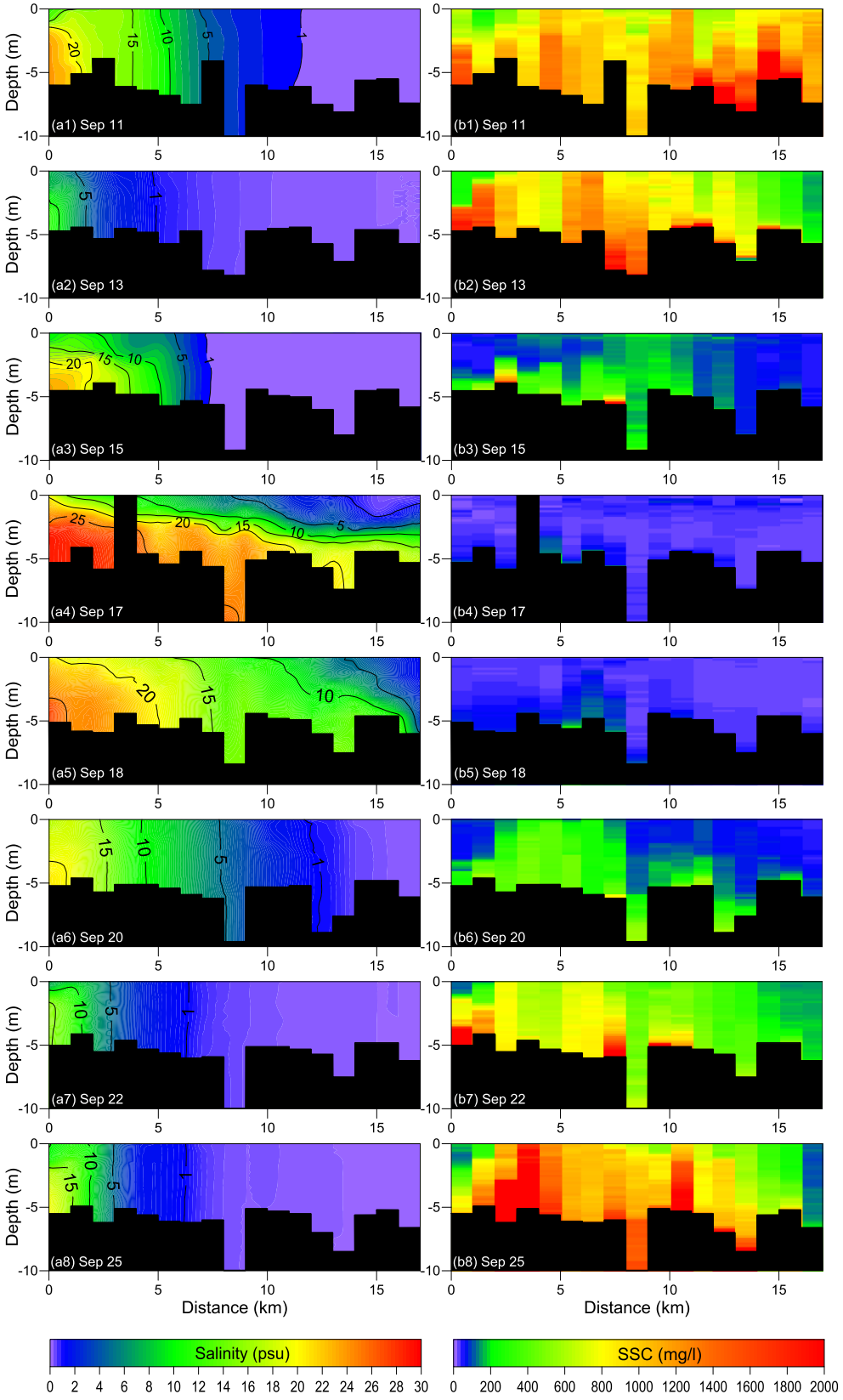

Fig. 3.35 Longitudinal and vertical distributions of (a) salinity, and (b) SSC during the semilunar tidal cycle. Data measured during flood tide were used.

3.2 Discussion

All types of mixing conditions were found in the Chikugo River estuary and the SSC varied widely during the semilunar tidal cycle. Thus, it is possible to investigate the dominant factors involved in ETM occurrence from various points of view: as a ratio of freshwater discharge and tidal flow, as a relationship between salinity and SSC, and as a relationship between mixing strength and SSC.

Because the salinity interface gradient (SIG) exceeded 0.005 on September 11 (Fig. 3.36b), the estuary was well mixed during the spring tide. The SIG settled into a range between 0.005 and 0.001 on September 13, 15, 22, and 25; thus, the estuary was partially mixed. The SIG was less than 0.001 on September 17 and 18, and the estuary was considered to be in a stratified condition during the neap tide.

3.2.1 Magnitude of the ETM

The Tay estuary, which is a macrotidal estuary with a normal tidal range of 5 m during spring tide and 2.5 m during neap tide, has a maximum SSC of 35 mg/l at high tide and 84 mg/l at low tide (Dobereiner and Mcmanus, 1983). The macrotidal Scheldt estuary had a peak SSC of 300–400 mg/l. The Scheldt estuary was influenced by a mean tidal range of 4.85 m during spring tide and 2.81 m during neap tide (Chen *et al.*, 2005). The Weser estuary had a peak SSC of 400–700 mg/l with a mean tidal range of 4.2 m during spring tide and 3.1 m during neap tide. The mean SSC during flood tide in the Humber estuary was generally lower than the mean ebb SSC, and the peak SSC at the ETM was 10,000–15,000 mg/l with mean tidal range of 6.4 m during spring tide and 3.4 m during neap tide (Mitchell, 2013). The Tamar is a coastal plain estuary where the SSC can exceed 5,000 mg/l during spring tide and 500 mg/l during neap tide. The Tamar estuary had a mean tidal range of 4.7 m during spring tide and 2.2 m during neap tide (Grabemann *et al.*, 1997). The macrotidal Konkoure estuary had an SSC of 100 mg/l at the surface and 1,500 mg/l on the bottom with a mean tidal range of 4.2 m during spring tide and 1.3 m during neap tide (Capo *et al.*, 2006). The SSC, in macrotidal estuaries worldwide, ranges widely from 35 mg/l to 15,000 mg/l and it is thought that the SSC in the Chikugo River estuary was at the higher end of this range.

3.2.2 Flow Ratio

Ji *et al.* (2007) used a flow ratio (which is the ratio of total volume of freshwater over a tidal cycle to the tidal prism, entering an estuary each flood tide) to explain the estuarine stratification with the significant effect of additional factors on stratification. In the St. Lucie estuary, the dominant force on the flow ratio was freshwater discharge because of the small tidal range. Hence, the effect of tidal variations during the semilunar tidal cycle was not documented. Simmons (1955) explained that when the flow ratio was 1.0 or greater, the estuary was highly stratified. When the flow ratio was less than 0.1, the estuary was well-mixed. However, the Chikugo River estuary had a flow ratio of 0.1 to 0.3 when the salinity distribution was stratified and 0.01 to 0.03 when it was well-mixed (Fig. 3.36d).

The flow ratio displayed three peaks over two weeks (Fig. 3.36d). The peak flow ratio on September 17 was caused by the low tidal range of the neap tide. The peaks on September 13 and 23 were a consequence of rainfall runoff. Although the tidal amplitude increased from the half tide (September 22) toward the spring tide (September 25), the flow ratio on both days was the same because of the increase in fresh water discharge. Therefore, the variation of both tidal flow during the semi-lunar tidal cycle and the daily freshwater flow significantly affected the flow ratio of the estuary.

The velocity of the flood current exceeded 1.25 m/s whereas the velocity of the ebb current was lower than 1.0 m/s on September 11 (Fig. 3.36e). Because the estuary has a funnel-shape, the semidiurnal tidal cycle becomes asymmetric, and the current velocity of the flood tide becomes greater than that of the ebb tide (Muylaert *et al.*, 2005). The velocity decreased to below 0.4 m/s during the neap tide, which was one-third of the maximum speed. The maximum concentration of suspended sediment, which exceeded 3,500 mg/l, occurred during the spring tide and the SSC ranged from 10 to 30 mg/l during the neap tide, i.e., it decreased to 150^{th} of the maximum rate (Fig. 3.36f). The SSC was sensitive to changes in the tidal current.

However, the response of the SSC to water velocity changed on September 23. The velocity of the ebb current exceeded 1.0 m/s and was greater than the velocity of the flood current. Because a fresh water discharge of 350 m^3/s from the basin toward the sea was added to the tidal current (Fig. 3.1b), the ebb current accelerated and the flood current was reduced. The peak SSC was 200 mg/l, which was one-tenth of the SSC on

September 13, whereas the tidal range on September 23 was almost the same as it was on September 13. It is likely that the ETM was diluted by water with a low SSC that ranged 20–56 mg/l from the basin (Fig. 3.36f) and it did not respond to the increase in the ebb current. Those phenomena indicate that the flow ratio affects the velocity and the SSC.

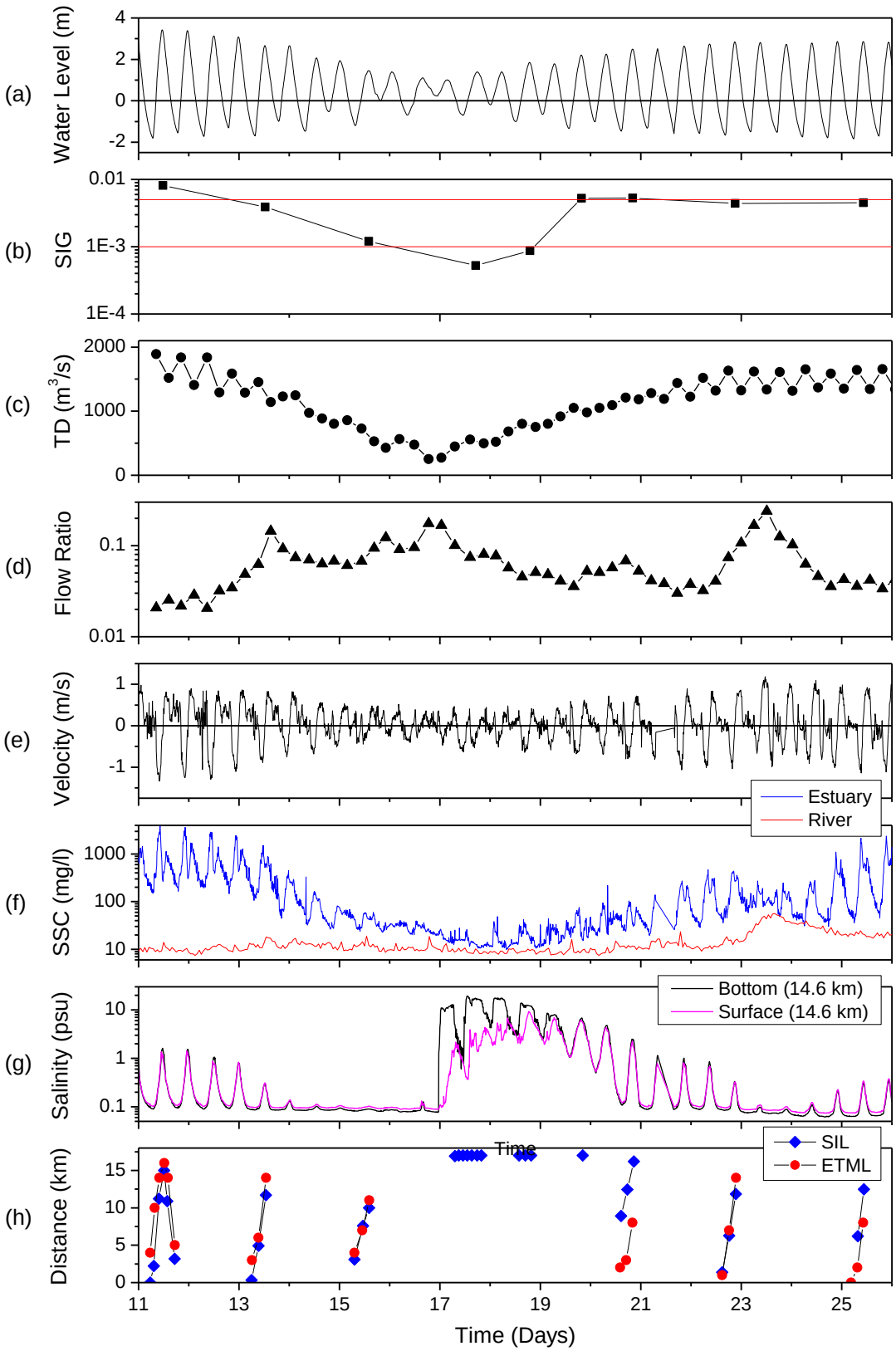

Fig. 3.36 Temporal variation of (a) water level, (b) SIG, (c) tidal discharge, (d) flow ratio, (e) bottom velocity at 14.6 km upstream, (f) bottom SSC of estuary at 14.6 km upstream and river at 25 km upstream gauge station, and (g) salinity in the surface and bottom at 14.6 km upstream (h) location of saltwater intrusion and the ETM.

The relationship between flow ratio and average SSC produced a uniformly linear relation during the fortnightly tidal cycle (Fig. 3.37). The flow ratio ranged between 0.2 and 0.02, which indicates that the tidal discharge was 5–50 times larger than the freshwater discharge. For example, the tidal discharge was approximately 500 m^3/s during the neap tide and reached 2,000 m^3/s during the spring tide; on the other hand freshwater discharge was below 50 m^3/s during normal days and it increased 200 – 360 m^3/s on rainy days (Fig. 3.1b). On a yearly basis, the freshwater discharge in the dry season was 40 m^3/s and the mean annual peak discharge was 2,800 m^3/s. On average, there were 11 days when the freshwater discharge exceeded 500 m^3/s and 39 days when it exceeded 200 m^3/s. Therefore, the daily tidal discharge was much larger than the freshwater discharge for 11 months (Fig. 3.1a).

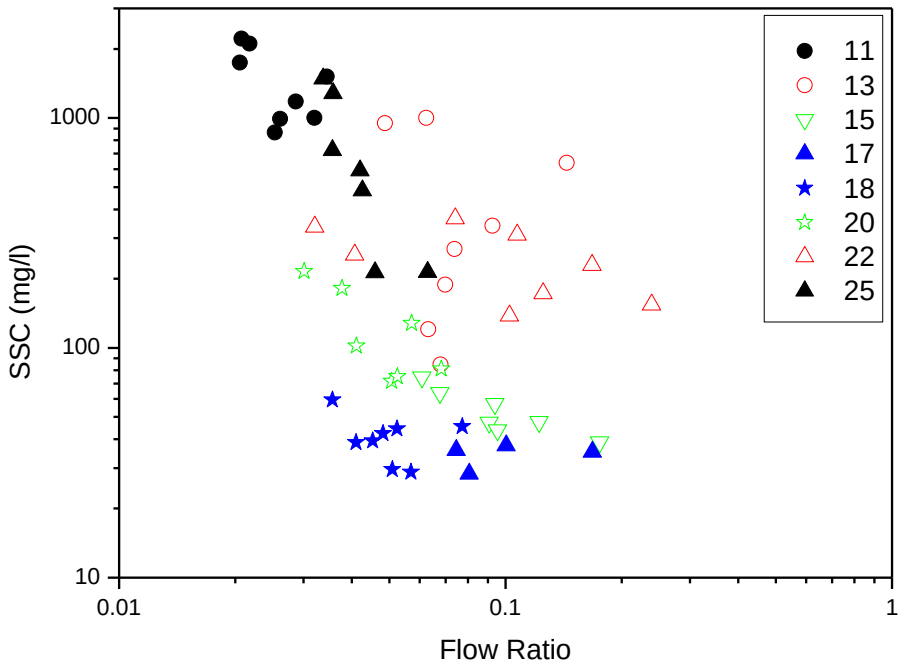

Fig. 3.37 A plot of the flow ratio against SSC. The average bottom SSC at 14.6 km upstream was calculated for the duration of each flood and ebb tide. The relationship was plotted during spring tide (black), half tides (red and green), and neap tide (blue).

The SSC was approximately 30 to 300 mg/l when the flow ratio was 0.1, and was over 1,000 mg/l when the flow ratio was less than 0.03; thus, the SSC increased as the flow ratio decreased. The plots for September 13 and 22 show dispersed data points, which reduced the correlation between the flow ratio and SSC. The rapid supply of

freshwater on September 13 and 22 disturbed the processes that influence the ETM such as resuspension of bottom sediment, settling of suspended particles, and the advection of those sediments. With the exception of the rapid variation of the freshwater discharge following heavy rainfall, ETM growth was dominated by both tidal forcing and the freshwater flow. The ETM in the upper Humber and Ouse estuary (Uncles *et al.*, 2006), Delaware estuary (Cook *et al.*, 2007) and Tana estuary (Kitheka *et al.*, 2005) was mainly dependent on freshwater inflow and the influence of tidal force was less. Although the previous studies on the relationship between flow ratio and SSC were limited, Fig. 3.37 shows the relationship and the importance of both tidal variation and freshwater inflow in ETM.

Flow ratio is a useful index that provides an outline of the estuarine mixing and the SSC when an actual tidal prism is calculated. However, the spatial characteristics of mixing and the SSC cannot be considered using the flow ratio. The flow ratio consists of topographic volume and freshwater quantity, and neither parameter includes spatial information. Therefore, it is necessary to apply another index to consider the location and time of the occurrence of large SSCs.

3.2.3 Salinity Intrusion and Movement of ETM

The salinity intrusion length (SIL) indicates the interface between sea water and freshwater, which was located at the river mouth in low tide conditions during the spring and half tides (Fig. 3.36g and Fig. 3.36h). The interface moved landward during the flood tide and reached the upper estuary at high tide. As the tidal amplitude changed from spring to half tide, the SIL decreased from 16 km to 10 km. The maximum SIL occurred during the neap tide because a salt wedge developed. The location of the ETM zone moved landward or seaward and the movement was similar to the SIL. It is suggested that the ETM zone was located near the interface between salt water and freshwater.

There was a strong ETM zone found at both the lower and upper estuary (Fig. 3.38). The ETM zone moved along the edge of the freshwater-saltwater interface. The ETM zone at the estuary mouth may occur due to erosion from the tidal flat. The ETM zone observed upstream may arise due to transport and erosion.

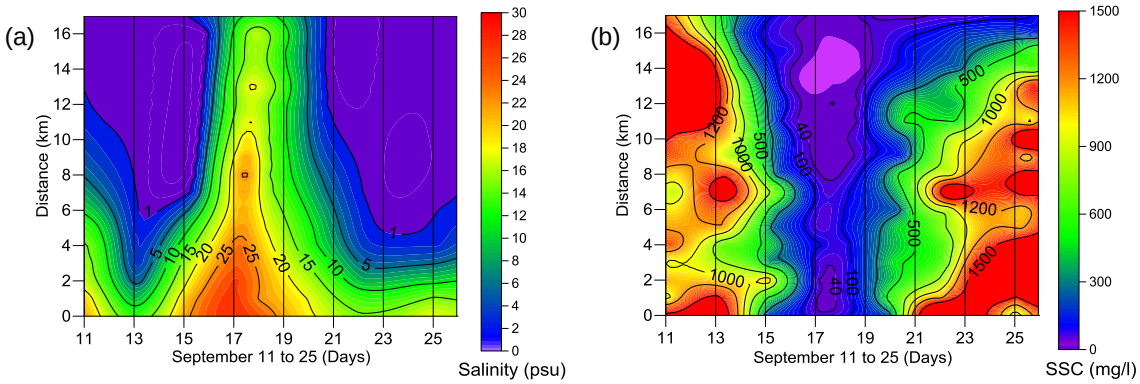

Fig. 3.38 Time-distance isopleth of (a) salinity and (b) SSC at flood phase on the surface.

To determine the effect of salinity on the SSC, the relationship between bottom salinity and SSC at the lower (0–4 km), middle (5–9 km), and upper (10–17 km) parts of estuary during the semi-lunar tidal cycle was investigated (Fig. 3.39). In the lower estuary, the ETM zone was mainly located near the region with a salinity of 10 psu (Fig. 3.39a). The SSC became greater where the salinity was 0.5 psu during the spring tide in the upper estuary (Fig. 3.39c). The ETM zone in the upper estuary developed at the saltwater-freshwater interface. There were two peaks of SSC in the middle estuary (Fig. 3.39b), in the areas with salinity around 0.5 psu and 10 psu, which indicates a transitional behavior between the lower and upper estuary.

In general, the ETM zone is found near the low salinity reaches of upper estuaries (Festa and Hansen, 1978; Uncles, 2002) and the results shown in Fig. 3.36g and Fig. 3.39c support that observation. The occurrence of the ETM in the upper reaches was caused by the resuspension of bottom sediment. The resuspension of bottom sediment is particularly significant in shallow, tidally dominated estuaries, which are driven by turbulent vertical mixing (Byun *et al.* 2007). Much of the suspended sediment settles out during the slack tide because of flocculation. The flocculated particles are mostly inorganic material in macrotidal estuaries (Wolanski *et al.*, 2001; Yokoyama, 2013).

Because the Chikugo River estuary was well-mixed, with a tidal velocity of 1.3 m/s during spring tide (Fig. 3.36b and Fig. 3.36e), the transported suspended sediment was flocculated and accumulated by estuarine mixing at the salinity front in the upper estuary (Fig. 3.39c). The SSC decreased during the half tide, and the water became clear during the neap tide. Estuarine mixing changed with the tidal variation and velocity

gradually decreased to 0.8 m/s during the half tide and became stable (< 0.5 m/s) during the neap tide. This transition process affected the strength of the ETM in this region.

Fig. 3.39a clearly shows the existence of other processes that influence the occurrence of the ETM. The peak SSC appeared in the region of seawater (10 psu), not in the interface between sea water and freshwater (0.5 psu). Suspended sediment originated from bed erosion in the offshore tidal flat from seawater intrusion. Figure 6b illustrates the transportation process of the suspended sediment in the estuarine channel. A high SSC occurred because of the landward transportation of fine sediment that was eroded from the offshore area and the development of an ETM at the salinity front.

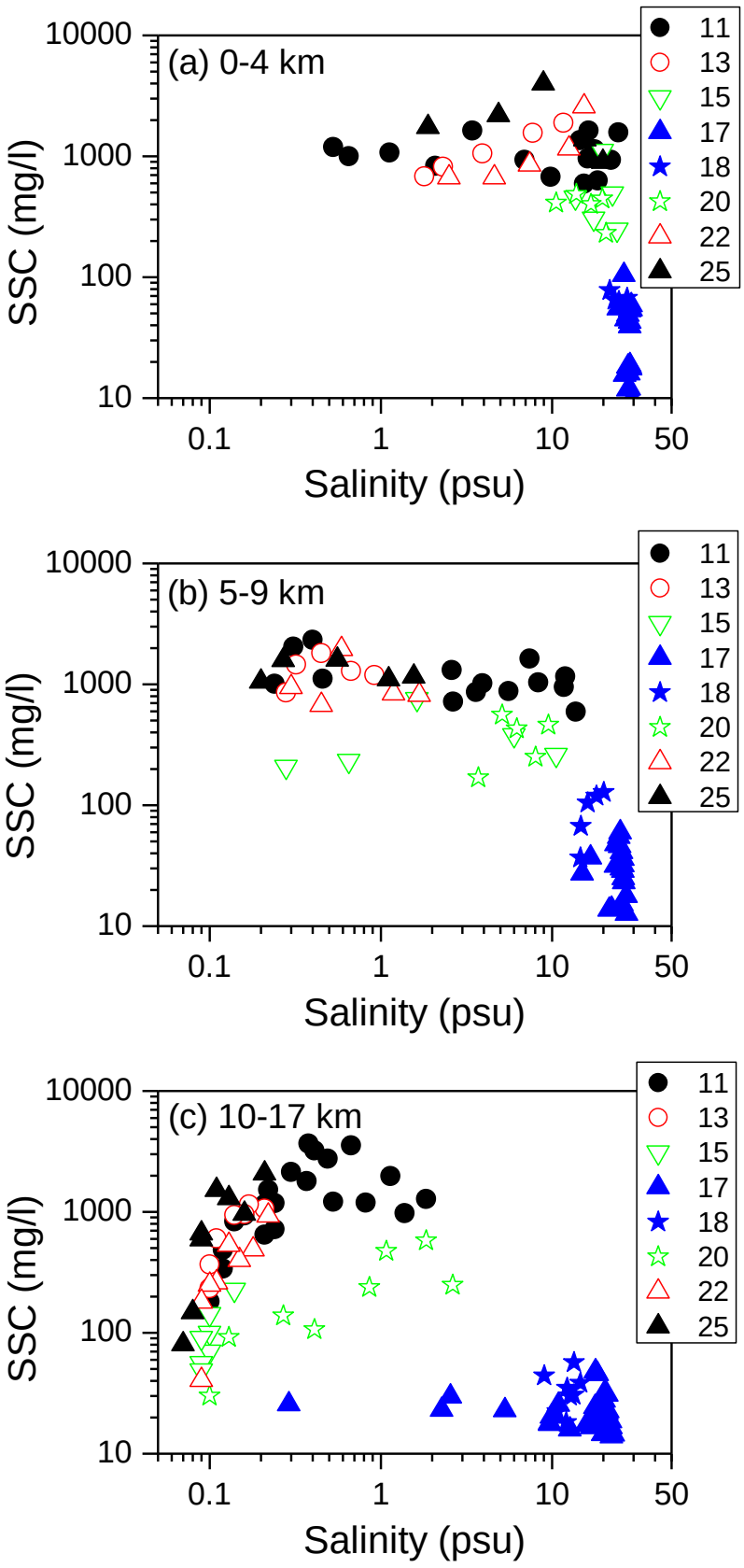

Fig. 3.39 Relationship between salinity and SSC for (a) the lower estuary, (b) the middle estuary, and (c) the upper estuary.

3.2.4 MS and SSC

The spatio-temporal distribution of the mixing strength (MS) during high tide is shown in Fig. 3.40. The value of the MS is inversely proportional to the actual mixing state, i.e., the MS becomes small when the estuary is well mixed. The MS was low (< 0.1) in the region from 10 to 17 km during the period from September 11 to 15 and from September 20 to 25. Vertically strong mixing occurred during the spring and half tides in the upper estuary.

In contrast, the MS increased in the lower estuary and was 0.5–1.0 in the region around the river mouth for the same period. Because there was heavy rain in the area around the river mouth on September 22 and 23, with freshwater flowing directly into the lower estuary, the MS increased substantially. In addition to the rainfall effect, there was a tendency for the MS to increase toward the river mouth on other days during the spring and half tides. Compared with the upper estuary, vertical mixing was reduced in the lower estuary. The position where the maximum mixing (minimum MS) occurred corresponded to the location of the salinity front (Fig. 3.36g). Vertical mixing in the estuary increased at the interface between seawater and freshwater during the spring and half tides.

The MS was large on September 17 when it exceeded 2.0 during the neap tide. The estuary was vertically stratified and was in a stable state. Furthermore, the MS reached a maximum in the region 15 km upstream from a longitudinal perspective. It is likely that both vertical mixing during the spring-half tide and gravitational stability during the neap tide are high in the upper estuary. The dynamism of the salinity movement was much greater in the upper estuary than it was in the lower estuary.

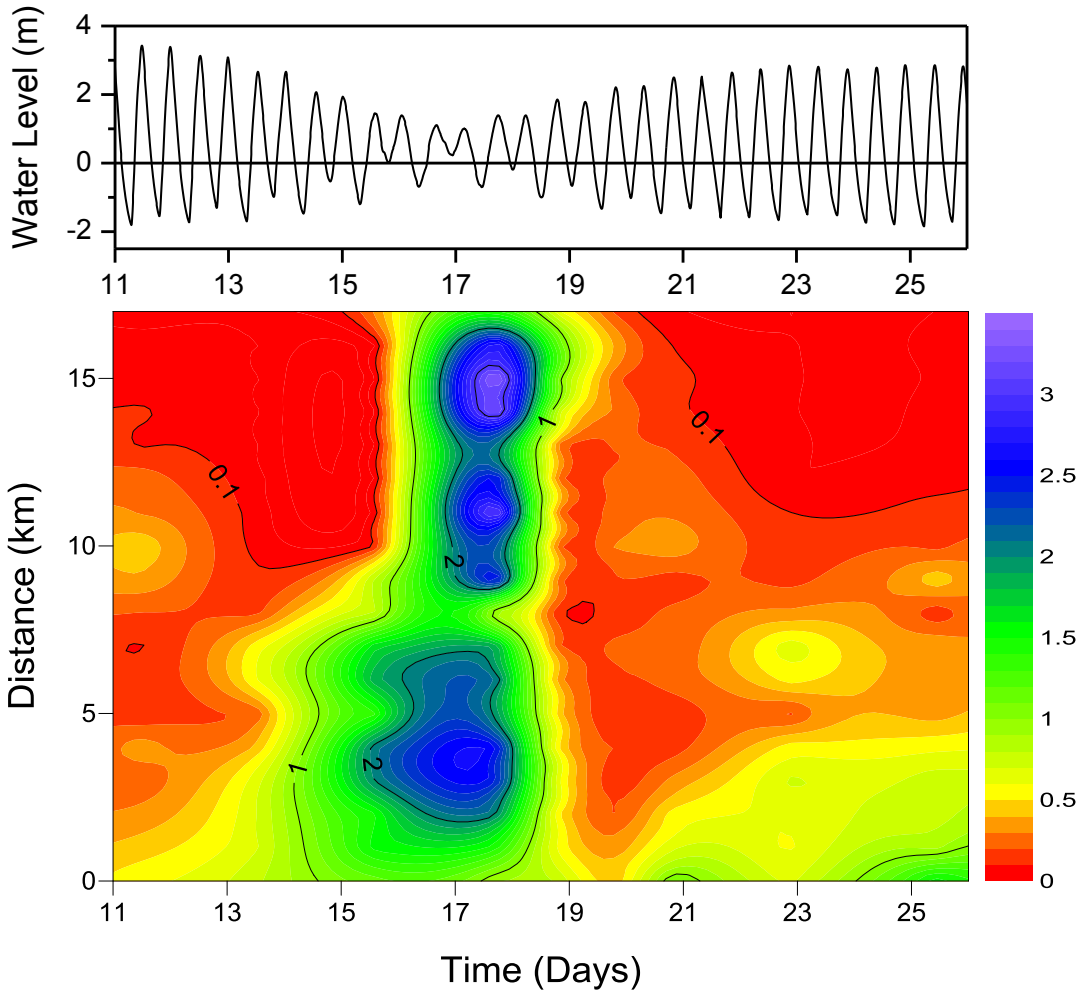

Fig. 3.40 (a) Temporal variation of the water level and (b) spatio-temporal distribution of MS.

The MS was plotted against the depth-averaged SSC for the lower, middle, and upper parts of the estuary (Fig. 3.41). The SSC was correlated with MS in each part of the estuary. When the MS was high (> 1.0), the SSC was around 20 mg/l. A high MS corresponds to a strongly stratified salinity distribution and the stable water body did not generate suspended sediment. The SSC increased with a decrease in the MS, and it reached 1,000 mg/l when the MS decreased to below 0.1. A low MS corresponds to vertically well-mixed conditions, where a strong current can erode the bottom sediment and the turbulence can suspend fine particles.

Furthermore, the relationship varied longitudinally during the spring and half tides. Although the SSC was almost the same in all fields when the MS was lower than 0.01 and was higher than 1.0, the SSC plotted in the transition zone of the MS was different in every field. The SSC in the lower estuary was greater than it was in the

upper estuary. For example, when the MS was 0.1, the SSC was around 900 mg/l, 300 mg/l, and 100 mg/l in the lower, middle, and upper parts of the estuary, respectively.

The difference in SSC for the same MS indicates that suspended sediment was generated more easily in the lower estuary in comparison with the upper estuary. The fact that the maximum and minimum concentrations of suspended sediment were approximately equal in all locations of the estuary and that the midrange concentration was highest in the lower estuary led us to conclude that the bottom sediment in the lower estuary was easily eroded during an acceleration stage (*e.g.*, neap to spring tides) and that suspended sediment did not settle appreciably during a reduction stage (*e.g.*, spring to neap tides). In contrast, the bottom sediment in the upper estuary was stiffer than it was in the lower estuary, and the settling velocity of fine particles in the upper estuary was greater than that in lower estuary.

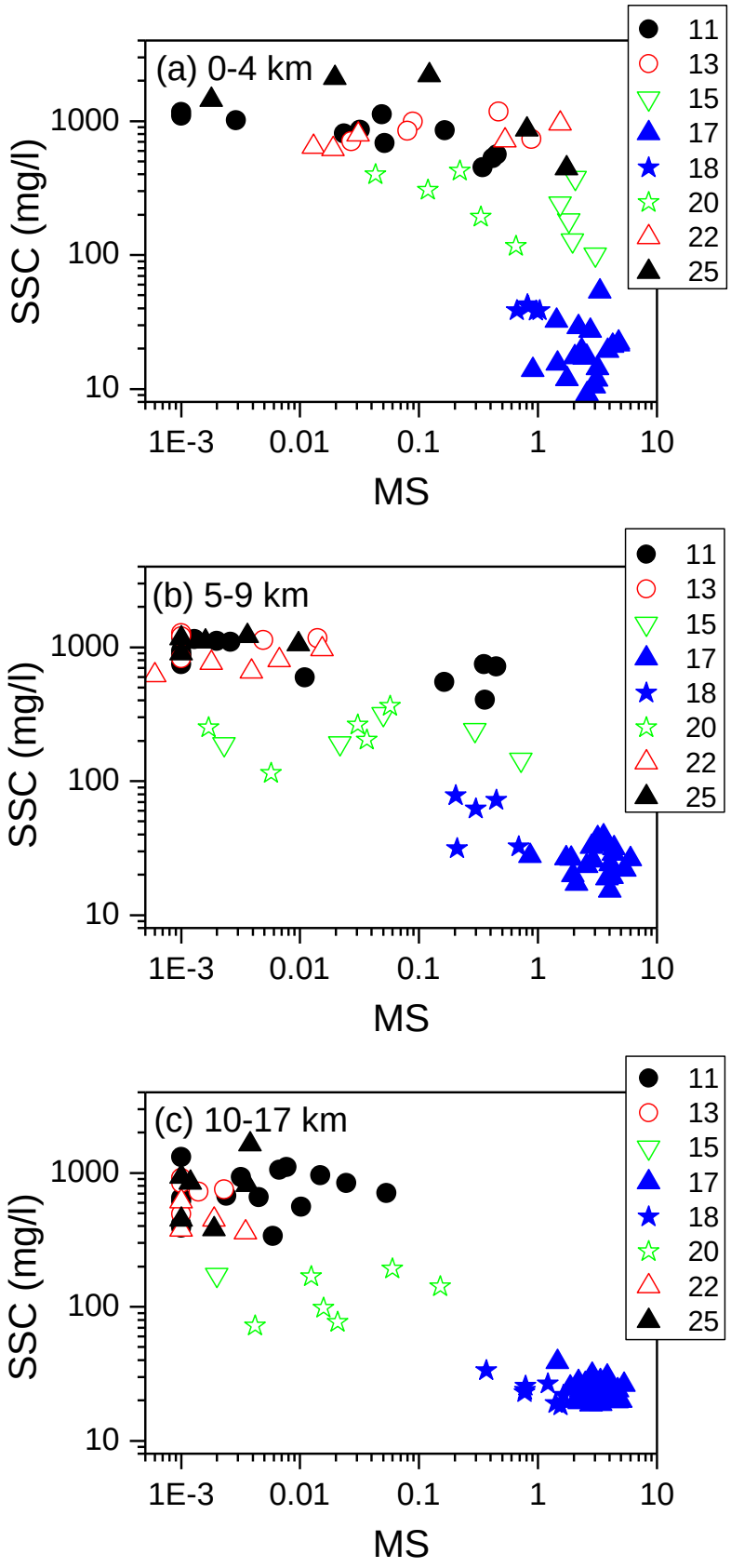

Fig. 3.41 Relationship between MS and depth averaged SSC for (a) the lower estuary, (b) the middle estuary, and (c) the upper estuary.

Trevethan *et al.* (2007) obtained detailed field measurements of turbulence and suspended sediment simultaneously and continuously at high frequency in a small subtropical estuary with semi-diurnal tides. They found that the SSC was dominated mainly by turbulent processes during a flood tide. Xie and Pan (2013) found a linear relationship between bottom shear stress and the SSC in the Yanguan section of the Qiantang River. Andersen *et al.* (2007) estimated the bed shear stress using an acoustic Doppler velocimeter (ADV) at the Kongsmark mudflat, and found that most of the erosion occurred in shallow water, and once the sediment surface was broken, the erosion of the underlying sediment could proceed at a substantially lower bed shear stress. Deloffre *et al.* (2007) reported that bottom shear stress prevented deposition, and the SSC in the water column remained high (up to 1,000 mg/l). Sottolichio *et al.* (2011) also measured SSC and turbulent kinetic energy (TKE) by using high frequency velocity data recorded by an ADV. It was not possible to directly demonstrate the relationship between SSC and TKE from the dataset they obtained.

Although the bottom shear stress and turbulent processes are the direct forces that generate suspended sediment, it is considerably difficult to prepare and mount recording equipment longitudinally. Actually, almost all field measurements on the bottom shear stress were conducted at one or two stations and the longitudinal change of the relationship between bottom shear stress and SSC were scarcely discussed. In contrast, the determination of MS is easily accomplished using a CTD, and we can understand the temporal and spatial characteristics of SSC through the MS.

3.2.5 The ETM Process

Many studies have compared the ETM process on spring and neap tides, and the ETM process has mainly been discussed during spring tides (*e.g.*, Uncles and Stephens, 2010; Wolanski *et al.*, 1995). This study showed the spring-neap transition process in detail and there was sufficient SSC in the intermediate half tides.

The discussion of the relationship between SSC and MS (Fig. 3.41) reached a similar conclusion as that of SSC *vs.* salinity (Fig. 3.39). The main source of suspended sediment in the lower estuary was eroded bottom sediment; on the other hand, the main factor influencing SSC occurrence in the upper estuary was accumulation by salinity intrusion.

Based on the relationship between the flow ratio and SSC, salinity and SSC, and the MS and SSC, the suspended sediment process can be summarized as follows: Suspended sediment is generated when seawater erodes the muddy bed around the river mouth, and it accelerates with a decrease in the flow ratio, i.e., an increase of tidal discharge and a decrease of freshwater discharge. Suspended sediment migrates landward during a flood tide and it forms flocs at the seawater-freshwater interface. The settling velocity of the flocs is larger than that of the single particles that comprise the flocs, and floc particles are deposited on the bottom of the upper estuary. The deposited particles are consolidated and become mud because of the bonding materials contained in the floc particles (Hir *et al.*, 2007; Tolhursf *et al.*, 2002). The erodibility of the bottom sediment in the upper estuary is then reduced compared with the sediment in the lower estuary.

3.3 Conclusions

The spatial distribution and temporal variation of salinity and SSC in the highly turbid Chikugo River estuary, Japan, was continuously measured for two weeks, and the transition process of mixing conditions and ETM process during a semi-lunar tidal cycle were examined. The estuary gradually changed from a vertically well-mixed condition during the spring tide to a strongly stratified condition during the neap tide via a partially mixed condition during intermediate half tides.

The flow ratio of the estuary was significantly affected by both the tidal prism during the semi-lunar tidal cycle and daily freshwater discharge. The SSC was explained by the flow ratio, thus, ETM growth was dominated by both tidal forcing and the freshwater flow, with the exception of the rapid variation of the freshwater discharge following heavy rainfall.

The relationship between salinity and the SSC was investigated longitudinally. In the lower estuary, the SSC was high near the region with a salinity of 10 psu. The SSC was high when salinity was 0.5 psu in the upper estuary. There were two peaks of SSC in the middle estuary when salinity was around 0.5 psu and 10 psu. This suggested there are two processes on suspended sediment occurrence and transport.

The spatio-temporal characteristics of SSC were explained through the MS. The SSC in the lower estuary was higher than in the upper estuary for the same MS. This indicated that bottom sediment in the lower estuary was easily eroded during neap-

spring transition and that suspended sediment did not settle appreciably during spring-neap transition. In contrast, the settling velocity of fine particles in the upper estuary increased due to flocculation.

Based on the flow ratio, salinity and MS, the occurrence of the ETM and its development at the macrotidal Chikugo river estuary was a consequence of three processes: bed sediment erosion by sea water in the lower estuary, sediment transport in the estuarine channel by the tidal current and freshwater flow, and sediment accumulation at the salinity front in the upper estuary.

Chapter 4

Effect of Estuarine Mixing and ETM on the Phytoplankton Process

This chapter includes the studies about the influence of estuarine mixing and ETM on the phytoplankton process.

Abstract

Spatial distribution and temporal variation of salinity, suspended sediment concentration (SSC) and chlorophyll pigments in the macro-tidal Chikugo river estuary, Japan, were measured for two weeks and investigated the effect of salinity mixing and the estuarine turbidity maximum (ETM) on the state of phytoplankton. The estuary was in a vertically well-mixed condition during spring tide with SSC exceeded 1,000 mg/l. The estuary changed to stratified condition during the neap tide with SSC of less than 20 mg/l. Strong relation between light attenuation coefficient (K) and SSC indicate that the SSC was the key driver of light availability in the Chikugo river estuary. Although light scarcely penetrated into the water column during spring tide, a definite quantity of living phytoplankton (Chl-a) existed throughout the semilunar tidal cycle. Mean concentration of Chl-a in the daytime and in the upper estuary against the ratio of photic depth to mixing depth (Zp:Zm ratio) showed the hysteresis loop and it was found that phytoplankton growth has a time lag of three days. Good relationship between surface salinity reach (SSR) and Chl-a length showed that the phytoplankton mainly inhabit in brackish water below 1psu. Pheo-a (dead phytoplankton cells) had high correlation for SSC, K and Zp:Zm ratio. This shows that phytoplankton deactivation and Pheo-a production were caused by the light limitation due to suspended sediment. Good relationship between location of Surface SSC maximum (SSM) and Pheo-a length indicated that the detritus migrated by adhering to inorganic sediment. It was concluded that estuarine mixing, development of the ETM and phytoplankton process interact.

Content of this chapter was constructed from following papers:

Azhikodan, G. and Yokoyama, K. 2014. Estuarine Mixing and Spatial Distribution of Phytoplankton in the Chikugo River Estuary, *Journal of JSCE, Ser. B2 (Coastal Engineering)*, Accepted.

4.1 Results

4.1.1 Weather

The time series of the water level at the station 14.6 km upstream, daily solar radiation, mean wind speed, hourly river discharge and hourly rainfall during the field measurements are shown in Fig. 4.1. The shaded area in the water level indicates the actual measurement time during the period of the field survey.

On September 11 and 25, a spring tide occurred with a tidal range of 5.1 m and 4.7 m, respectively. A neap tide occurred on September 17 with a tidal range of 2 m (Fig. 4.1a). Amount of solar radiation was also very high during most of the days with the exception of rainy days (Fig. 4.1b). The mean wind speed was greater than 4 m/s during spring tides (September 11, 12, and 23 to 25). The wind speed was 2 m/s during September 13 to 22 (Fig. 4.1c). Rainfall events of upto 20 mm occurred on September 13, 22, and 23. A sudden peak discharge on September 13 and 23 was observed due to these rainfall events. The freshwater discharge patterns revealed significant temporal variations with the influence of rainfall. Freshwater discharges in the Chikugo River estuary in the period from September 11 to 25 ranged from 50 m^3/s (during the normal period) to more than 300 m^3/s during rainy days (Fig. 4.1d).

As it was mentioned in Chapter 3, the physical and biological process in an estuary are significantly affected by the influence of both freshwater and seawater. The tidal flow in the Chikugo river estuary is 5–50 times larger than the freshwater discharge.

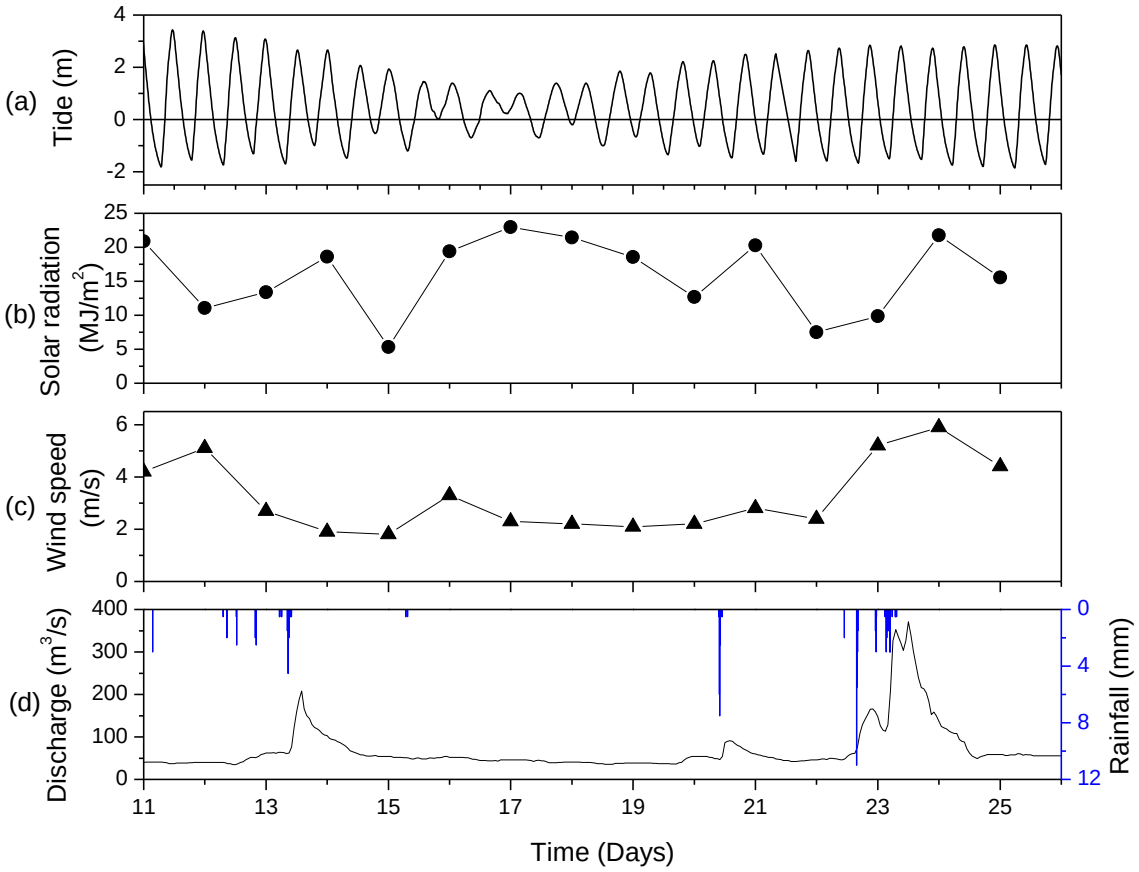

Fig. 4.1 Weather conditions of the study area during September 11 to 25, 2010.

4.1.2 Relationship between in-situ Chl-a and analysed phytoplankton

The in-situ Chl-a concentration by fluorescent sensor was plotted against the analysed Chl-a concentration in laboratory (Fig. 4.2). There was no relationship found between in-situ Chl-a and analysed Chl-a during September 11 (Fig. 4.2a), 13 (Fig. 4.2b), and 15 (Fig. 4.2c). That means the in-situ sensor may catch not only Chl-a but also some inorganic matter or dead phytoplankton. The relation was better during neap tide and it becomes good during September 20, 22, and 25. The slope indicates the proportion of actual Chl-a content in the in-situ Chl-a value and it changed gradually.

The in-situ Chl-a concentration by fluorescent sensor was plotted against the analysed Pheo-a concentration in laboratory (Fig. 4.3). The relation was good during September 11, 13, 22, and 25 where those days have high tidal amplitude. The relation was bad during half tides and neap tide.

In-situ Chl-a sensor directly measure the reflection from the total suspended matter in the water which may include living phytoplankton, deactivated phytoplankton

and suspended sediment. For the laboratory analysis, fluorometer measures the reflection of Chl-a extracted in the DMF. The laboratory analysis will give the accurate result of Chl-a concentration. Therefore, Fig. 4.2 and Fig. 4.3 indicate the activity of phytoplankton and components of suspended matter.

In general, high correlation was found between Chl-a concentration measured by in-situ sensor and that by laboratory analysis, thus, Chl-a concentration in water column was obtained from in-situ fluorescent sensorquickly by using regression equation. Although relationship between two Chl-a values was found in each day, the relationship changed gradually. It was hard to estimate the temporal and spatial Chl-a distribution collectively by using in-situ sensor in the Chikugo river estuary. Therefore, analyzed Chl-a concentration at the water surface was applied for the following investigation.

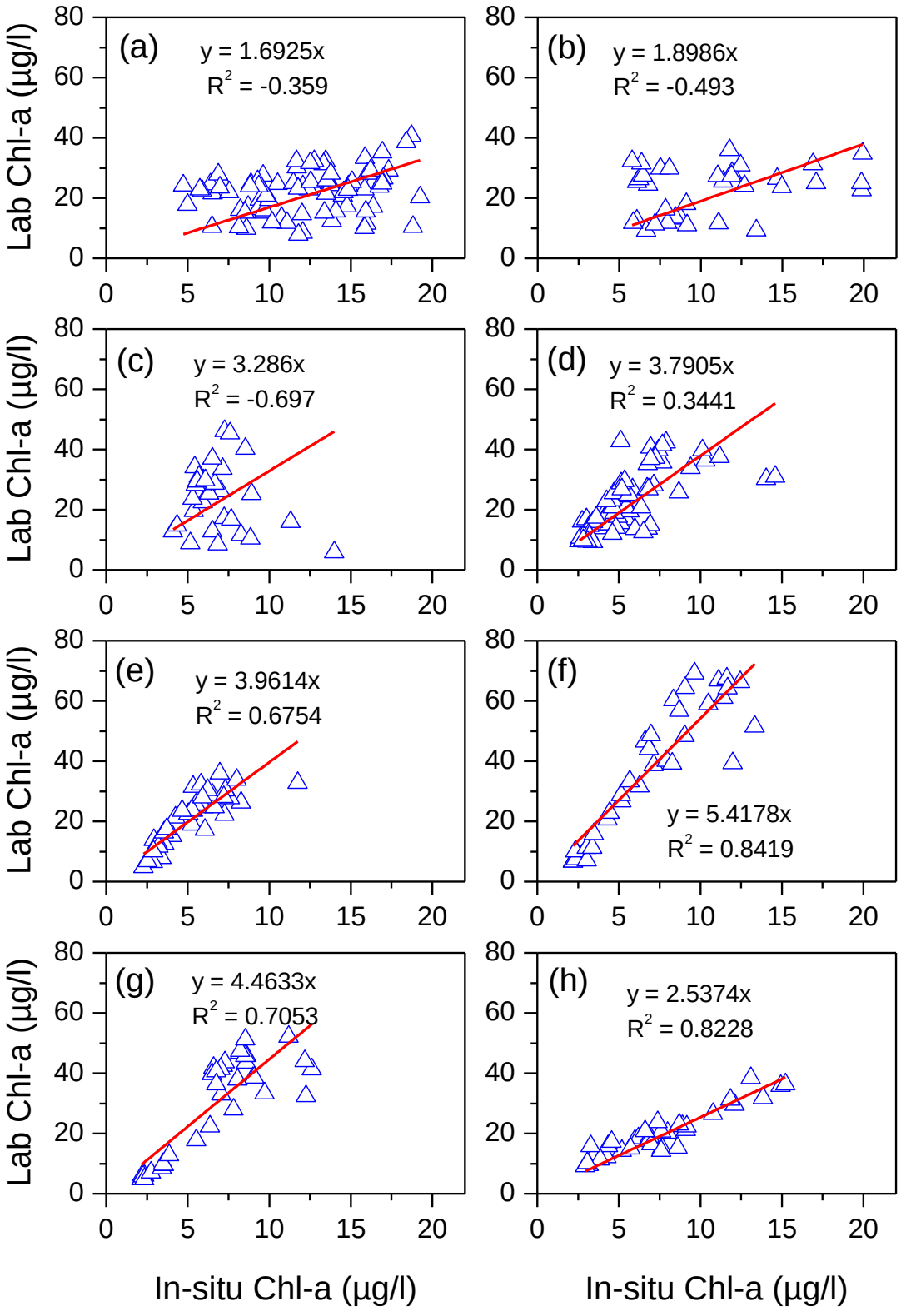

Fig. 4.2 In-situ Chl-a (surface) vs laboratory analysed Chl-a (surface) for (a) September 11, (b) September 13, (c) September 15, (d) September 17, (e) September 18, (f) September 20, (g) September 22, and (h) September 25.

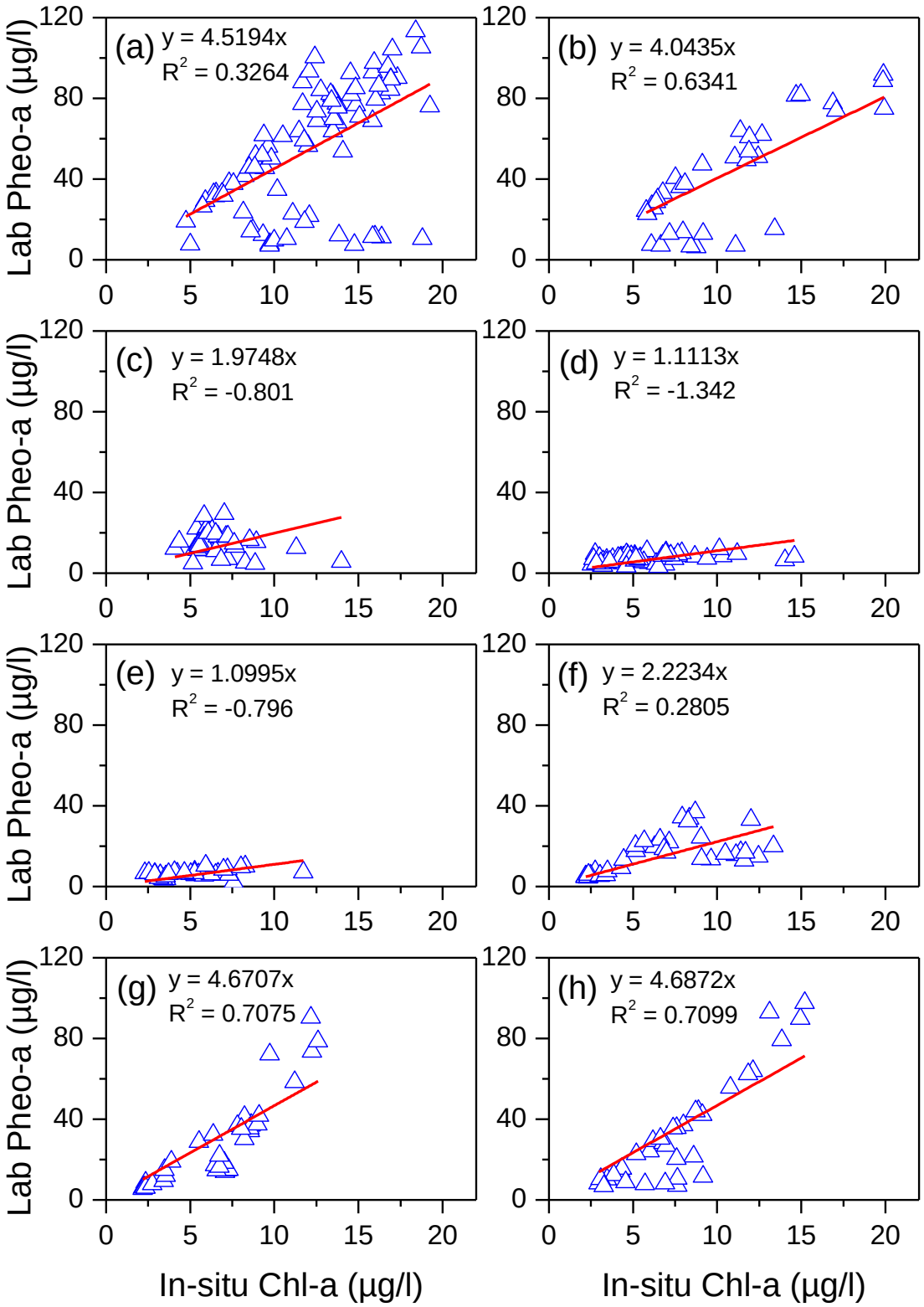

Fig. 4.3 In-situ Chl-a (surface) vs laboratory analysed Pheo-a (surface) for (a) September 11, (b) September 13, (c) September 15, (d) September 17, (e) September 18, (f) September 20, (g) September 22, and (h) September 25.

4.1.3 Spring - Neap - Spring Transition

The temporal variation of the tide, vertical and horizontal spatial distributions of the salinity, SSC and light intensity, and longitudinal distribution of Chl-a (surface) and Pheo-a (surface) during each tidal cruise of the fortnightly tidal cycles (September 11 to 25) were shown in Fig. 4.4 to Fig. 4.36. The blue shade on the tide shows the time of measurement for respective cruise. Since the distributions of salinity and SSC were discussed in section 3.1.2, the distribution of light, Chl-a and Pheo-a were described mainly in this section.

(a) Spring Tide to Neap Tide Transition

During spring tide the light intensity in the water column was very low during low water (Fig. 4.4d and Fig. 4.5d) and flood water (Fig. 4.6d) because of the extreme turbidity with an SSC of 1000 to 2000 mg/l (Fig. 4.4c to Fig. 4.6c). There was increase in light intensity during the high water (Fig. 4.7d) when the suspended sediment was started to deposit and the surface layer SSC decreased to <100 mg/l for the stations 0 to 11 km (Fig. 4.7c). Again the light intensity starts to decrease during the ebb phase (Fig. 4.8d) when the SSC started to exceed 250 mg/l with strong currents (Fig. 4.8c). A definite quantity of Chl-a (10–40 µg/l) was existed during spring tide despite the strong currents and light limitations (Fig. 4.4e to Fig. 4.10e). Amount of Pheo-a was more than 50 µg/l most of the time and sometimes it exceeded 100 µg/l. There was an exception that both Chl-a and Pheo-a was decreased during high water when the estuary was filled with intruded seawater (Fig. 4.7e). The position of highest Pheo-a was coincided with the ETM zone. During spring tide estuary was vertically homogenous salinity distribution with weak vertical stratification.

During spring tides (September 11 and 25) and half tides (September 13, 15, 20 and 22) salinity intrusion was showing an increasing trend towards upstream as the tidal phase changes from low water to high water and going back seaward during the ebb water.

The salinity intrusion and movement of ETM during the half tides 13 (Fig. 4.11 to Fig. 4.13) and 15 (Fig. 4.14 to Fig. 4.16) were found similar to the spring tide. During September 13, the tidal amplitude decreased to 4.1 m (Fig. 4.11a to Fig. 4.13a) and the SSC in the ETM zone was nearly 1000 mg/l (Fig. 4.11c to Fig. 4.13c). Therefore light intensity in the water column was limited during low water (Fig. 4.11d) and flood water

(Fig. 4.12d). There was an increase in light intensity during high water (Fig. 4.13d) when the SSC was decreased in the lower estuary (Fig. 4.13c). The Chl-a and Pheo-a during low water (Fig. 4.11e) were similar to the spring tide. During high water Pheo-a decreased drastically and Chl-a was also decreased (Fig. 4.13e).

Then during the following half tide (September 15), the tidal amplitude decreased to 2.4 m (Fig. 4.14a to Fig. 4.16a) and the SSC in the maximum zone decreased to 500 mg/l (Fig. 4.14c to Fig. 4.16c). The amount of light in the water column was started to increase when the tidal phase changes from low water (Fig. 4.14d) to high water (Fig. 4.16d). Because of this amount of Pheo-a was very less and a small increase in amount of Chl-a was seen (Fig. 4.14e and Fig. 4.16e).

The light intensity in the water column was very high throughout the neap tidal cycle (Fig. 4.17d to Fig. 4.23d) as the estuarine water was found very clear with an SSC of 20–50 mg/l (Fig. 4.17c to Fig. 4.23c). Therefore, amount of Pheo-a were less than 10 µg/l throughout the day. The Chl-a was 10 – 18 µg/l in the morning (Fig. 4.17e) and then it gradually increases during the day time with the favorable conditions of weak currents, low SSC, and light availability. Chl-a concentration reached 10 – 40 µg/l in the evening (Fig. 4.21e and Fig. 4.23e).

(b) Neap Tide to Spring Tide Transition

The light intensity was very during September 18 (Fig. 4.24d and Fig. 4.25d) as it was during neap tide because of the low SSC in the water column (Fig. 4.24c to Fig. 4.26c). Distribution of Chl-a and Pheo-a during low water (Fig. 4.24e) were similar to their distributions during neap tide. Amount of Chl-a becomes < 13 µg/l at 5 km to 12 km during the night time (Fig. 4.26e).

During September 20 the light intensity was relative high at low water (Fig. 4.28d) with low SSC (Fig. 4.28c). However it was less compared with September 17 and 18. The light intensity further decreased during the flood water (Fig. 4.29d) with an increase in SSC up to 500 mg/l (Fig. 4.29c) in the lower estuary. The measurement during flood water was carried out in the evening and high water in the night (Fig. 4.29a and Fig. 4.30a). This was additional reason for decrease in light intensity during flood water and no data during high water. Amount of Chl-a reached maximum value of 50 – 70 µg/l most part of the estuary during low water in the day time despite the increase in

tidal amplitude (Fig. 4.28e). The Pheo-a concentration was also increased to 13 – 36 µg/l. The Chl-a and Pheo-a decreased during high water in the night time (Fig. 4.30e).

The salinity and SSC distribution during September 22 (Fig. 4.31 to Fig. 4.33) were found similar to their distributions during September 13 (Fig. 4.11 to Fig. 4.13). During September 22, there was some light available in the surface layer at low water (Fig. 4.31d) with an SSC of more than 500 mg/l. The light availability was totally limited during flood water (Fig. 4.32d) because of increase in SSC (500–1000 mg/l) and the approach of sunset. There was no light data during high water (Fig. 3.33d) due to the measurement at night time. The Chl-a during low water was 32–52 µg/l with Pheo-a concentration of 30–90 µg/l for 0 to 9 km and approximately 15 µg/l for upper estuary (Fig. 4.31e). Both Chl-a and Pheo-a decreased during high water and it was slightly high in the upper estuary (4.33e).

During September 25, the measurement at the low water was carried out before sunrise and the light data was not available (Fig. 4.34d). At flood water the light intensity was limited with high SSC of 1000–2000 mg/l despite the strong solar radiation on the surface (Fig. 4.35d). The light intensity was increased at high water for the lower estuary (Fig. 4.36d) as the SSC in the lower estuary becomes <100 mg/l (Fig. 4.36c). A definite quantity of Chl-a (10–30 µg/l) were existed at both low water (Fig. 4.34e) and high water (Fig. 4.36e) with high Pheo-a concentration.

Throughout the semilunar tidal cycle, the peak Chl-a was seen landward of the freshwater-salt water interface. Also the peak Pheo-a was seen near the ETM zone.

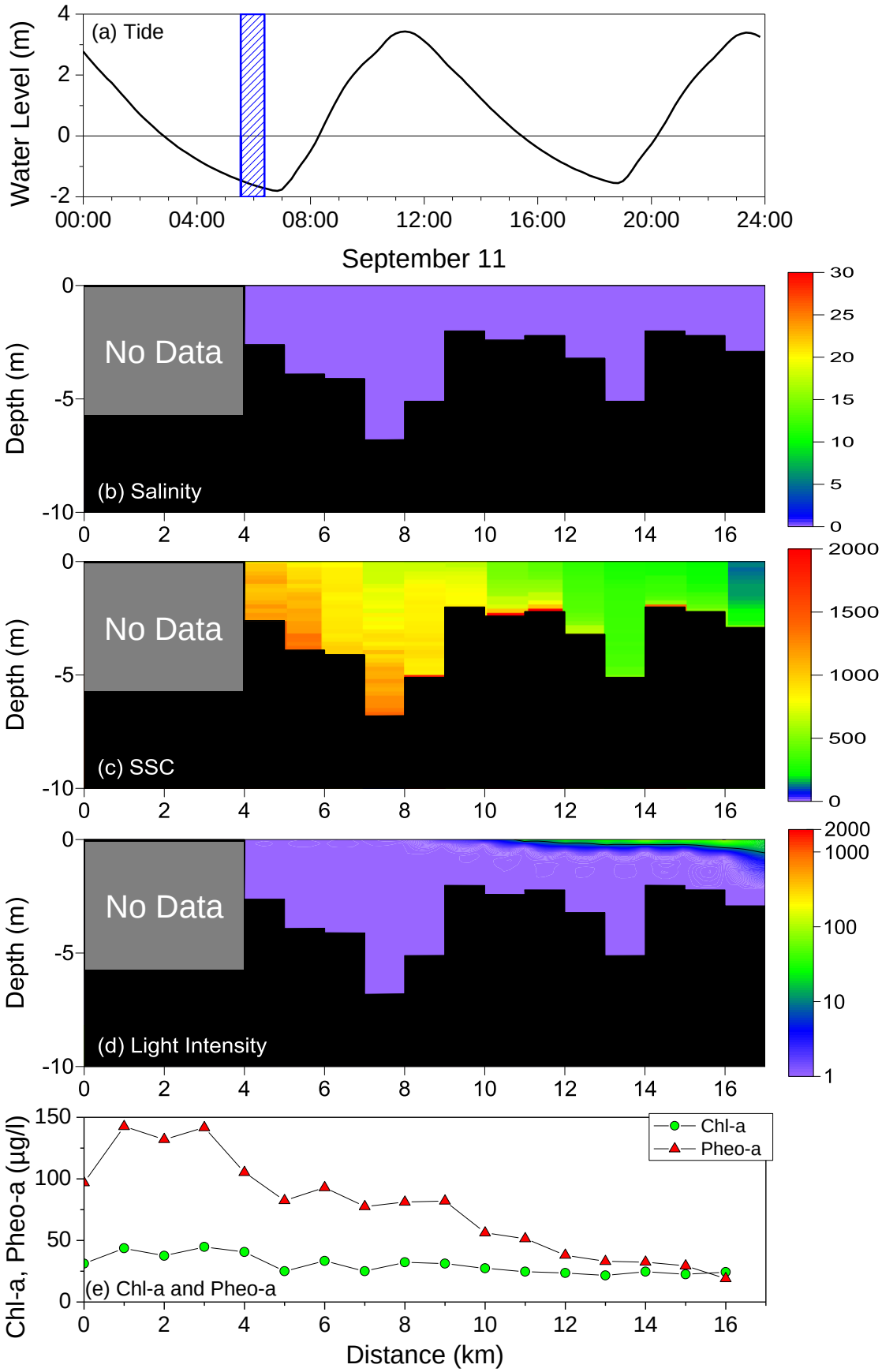

Fig. 4.4 (a) temporal variation of tide; longitudinal and vertical distributions of (b) salinity in psu, (c) SSC in mg/l, and (d) light intensity in µmol/m^{2}s; and (e) longitudinal distributions of Chl-a (surface) and Pheo-a (surface) during September 11 (Round 1).

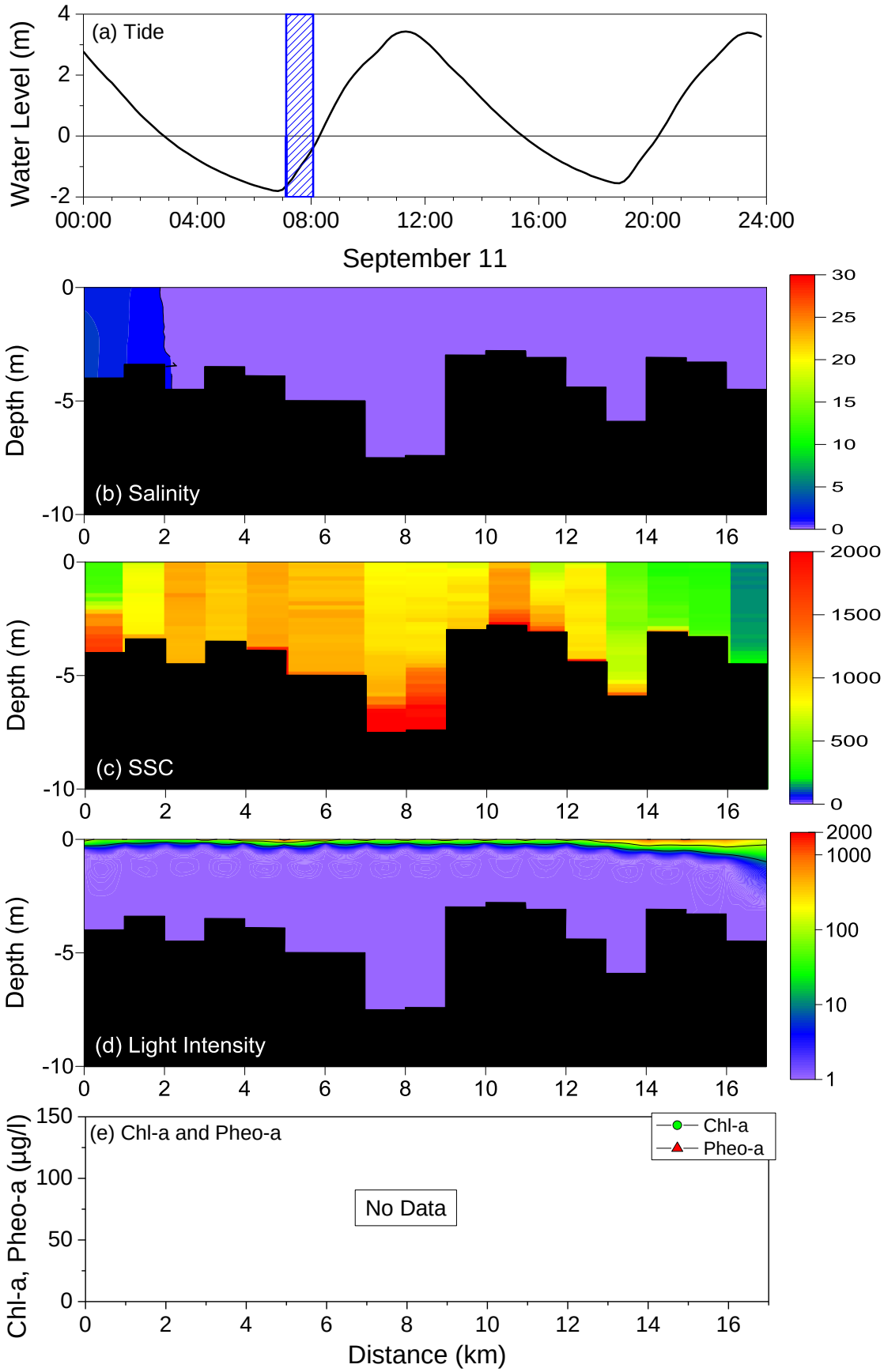

Fig. 4.5 (a) temporal variation of tide; longitudinal and vertical distributions of (b) salinity in psu, (c) SSC in mg/l, and (d) light intensity in µmol/m^{2}s; and (e) longitudinal distributions of Chl-a (surface) and Pheo-a (surface) during September 11 (Round 2).

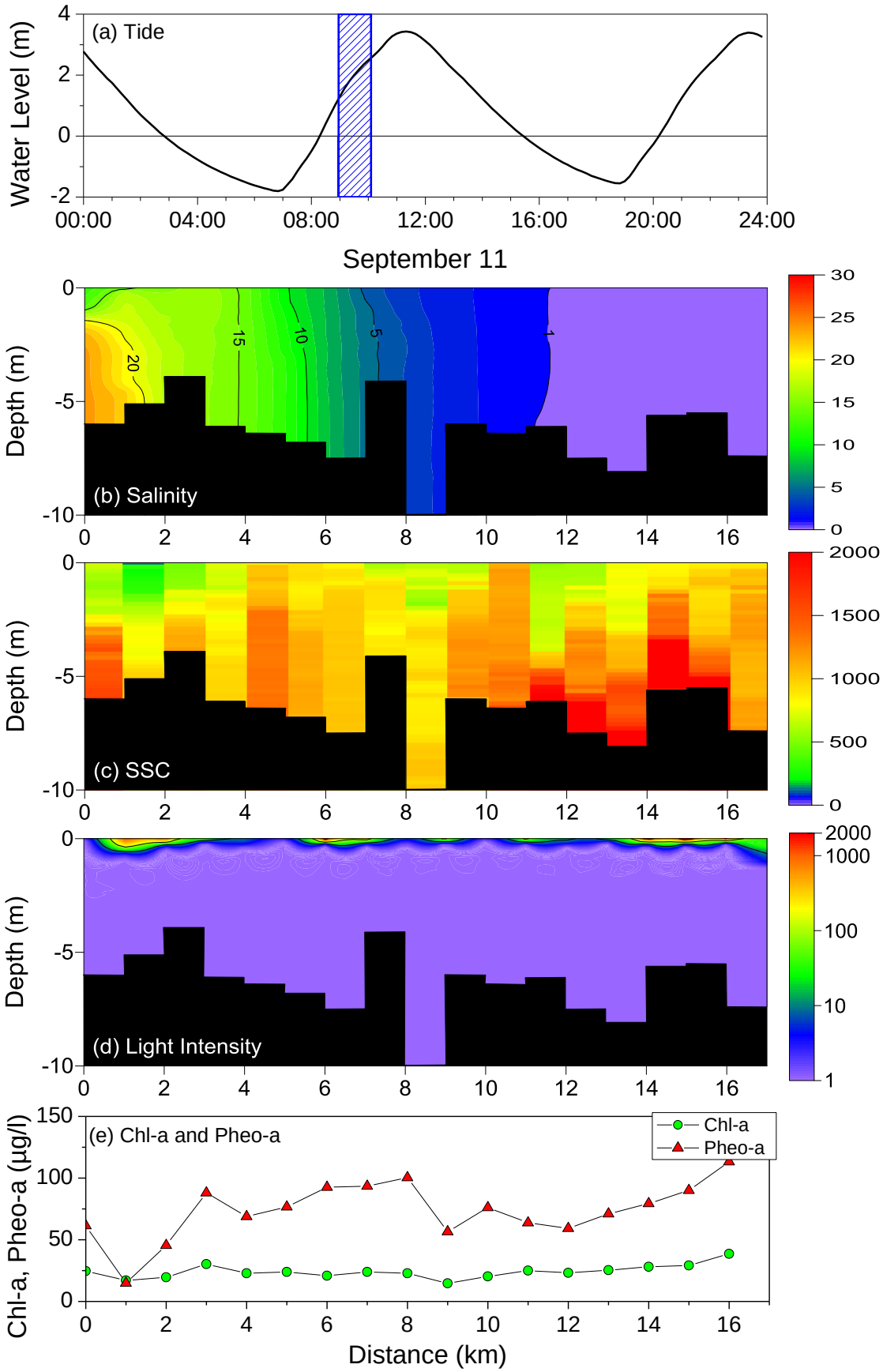

Fig. 4.6 (a) temporal variation of tide; longitudinal and vertical distributions of (b) salinity in psu, (c) SSC in mg/l, and (d) light intensity in µmol/m^{2}s; and (e) longitudinal distributions of Chl-a (surface) and Pheo-a (surface) during September 11 (Round 3).

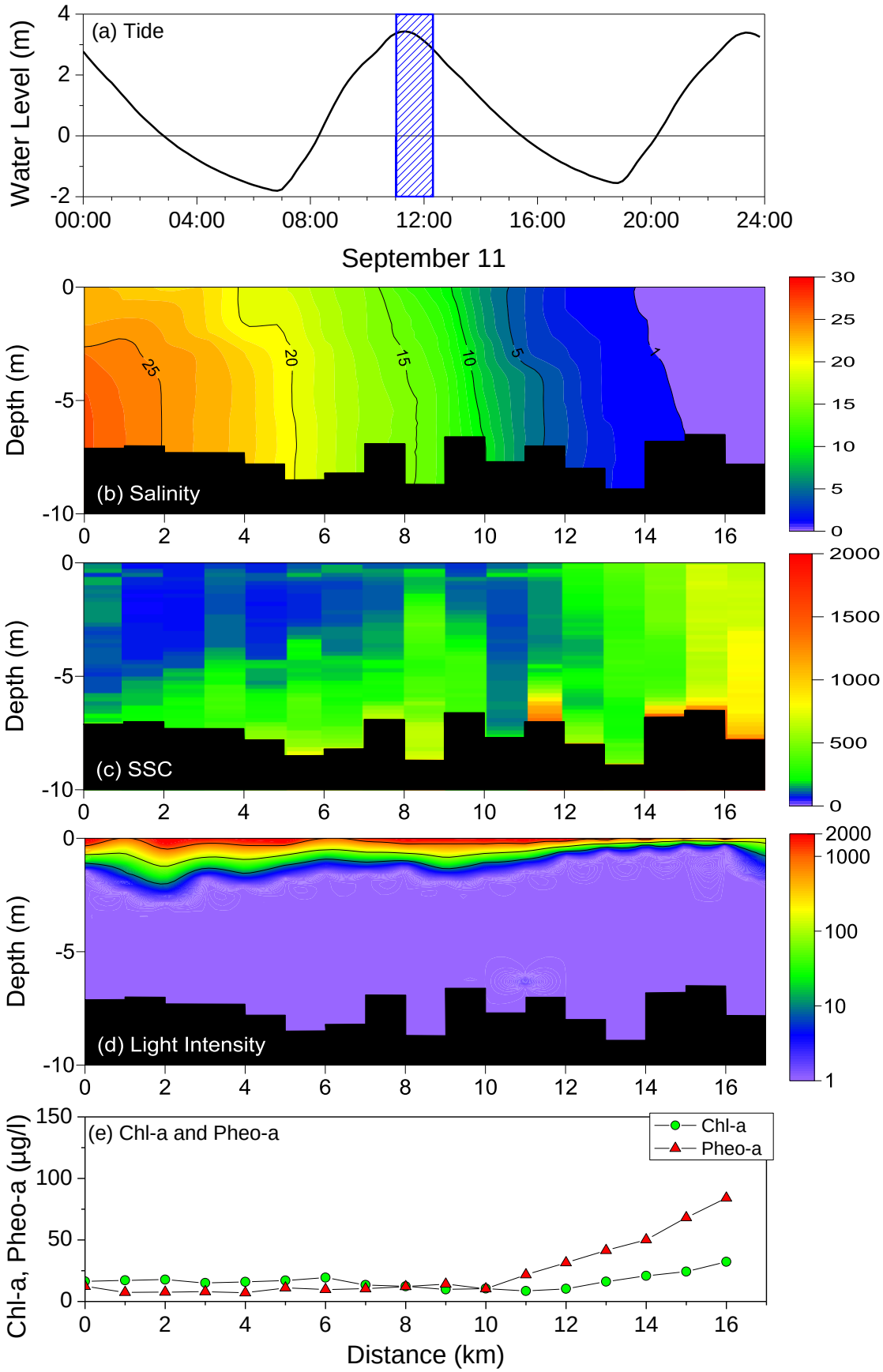

Fig. 4.7 (a) temporal variation of tide; longitudinal and vertical distributions of (b) salinity in psu, (c) SSC in mg/l, and (d) light intensity in µmol/m^{2}s; and (e) longitudinal distributions of Chl-a (surface) and Pheo-a (surface) during September 11 (Round 4).

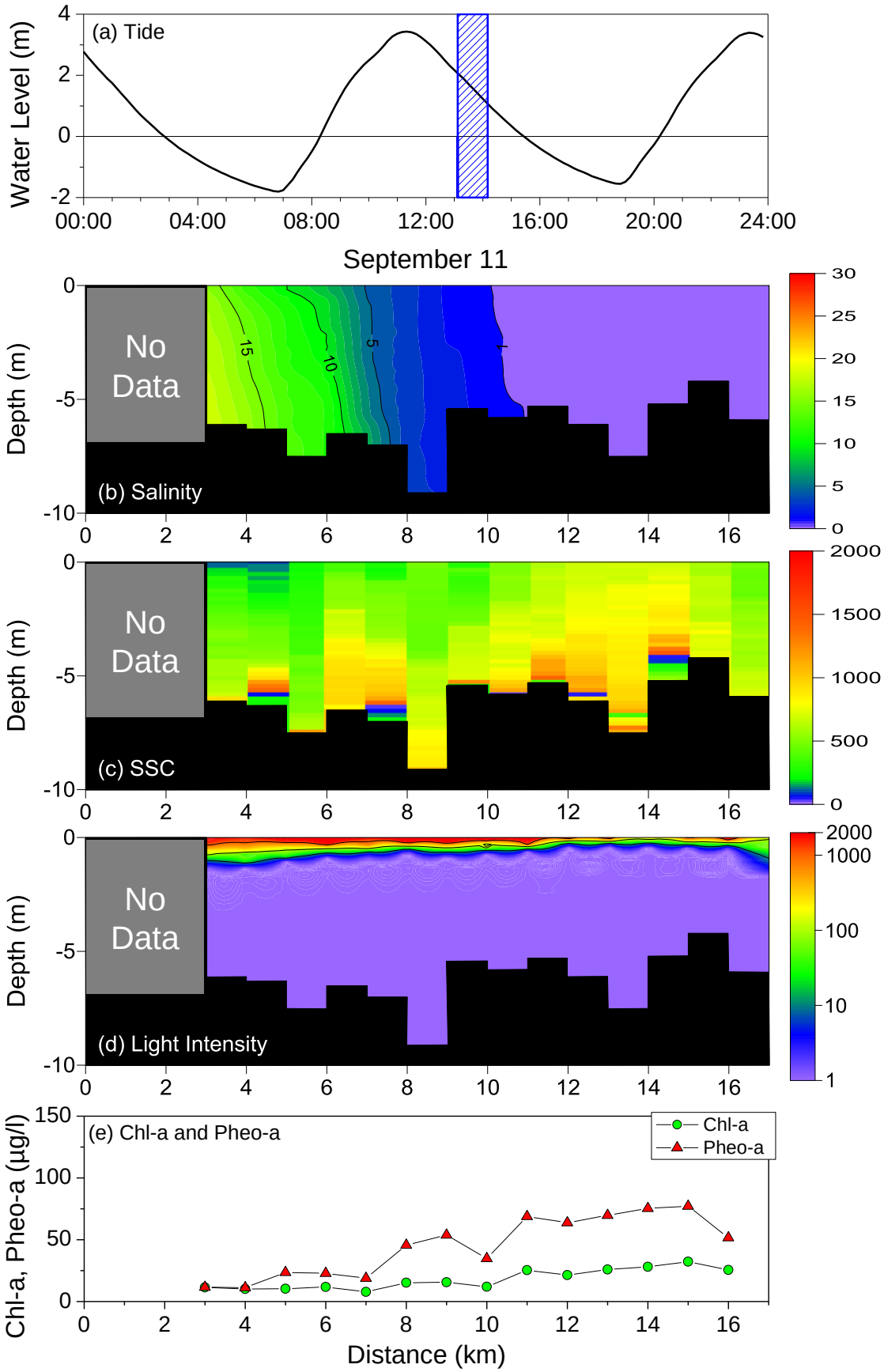

Fig. 4.8 (a) temporal variation of tide; longitudinal and vertical distributions of (b) salinity in psu, (c) SSC in mg/l, and (d) light intensity in µmol/m^{2}s; and (e) longitudinal distributions of Chl-a (surface) and Pheo-a (surface) during September 11 (Round 5).

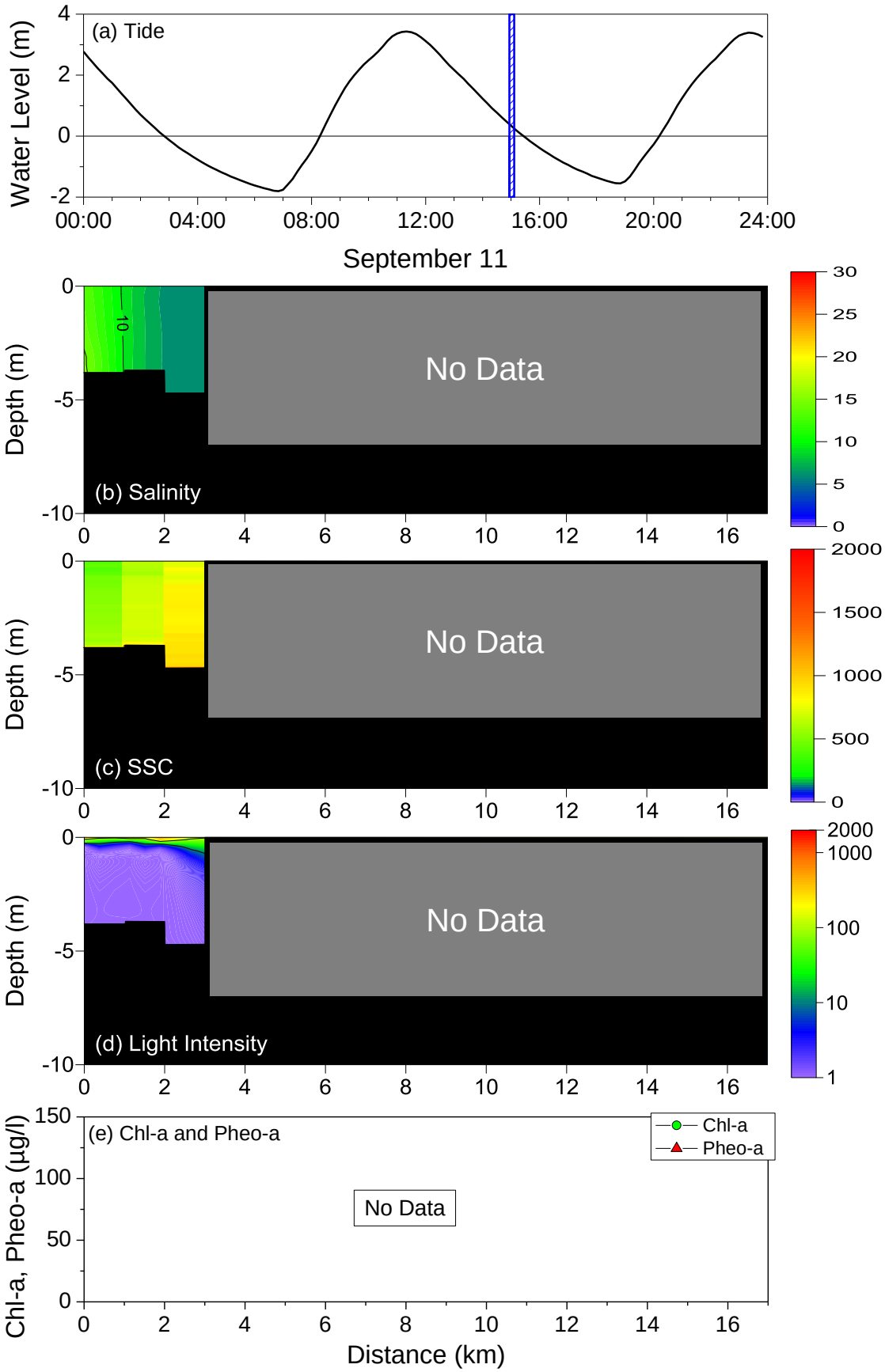

Fig. 4.9 (a) temporal variation of tide; longitudinal and vertical distributions of (b) salinity in psu, (c) SSC in mg/l, and (d) light intensity in µmol/m^{2}s; and (e) longitudinal distributions of Chl-a (surface) and Pheo-a (surface) during September 11 (Round 6).

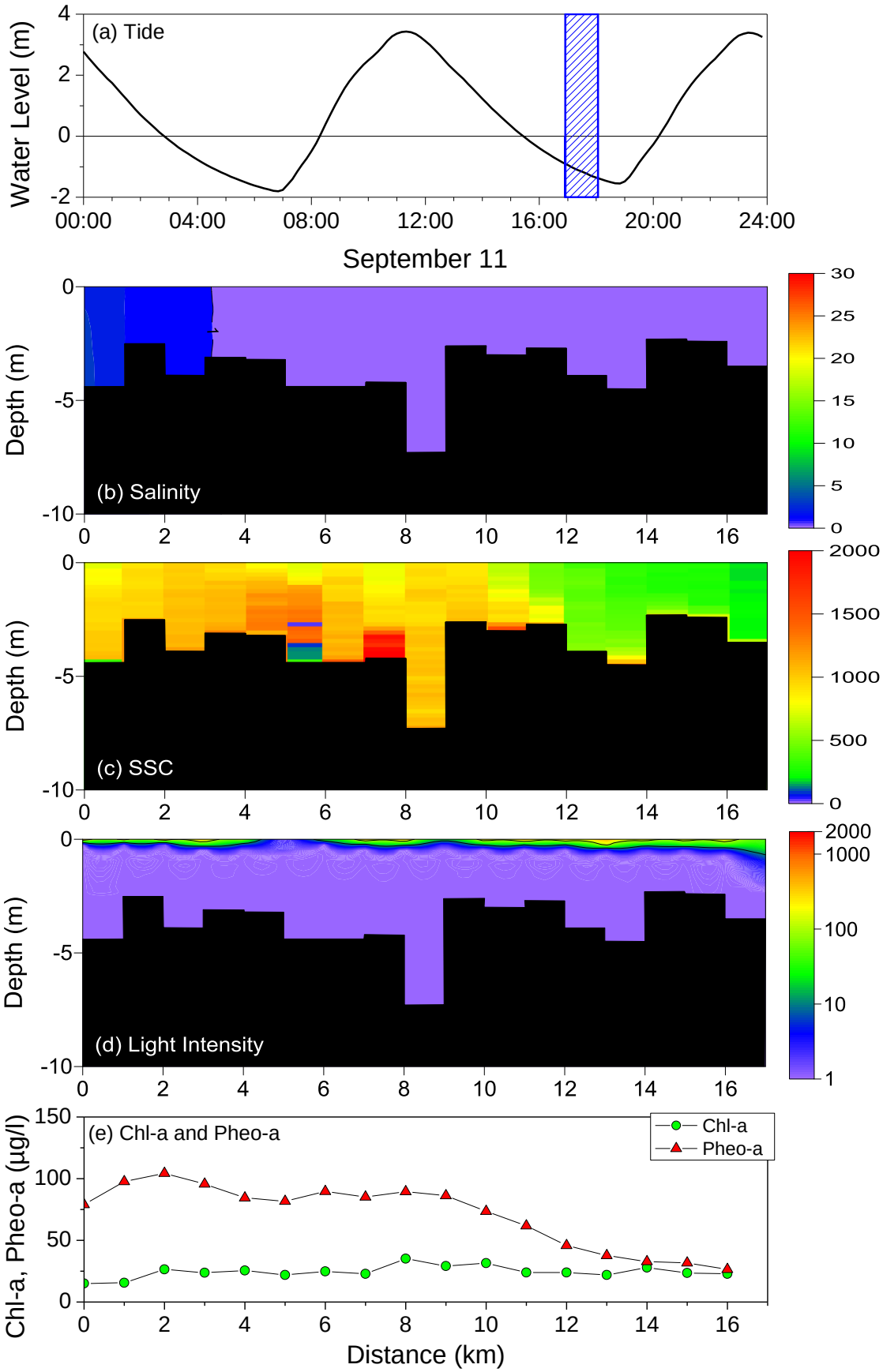

Fig. 4.10 (a) temporal variation of tide; longitudinal and vertical distributions of (b) salinity in psu, (c) SSC in mg/l, and (d) light intensity in µmol/m^{2}s; and (e) longitudinal distributions of Chl-a (surface) and Pheo-a (surface) during September 11 (Round 7).

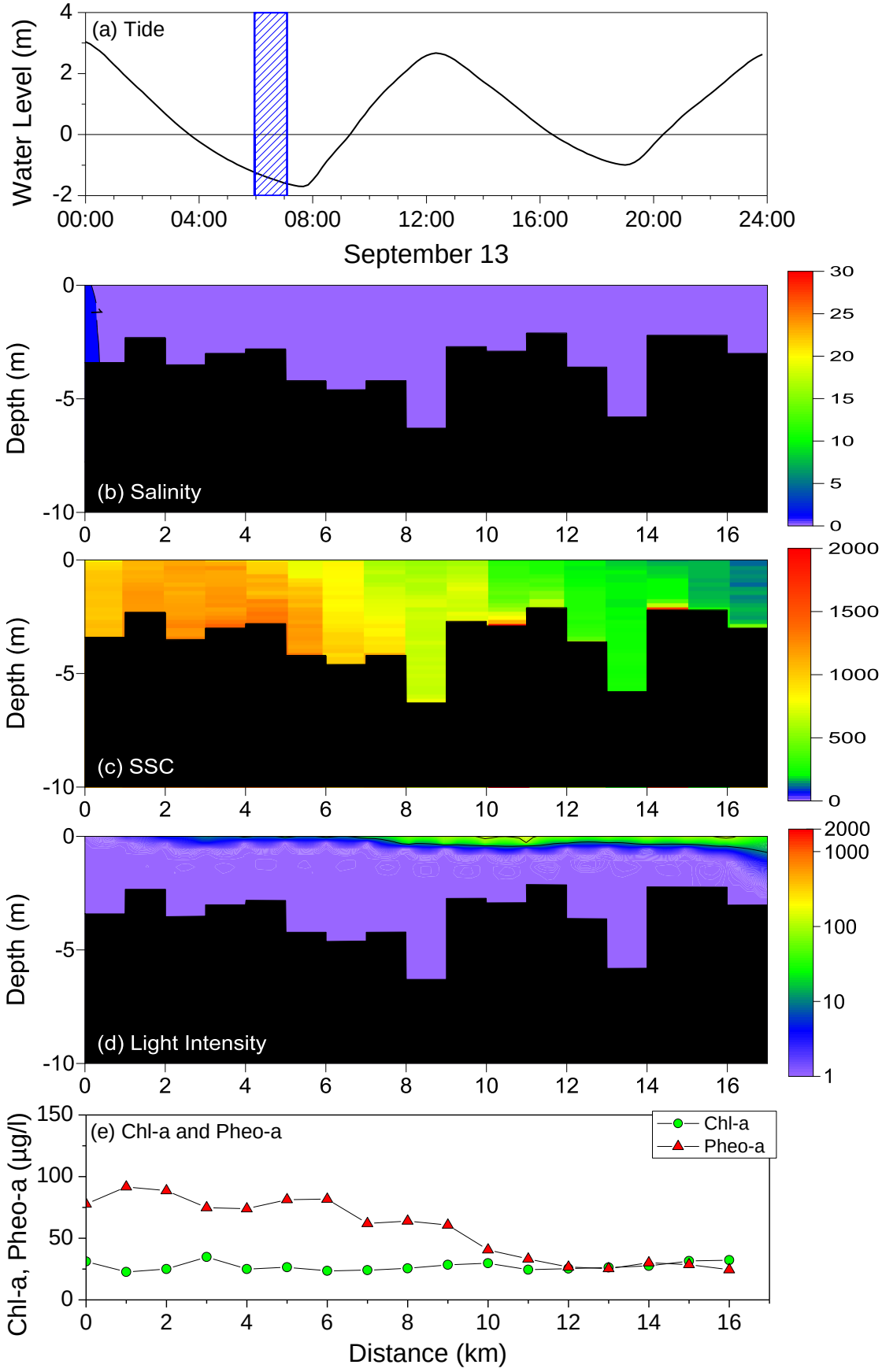

Fig. 4.11 (a) temporal variation of tide; longitudinal and vertical distributions of (b) salinity in psu, (c) SSC in mg/l, and (d) light intensity in µmol/m^{2}s; and (e) longitudinal distributions of Chl-a (surface) and Pheo-a (surface) during September 13 (Round 1).

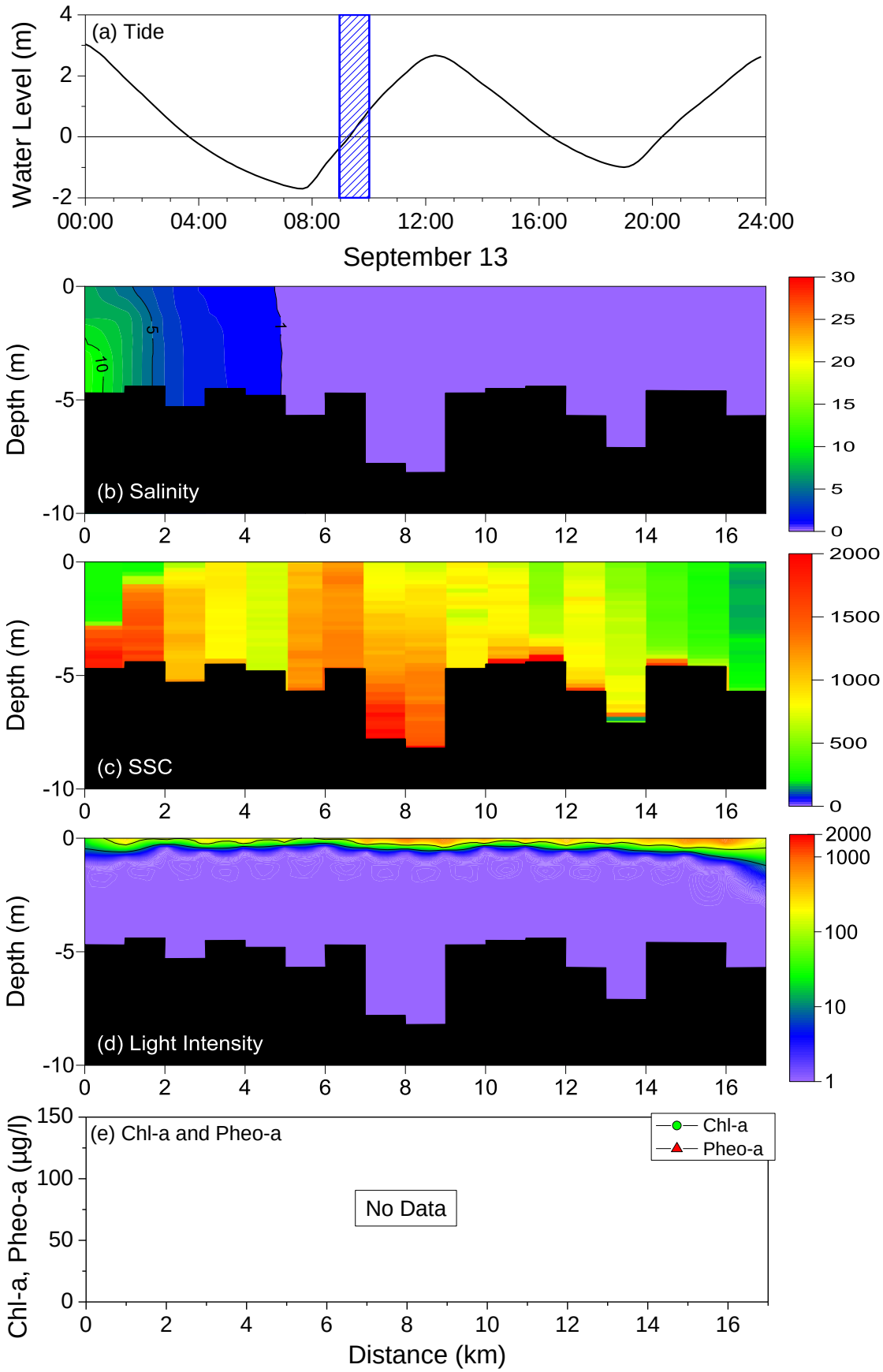

Fig. 4.12 (a) temporal variation of tide; longitudinal and vertical distributions of (b) salinity in psu, (c) SSC in mg/l, and (d) light intensity in µmol/m^{2}s; and (e) longitudinal distributions of Chl-a (surface) and Pheo-a (surface) during September 13 (Round 2).

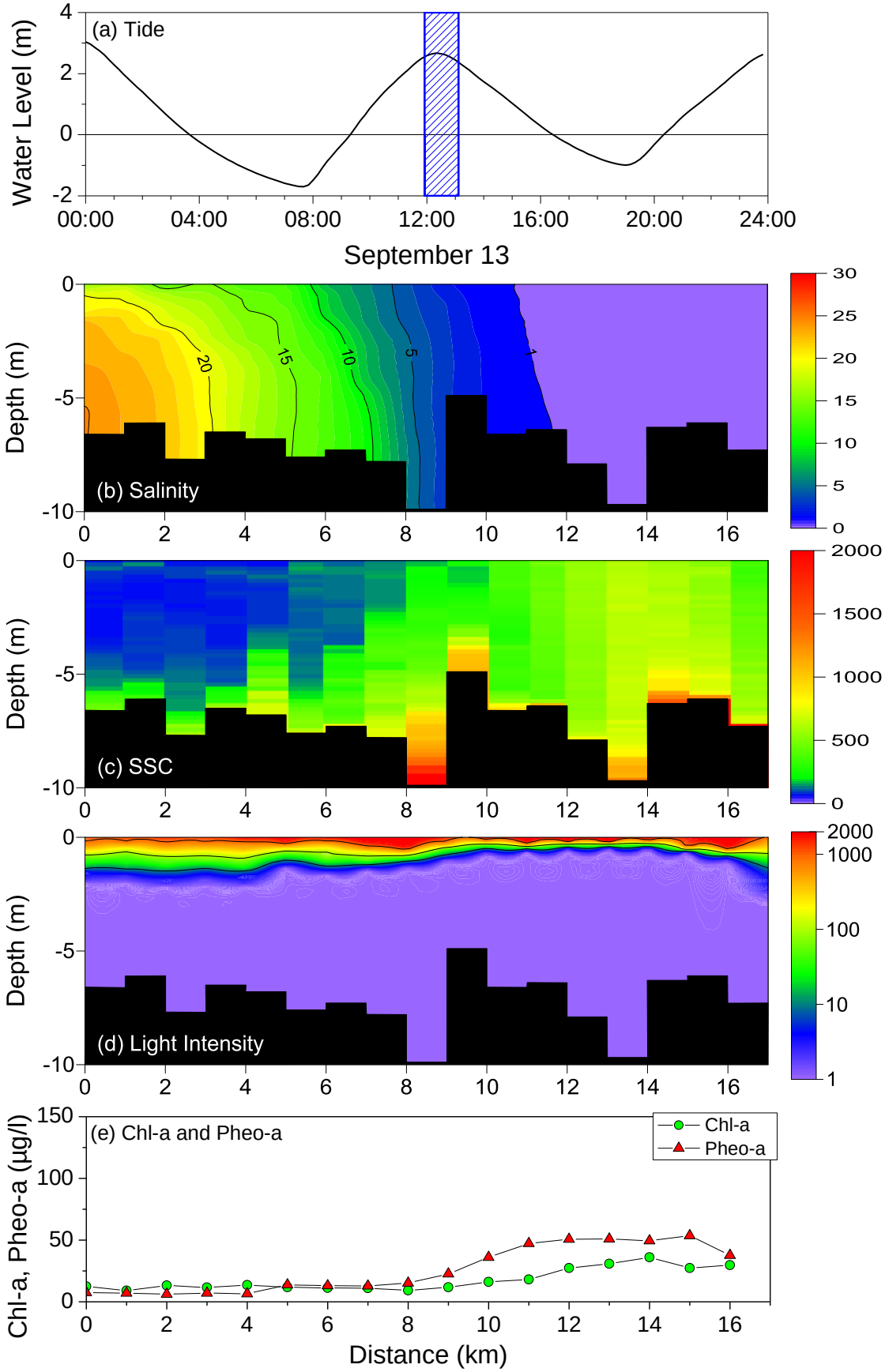

Fig. 4.13 (a) temporal variation of tide; longitudinal and vertical distributions of (b) salinity in psu, (c) SSC in mg/l, and (d) light intensity in µmol/m^{2}s; and (e) longitudinal distributions of Chl-a (surface) and Pheo-a (surface) during September 13 (Round 3).

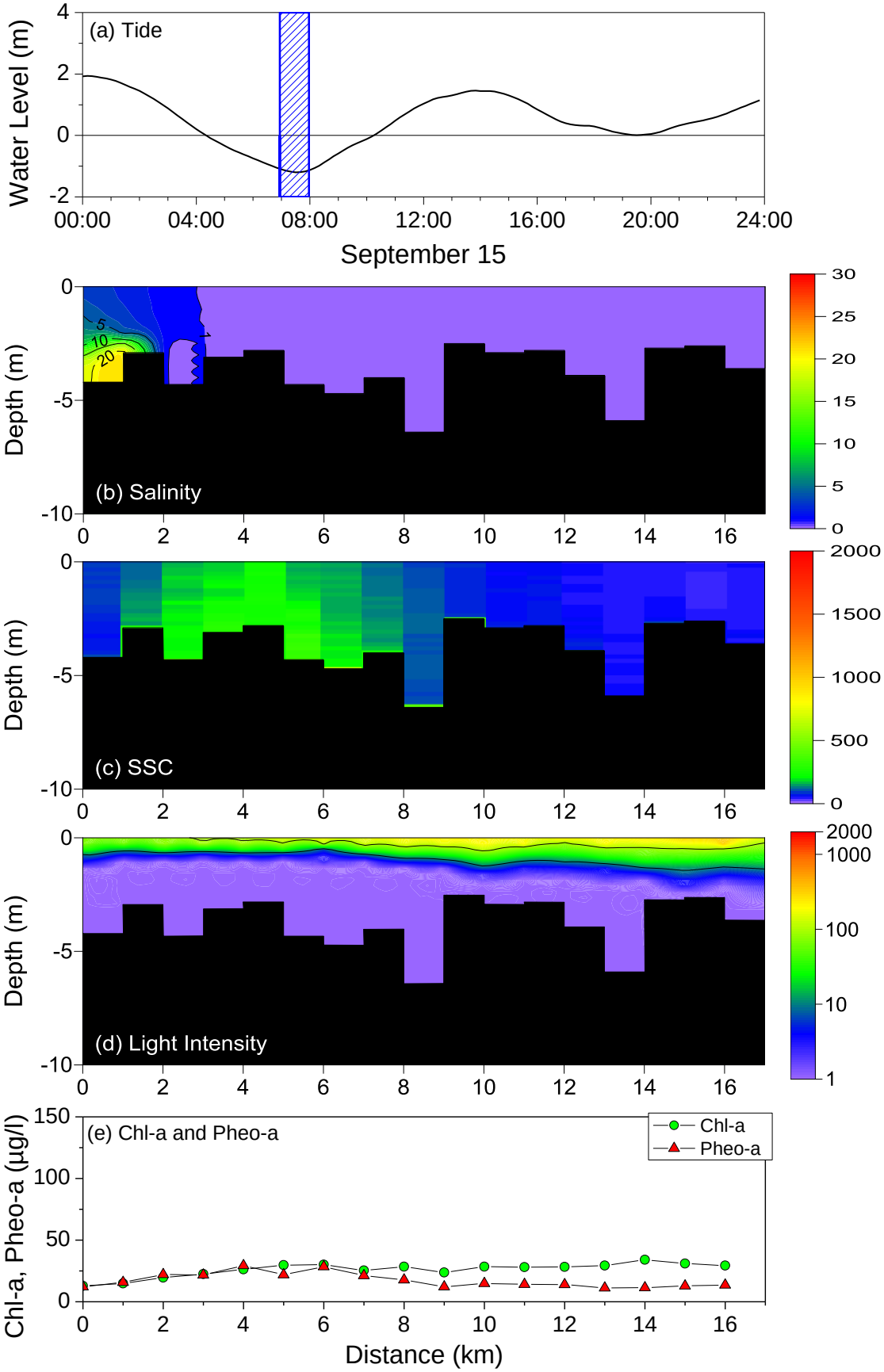

Fig. 4.14 (a) temporal variation of tide; longitudinal and vertical distributions of (b) salinity in psu, (c) SSC in mg/l, and (d) light intensity in µmol/m^{2}s; and (e) longitudinal distributions of Chl-a (surface) and Pheo-a (surface) during September 15 (Round 1).

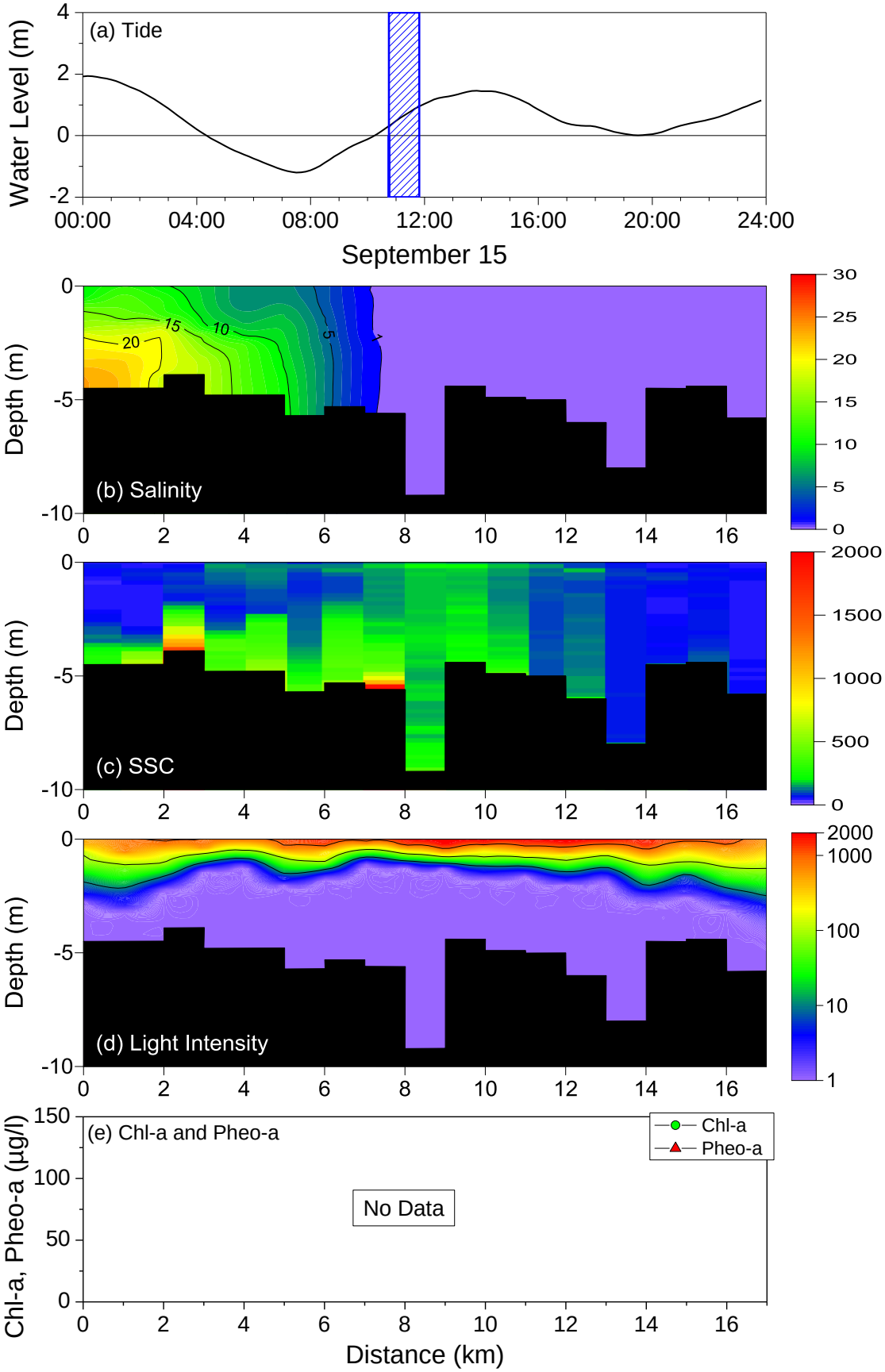

Fig. 4.15 (a) temporal variation of tide; longitudinal and vertical distributions of (b) salinity in psu, (c) SSC in mg/l, and (d) light intensity in µmol/m^{2}s; and (e) longitudinal distributions of Chl-a (surface) and Pheo-a (surface) during September 15 (Round 2).

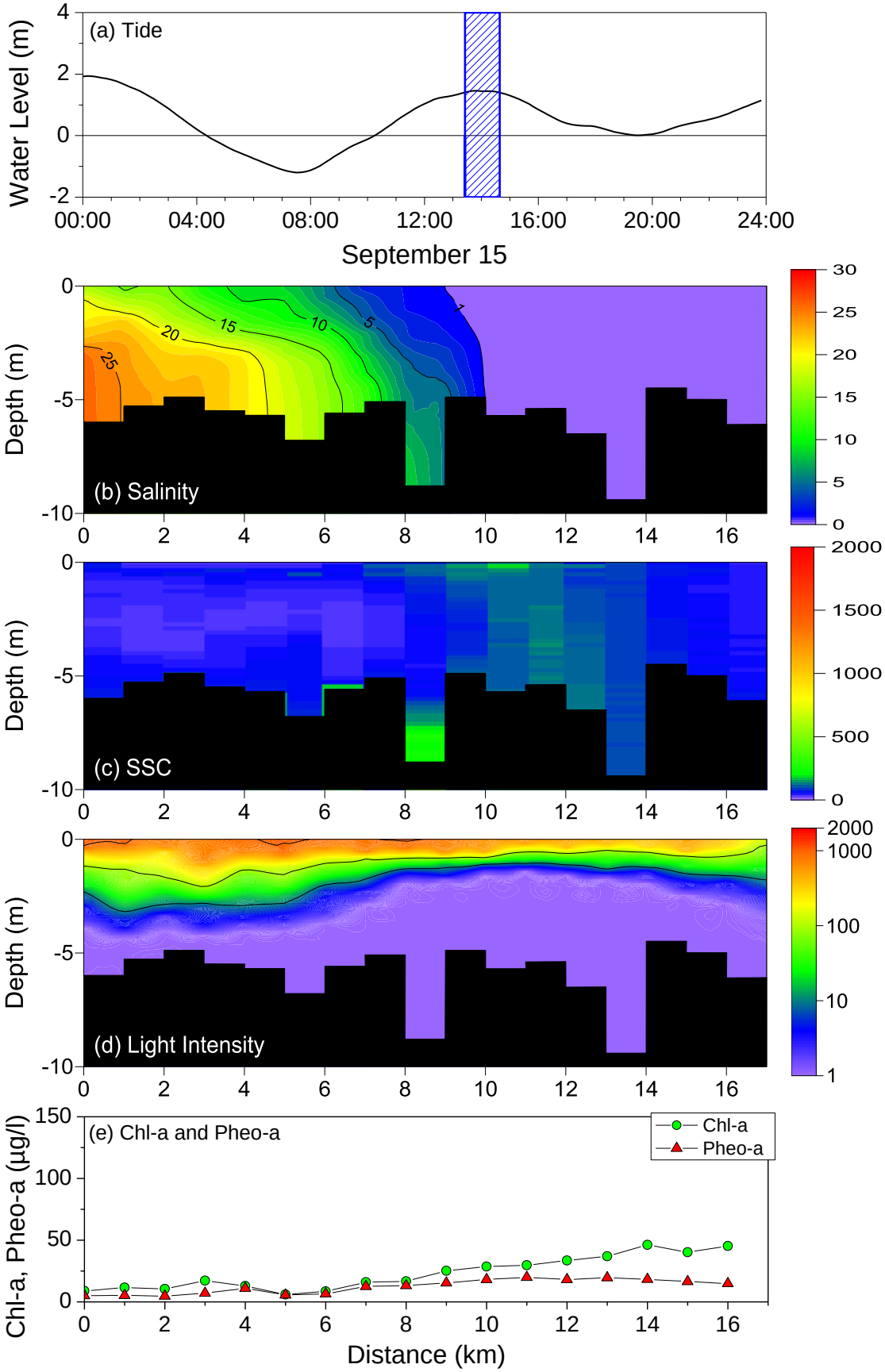

Fig. 4.16 (a) temporal variation of tide; longitudinal and vertical distributions of (b) salinity in psu, (c) SSC in mg/l, and (d) light intensity in µmol/m^{2}s; and (e) longitudinal distributions of Chl-a (surface) and Pheo-a (surface) during September 15 (Round 3).

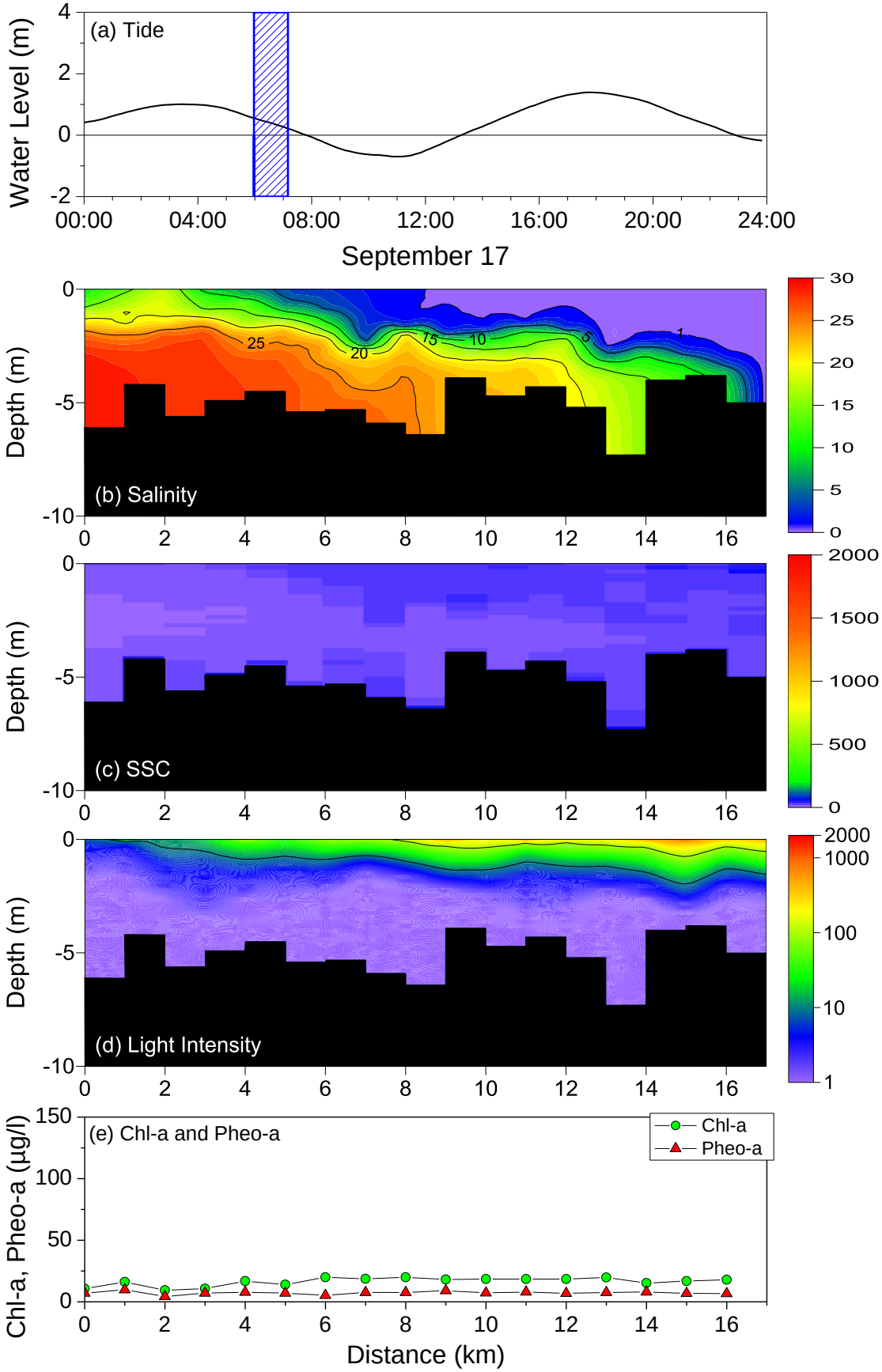

Fig. 4.17 (a) temporal variation of tide; longitudinal and vertical distributions of (b) salinity in psu, (c) SSC in mg/l, and (d) light intensity in µmol/m^{2}s; and (e) longitudinal distributions of Chl-a (surface) and Pheo-a (surface) during September 17 (Round 1).

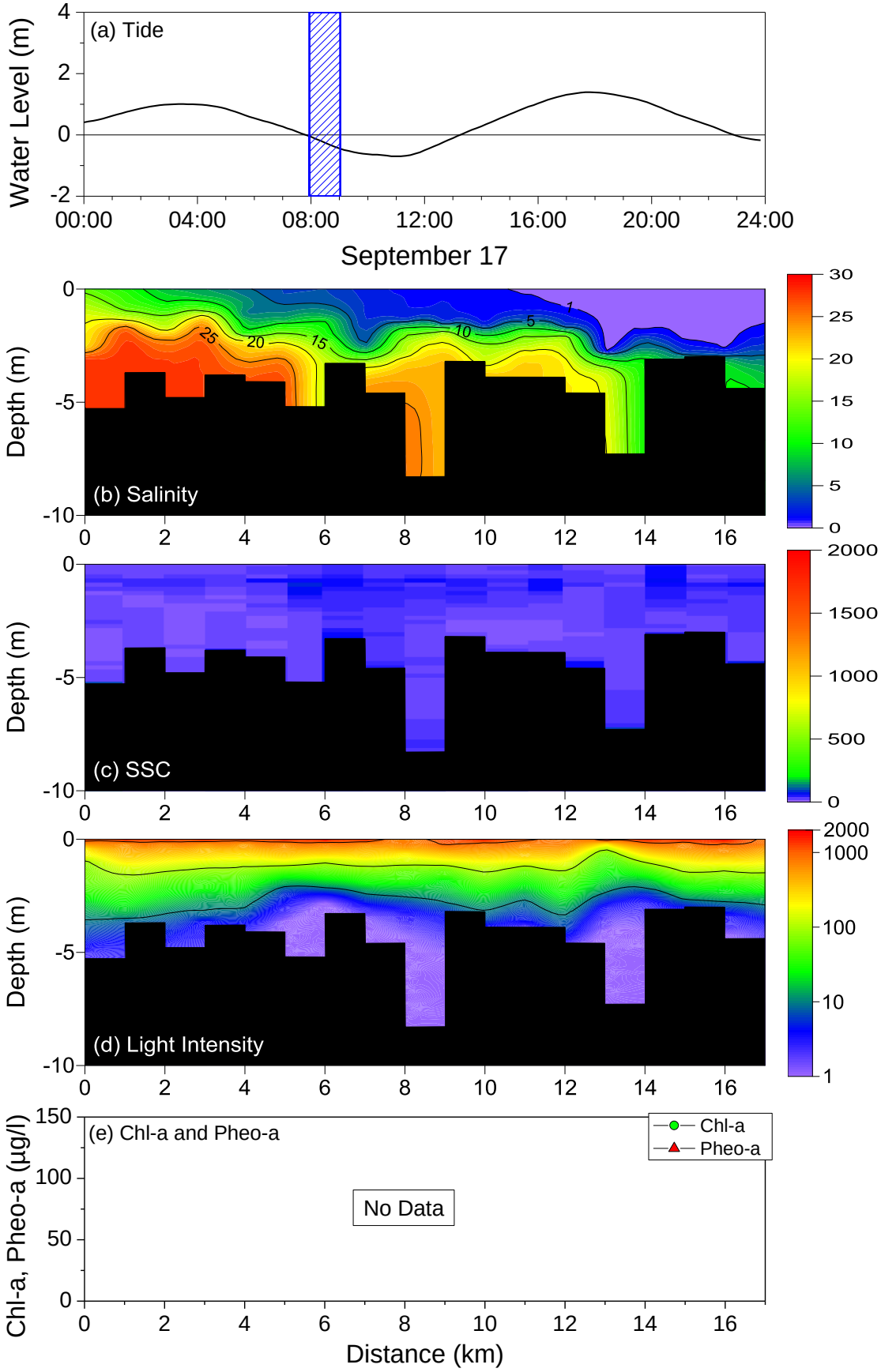

Fig. 4.18 (a) temporal variation of tide; longitudinal and vertical distributions of (b) salinity in psu, (c) SSC in mg/l, and (d) light intensity in µmol/m^{2}s; and (e) longitudinal distributions of Chl-a (surface) and Pheo-a (surface) during September 17 (Round 2).

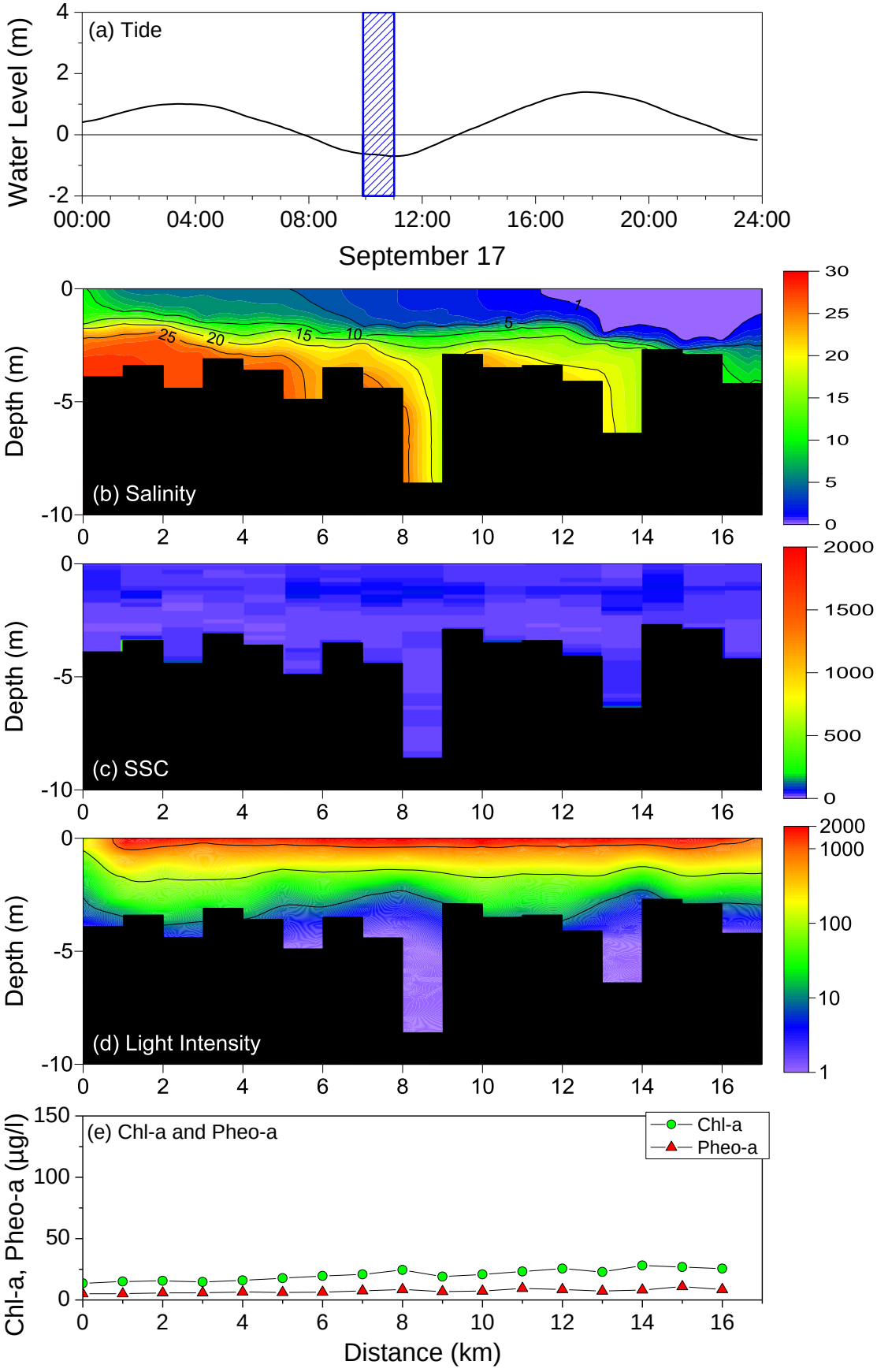

Fig. 4.19 (a) temporal variation of tide; longitudinal and vertical distributions of (b) salinity in psu, (c) SSC in mg/l, and (d) light intensity in µmol/m^{2}s; and (e) longitudinal distributions of Chl-a (surface) and Pheo-a (surface) during September 17 (Round 3).

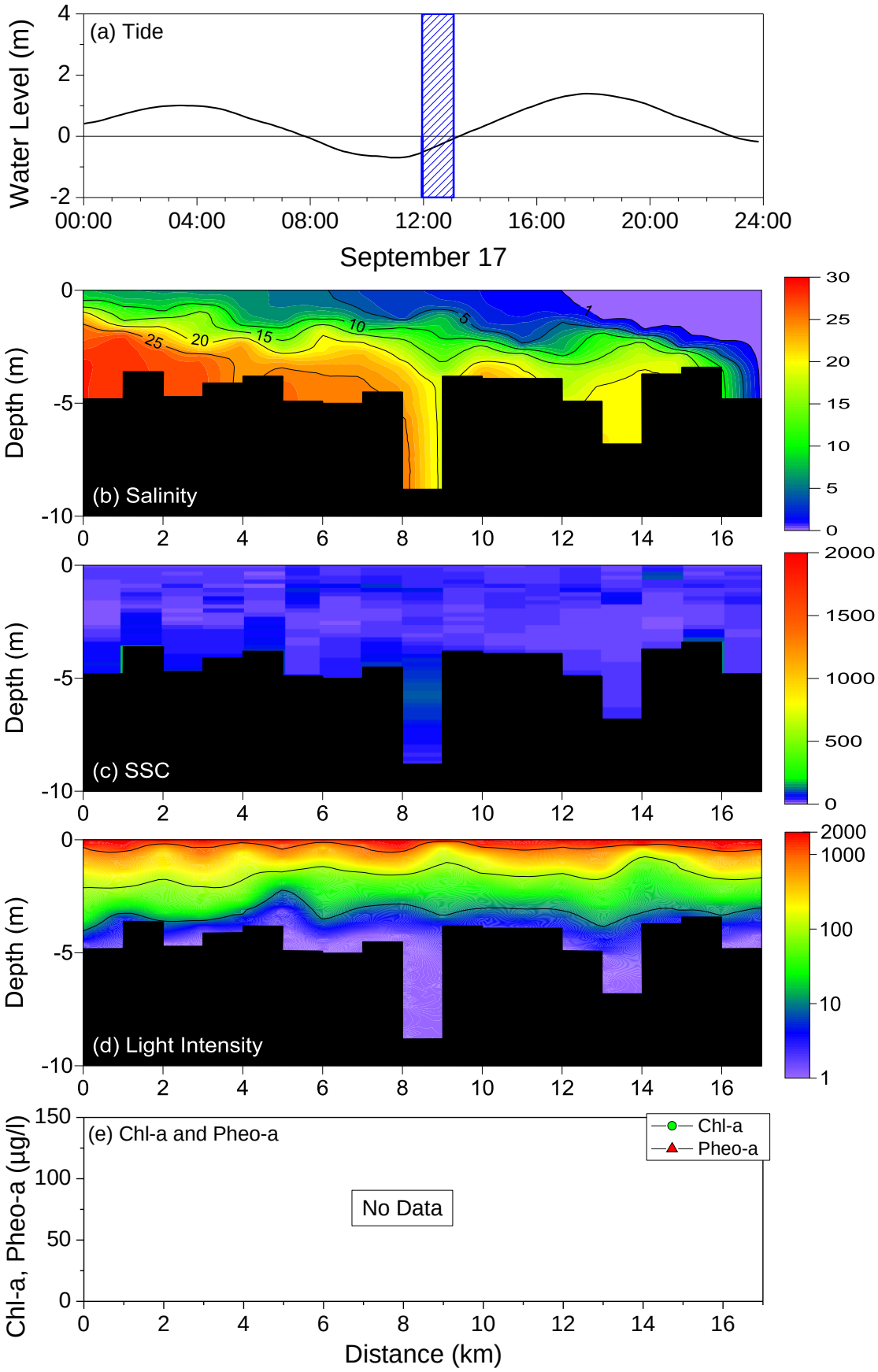

Fig. 4.20 (a) temporal variation of tide; longitudinal and vertical distributions of (b) salinity in psu, (c) SSC in mg/l, and (d) light intensity in µmol/m^{2}s; and (e) longitudinal distributions of Chl-a (surface) and Pheo-a (surface) during September 17 (Round 4).

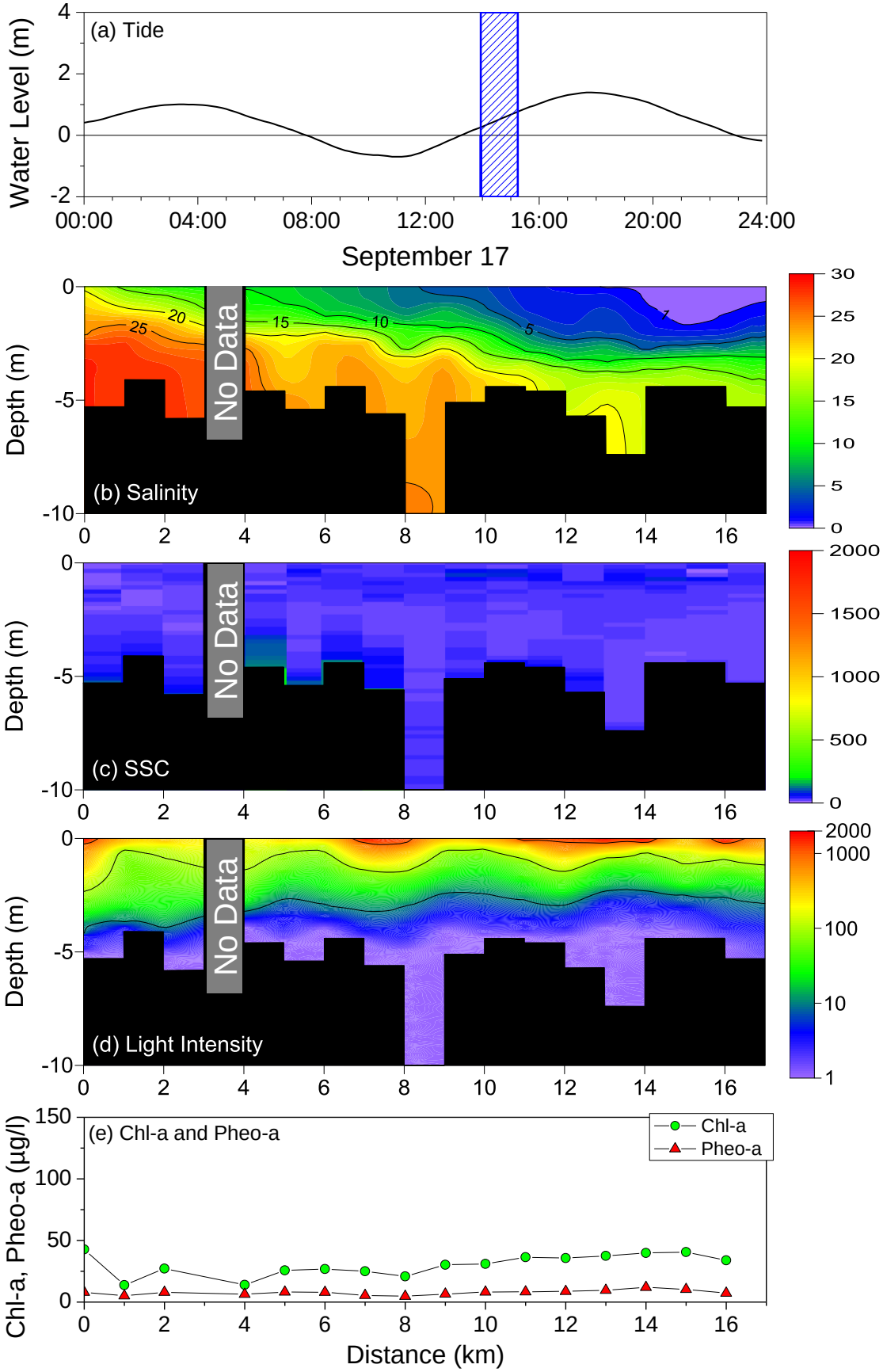

Fig. 4.21 (a) temporal variation of tide; longitudinal and vertical distributions of (b) salinity in psu, (c) SSC in mg/l, and (d) light intensity in µmol/m^{2}s; and (e) longitudinal distributions of Chl-a (surface) and Pheo-a (surface) during September 17 (Round 5).

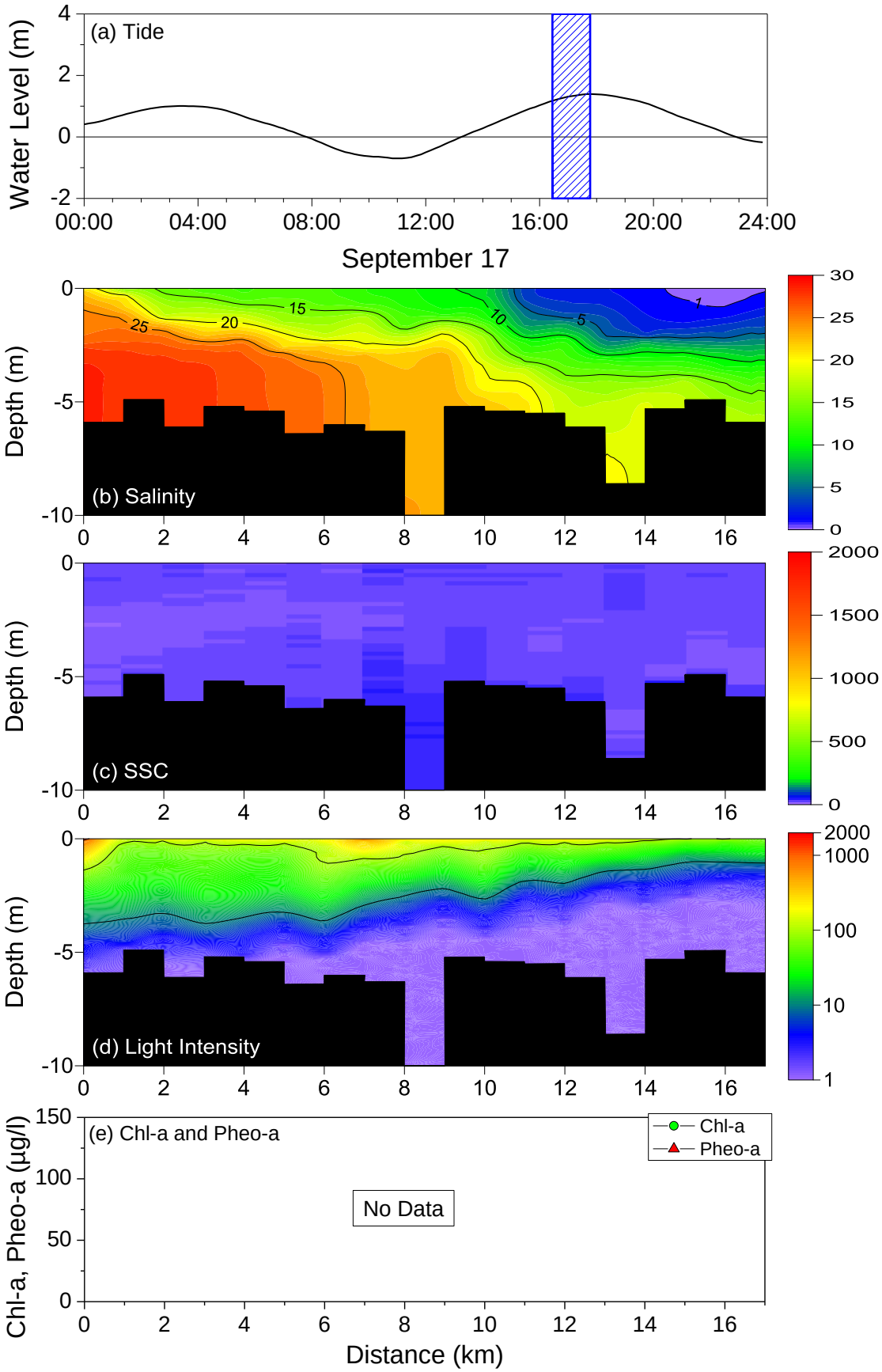

Fig. 4.22 (a) temporal variation of tide; longitudinal and vertical distributions of (b) salinity in psu, (c) SSC in mg/l, and (d) light intensity in µmol/m^{2}s; and (e) longitudinal distributions of Chl-a (surface) and Pheo-a (surface) during September 17 (Round 6).

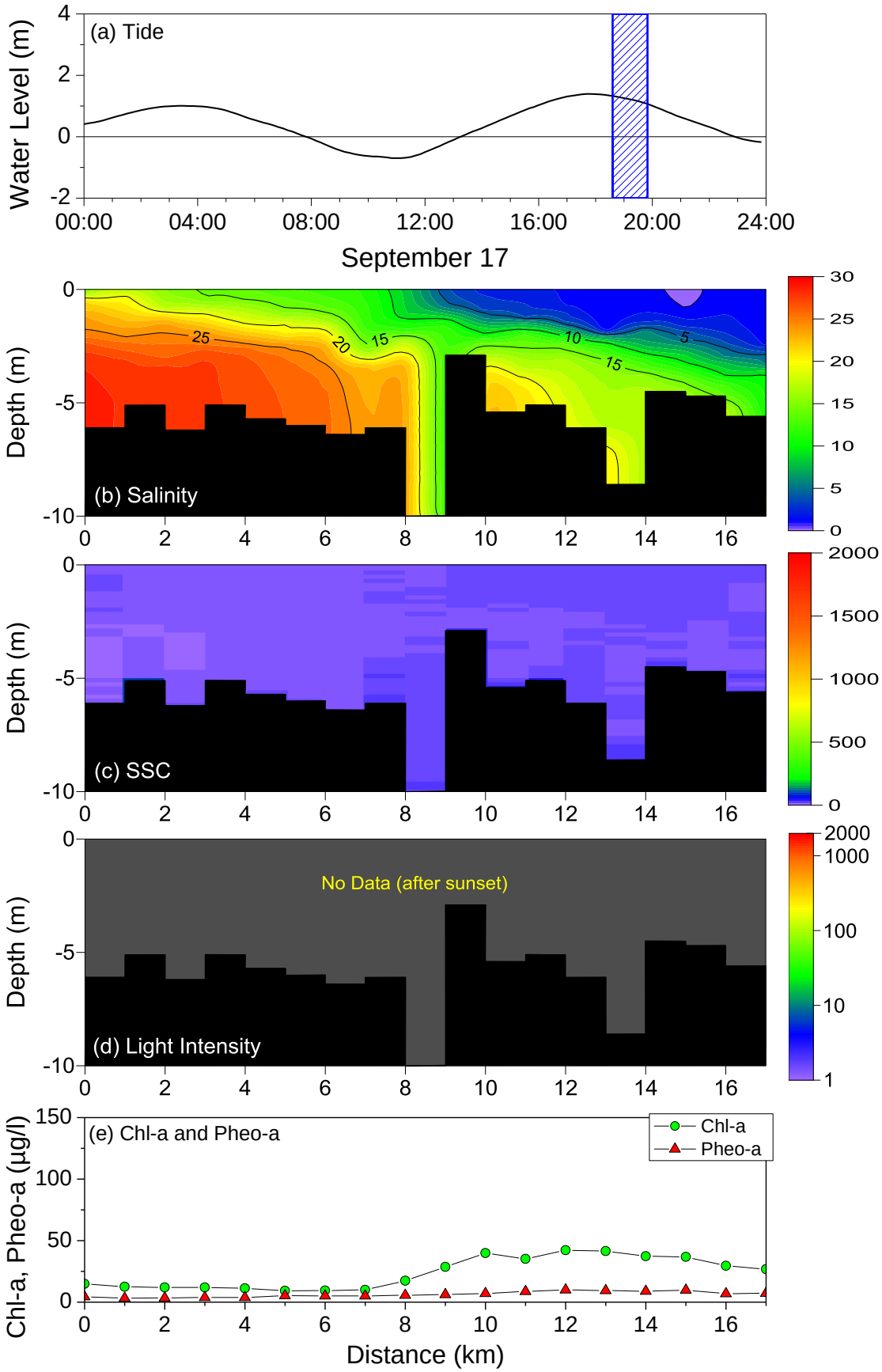

Fig. 4.23 (a) temporal variation of tide; longitudinal and vertical distributions of (b) salinity in psu, (c) SSC in mg/l, and (d) light intensity in µmol/m^{2}s; and (e) longitudinal distributions of Chl-a (surface) and Pheo-a (surface) during September 17 (Round 7).

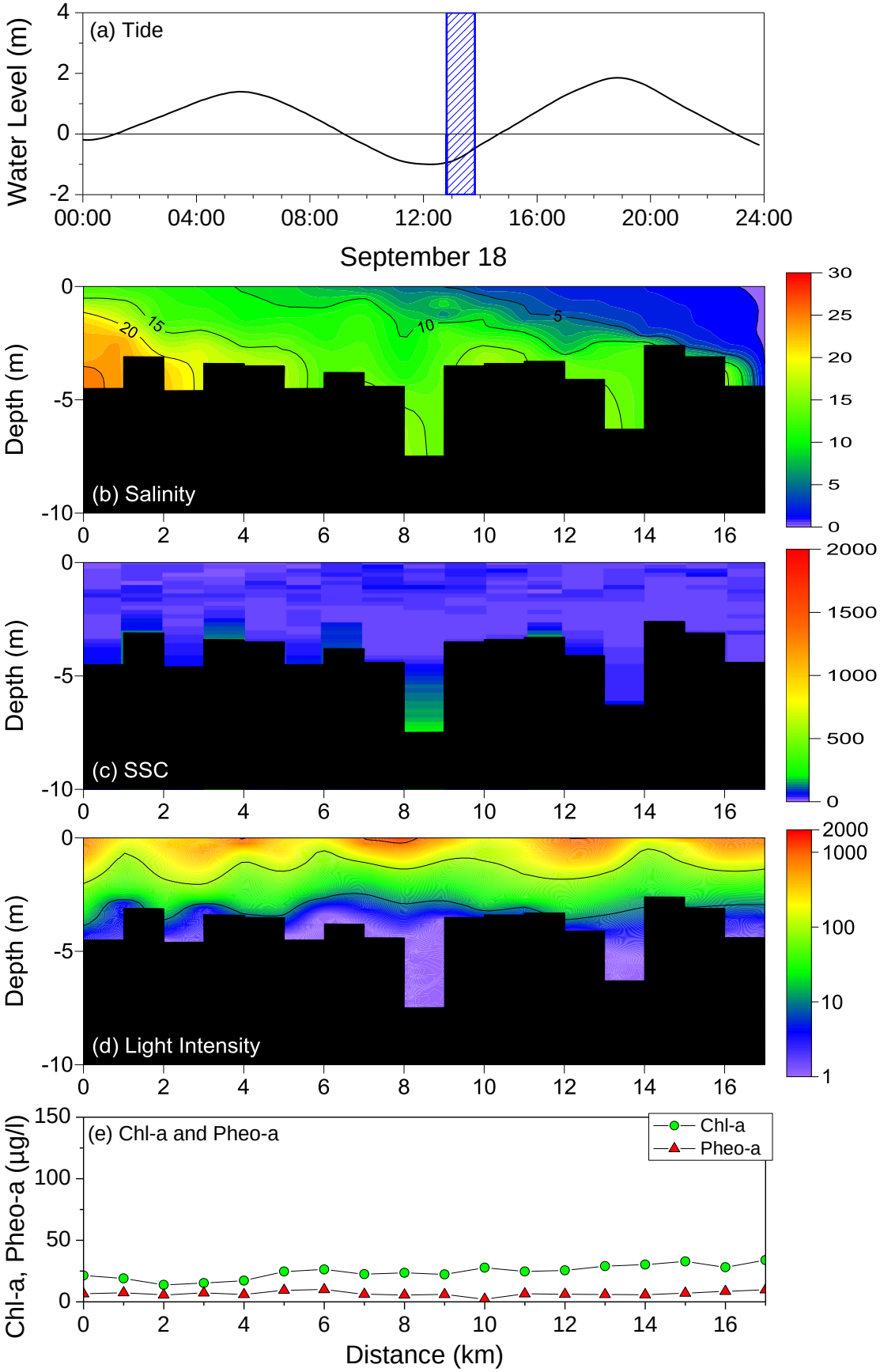

Fig. 4.24 (a) temporal variation of tide; longitudinal and vertical distributions of (b) salinity in psu, (c) SSC in mg/l, and (d) light intensity in µmol/m^{2}s; and (e) longitudinal distributions of Chl-a (surface) and Pheo-a (surface) during September 18 (Round 1).

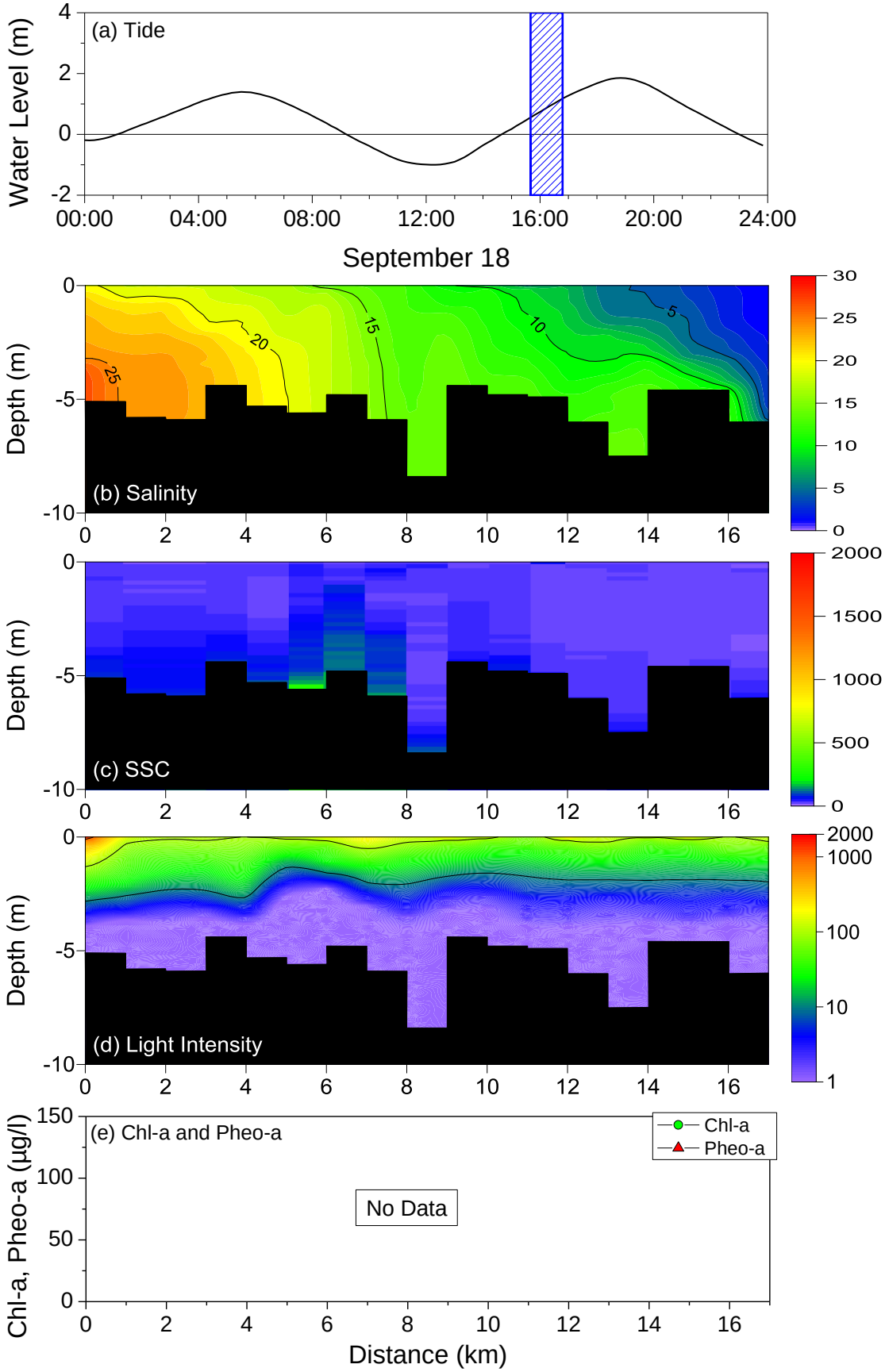

Fig. 4.25 (a) temporal variation of tide; longitudinal and vertical distributions of (b) salinity in psu, (c) SSC in mg/l, and (d) light intensity in µmol/m^{2}s; and (e) longitudinal distributions of Chl-a (surface) and Pheo-a (surface) during September 18 (Round 2).

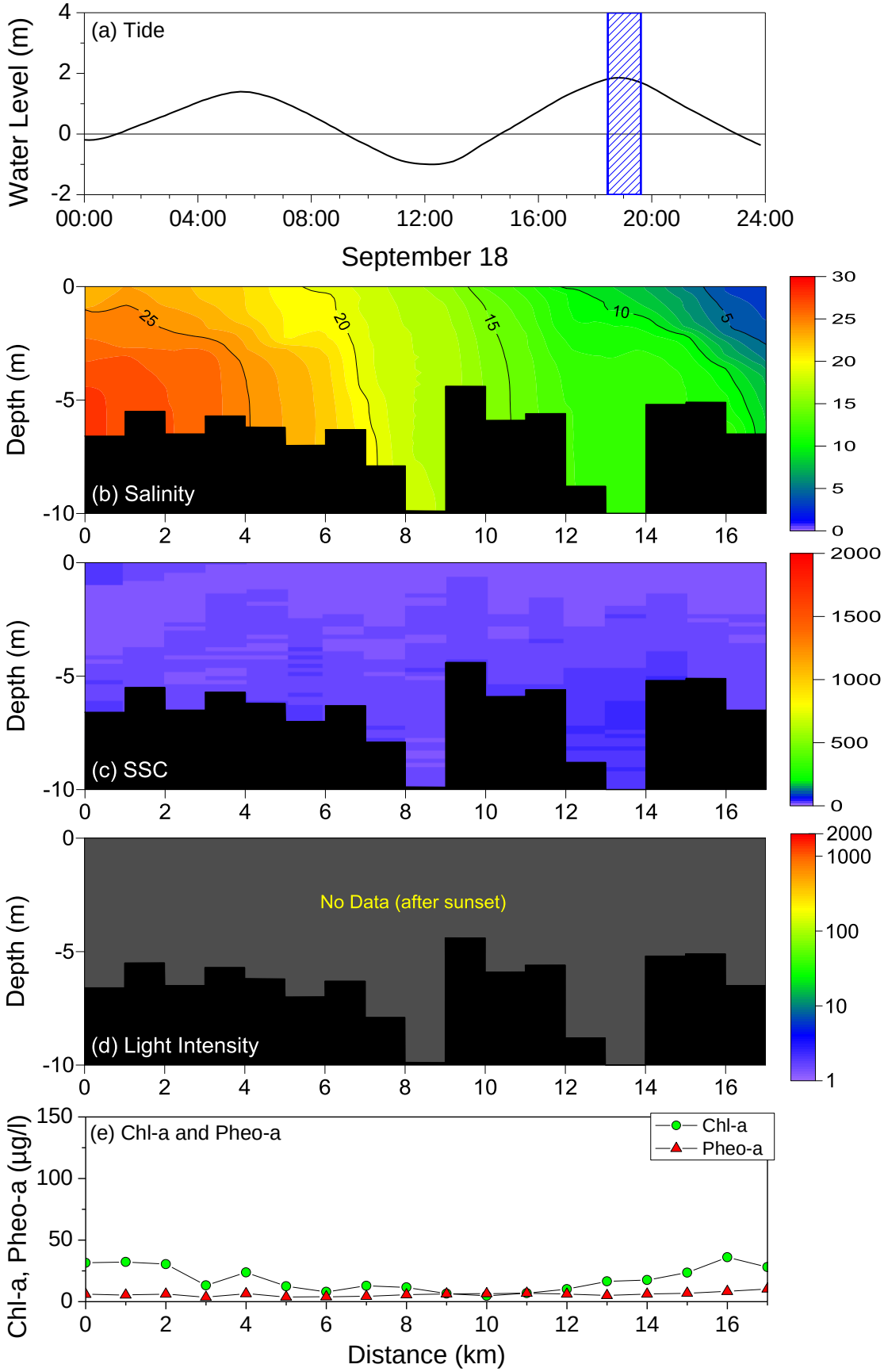

Fig. 4.26 (a) temporal variation of tide; longitudinal and vertical distributions of (b) salinity in psu, (c) SSC in mg/l, and (d) light intensity in µmol/m^{2}s; and (e) longitudinal distributions of Chl-a (surface) and Pheo-a (surface) during September 18 (Round 3).

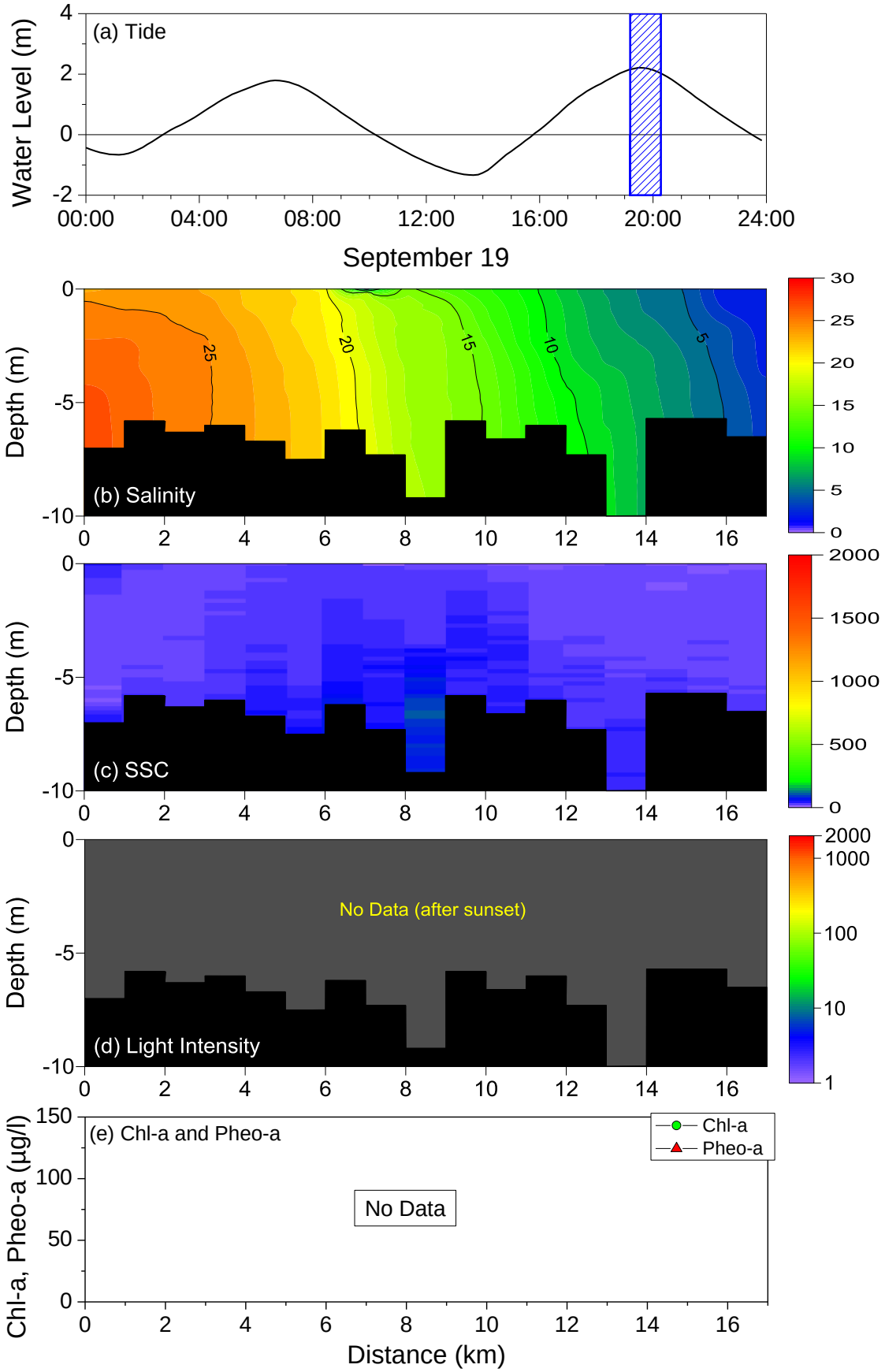

Fig. 4.27 (a) temporal variation of tide; longitudinal and vertical distributions of (b) salinity in psu, (c) SSC in mg/l, and (d) light intensity in µmol/m^{2}s; and (e) longitudinal distributions of Chl-a (surface) and Pheo-a (surface) during September 19 (Round 1).

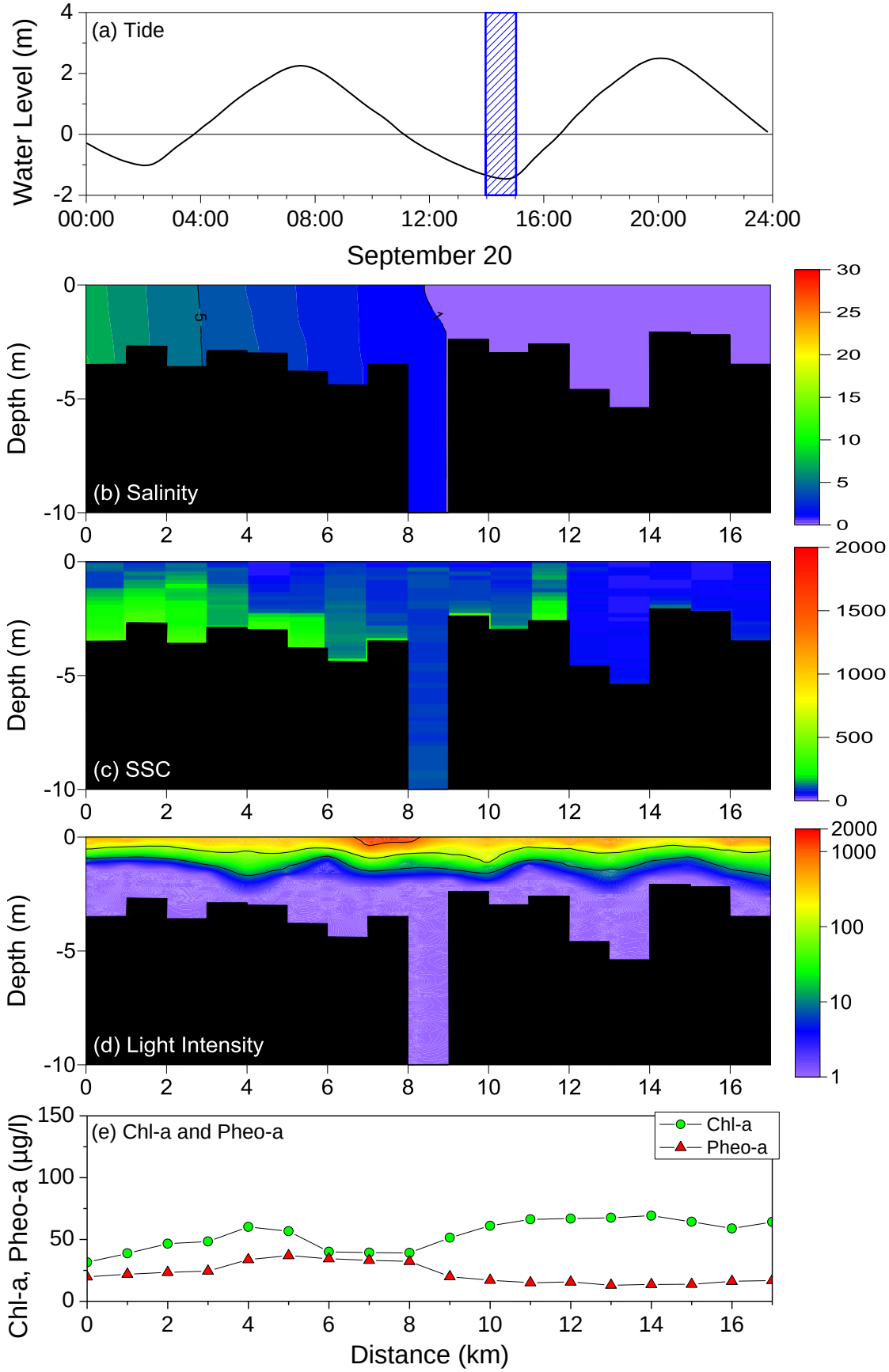

Fig. 4.28 (a) temporal variation of tide; longitudinal and vertical distributions of (b) salinity in psu, (c) SSC in mg/l, and (d) light intensity in µmol/m^{2}s; and (e) longitudinal distributions of Chl-a (surface) and Pheo-a (surface) during September 20 (Round 1).

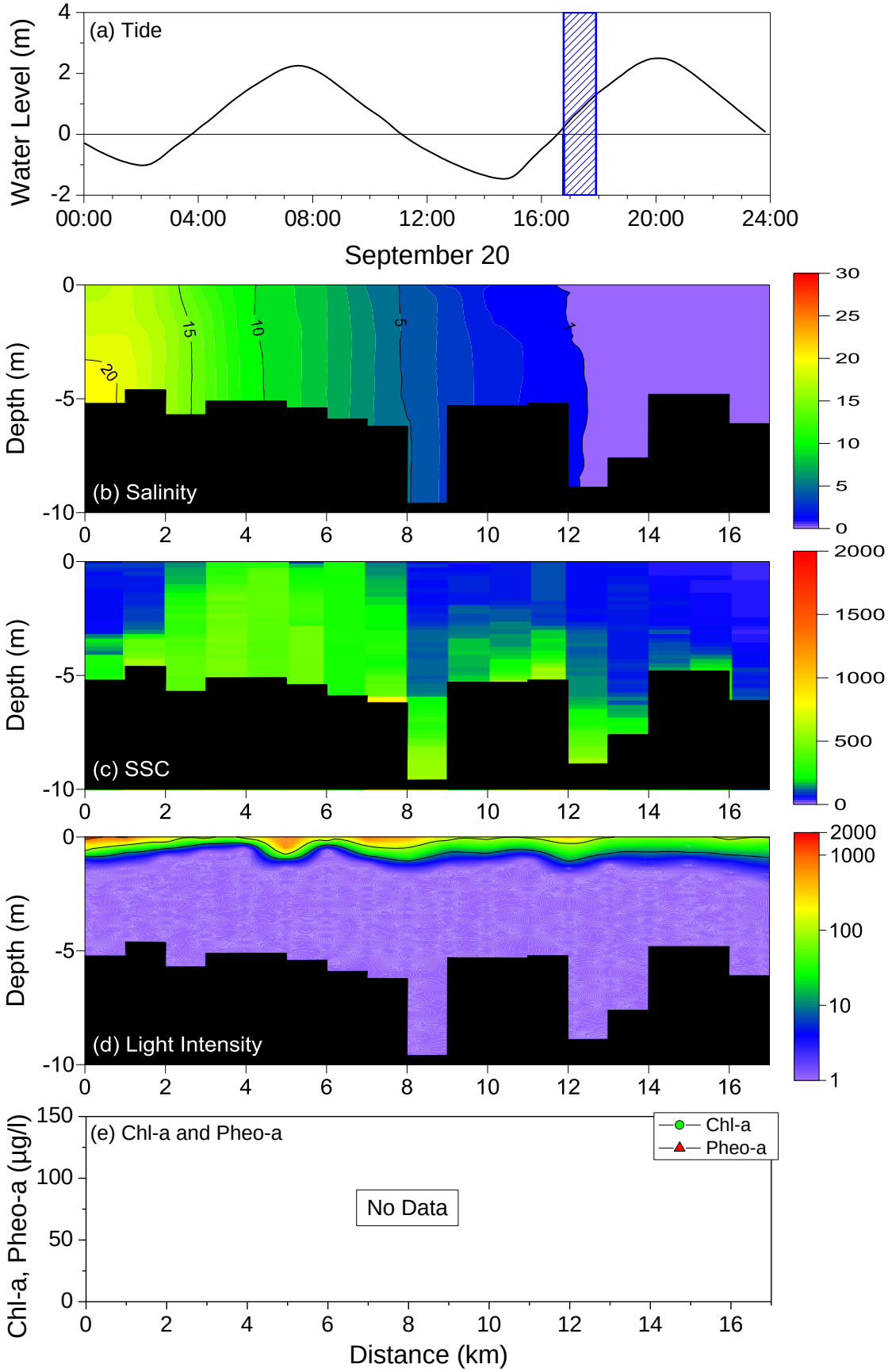

Fig. 4.29 (a) temporal variation of tide; longitudinal and vertical distributions of (b) salinity in psu, (c) SSC in mg/l, and (d) light intensity in µmol/m^{2}s; and (e) longitudinal distributions of Chl-a (surface) and Pheo-a (surface) during September 20 (Round 2).

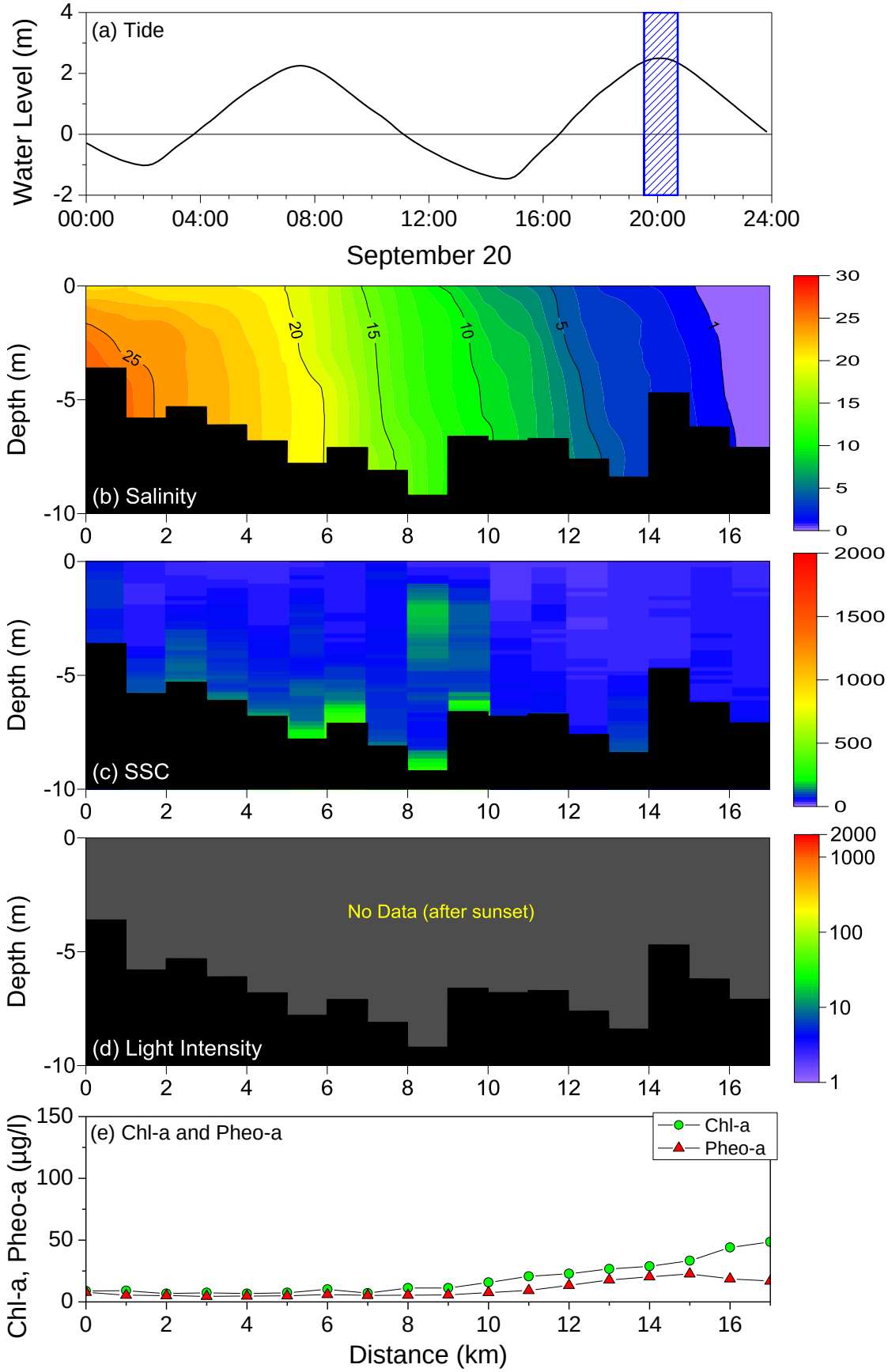

Fig. 4.30 (a) temporal variation of tide; longitudinal and vertical distributions of (b) salinity in psu, (c) SSC in mg/l, and (d) light intensity in µmol/m^{2}s; and (e) longitudinal distributions of Chl-a (surface) and Pheo-a (surface) during September 20 (Round 3).

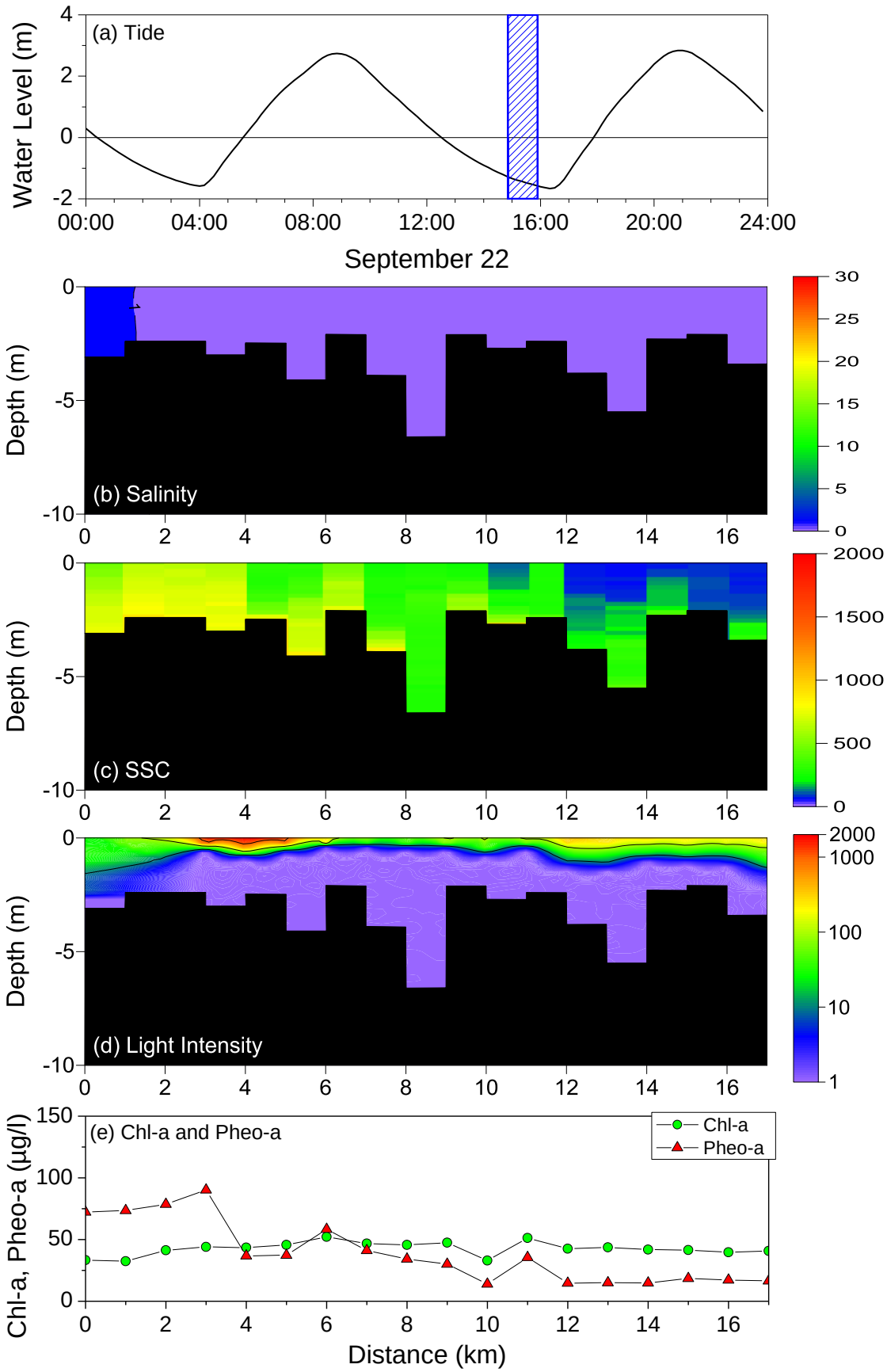

Fig. 4.31 (a) temporal variation of tide; longitudinal and vertical distributions of (b) salinity in psu, (c) SSC in mg/l, and (d) light intensity in µmol/m^{2}s; and (e) longitudinal distributions of Chl-a (surface) and Pheo-a (surface) during September 22 (Round 1).

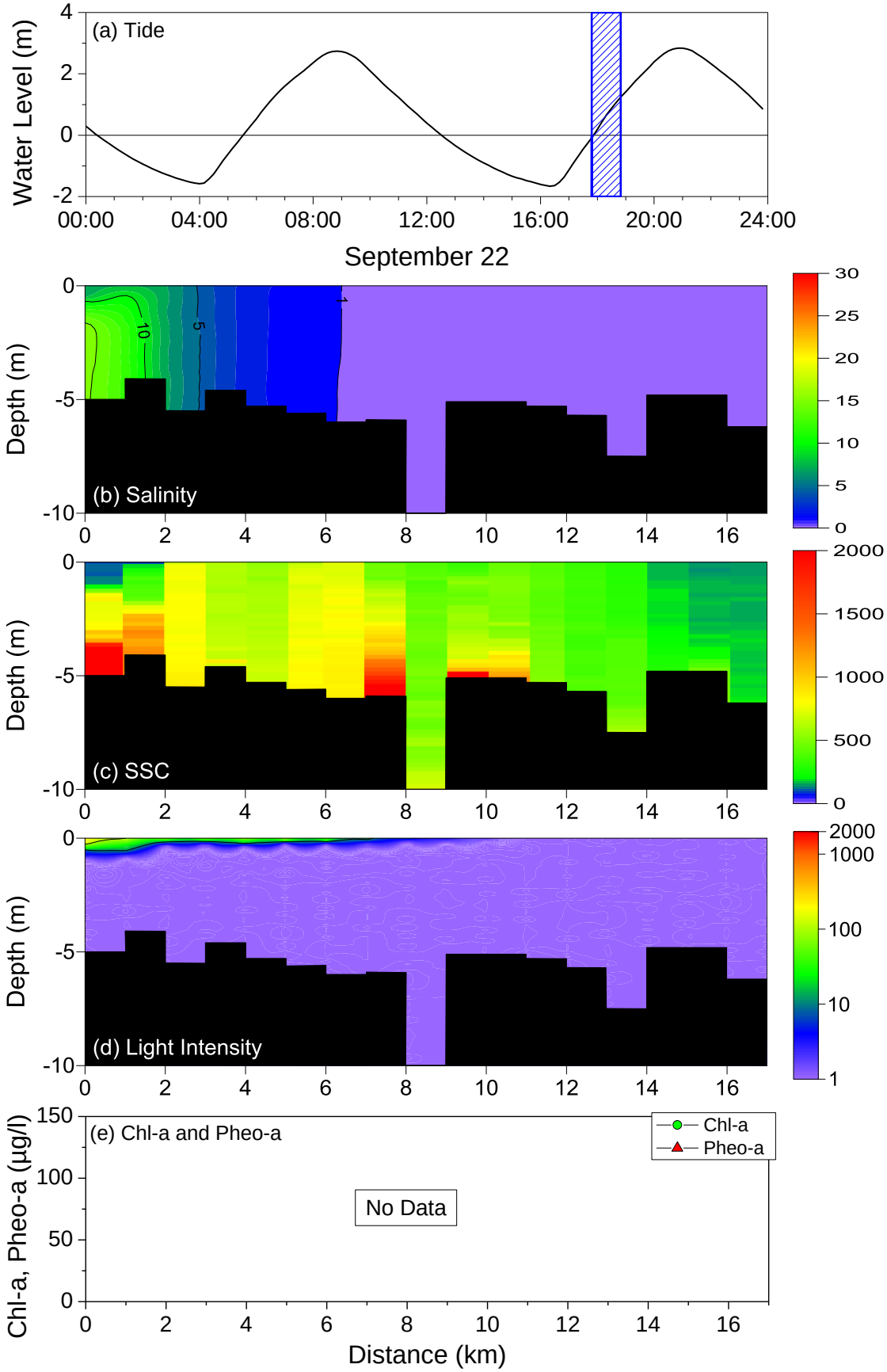

Fig. 4.32 (a) temporal variation of tide; longitudinal and vertical distributions of (b) salinity in psu, (c) SSC in mg/l, and (d) light intensity in µmol/m^{2}s; and (e) longitudinal distributions of Chl-a (surface) and Pheo-a (surface) during September 22 (Round 2).

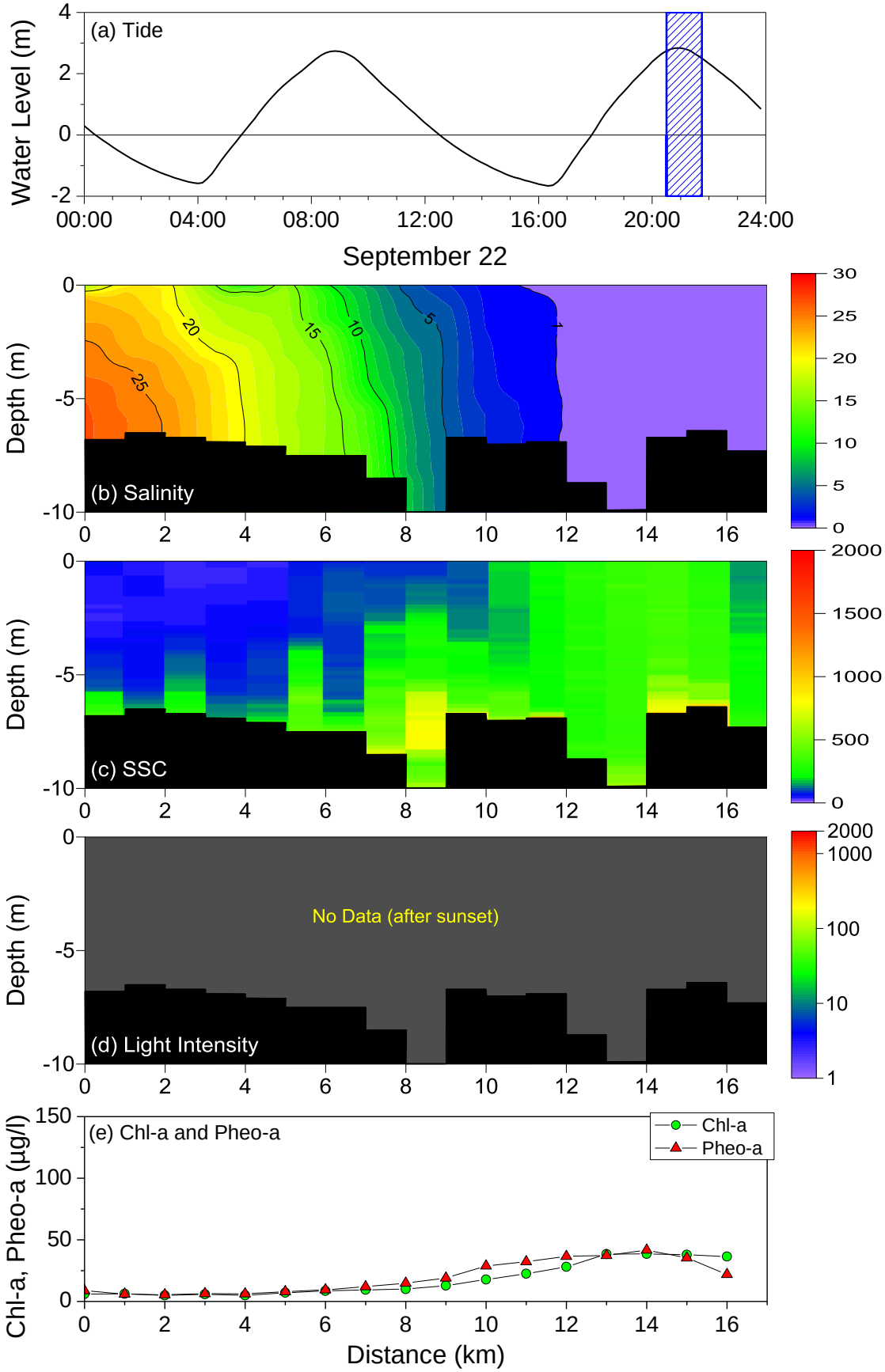

Fig. 4.33 (a) temporal variation of tide; longitudinal and vertical distributions of (b) salinity in psu, (c) SSC in mg/l, and (d) light intensity in µmol/m^{2}s; and (e) longitudinal distributions of Chl-a (surface) and Pheo-a (surface) during September 22 (Round 3).

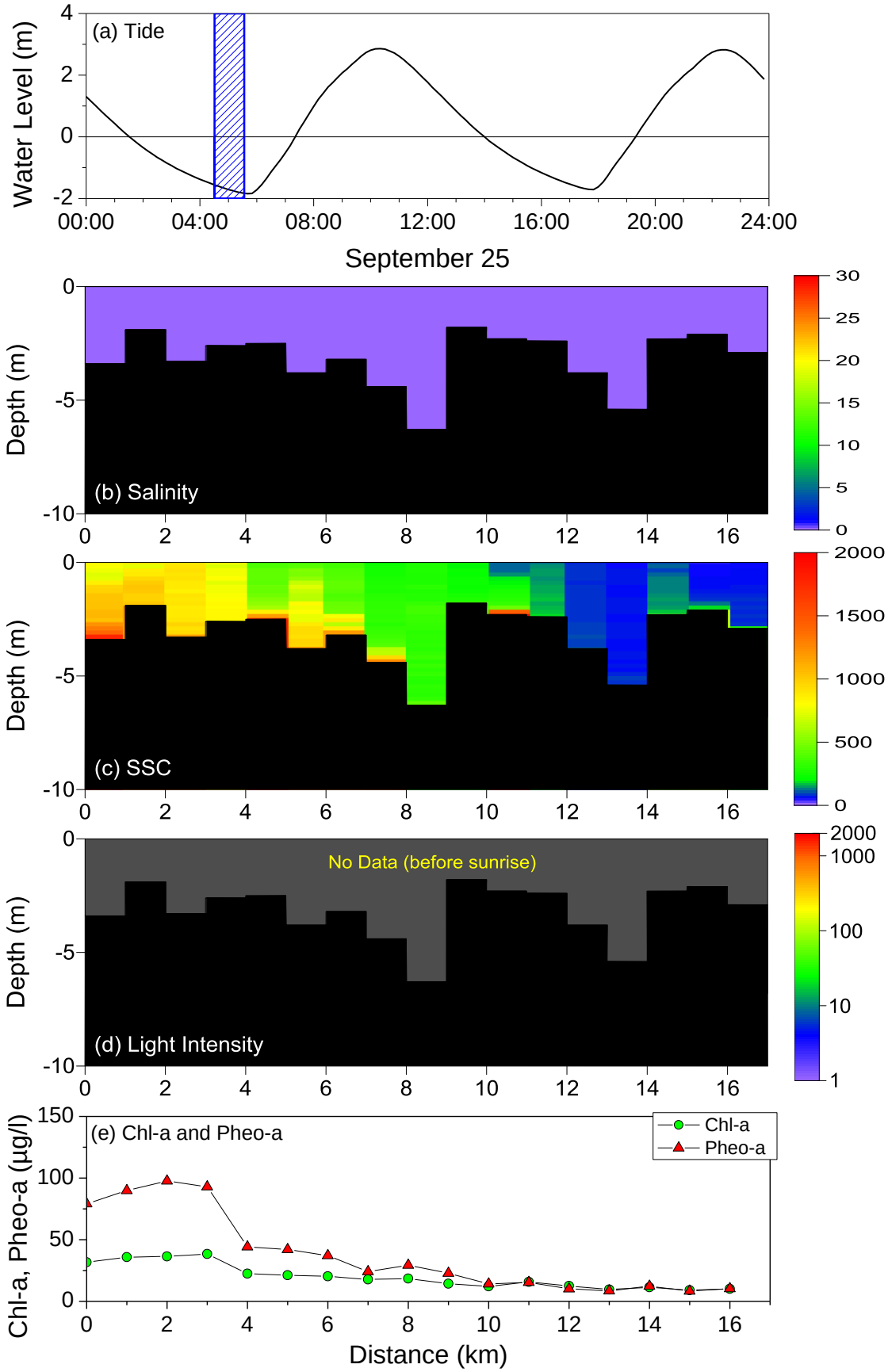

Fig. 4.34 (a) temporal variation of tide; longitudinal and vertical distributions of (b) salinity in psu, (c) SSC in mg/l, and (d) light intensity in µmol/m^{2}s; and (e) longitudinal distributions of Chl-a (surface) and Pheo-a (surface) during September 25 (Round 1).

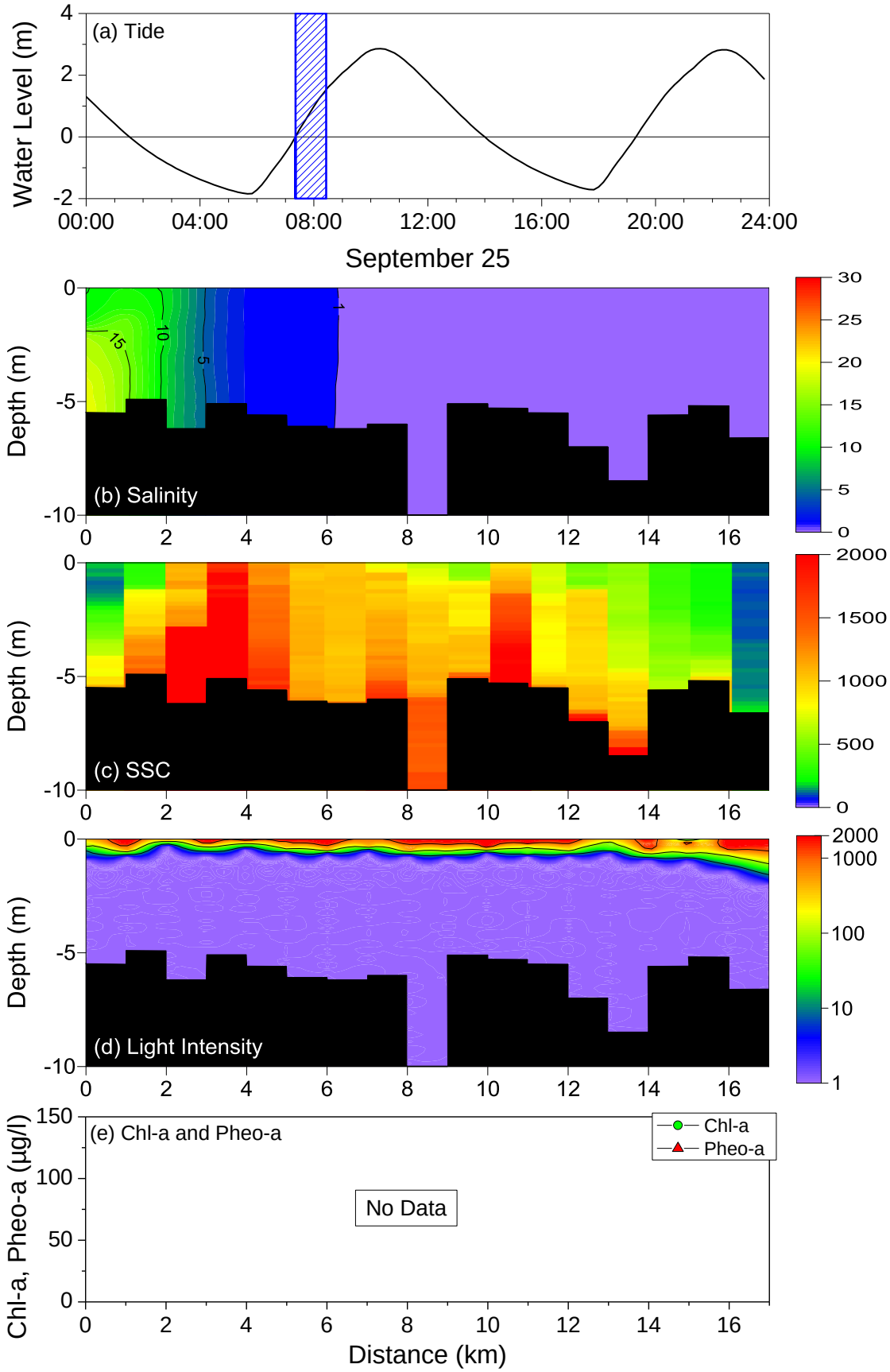

Fig. 4.35 (a) temporal variation of tide; longitudinal and vertical distributions of (b) salinity in psu, (c) SSC in mg/l, and (d) light intensity in µmol/m^{2}s; and (e) longitudinal distributions of Chl-a (surface) and Pheo-a (surface) during September 25 (Round 2).

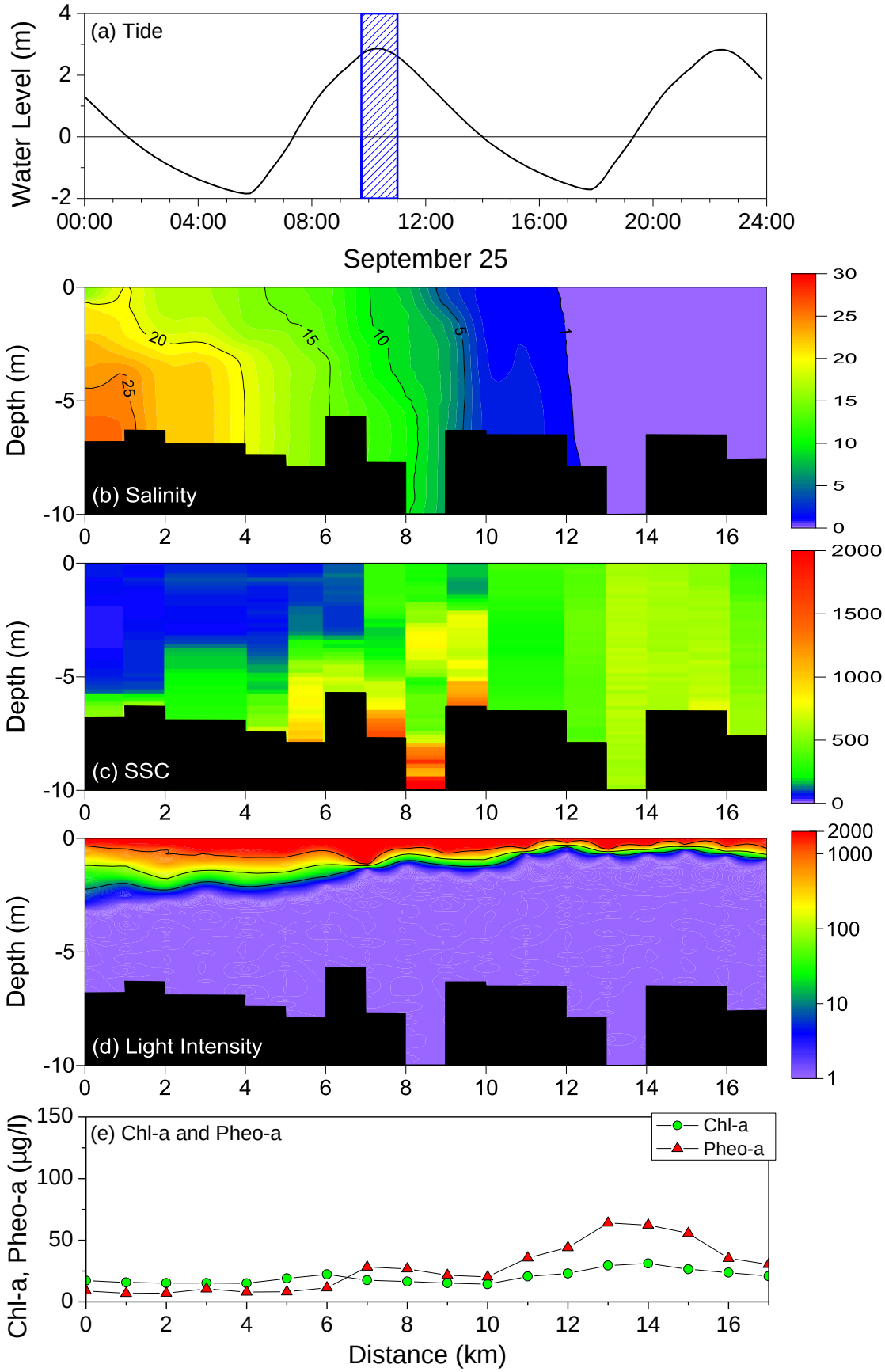

Fig. 4.36 (a) temporal variation of tide; longitudinal and vertical distributions of (b) salinity in psu, (c) SSC in mg/l, and (d) light intensity in µmol/m^{2}s; and (e) longitudinal distributions of Chl-a (surface) and Pheo-a (surface) during September 25 (Round 3).

4.2 Discussion

4.2.1 Light Attenuation in the Water Column

The light attenuation coefficient (K) in the Chikugo river estuary was changing with fortnightly tidal cycle and spatially (Fig. 4.37a). For Chikugo river estuary light attenuation coefficient exceeded 30 m^{-1} during spring tide and it gradually decreases during the half tides and reaches <2 m^{-1} during neap tide. Therefore, the photic depth becomes greater than 4 m during the neap tide compared to less than 0.2 m during the spring tide (Fig. 4.37b). The photic depth of large rivers and river dominated estuaries is typically less than 5 m (Cloern, 1987), but Chikugo river estuary is mainly tidally dominated estuary with the influence of river discharge. The photic depth in the estuaries worldwide ranges widely from 0 to 26 m. The Tamar estuary, Columbia River estuary and Northern San Francisco (San Pablo) Bay have the similar photic depth ranges of Chikugo river estuary (Owens, 1985; Small and Frey, 1984; Cloern *et al*., 1985).

The mixing depth (Fig. 4.37c) during spring tide was more than 10 times the photic depth for the whole estuary except river mouth and 17 km upstream. For the half tide Zp:Zm ratio was ranged between 0.2 to 1. The mixing depth reduced during neap tide and the Zp:Zm ratio was ranged between 1 to more than 10.

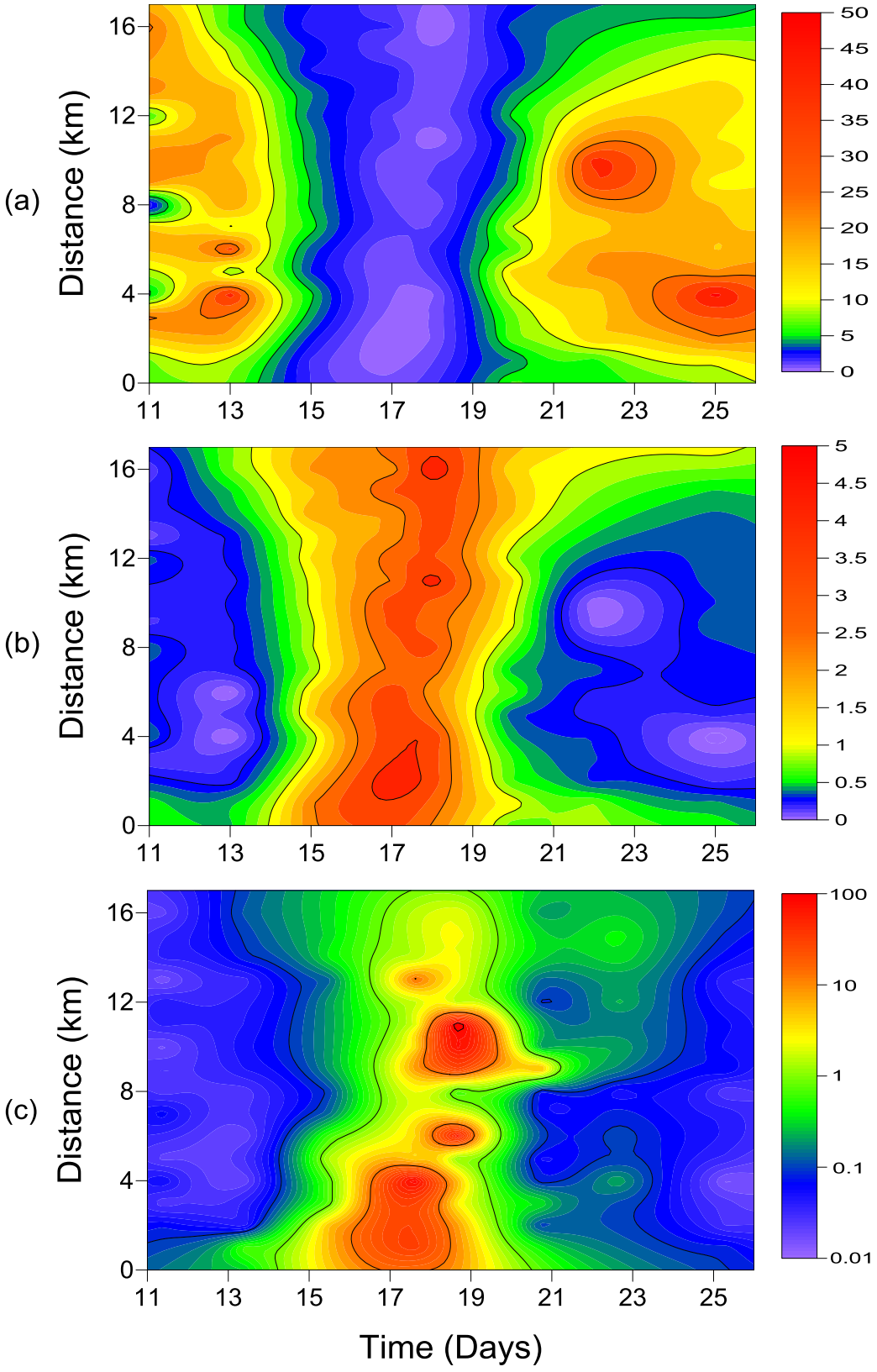

Fig. 4.37 Spatio-temporal distribution of (a) Light attenuation coefficient (K) in m^{-1}, (b) Photic Depth (Zp) in m, and (c) Zp:Zm ratio (Zp/Zm).

Light attenuation coefficient (K) shows a linear relation with the depth averaged SSC in the photic zone (Fig. 4.38a) for the fortnightly sampling days. Light attenuation and SSC was gradually changing from spring tide to neap tide. However, they do not show big change spatially. The light penetration was more than 2 m when the SSC was below 30 mg/l during neap tide. The light penetration decreased from 1.5 m to 30 cm when the SSC increased from 100 to 300 mg/l. The light penetration significantly reduced and approached 10 – 20 cm when the SSC exceeded 500 mg/l during spring tide. This indicates that the water transparency of Chikugo river estuary was regulated by the fortnightly variations of suspended sediment dynamics. Strong relation between K and SSC indicate that the SSC is the key driver of light attenuation in the Chikugo river estuary by spatially and temporally. Zp:Zm ratio shows an inverse relation with K (Fig. 4.38b). This means that the light penetration in the water column of Chikugo river estuary is related with the ratio of photic depth to mixing depth. The light attenuation coefficient is influenced by SSC and mixing. Hence the Zp:Zm ratio can be represented as the function of light availability in the Chikugo River estuary.

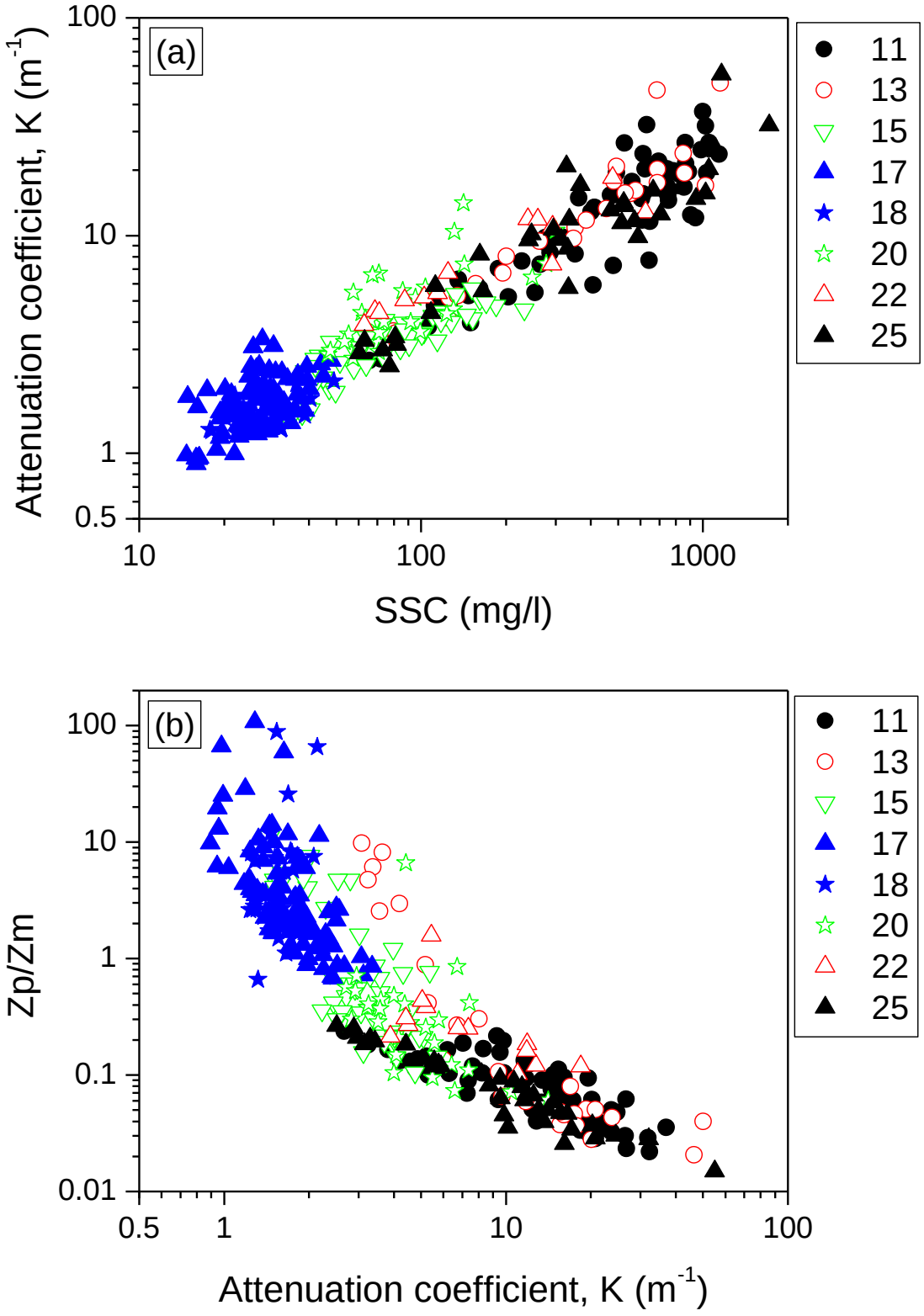

Fig. 4.38 Relationship between (a) light attenuation coefficient and depth averaged SSC in the photic zone and (b) light attenuation coefficient and Zp:Zm ratio.

4.2.2 Phytoplankton

(a) Semidiurnal Variation of Phytoplankton

Spatio-temporal variation of salinity, SSC, analyzed Chl-a and analyzed Pheo-a during spring and neap tide were plotted (Fig. 4.39). All the values are taken from surface layers. Seawater movement to upstream was (Fig. 4.39a1) seen during spring tide from low tide and flood tide and reaching more than 10 km upstream at high tide. Then the seawater retreated back to the ocean at the ebb tide. The SSC was very high in both lower and upper estuary and the distribution of SSC was moving with the seawater (Fig. 4.39a2). During neap tide SSC was ranged between 10 to 40 mg/l on the water surface (Fig. 4. 39b2).

Analyzed Chl-a was ranged from 10 to 50 μg/l, it was relatively low during spring tide (Fig. 4.39a3) and became high during neap tide (Fig. 4.39b3). The Chl-a concentration in spring tide was relatively high during the low water. During neap tide Chl-a was nearly 20 μg/l at morning and it increased to more than 40 μg/l at the evening. Chl-a was slightly high in the upper estuary for both spring and tide.

Pheo-a concentration was very high during spring tide especially for flood and ebb phase (Fig. 4.39a4). Pheo-a was high near the river mouth during low tide and it was high at the upper estuary during high tide, then again it became high near the river mouth during the succeeding low tide. Therefore, Pheo-a was moving from the river mouth to the upper estuary during flood tide and moving back to lower estuary during ebb tide. Pheo-a was ranged 5–10 μg/l during neap tide (Fig. 4.39b4).

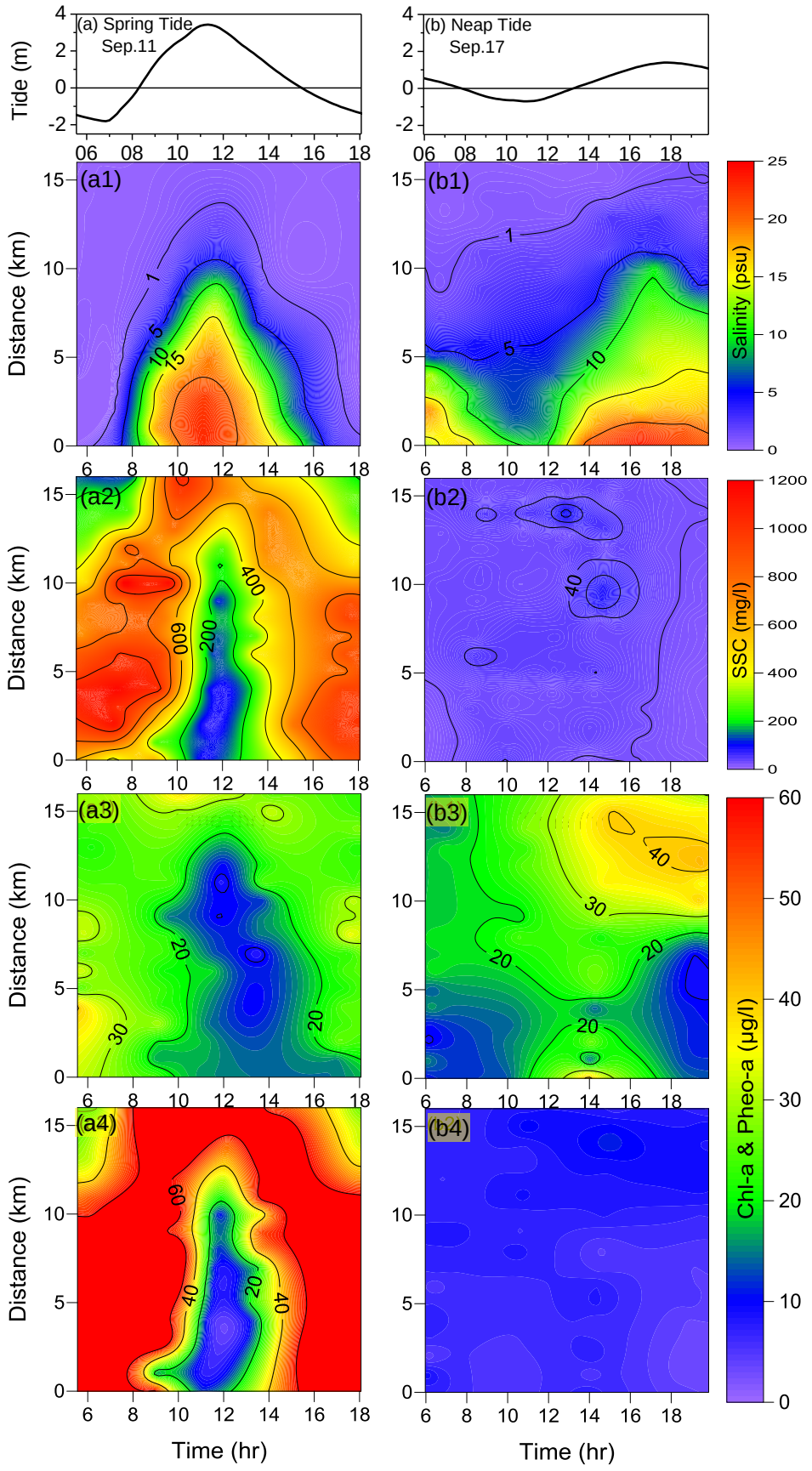

Fig. 4.39 (1) Surface Salinity, (2) Surface SSC, (3) Chl-a, and (4) Pheo-a during (a) spring and (b) neap tide.

(b) Semilunar Variation of Phytoplankton

Analyzed Chl-a was relatively high during spring tide ranged from 7 to 30 μg/l. Although the growth of phytoplankton was inhibited due to high SSC and strong mixing during spring tide, a definite quantity of living phytoplankton existed. The Chl-a concentration became 10–50 μg/l during neap (Fig.4.40c). The Chl-a concentration reached the peak with 70 μg/l on September 20 which is three days after the neap tide.

The phytoplankton was activated and started to grow during neap tide at morning with favorable condition and its growth increases towards the evening. The phytoplankton growth reached the maximum on September 20 at day time and started to deactivate with the strong currents and high SSC. This is showing a 2 to 3 days of timelag in phytoplankton growth with the tidal cycle. A definite quantity of phytoplankton was present in all the days and Chl-a concentration was slightly high in the upper estuary.

Pheo-a concentration was high during spring tide and it became low during neap tide (Fig.4.40d). The trend on the Pheo-a variation for the lower and upper estuary was found opposite. It indicated that Pheo-a migrated from the river mouth to the upper estuary during flood tide.

Chl-a rate in total phytoplankton concentration was 20–60% during spring tide and it reached 90% during neap tide (Fig.4.40e). Chl-a rate became high in the upper estuary during half tide. The upper estuary was suitable for the growth of phytoplankton during the transition phase of mixing.

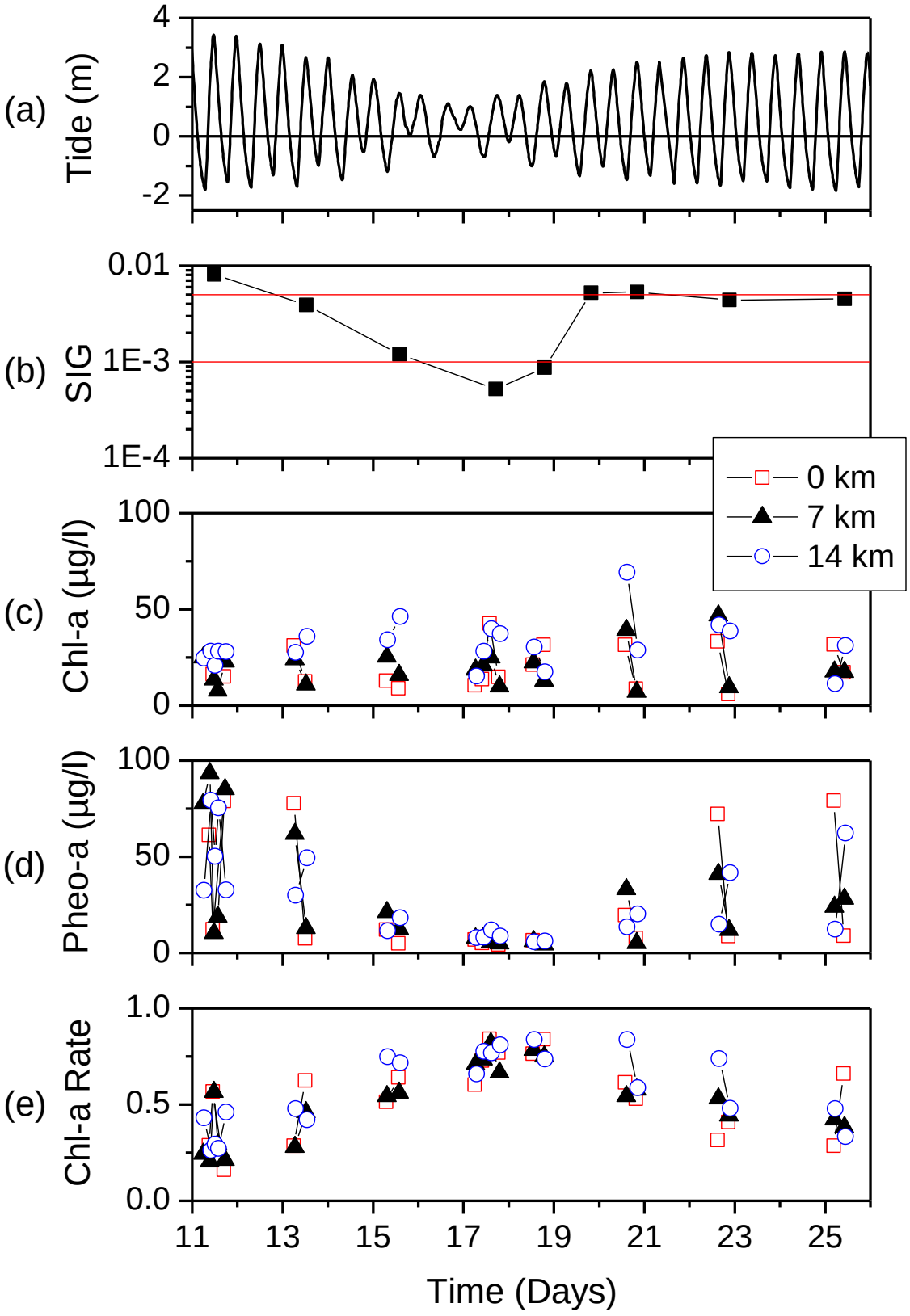

Fig. 4.40 Temporal variations of (a) tide, (b) SIG, (c) chl-a, (d) pheo-a, and (e) chl-a rate.

(c) Spatial Variation of Phytoplankton

Although the growth of phytoplankton was inhibited due to high SSC and strong mixing during spring tide, a definite quantity of living phytoplankton existed (Fig. 4.41). Chl-a and Pheo-a concentration was significantly high in the upper estuary which was coincided with the freshwater salt water interface and high SSC. However Chl-a concentration was negatively correlated with Zp:Zm ratio by spatially.

During September 13 (Fig. 4.42), the peak value of Chl-a was coincided with the low salinity region peak value of Pheo-a coincided with the high SSC. Chl-a concentration was negatively correlated with Zp:Zm ratio by spatially.

During September 15 (Fig. 4.43), the increase in Chl-a concentration was seen and it was near the low salinity region. The Pheo-a concentration was decreased compared with it was during September 13. Chl-a concentration was negatively correlated with Zp:Zm ratio by spatially.

The Chl-a concentration significantly increased during neap tide (Fig. 4.44). The Chl-a was slightly high in the upper estuary. The surface water was diluted by the freshwater since the tidal current was very weak. The estuary was almost clear with low SSC. The Zp:Zm ratio showed a negative relation with Chl-a by spatially similar with spring tide and half tides. The spatial trend of Chl-a and Pheo-a with salinity, SSC and Zp:Zm ratio during September 18 (Fig. 4.45) were similar to the trend as it was during neap tide.

The Chl-a and Pheo-a increased during September 20 (Fig. 4.46) throughout the estuary. The spatial trend of Chl-a and Pheo-a was not showing any relationship with salinity, SSC and Zp:Zm ratio.

The Chl-a during September 22 (Fig. 4.47) was very high with freshwater throughout the estuary. The peak Pheo-a was found near lower estuary where high SSC was seen. There was no relationship found between Chl-a and Zp:Zm ratio.

The spatial trend of Chl-a and Pheo-a with salinity, SSC and Zp:Zm ratio during September 25 (Fig. 4.48) was similar to that it was during September 11.

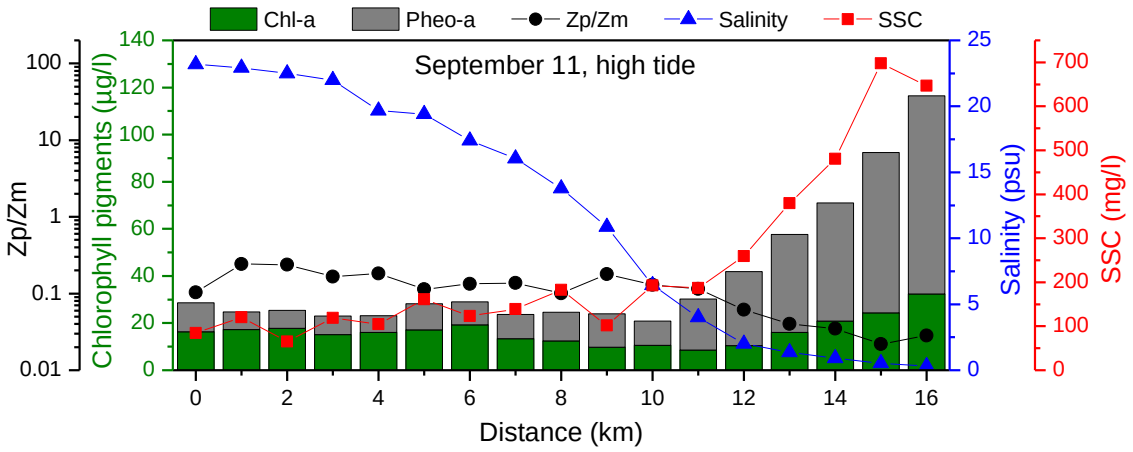

Fig. 4.41 Spatial variation of Chl-a and Pheo-a with Zp:Zm ratio, salinity and SSC during September 11 at high tide.

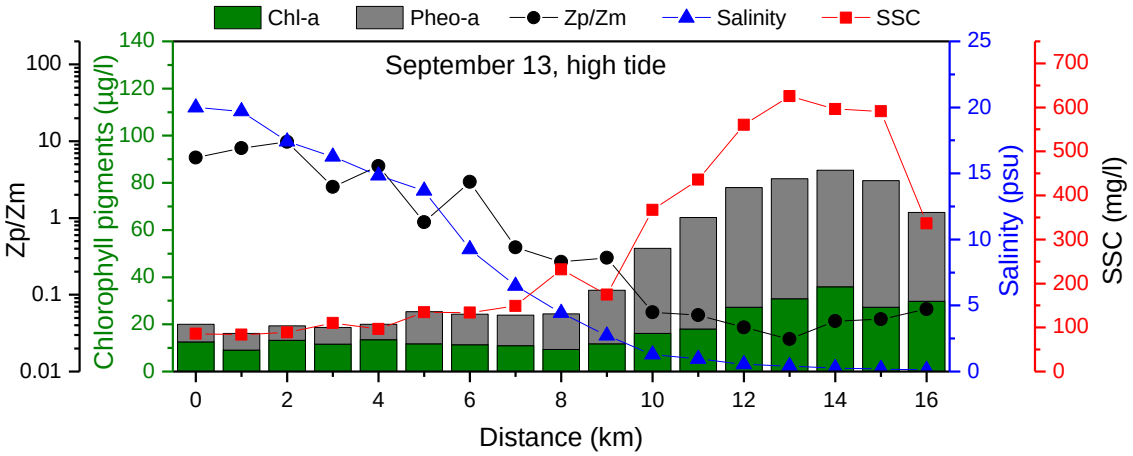

Fig. 4.42 Spatial variation of Chl-a and Pheo-a with Zp:Zm ratio, salinity and SSC during September 13 at high tide.

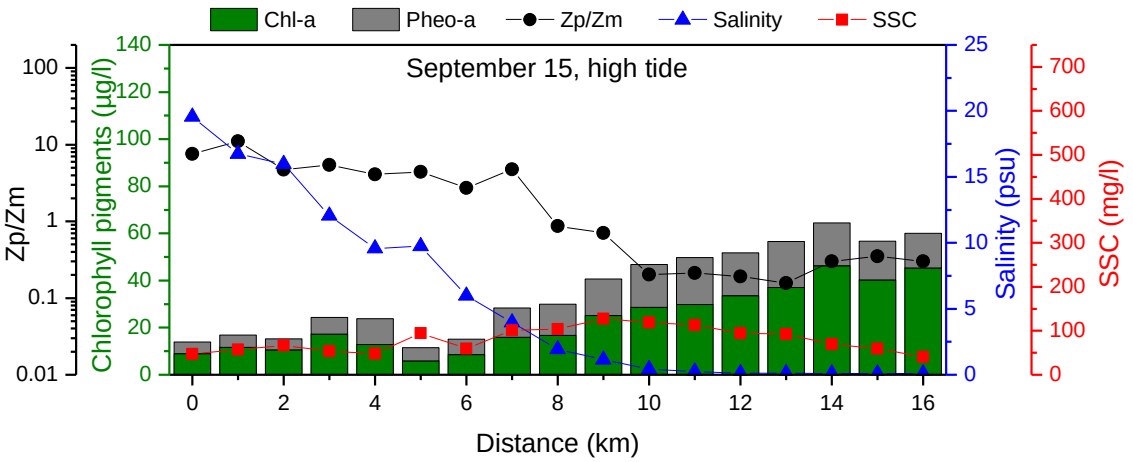

Fig. 4.43 Spatial variation of Chl-a and Pheo-a with Zp:Zm ratio, salinity and SSC during September 15 at high tide.

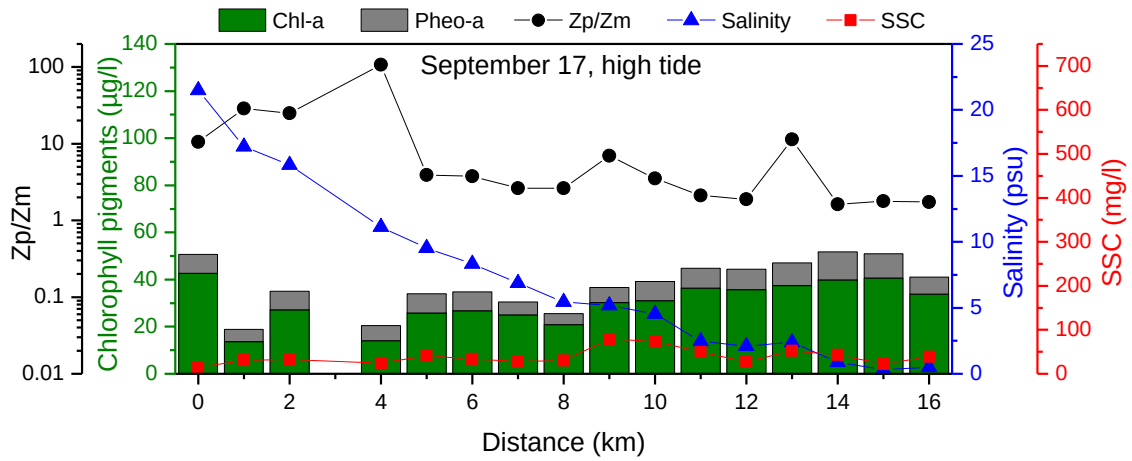

Fig. 4.44 Spatial variation of Chl-a and Pheo-a with Zp:Zm ratio, salinity and SSC during September 17 at high tide.

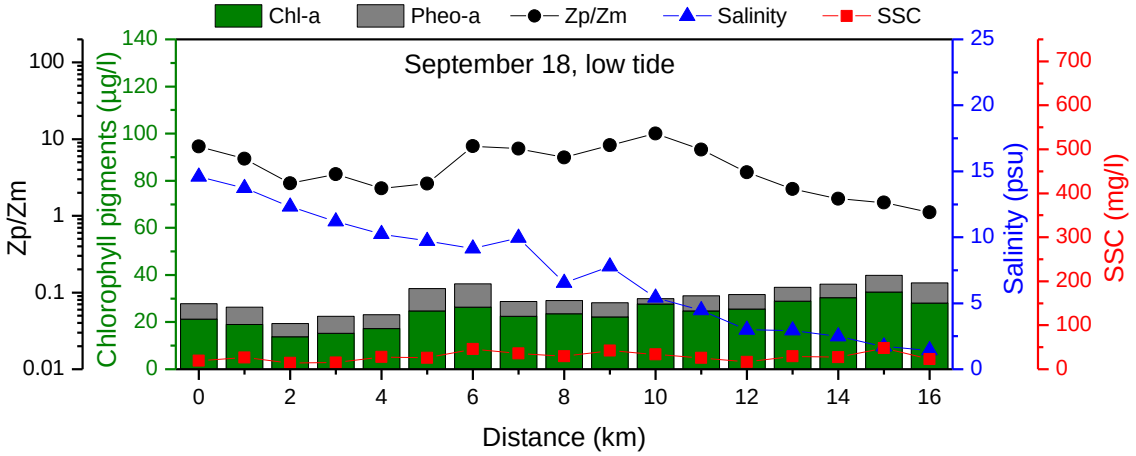

Fig. 4.45 Spatial variation of Chl-a and Pheo-a with Zp:Zm ratio, salinity and SSC during September 18 at low tide.

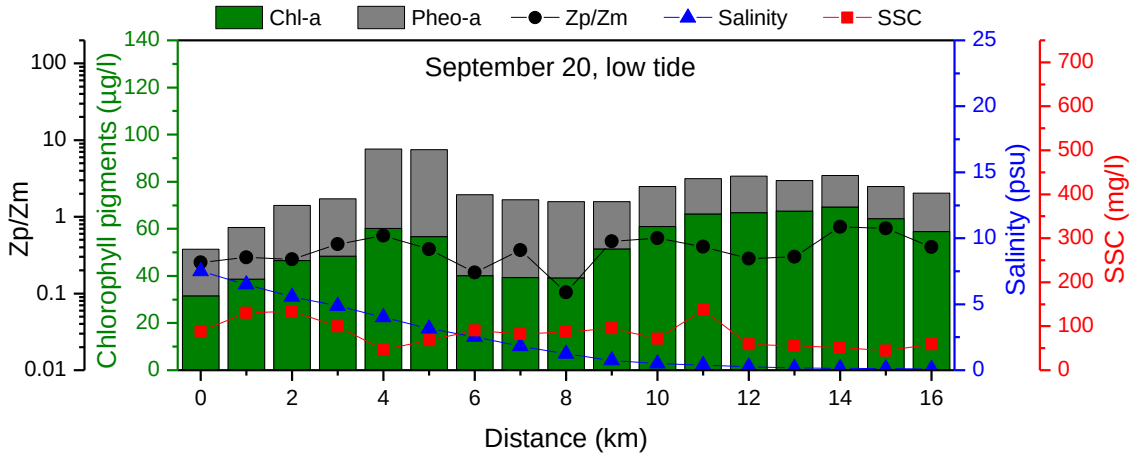

Fig. 4.46 Spatial variation of Chl-a and Pheo-a with Zp:Zm ratio, salinity and SSC during September 20 at low tide.

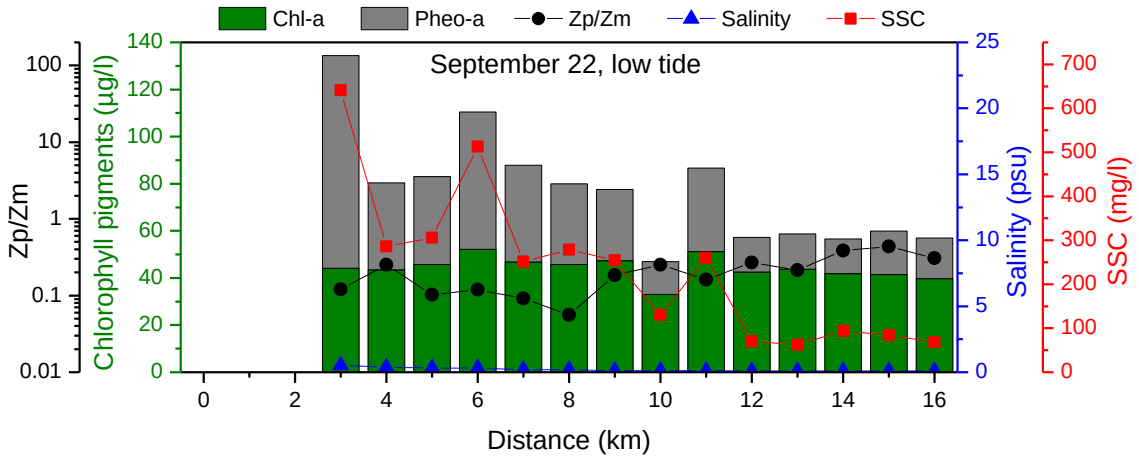

Fig. 4.47 Spatial variation of Chl-a and Pheo-a with Zp:Zm ratio, salinity and SSC during September 22 at low tide.

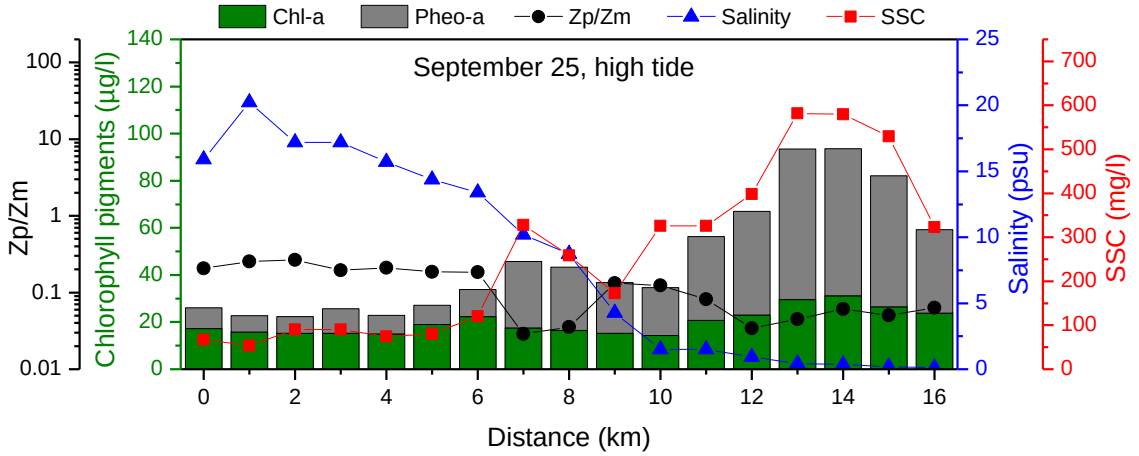

Fig. 4.48 Spatial variation of Chl-a and Pheo-a with Zp:Zm ratio, salinity and SSC during September 25 at high tide.

4.2.3 Zp:Zm Ratio and Activity of Phytoplankton

Cloern (1987) and Grobbelaar *et al.* (1990) suggested that Zp:Zm ratio can explain the fundamental property of highly turbid environments. According to them, phytoplankton production decreases rapidly when ratio of photic depth to mixing depth becomes less than 1 and the estuary becomes sink for phytoplankton when the ratio reaches 0.2. Chl-a distribution was not showing any relationship with the Zp:Zm ratio during semilunar tidal cycle (Fig. 4.49a). Highest concentration of Chl-a was seen on September 20 which is three days after the neap tide. This means that Chl-a was present in all the days; however the Chl-a starts to grow during the neap tide at morning with

favorable condition and its growth increases towards the evening. Then the concentration of Chl-a reaches the peak on September 20 and start to deactivate with the strong currents and high SSC. This is showing 2 to 3 days of time-lag in phytoplankton growth with the tidal cycle.

The above finding is supported by the good relationship between Pheo-a and Zp:Zm ratio (Fig. 4.49b). Pheo-a pigments are the dead phytoplankton cells. The good relation shows that the light availability is strongly influence the activity of phytoplankton. The amount of phytoplankton was below 10μg/l during the neap tide and it gradually decrease during the half tides and Pheo-a becomes more than 100μg/l during spring tide.

The relationship between Chl-a rate and Zp:Zm ratio (Fig. 4.49c) indicate that the Chl-a was inversely proportional to the ratio of photic depth to mixing depth. The phytoplankton starts to grow during neap tide and the amount of living phytoplankton reaches the peak on September 20 with high Chl-a rate. For the Chikugo River estuary, the bottom sediment eroded from the tidal flat during spring tide with high currents and the estuary becomes highly turbid. Then the phytoplankton plants lose the activity to do photosynthesis and gradually die during spring tide due to the limitation of available light and strong tidal currents. Light availability and deactivation of phytoplankton were strongly linked during the semilunar tidal cycle.

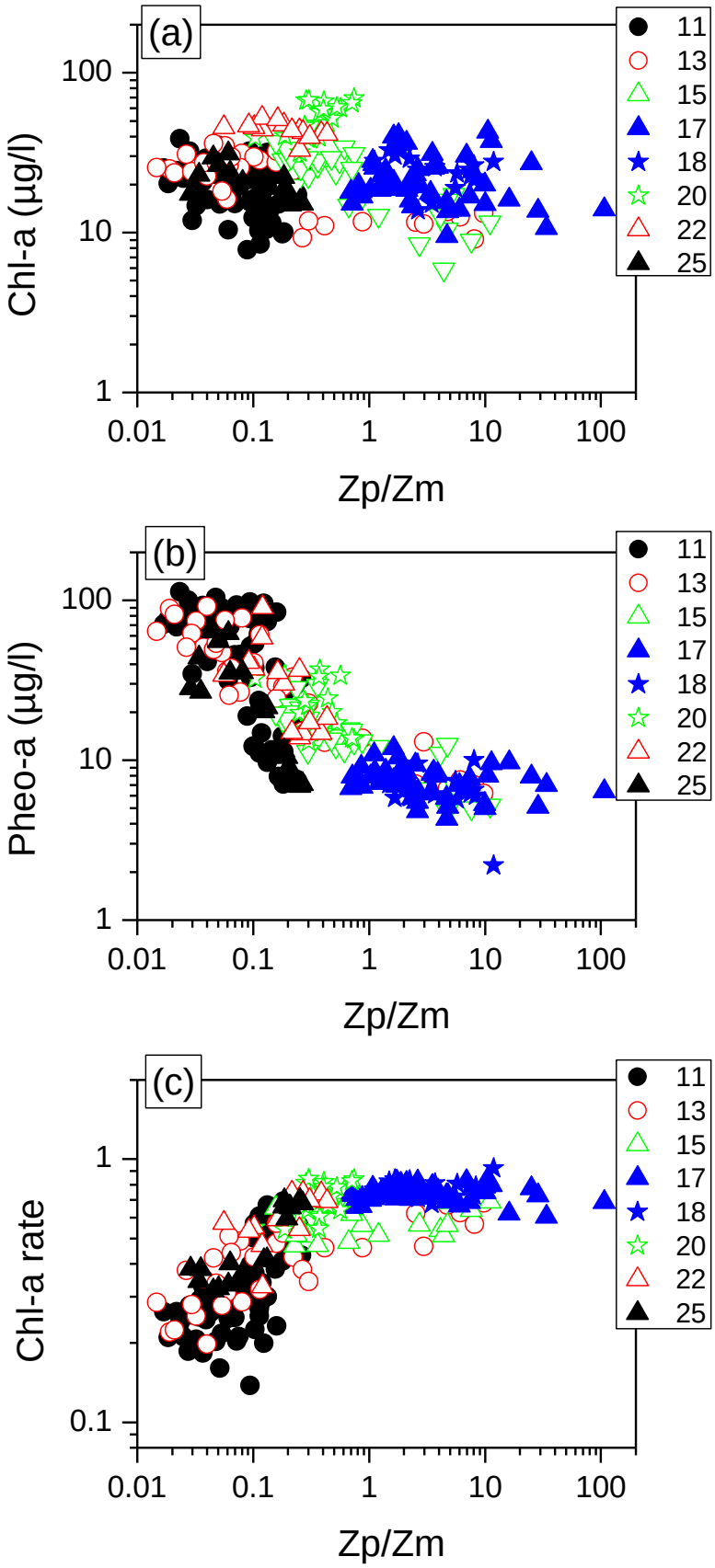

Fig. 4.49 Zp:Zm ratio against chl-a. pheo-a and chl-a rate.

It has been reported that spatial and temporal variability patterns of light available to phytoplankton in the Guadiana estuary are controlled by changes in the levels of suspended sediment (Domingues *et al.*, 2012). Romana (1979) and Edmond *et al.*, (1981) in their studies reported that the major phytoplankton blooms near the mouth of the Seine and Amazon rivers are limited by the severe light attenuation due to high SSC from the rivers. Phytoplankton started to appear only after the SSC reduced by sinking and dilution with seawater.

4.2.4 Time lag of Phytoplankton Growth

The peak value of Chl-a was found near the low salinity region and day time. Therefore, the Chl-a and its mean concentration in the day time and brackish water region (region with salinity of (0.5–2 psu) was plotted against the ratio of photic depth to mixing depth (Fig. 4.50). The relationship showed the hysteresis loop during spring – neap – spring tidal cycle. The Chl-a concentration starts to increase with increase in Zp:Zm ratio during spring tide to neap tide. The Zp:Zm ratio starts to decrease after neap tide and reach the minimum during next spring tide. However the Chl-a concentration reached its peak on three days after the neap tide and then it starts to decrease during the successive days.

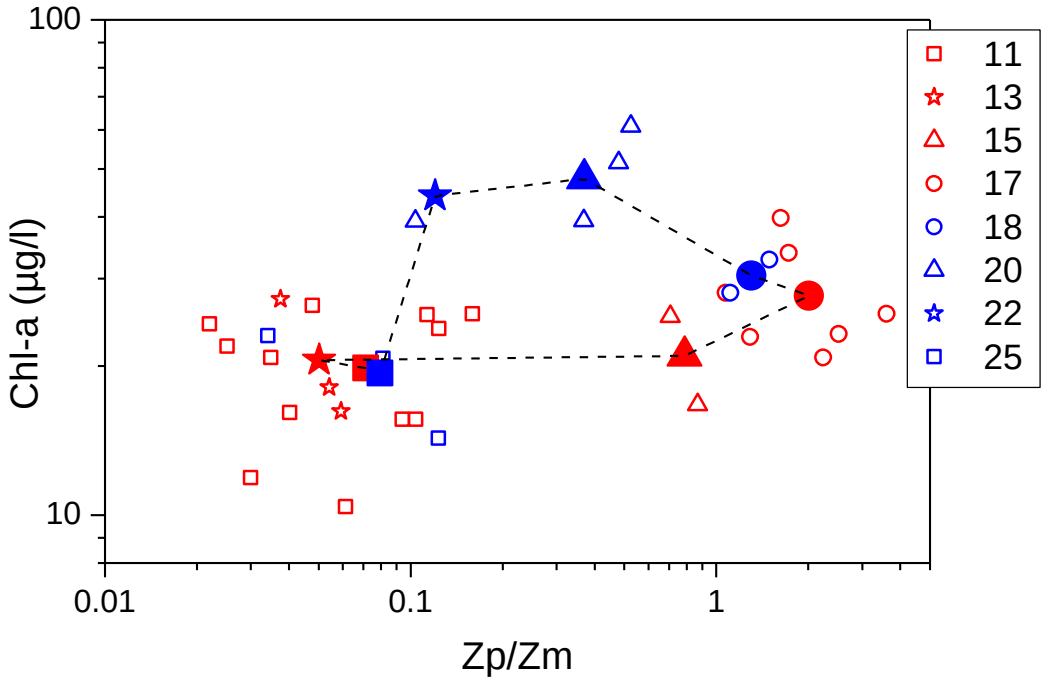

Fig. 4.50 Zp:Zm ratio vs chl-a for brackish water.

The relationship between in-situ Chl-a and analysed Chl-a (Fig. 4.2) supports the discussion about the time lag. The slope of the relationship indicates the proportion of actual Chl-a content in the in-situ Chl-a value and it changed gradually. The time series of slope was plotted with respect to tide (Fig. 4.51).The slope was 1.69 during spring tide and it gradually increased during half tides. It reached 3.79 during neap tide. The peak value was found during September 20 which three days after neap tide. Then the slope started to decrease during September 22 and 25.

This shows that phytoplankton growth has three days of time lag with the physical process in the Chikugo River estuary.

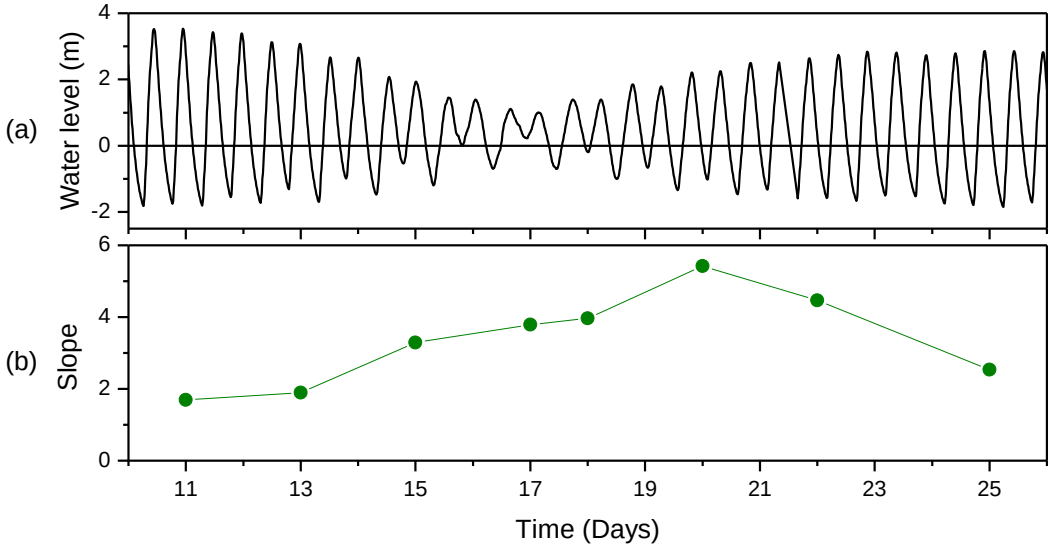

Fig. 4.51 Time series of the (a) water level and (b) slope of the relationship between in-situ Chl-a and analysed Chl-a.

In seasonal perspective, temporal variation of freshwater flow drive the annual growth cycle of phytoplankton in estuaries (Sinclair *et al.*, 1981). For the fortnightly basis, phytoplankton production was influenced by spring-neap tidal cycle for various estuaries (Cloern, 1984; Demers *et al.*, 1979; Haas, 1977; Sinclair, 1978; Takahashi *et al.*, 1977; Winter *et al.*, 1975). In several estuaries, highest amount of phytoplankton was found during the neap tide with low SSC and strong stratification. On the other hand a rapid decline in phytoplankton production occurred during spring tide with high SSC and weak stratification (Cloern, 1996). Phytoplankton growth cycle of the Chikugo river estuary was also influenced by the spring-neap-spring tidal cycle. However, it was found that phytoplankton growth cycle of the Chikugo River estuary has three days of time lag with the physical process in the estuary.

4.2.5 Migration of Phytoplankton

Surface salinity reach (SSR) was plotted against Chl-a length and showed good relationship (Fig. 4.52a). Furthermore, good relationship was found between surface SSC maximum (SSM) and Pheo-a length (Fig. 4.52b). The Chl-a length and Pheo-a length showed the location of peak concentration of Chl-a and Pheo-a respectively. The peak concentration of Chl-a was located in the upper reach of the salinity front. The location of the peak Pheo-a was coincided with the ETM zone.

Location of peak Chl-a concentration in the open ocean was discussed by many researchers (Furuya, 1990; Hobson and Lorenzen, 1972; Lips et al., 2010; Messie and Radenac, 2006; Perry et al., 2008). However studies about the peak Chl-a in estuaries were limited. Fisher et al. (1988) reported that peak Chl-a was found seaward of the ETM zone for Chesapeake and Delaware Bay estuaries, USA. The salinity at the location of peak Chl-a concentration were <20 psu for Chesapeake Bay and 15 – 30 psu for Delaware Bay. Furthermore, peak Chl-a was found at the ETM zone itself in the northern San Francisco Bay Estuary (Cloern et al., 1983), Colne estuary (Kocum et al., 2002), and Hudson River estuary (Cole *et al.*, 1992). Additionally, peak Chl-a was found at the freshwater region of James, York and Rappahannock river estuaries which are the sub estuaries of Chesapeake Bay (Anderson, 1986).

From the relationship between SSR and Chl-a length, it was found that the phytoplankton in the Chikugo River estuary mainly inhabit in brackish water below 1psu. Good relationship between surface SSC maximum (SSM) and Pheo-a length indicated that the dead phytoplankton adhered to the inorganic sediment and moved with ETM zone. Therefore, development of the ETM and the deactivation of phytoplankton were interacting.

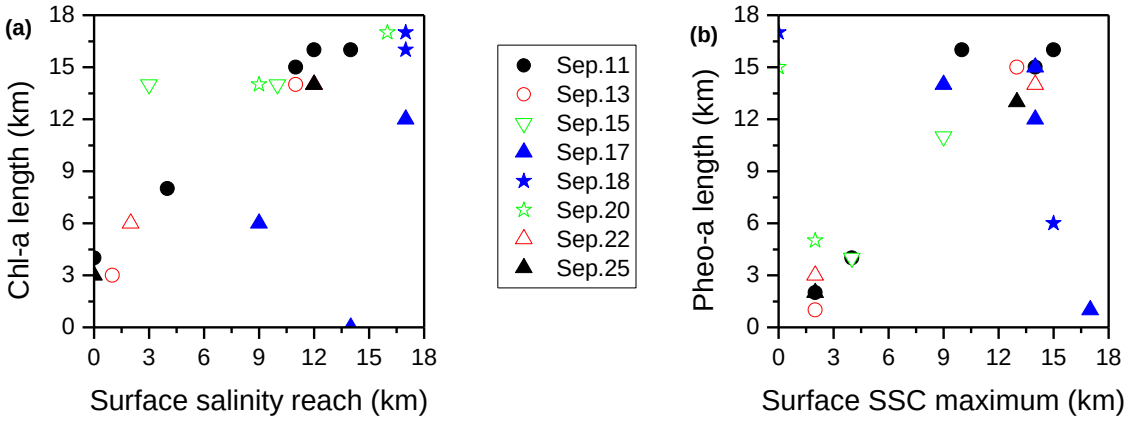

Fig. 4.52 (a) Chl-a length against Surface SIL, and (b) Pheo-a length against Surface SSC length.

4.3 Conclusions

The photic depth became less than 0.2 m during spring tide and it gradually increased during the half tides and reached 4 m during neap tide. The mixing depth during spring tide was more than 10 times the photic depth for the whole estuary except river mouth and 17 km upstream. For the half tide Zp:Zm ratio was ranged between 0.2 to 1. The mixing depth reduced during neap tide and the Zp:Zm ratio was ranged between 1 to more than 10. Strong relation between K and SSC indicate that the SSC was the key driver of light availability in the Chikugo river estuary.

Although light scarcely penetrated into the water column during spring tide, a definite quantity of living phytoplankton (Chl-a) existed throughout the semilunar tidal cycle. Mean concentration of Chl-a in the daytime and in the upper estuary against Zp:Zm ratio showed the hysteresis loop and it was found that phytoplankton growth has a time lag of three days. Good relationship between SSR and Chl-a length showed that the phytoplankton mainly inhabit in brackish water below 1psu.

Pheo-a (dead phytoplankton cells) had high correlation for SSC, K and Zp:Zm ratio. This shows that phytoplankton deactivation and Pheo-a production were caused by the light limitation due to suspended sediment. Good relationship between location of SSM and Pheo-a length indicated that the detritus migrated by adhering to inorganic sediment. It was concluded that estuarine mixing, development of the ETM and phytoplankton process interact.

Chapter 5

Conclusions

This chapter gives the summary of main conclusions of each chapter and the future issues.

The spatial distribution and temporal variation of salinity and SSC in the highly turbid Chikugo River estuary, Japan, was continuously measured for two weeks, and the transition process of mixing conditions and ETM process during a semi-lunar tidal cycle were examined.

5.1 Salinity Intrusion, Mixing and Suspended Sediment Dynamics

The estuary gradually changed from a vertically well-mixed condition during the spring tide to a strongly stratified condition during the neap tide via a partially mixed condition during intermediate half tides.

Salinity intrusion was showing an increasing trend towards upstream as the tidal phase changes from low tide to high tide and going back seaward during the ebb phase. Also it shows a well-mixed condition with weak vertical stratification & halocline throughout the spring tidal cycle. Isohalines looks almost vertical and there were no two layered net circulation. Location of ETM zone was moving landward or seaward depending upon the tidal phase. The spring tidal cycle affects locations of ETM. ETM zone was located near or landward of the fresh-salt water interface. The highest SSC was found during the flood tides due to high current velocity.

The flow ratio of the estuary was significantly affected by both the tidal prism during the semi-lunar tidal cycle and daily freshwater discharge. The SSC was explained by the flow ratio, thus, ETM growth was dominated by both tidal forcing and the freshwater flow, with the exception of the rapid variation of the freshwater discharge following heavy rainfall.

The relationship between salinity and the SSC was investigated longitudinally. In the lower estuary, the SSC was high near the region with a salinity of 10 psu. The SSC was high when salinity was 0.5 psu in the upper estuary. There were two peaks of SSC in the middle estuary when salinity was around 0.5 psu and 10 psu. This suggested there are two processes on suspended sediment occurrence and transport.

The spatio-temporal characteristics of SSC were explained through the MS. The SSC in the lower estuary was higher than in the upper estuary for the same MS. This indicated that bottom sediment in the lower estuary was easily eroded during neap-spring transition and that suspended sediment did not settle appreciably during spring-neap transition. In contrast, the settling velocity of fine particles in the upper estuary increased due to flocculation.

Based on the flow ratio, salinity and MS, the occurrence of the ETM and its development at the macrotidal Chikugo river estuary was a consequence of three processes: bed sediment erosion by sea water in the lower estuary, sediment transport in the estuarine channel by the tidal current and freshwater flow, and sediment accumulation at the salinity front in the upper estuary.

5.2 Estuarine Mixing and ETM on Phytoplankton Process

The photic depth became less than 0.2 m during spring tide and it gradually increased during the half tides and reached 4 m during neap tide. The mixing depth (Fig. 5c) during spring tide was more than 10 times the photic depth for the whole estuary except river mouth and 17 km upstream. For the half tide Zp:Zm ratio was ranged between 0.2 to 1. The mixing depth reduced during neap tide and the Zp:Zm ratio was ranged between 1 to more than 10. Strong relation between K and SSC indicate that the SSC was the key driver of light availability in the Chikugo river estuary.

Although light scarcely penetrated into the water column during spring tide, a definite quantity of living phytoplankton (Chl-a) existed throughout the semilunar tidal cycle. Mean concentration of Chl-a in the daytime and in the upper estuary against Zp/Zm showed the hysteresis loop and it was found that phytoplankton growth has a time lag of three days. Good relationship between SSR and Chl-a length showed that the phytoplankton mainly inhabit in brackish water below 1psu. The peak value of Chl-a was located near the low salinity region.

Pheo-a (dead phytoplankton cells) had high correlation for SSC, K and Zp/Zm. This shows that phytoplankton deactivation and Pheo-a production were caused by the light limitation due to suspended sediment. Good relationship between location of SSM and Pheo-a length indicated that the detritus migrated by adhering to inorganic sediment. The peak value of Pheo-a was located near the ETM zone. It was concluded that estuarine mixing, development of the ETM and phytoplankton process interact.

5.3 Future Works

The environment of river estuary consists of many elements, such as physical processes, chemical reactions, and biological structures. All elements are interconnected, and the relationship between elements varies temporally and spatially. Time scales are various, including semidiurnal, semilunar tidal cycles, and monthly variations in freshwater discharge. Spaces are longitudinally, upper, middle, and lower estuaries, horizontally, salt marsh, tidal flat and deep channel, and vertically, dry and wet zones.

Since environmental processes in estuaries are very complex, and since there are many environmental issues affecting these environments, it is necessary for the river engineer to understand both individual elements and the interaction between those elements. For example, construction of an estuary barrage changes flow and salinity. An estuary barrage interrupts movement of freshwater towards the sea and salt water intrusion in land become stagnated, possibly leading to a decrease in dissolved oxygen. Hypoxia then occurs in the salt wedge, and non-oxygenated water damages shellfish inhabiting the estuarine channel. Ultimately, fishermen will be unable to maintain the levels of shellfish catch which existed prior to construction of the estuary barrage, and their livelihoods suffer as a result. In the meantime, city dwellers will also be unable to consume the shellfish.

Therefore it is important to reproduce and predict the estuarine changes using numerical simulation for the better management of the aquatic environment of river estuaries.

When using numerical models, dimension and orientation suitable for the target area should be chosen. Depending on the type of estuary, several types of models can be used. A 1D model along an estuarine channel is applicable to a well-mixed estuary with a single channel. A depth-averaged 2D model is applicable to a well-mixed estuary with multi-channel or with complex planar topography, and this model is suitable for

understanding horizontal circulation and differences between the center of the channel and the near-shore area. A width-averaged 2D model is generally utilized in partially mixed estuaries and stratified estuaries with a single channel. A 3D model is applicable for all situations with more complex systems and processes; however computation time for such model is very long. 1D or 2D models were not appropriate for Chikugo river estuary as the estuary was influenced by all types of mixing conditions.

The process for achieving the objectives in this study includes:

- Investigate the processes during the lifecycle of phytoplankton (Skeletonema costatum).
- Development of a new three dimensional numerical simulation model to analyse the aquatic ecosystem of the Chikugo River estuarine channel considering their interactions with the physical environment.
- Analyse the complex tidal dynamics by predicting the mixing and salinity intrusion using estuarine bathymetry, tides, and climate. Continuous changes in climate can cause variability in the freshwater runoff and evaporation regimes.
- Then result from the above prediction of mixing and salinity intrusion can be used to assist the interpretation of magnitude and movement of estuarine turbidity maximum (ETM) and potential areas of erosion.
- Finally predict the migration and lifecycle of phytoplankton ecosystems in the Chikugo River estuary considering the variability and interaction of physical drivers in a large number of ways.

The numerical simulation modeling can help our understanding of the complex hydraulic processes, morphodynamics and changes in environmental and ecological condition of the Chikugo River estuary. The modelling can be applicable to the branched estuarine systems of Asian developing countries (*e. g.*, Ganges delta in India and Bangladesh, Mekong Delta in Vietnam) and helps for the better planning and management of their aquatic environment.

References:

Allen, G.P., Salomon, J.C., Bassoullet, P., Penhoat, Y.D., Grandpre, C.D., 1980. Effects of tides on mixing and suspended sediment transport in macrotidal estuaries. Sedimentary Geology 26, 69–90.

Anderson, G.F., 1986. Silica, diatoms and a freshwater productivity maximum in Atlantic Coastal Plain estuaries, Chesapeake Bay. Estuarine, Coastal and Shelf Science 22, 183–197.

Andersen, T.J. Fredsoe, J., Pejrup, M., 2007. In situ estimation of erosion and deposition thresholds by Acoustic Doppler Velocimeter (ADV). Estuarine, Coastal and Shelf Science 75, 327–336.

Baeyens, W., Eck, B.V., Lambert, C., Wollast, R., Goeyens, L., 1998. General description of the Scheldt estuary, Hydrobiologia 366, 1–14.

Barbosa, A.B., Domingues, R.B., Galvão, H.M., 2010. Environmental forcing of phytoplankton in a Mediterranean estuary (Guadiana estuary, south-western Iberia): a decadal study of climatic and anthropogenic influences. Estuarine Coastal and Shelf Science 33, 324–41.

Boyer, J.N., Kelble, C.R., Ortner, P.B., Rudnick, D.T., 2009. Phytoplankton bloom status: Chlorophyll a biomass as an indicator of water quality condition in the southern estuaries of Florida, USA. Ecological Indicators 9, S56–S67.

Bruno, S.F., Staker, R.D., Sharma, G.M., 1980. Dynamics of Phytoplankton Productivity in the Peconic Bay Estuary, Long Island. Estuarine and Coastal Marine Science 10, 247–263.

Byun, D.S., Wang, X.H., Zavatarelli, M., Cho, Y.K., 2007. Effects of resuspended sediments and vertical mixing on phytoplankton spring bloom dynamics in a tidal estuarine embayment. Journal of Marine Systems 67, 102–118.

Cameron, W.M., Pritchard, D.W., 1963. Estuaries. In: The Sea (Ed. MN Hill), **2**, Wiley, New York, 306–324.

Capo, S., Sottolichio, A., Brenon, I., Castaing, P., Ferry, L., 2006. Morphology, hydrography and sediment dynamics in a mangrove estuary: The Konkoure Estuary., Guinea. Marine Geology 230, 199–215.

Chen, M.S., Wartel, S., Eck, B.V., Maldegem, D.V., 2005. Suspended matter in the Scheldt estuary. Hydrobiologia 540, 79–104.

Cloern, J.E., Alpine, A.E., Cole, B.E., Wong, R.L.J., Arthur, J.F., Ball, M.D., 1983. River discharge controls phytoplankton dynamics in the northern San Francisco Bay estuary. Estuarine, Coastal and Shelf Science 16, 415–429.

Cloern, J.E., 1984. Temporal dynamics and ecological significance of salinity stratification in an estuary (South San Francisco Bay, USA). Oceanologica Acta 7, 137–141.

Cloern, J.E., Cole, B.E., Wong, R.L.J., Alpine, A.E., 1985. Temporal dynamics of estuarine phytoplankton. A case study of San Francisco Bay. Hydrobiologia 129, 153–176.

Cloern, J.E., 1987. Turbidity as a control on phytoplankton biomass and productivity in estuaries. Continental Shelf Research 7, 1367–1381.

Cloern, J.E., Powell, T.M., Huzzey, L.M., 1989. Spatial and Temporal Variability in South San Francisco Bay (USA). II. Temporal Changes in Salinity, Suspended Sediments, and Phytoplankton Biomass and Productivity Over Tidal Time Scales. Estuarine, Coastal and Shelf Science 28, 599–613.

Cloern, J.E., 1996. Phytoplankton bloom dynamics in coastal ecosystems: A review with some general lessons from sustained investigation of San Francisco Bay, California. Review of Geophysics 34, 127–168.

Cloern, J.E., Jassby, A.D., 2010. Patterns and Scales of Phytoplankton Variability in Estuarine–Coastal Ecosystems. Estuaries and Coasts 33, 230–241.

Cole, J.J., Caraco, N.F., Peierls, B.L., 1992. Can phytoplankton maintain a positive carbon balance in a turbid, freshwater, tidal estuary? Limnology and Oceanography 37, 1608–1617.

Cook, T.L., Sommerfield, C.K., Wong, K., 2007. Observations of tidal and springtime sediment transport in the upper Delaware Estuary. Estuarine, Coastal and Shelf Science 72, 235–246.

Davies, J.L., 1964. A morphogenetic approach to world shorelines. Zeitschrift fur Geomorphologie 8, 127–142.

Deloffre, J., Verney, R., Lafite, R., Lesueur, P., Lesourd, S., Cundy, A.B., 2007. Sedimentation on intertidal mudflats in the lower part of macrotidal estuaries: Sedimentation rhythms and their preservation. Marine Geology 241, 19–32.

Demers, S., Lafleur, P.E., Legendre, L., Trump, C.L., 1979. Short-term covariability of Chlorophyll and Temperature in the St. Lawrence Estuary. Journal of the Fisheries Research Board of Canada 36, 568–573.

Dobereiner, C., McManus, J., 1983. Turbidity maximum migration and harbour siltation in the Tay estuary. Canadian Journal of Fisheries and Aquatic Sciences 40(S1), 117–129.

Domingues, R.B., Barbosa, A., Galvao, H., 2005. Nutrients, light and phytoplankton succession in a temperate estuary (the Guadiana, south-western Iberia. Estuarine, Coastal and Shelf Science 64, 249–260.

Domingues, R.B., Anselmo, T.P., Barbosa, A.B., Sommer, U., Galvão, H.M., 2011. Light as a driver of phytoplankton growth and production in the freshwater tidal zone of a turbid estuary. Estuarine Coastal and Shelf Science 91, 526–35.

Domingues, R.B., Barbosa, A.B., Sommer, U., Galvao, H.M., 2012. Phytoplankton composition, growth and production in the Guadiana estuary (SW Iberia): Unraveling changes induced after dam construction. Science of the Total Environment 416, 300–313.

Dyer, K.R., 1986. Coastal and Estuarine Sediment Dynamics. John Wiley & Sons, Chichester.

Dyer, K.R., 1997. Estuaries, A Physical Introduction, 2nd Edition, John Wiley, London, UK, 195 pp.

Dyer, K.R., Ramamoorthy, K., 1969. Salinity and water circulation in the Vellar estuary. Limnology and Oceanography 14, 4–15.

Edmond, J.M., Boyle, E.A., Grant, B., Stallard, R.F., 1981. The chemical mass balance in the Amazon plume I: The nutrients. Deep Sea Research 28, 1339–1374.

Festa, J.F., Hansen, D.V., 1978. Turbidity maxima in partially mixed estuaries: A two-dimensional numerical model. Estuarine, and Coastal Marine Science 7, 347–359.

Feuillet, J.P., Fleischer, P., 1980. Estuarine circulation: Controlling factor of clay mineral distribution in James River Estuary, Virginia. Journal of Sedimentary Petrology 50, 267 – 279.

Fisher, T.R., Harding, L.W., Stanley, D.W., Ward, L.G., 1988. Phytoplankton, nutrients, and turbidity in the Chesapeake, Delaware, and Hudson estuaries. Estuarine, Coastal and Shelf Science 27, 61–93.

Furuya, K., 1990. Subsurface chlorophyll maximum in the tropical and subtropical western Pacific Ocean: vertical profiles of phytoplankton biomass and its relationship with chlorophyll a and particulate organic carbon. Marine Biology 107, 529–539.

Gameiro, C., Cartaxana, P., Brotas, V., 2007. Environmental drivers of phytoplankton distribution and composition in Tagus Estuary, Portugal. Estuarine, Coastal and Shelf Science 75, 21–34.

Gelfenbaum, G., 1983. Suspended-sediment response to semidiurnal and fortnightly tidal variations in a mesotidal estuary: Columbia River, U.S.A. Marine Geology 52, 39–57.

Grabemann, I., Uncles, R.J., Krause, G., Stephens, J.A., 1997. Behaviour of Turbidity Maxima in the Tamar (U.K.) and Weser (F.R.G.) Estuaries. Estuarine, Coastal and Shelf Science 45, 235–246.

Grobbelaar, J.U., Soeder, C.J., Stengel, E., 1990. Modeling algal productivity in large outdoor cultures and waste treatment systems. Biomass 21, 297–314.

Haas, L.W., 1977. The effect of the spring-neap tidal cycle on the vertical salinity structure of the James, York and Rappahannock Rivers, Virginia, U.S.A. Estuarine and Coastal Marine Science 5, 485–496.

Hir, P.L., Monbet, Y., Orvain, F., 2007. Sediment erodability in sediment transport modeling: Can we account for biota effect. Continental Shelf Research 27, 1116–1142.

Hobson, L.A., Lorenzen, C.J., 1972. Relationships of chlorophyll maxima to density structure in the Atlantic Ocean and Gulf of Mexico. Deep-Sea Research 19, 297–306.

Jago, C.F., Ishak, A.K., Jones, S.E., Goff, M.R.G., 2006. An Ephemeral Turbidity Maximum Generated by Resuspension of Organic-rich Matter in a Macrotidal Estuary, S.W. Wales. Estuaries and Coasts 29, 197–208.

Ji, Z.-H., Hu, G., Shen, J., Wan, Y., 2007. Three-dimensional modeling of hydrodynamic processes in the St. Lucie Estuary. Estuarine, Coastal and Shelf Science 73, 188–200.

Kasai, A., Kurikawa, Y., Ueno, M., Robert, D., Yamashita, Y., 2010. Salt-wedge intrusion of seawater and its implication for phytoplankton dynamics in the Yura Estuary, Japan. Estuarine, Coastal and Shelf Science 86, 408–414.

Kitheka, J.U., Obiero, M., Nthenge, P., 2005. River discharge, sediment transport and exchange in the Tana Estuary, Kenya. Estuarine, Coastal and Shelf Science 63, 455–468.

Kocum, E., Underwood, G.J.C., Nedwell, D.B., 2002. Simultaneous measurement of phytoplanktonic primary production, nutrient and light availability along a turbid, eutrophic UK east coast estuary (the Colne Estuary). Marine Ecology Progress Series 231, 1–12.

Lips, U., Lips, I., Liblik, T., Kuvaldina, N., 2010. Processes responsible for the formation and maintenance of sub-surface chlorophyll maxima in the Gulf of Finland. Estuarine, Coastal and Shelf Science 88, 339–349.

May, C.L., Koseff, J., Lucas, L.V., Cloern, J.E., Schoellhamer, D.H., 2003. Effects of spatial and temporal variability of turbidity on phytoplankton blooms. Marine Ecology Progress Series 254, 111–128.

Messie, M., Radenac, M.H., 2006. Seasonal variability of the surface chlorophyll in the western tropical Pacific from SeaWiFS data. Deep-Sea Research Part I 53, 1581–1600.

Mitchell, S.B., 2013. Turbidity maxima in four macrotidal estuaries. Ocean & Coastal Management 79, 62–69.

Muylaert, K., Sabbe, K., Vyverman, W., 2000. Spatial and temporal dynamics of phytoplankton communities in a freshwater tidal estuary (Schelde, Belgium). Estuarine, Coastal and Shelf Science 50, 673–687.

Muylaert, K., Tackx, M., Vyverman, W., 2005. Phytoplankton growth rates in the freshwater tidal reaches of the Schelde estuary (Belgium) estimated using a simple light-limited primary production model. Hydrobiologia 540, 127–140.

Newell, R.I.E., 1988. Ecological changes in Chesapeake Bay: Are they the result of over-harvesting the American oyster, Crassostrea virginica? In Understanding the Estuary: Advances in Chesapeake Bay Research. M. Lynch and E.C. Krome (eds.). Chesapeake Research Consortium, Solomons, MD, pp. 536–546.

Owens, N.J.P., 1985. Variations in the natural abundance of 15N in estuarine suspended particulate matter: A specific indicator of biological processing. Estuarine, Coastal and Shelf Science 20, 505–510.

Patchineelam, S.M., Kjerfve, B., 2004. Suspended sediment variability on seasonal and tidal time scales in the Winyah Bay estuary, South Carolina, USA. Estuarine, Coastal and Shelf Science 59, 307–318.

Pennock, J.R., 1985. Chlorophyll Distributions in the Delaware Estuary: Regulation by Light-limitation. Estuarine, Coastal and Shelf Science 21, 711–725.

Pennock, J.R., Sharp, J.H., 1986. Phytoplankton production in the Delaware Estuary: temporal and spatial variability. Marine ecology 34, 143–155.

Pennock, J.R., 1987. Temporal and Spatial Variability in Phytoplankton Ammonium and Nitrate Uptake in the Delaware Estuary. Estuarine, Coastal and Shelf Science 24, 841–857.

Perry, M.J., Sackmann, B.S., Eriksen, C.C., Lee, C.M., 2008. Seaglider observations of blooms and subsurface chlorophyll maxima off the Washington coast. Limnology and Oceanography 53, 2169–2179.

Peterson, O.H., Festa, J.P., 1984. Numerical simulation of phytoplankton productivity in partially mixed estuaries. Estuarine, Coastal and Shelf Science 19, 563–589.

Pierson, D.C., Markensten, H., Strombeck, N., 2003. Long and short term variations in suspended particulate material: The influence on light available to the phytoplankton community. Hydrobiologia 494, 299–304.

Pritchard, D.W., 1967. What is an estuary: physical viewpoint. In Lauf, G. H. Estuaries. A.A.A.S. Publ. 83. Washington, DC. pp. 3–5.

Romana, L.A., 1979. Role du bouchon vaseaux duns un ecosysteme estuarien. 2es Journees de la thermoecologie, Institute Scientifique et Technique des Peches Maritimes, pp. 121–140.

Rothschild, B.J., Ault, J.S., Goulletquer, P., Heral, M., 1994. Decline of the Chesapeake Bay oyster population: a century of habitat destruction and overfishing, Marine Ecology Progress Series 111, 29–39.

Schubel, J.R., 1968. Turbidity maximum of the northern Chesapeake Bay. Science 161, 1013–1015.

Shi, K., Zhang, Y., Liu, X., Wang, M., Qin, B., 2014. Remote sensing of diffuse attenuation coefficient of photosynthetically active radiation in Lake Taihu using MERIS data. Remote Sensing of Environment 140, 365–377.

Simmons, H.B., 1955. Some effects of upland discharges on estuarine hydraulics. Proceedings of 81st Conference of American Society of Civil Engineers (Reston, Virginia, ASCE), pp. 792.

Sinclair, M., 1978. Summer Phytoplankton Variability in the Lower St. Lawrence

Estuary. Journal of the Fisheries Research Board of Canada 35, 1171–1185.

Sinclair, M., Rao, D.V.S., Couture, R., 1981. Phytoplankton temporal distributions in estuaries. Oceanologica Acta 4, 239–246.

Small, L.F., Frey, B.E., 1984. Water column primary production in the Columbia River Estuary. Final Report, Columbia River Estuary Data Development program, Astoria, Oregon, 133 pp.

Smith, R.C., Baker, K.S., 1978. The bio-optical state of ocean waters and remote sensing. Limnology and Oceanography 23, 247–259.

Somlyody, L., Koncsos, L., 1991. Influence of Sediment Resuspension on the Light Conditions of Algal Growth in Lake Balaton. Ecological Modelling 57, 173–192.

Sommerfield, C.K., Wong, K.C., 2011. Mechanisms of sediment flux and turbidity maintenance in the Delaware Estuary. Journal of Geophysical Research: Oceans 116 (C1).

Sottolichio, A., Hurther, D., Gratiot, N., Bretel, P., 2011. Acoustic turbulence measurements of near-bed suspended sediment dynamics in highly turbid waters of a macrotidal estuary. Continental Shelf Research 31, S36–S49.

Suzuki, K.W., Kasai, A., Isoda, T., Nakayama, K., Tanaka, M., 2008. Distinctive stable isotope ratios in important zooplankton species in relation to estuarine salinity gradients: Potential tracer of fish migration. Estuarine, Coastal and Shelf Science 78, 541–550.

Suzuki, K.W., Nakayama, K., Tanaka, M., 2009. Horizontal distribution and population dynamics of the dominant mysid *Hyperacanthomysis longirostris* along a temperate macrotidal estuary (Chikugo River estuary, Japan). Estuarine, Coastal and Shelf Science 83, 516–528.

Suzuki, K.W., Kasai, A., Nakayama, K., Tanaka, M., 2012. Year-round accumulation of particulate organic matter in the estuarine turbidity maximum: comparative observations in three macrotidal estuaries

(Chikugo, Midori, and Kuma Rivers), southwestern Japan. Journal of Oceanographer 68, 453–471.

Suzuki, K.W., Nakayama, K., Tanaka, M., 2013. Distinctive copepod community of the estuarine turbidity maximum: comparative observations in three macrotidal estuaries (Chikugo, Midori, and Kuma Rivers), southwestern Japan. Journal of Oceanographer 69, 15–33.

Takahashi, M., Seibert, D.L., Thomas, W.H., 1977. Occasional blooms of phytoplankton during summer in Saanich Inlet, B.C., Canada. Deep Sea Research 24, 775–780.

Tolhursf, T.J., Gust, G., Paterson, D.M., 2002. The influence of an extracellular polymeric substance (EPS) on cohesive sediment stability. Proceedings in Marine Science 5, 409–425.

Trevethan, M., Chanson, H., Takeuchi, M., 2007. Continuous high-frequency turbulence and suspended sediment concentration measurements in an upper estuary. Estuarine, Coastal and Shelf Science 73, 341–350.

Uncles, R.J., 2002. Estuarine Physical Processes Research: Some Recent Studies and Progress. Estuarine, Coastal and Shelf Science 55, 829–856.

Uncles, R.J., Stephens, J.A., Haris, C., 2006. Runoff and tidal influences on the estuarine turbidity maximum of a highly turbid system: The upper Humber and Ouse Estuary, UK. Marine Geology 235, 213–228.

Uncles, R.J., Stephens, J.A., 2010. Turbidity and sediment transport in a muddy sub-estuary. Estuarine, Coastal and Shelf Science 87, 213–224.

Van Dijik, G.M., Achterberg, E.P., 1992. Light climate in the water column of a shallow eutrophic lake (Lake Veluwe) in the Netherlands. Archiv für Hydrobiologie 125, 257–278.

Van Spaendonk, J.C.M., Kromkamp, J.C., De Visscher, P.R.M., 1993. Primary production of phytoplankton in a turbid coastal plain estuary, the Westerschelde (The Netherlands). Netherlands Journal of Sea Research 31, 267–279.

Watanabe, K., Kasai, A., Antonio, E.S., Suzuki, K., Ueno, M., Yamashita, Y., 2014.

Influence of salt-wedge intrusion on ecological processes at lower trophic levels in the Yura Estuary, Japan. Estuarine, Coastal and Shelf Science 139, 67–77.

Winter, D.F., Banse, K., Anderson, G.C., 1975. The dynamics of phytoplankton blooms in Puget Sound, a fjord in the northwestern United States. Marine Biology 29, 139–176.

Wolanski, E., King, B., Galloway, D., 1995. Dynamics of the Turbidity Maximum in the Fly River Estuary, Papua New Guinea. Estuarine, Coastal and Shelf Science 40, 321–337.

Wolanski, E., Moore, K., Spagnol, S., Adamo, N.D., Pattiaratchi, C., 2001. Rapid, Human-Induced Siltation of the Macro-Tidal Ord River Estuary, Western Australia. Estuarine, Coastal and Shelf Science 53, 717–732.

Wolanski, E., Williams, D., Spagnol, S., Chanson, H., 2004. Undular tidal bore dynamics in the Daly Estuary, Northern Australia. Estuarine, Coastal and Shelf Science 60, 629–636.

Xie, D.F., Pan, C.H., 2013. A preliminary study of the turbulence features of the tidal bore in the Qiantang River, China. Journal of Hydrodynamics 25, 903–911.

Yokoyama, K., 2013. Organic and inorganic components of suspended matter in the Chikugo river estuary. XVIII Conference on Hydraulics, Water Resources, Coastal and Environmental Engineering. Proceedings of HYDRO 2013 INTERNATIONAL (IIT Madras, INDIA), pp. 441–446.

Zhai, L., Tang, C., Platt, T., Sathyendranath, S., 2011. Ocean response to attenuation of visible light by phytoplankton in the Gulf of St. Lawrence. Journal of Marine Systems 88, 285–297.